FLUORESCENT MOLECULAR PROBES TO DETECT METAL IONS/ANIONS

A Thesis submitted to the

UPES

For the Award of

Doctor of Philosophy

in

Chemistry

By

NIDHI GOSWAMI

January 2025

Supervisor

Dr. Pankaj Kumar

Co-Supervisor

Dr. Sushil Kumar

Department of Chemistry

School of Advanced Engineering

UPES

Dehradun- 248007: Uttarakhand, India

FLUORESCENT MOLECULAR PROBES TO DETECT METAL IONS/ANIONS

A Thesis submitted to the

UPES

For the Award of

Doctor of Philosophy

in

Chemistry

By

NIDHI GOSWAMI

SAP-ID: 500095524

January 2025

Supervisor

Dr. Pankaj Kumar

Professor

Department of Chemistry, SoAE, UPES

Co-Supervisor

Dr. Sushil Kumar

Associate Professor

Department of Chemistry, SoAE, UPES

Department of Chemistry

School of Advanced Engineering

UPES

Dehradun- 248007: Uttarakhand, INDIA

DECLARATION

I declare that the thesis entitled "**Fluorescent Molecular Probes to Detect Metal Ions/Anions**" has been prepared by me under the guidance of **Dr. Pankaj Kumar** (Supervisor), Professor, Department of Chemistry, UPES, Dehradun and **Dr. Sushil Kumar** (Co-supervisor), Associate Professor, Department of Chemistry, UPES, Dehradun. No part of this abstract has formed the basis for the award of any degree or fellowship previously.

Nidhi Goswami

Department of Chemistry

UPES

Dehradun-248007, Uttarakhand

Date: 31 July 2025

UPES
UNIVERSITY OF TOMORROW

Great Place To Work. Certified FEB 2024-FEB 2025 INDIA

CERTIFICATE

I certify that **Nidhi Goswami** has prepared her thesis entitled **"Fluorescent Molecular Probes to Detect Metal Ions/Anions"** for the award of PhD degree from the University under my guidance. She has carried out the work at the Department of Chemistry, UPES, Dehradun.

22/08/2024.

Supervisor

Dr. Pankaj Kumar

Department of Chemistry, SoAE,

UPES, Dehradun

248007

Date:

Co-supervisor

22/08/2024

Dr. Sushil Kumar

Department of Chemistry, SoAE,

UPES, Dehradun

248007

Date:

Energy Acres: Bidholi Via Prem Nagar, Dehradun 248 007 (Uttarakhand), India T: +91 135 277013 /2776053/54/9 , 2776201,9997799474 F: +91 135 2776090/95
Knowledge Acres: Kandoli Via Prem Nagar, Dehradun - 248 007 (Uttarakhand), India T: +91 8171979021/2/3, 7060111775

ABSTRACT

Small analytes, such as cations and anions, are integral to human health, material science, industrial processes, and biological systems. Metal ions, in particular, play essential roles in numerous biological functions due to their strong affinity for biomolecules. However, their improper handling or excessive use has led to significant environmental contamination, particularly in soil and water bodies. This necessitates the development of efficient and selective detection methods to monitor these analytes in biological and environmental samples, ensuring human and ecological health. Optical sensing, especially using fluorescent molecular probes, has emerged as a promising approach due to its simplicity, rapid detection, high sensitivity, and cost-effectiveness. These probes, incorporating receptor, signaling, and reporter units, have demonstrated great potential for applications across chemical, biological, and environmental domains.

This thesis focuses on the design, synthesis, and application of novel fluorescent chemosensors for the detection of various analytes. Key highlights include:

1. **Fluorescent and Colorimetric Probe for Al^{3+} Detection**

A quinoline-derived Schiff base (**QnSb**) was synthesized and extensively characterized using elemental analysis, spectroscopy, and single-crystal X-ray diffraction. The non-fluorescent **QnSb** exhibited a "turn-on" fluorescence response at 422 nm upon binding with Al^{3+} in a CH_3CN/H_2O medium. The probe demonstrated high selectivity, a detection limit of 15.8 nM (below WHO standards), and a 1:1 binding stoichiometry, as confirmed by Job's plot, ESI-MS, NMR, and DFT analyses. Applications included molecular logic gate development and Al^{3+} detection using filter paper strips.

2. **Schiff Base Probe for Al^{3+} Recognition in Biological and Environmental Samples**

Another Schiff base probe (**TQSB**) exhibited high selectivity for Al^{3+} with a detection limit of 7.0 nM. Fluorescence enhancement was attributed to CHEF (chelation-enhanced fluorescence) and restricted PET effects. Applications

included detecting Al^{3+} in soil samples, gastric tablets, and live-cell imaging with no cytotoxic effects.

3. Lewis Acid-Catalyzed Nucleophilic Reactions and Structural Insights

A robust synthetic approach emphasized on Lewis acid coordination to aromatic aldehydes was developed. This method stabilized transient gem-diol intermediates, confirmed by X-ray crystallography, absorption and emission spectral profiles, providing deeper insights into biomimetic reaction mechanisms.

4. Fluorogenic Probe for F^- and CN^- Detection

A phenanthroline-based probe (**bpmpip**) was developed for the selective and ratiometric fluorescence detection of fluoride and cyanide ions. The probe displayed nanomolar detection limits, distinct visual color changes, and successful applications in soil, environmental, and live-cell analyses. The binding mechanism, based on hydrogen bonding and deprotonation, was elucidated through Job's plot, NMR, and computational studies.

These findings advance the field of optical sensing, offering practical applications in environmental monitoring, biological imaging, and analytical chemistry.

ACKNOWLEDGEMENT

I am profoundly grateful to the Almighty Lord Shiva, whose divine guidance and blessings have steered me toward this significant milestone in my academic journey. With a heart full of reverence and humility, I extend my sincerest appreciation to all those whose unwavering support, encouragement, and kindness have paved the path to the successful completion of this research.

Foremost, I extend my sincere appreciation to my esteemed supervisors, Dr. Pankaj Kumar Thakur and Dr. Sushil Kumar, whose invaluable guidance, continuous encouragement, and unwavering faith in my abilities have been the bedrock of this thesis. Their mentorship, from the inception of my research to its completion, has not only shaped my academic development but also contributed significantly to my personal growth. The intellectual freedom they extended to me allowing exploration across topics and collaborations greatly enriched my understanding and broadened my academic perspective. I am especially thankful for the intellectually stimulating discussions we shared, often over evening coffee, which were both insightful and inspiring.

I would like to express my heartfelt gratitude to Dr. Ram Sharma, Vice Chancellor, University of Petroleum and Energy Studies (UPES), for his inspiring leadership and unwavering support throughout my research journey. I am deeply grateful to former Dean Dr. D. K. Avasthi and present Dean Dr. Ashwini Kumar Nangia; their guidance, motivation, and feedback significantly enriched my research. I also sincerely acknowledge UPES for providing financial assistance and an enriching academic environment during my Ph.D. tenure. The resources, facilities, and constant encouragement offered by the university have been instrumental in shaping this research. I would like to express my heartfelt thanks to Dr. Ranjeet Brajpuriya, Cluster Head, and Mrs. Bhawna Yadav Lamba, Ph.D. Coordinator, for their constructive feedback and guidance, which significantly enhanced the depth and clarity of my work. Their belief in my potential has been a source of motivation. I also extend my gratitude to the Department of Chemistry faculty members for their continuous assistance

during my research. My sincere thanks go to my departmental research committee (DRC) members: Dr. Aashish Mathur, Dr. Shefali Arora, and Dr. Sravendra Rana whose critical insights, motivation, and persistent reminders played a crucial role in keeping me focused and committed to completing my Ph.D. I am indebted to Dr. Manish Kumar, Dr. Balendu Shekhar Giri, Dr. Tridib Kumar Sinha, and Dr. Shalendra Kumar whose teachings and wisdom have greatly enriched my academic and research pursuits. I am also thankful to my collaborators: Dr. Ritesh Dubey, Dr. Tapas Goswami, Dr. Jimmy Mangalam, Dr. Samar Layek, Dr. Amit Kumar, and Mr. Rajneesh Budhwa from IIT Roorkee for their valuable contributions and collaborative spirit. I gratefully acknowledge the lab staff: Dr. Devendra Rawat, Mr. Tijendra Kumar, and Mr. Keshav Kumar Surya for their indirect yet vital support in the smooth execution of my research activities. I am also indebted to Mr. Abhishek Goel, Mr. Amit Kumar, and Mr. Yogesh Kumar Sharma for their kindness and support throughout this journey. My appreciation extends to the UPES academic and administrative staff, as well as the security personnel, for their consistent support and assistance.

The camaraderie and support of my lab mates have played an integral role in my academic life. I am especially thankful to Mr. Sudhanshu Naithani, Mrs. Pooja Sharma, Mr. Vikas Yadav, and Ms. Anjali Varshney, whose companionship and shared discussions have been both meaningful and memorable. I also cherish the time spent with Mrs. Sakshi Sharma, Mr. Kaushal, Mr. Rahul Chamola, and Ms. Huma Naaz. The lab's work desk has witnessed every stage of my journey from moments of triumph to setbacks, manuscript acceptances to rejections, all of which contributed to my growth and resilience. Beyond the confines of the lab, I am profoundly grateful to individuals who have stood by me during both academic and personal trials: Sonal Vilas Shah, Tej Bhan Singh, Dr. Dinesh Rathod, Shilpa Thakur, Mahima Pandey, Shivangi Jaryal, Dr. Poonam Singh, and Dr. Siddharth Singh. Their unwavering friendship and counsel have served as a strong anchor in my life. I am equally thankful to Jyoti Teotia, Anuradha, and Himani Bhardwaj for their steadfast support and encouragement. I would also like to acknowledge and thank my

travel companions on trips to Chakrata, Jaipur, Rishikesh, Renuka Ji, Amritsar, Kedarnath, and Badrinath. These experiences brought balance, joy, and unforgettable memories that enriched my Ph.D. journey.

Words are not enough to express my gratitude to my family. My father, Mr. Mukesh Puri, has been a pillar of strength, shielding us through both hardships and joyous times. My mother, Mrs. Ramkumari Puri, whose dreams and sacrifices shaped my identity, remains the most pivotal figure in my life. I offer heartfelt thanks to my uncles, Mr. Dori Puri, Mr. Sanjaya Puri, and Dr. Surendra Rana, and my aunts, Mrs. Manju Puri and Mrs. Manju Puri, for their continuous motivation and guidance. Special thanks to my brother Mr. Pradeep Puri and sister-in-law Mrs. Chhaya Puri, whose unwavering support and belief in my aspirations have been deeply encouraging. My heartfelt appreciation also goes to my brothers Mr. Lokendra Puri, Mr. Chandra Shekhar Goswami, Mr. Sandeep Singh, Mr. Jatin Puri, and Mr. Pravesh Goswami for being my constant support system. I am equally grateful to my sisters Mrs. Priya Goswami, Mrs. Varsha Puri, Mrs. Kiran, Ms. Soni, Ms. Madhuri, and Ms. Chhavi and my brothers-in-law Mr. Nitin Goswami and Mr. Nand Lal Goswami for their love and encouragement. To my beloved nephews Mr. Shaurya Puri, Mr. Iyan Goswami (Laddu), and Mr. Advik Goswami and niece, Ms. Yaara Goswami, I owe a special debt of gratitude. The time spent away from them in the lab was a personal sacrifice, and the joy in their eyes upon my accomplishments is my greatest reward. This thesis is dedicated with heartfelt reverence to the memory of my late grandparents, Mrs. Rukmani Puri and Mr. Mahesh Puri, whose blessings I feel have guided and protected me throughout this journey.

Lastly, I wish to extend my deepest gratitude to all those who were directly or indirectly associated with this journey. Even if your names are not mentioned here, please know that your support is deeply appreciated and remembered with sincere gratitude.

Thank you all, once again, from the bottom of my heart.

(Nidhi Goswami)

TABLE OF CONTENT

LIST OF FIGURES

LIST OF TABLES

LIST OF SCHEMES

ANNEXURE I

LIST OF FIGURES

LIST OF TABLES

CHAPTER 1

INTRODUCTION

1.1 Heavy metals: Sources and impact

Metals play a vital role in various biological processes and are essential in many aspects of daily life; however, many of them can have severe health effects. Among various metals, nickel (Ni), iron (Fe), copper (Cu), aluminum (Al), palladium (Pd), and platinum (Pt) are extensively utilized across industries, material science, biology, and many other aspects of human social life (Iftikhar et al., 2023; Loya et al., 2023; Shi et al., 2023; Yang et al., 2023; Ye et al., 2023) Over the past two decades, significant advancements have been made in developing metal-based catalysts for applications in organic chemistry, ranging from small-scale laboratory use to large-scale industrial processes (Afrin et al., 2023; Aruna et al., 2024; Iyer et al., 2023; Lalitha et al., 2023; Yang et al., 2024). These metals, in their ionic forms, exhibit unique coordination and reactivity, leading to the synthesis of various bioactive molecules, as reported in the literature (Table 1.1) (Majhi et al., 2024). However, the widespread use of these metals has resulted in severe ecological contamination, particularly in soil and water systems.

Table 1.1. Limits, sources, and effects of various heavy metals.

Analyte (Heavy metals)	WHO limits (mg L^{-1})	Sources	Effects	References
Cadmium (Cd)	0.005	Paints, synthetic rubber, plastics, etc.	Hypertension, lung cancer	(Huang et al., 2023)
Mercury (Hg)	0.001	Combustion of coal, volcanic emissions	Minamata disease	(Li et al., 2023)
Arsenic (As)	0.05	Fertilizers, pesticides	Anorexia, skin cancer	(Bhat et al., 2023)
Chromium (Cr)	0.05	Leather industry	Lung cancer, skin ulcer	(Liu et al., 2024)
Lead (Pb)	0.05	Agriculture, lead batteries	Alzheimer's disease, kidney damage	(Zhao et al., 2023)

Silver (Ag)	0.1	Refining of gold, copper, nickel, zinc	Mental fatigue	(Zhao et al., 2023)
Copper (Cu)	1.3	Fertilizers	Diabetes, kidney disorders	(Sun et al., 2023)
Iron (Fe)	0.3	Meat, seafood	Liver disease, heart problem	(Kumar et al., 2023)
Zinc (Zn)	5	Cosmetics and pigments	Respiratory disorders	(Naithani et al., 2023)

1.1.1 Aluminium (Al)

Although aluminum (Al) occurs naturally, human activities significantly contribute to its increased presence in the environment. Aluminium is the most abundant metal in the Earth's crust and the 3rd most abundant element in the lithosphere (*ca.* 8.0 % of total mineral substances). Al^{3+} ion is widely applied in different essential aspects of human social life, industries, material science, and biology; it has been typically employed in various household products, electrical and electronic components, building construction materials, and sophisticated medical devices, to name but a few (Heena et al., 2024; Naithani et al., 2023). Due to its extensive usage, more and more Al^{3+} ions enter the environment, leading to detrimental impact to human life. Excessive intake of Al^{3+} in humans has been linked to many inimical neurodegenerative disorders such as Parkinson's disease, Alzheimer's disease, as well as dialysis encephalopathy (Liu et al., 2024). Therefore, it has been categorized as a neurotoxic agent to humans. A high degree of Al^{3+} deposition causes the soil to become highly acidic which is deadly to the flora and aquatic fauna (Suguna et al., 2023; Zhou et al., 2024). Furthermore, other physiological dysfunctions such as gastrointestinal issues, interruption with Ca^{2+} metabolism, and reduced kidney and liver functioning can be caused by Al^{3+} toxicity. Due to a close relationship between Aluminium and human health, WHO (World Health Organisation) has limited the daily intake of Al^{3+} ion ranging from 3.0 to 10.0 mg/day while a limit of only 7.41 μM (200 μg/L) is allowed in the drinking water (Islam et al., 2024; Yao et al., 2023). Hence, there is an urgent need to develop selective and efficient methods for the detection and/or diagnosis of Al^{3+}, particularly in environmental and biological settings.

1.1.2 Nickel (Ni)

Nickel (Ni), the fifth most abundant metal on Earth, is vital for the activity of several enzymes that play significant roles in both plants and microorganisms (such as bacteria, fungi, algae and archaea) (Naithani et al., 2024). It acts as a co-factor in many fundamental biological and cellular events, more importantly in nitrogen metabolism and in energy-related processes (Loya et al., 2023). As compared to other biologically essential metals, Ni is found to be limited in eukaryotes. Nickel usually exists in Ni(0) and Ni(II) states while Ni(I) and Ni(IV) are hardly observed. Only a few nickel-based metalloenzymes including urease, nickel–superoxide dismutase (Ni–SOD) and [Ni–Fe] hydrogenase have been explored, so far (Sadia et al., 2023). On the other hand, no nickel-based enzyme has been discovered in mammals. Over the decades, the industrial utilization and demand for nickel has significantly expanded owing to its crucial roles in a diverse range of metallurgical and catalytic processes including alloy manufacturing, electroplating, paints and pigments, arcwelding, dental and surgical prostheses, magnetic tapes for computers, ceramics, hydrogenation catalysis and Ni-Cd batteries (Leslee et al., 2023). The industrial demand for Ni is leading to increased environmental pollution along with human health concerns. Notably, overexposure to Ni(II) (*via* either inhalation or dietary intake) may cause lung fibrosis, asthma, conjunctivitis, pneumonitis, and allergic contact dermatitis. Long-term exposure is also linked to malignancy issues of the stomach, throat, nasal, sinus, and lungs (Turhan et al., 2023). Though the influence and impact of nickel concentration on human beings is yet to be fully scrutinized, it is accepted today that an excess of nickel causes adverse health issues. This makes it crucial to detect nickel in the environment and biological systems. Contextually, several efficient methods have been developed to detect Ni(II) ions in a variety of materials including cellular organelles and other water bodies (Khan et al., 2023). Besides, there is a great deal of interest in learning more about Ni-based ions, with an emphasis on their physiological properties.

1.1.3 Palladium (Pd)

Palladium (Pd) belongs to the platinum group of transition metals along with platinum (Pt), ruthenium (Ru), rhodium (Rh), osmium (Os) and iridium (Ir) metals (Alqarni et al., 2024). The industrial demand for Pd is very high due to its crucial roles in many industrial processes including the production of fuel cells, dental alloys, automobiles, electric as well as electronic components (Ji et al., 2023). Through its variable oxidation states (i.e., 0, +2 and +4), palladium-based compounds have been widely employed as catalysts in various chemical, medicinal and petrochemical industries for the development of functional materials, supramolecules, drugs, natural products, polymers, etc. (Sharma et al., 2024). The increasing requirement of Pd in organic synthesis and catalysis can be highlighted by its high efficiency/ability to afford new carbon-carbon (C-C) and carbon-heteroatom (e.g., C-O, C-S, C-N etc.) bonds via Pd-catalyzed cross-coupling reactions (Gan et al., 2023). However, such an extensive usage of Pd has resulted in increased Pd-based pollution worldwide leading to a serious contamination of the environment and adverse effects on human health (Choudhury et al., 2023; Song et al., 2023). Pd(II), a soft acid, exhibits high affinity towards various biomolecules (thiol-based amino acids, proteins, DNA etc.), and thus it can easily accumulate in the food chain to cause severe health issues. For example, a high Pd(II) intake (more than 20 μg per day per person) is linked to dermatitis, nausea, loss of hair, asthma, and unusual abortion in humans (Sharma et al., 2024). Though various analytical methods have been successfully employed for the detection of metal ions, highly selective detection of Pd(II) is found to be underdeveloped, especially in complex environmental samples such as water and soil systems. The reason may lie behind the fact that the concentration of Pd(II) is remarkably low in such samples.

1.1.4 Platinum (Pt)

Platinum (Pt) is a precious metal that is widely employed in various catalytic conversions, gas adsorbing materials, fuel cells, therapeutic agents, jewels, dental crowns, etc. (Song et al., 2023). In particular as anticancer agents, Pt(II)-based compounds have exhibited remarkable optical, biological and catalytic properties (Alqarni et al., 2024). Catalysts with several activities, such

as carbophilic activation, oxidation, and hydration, can be developed from Pt(II) complexes (Sharma et al., 2023). Despite being implemented in many research areas, such compounds display remarkable toxicity to human beings. Frequent usage of Pt(II) salts is linked to the damage of intestines, kidneys, and bone marrow in addition to causing DNA abnormalities, malignancies, immune disorders, and respiratory and hearing issues (Das et al., 2024). This may be due to their preferential coordination to various soft donor sites (such as S, P, etc.) present in various biomolecules. Hence, the monitoring of Pt content in biosystems is crucial to diagnose and treat life-threatening diseases. Especially for cancer patients under treatment using Pt(II)-containing drugs (e.g., cisplatin), an accurate detection of Pt(II) content will certainly aid the therapy process. Regardless of the relevance of this metal in clinical research and biology, highly selective Pt(II) sensors have been less explored so far, which may be due to the comparable chemical features and reactivity of Pt(II) with Pd(II) (Sharma et al., 2023).

1.1.5 Mercury (Hg)

Mercury (Hg), in both its elemental and inorganic forms, is prevalent in the environment and poses significant toxicity to aquatic ecosystems, plants, and animals (Li et al., 2023). In aquatic systems, certain bacteria can transform inorganic Hg into the more hazardous monomethyl mercury(II) ions (An et al., 2024). This toxic element is highly detrimental to human health, capable of severely impairing the endocrine and central nervous systems. Prolonged or excessive exposure can result in serious conditions such as edema, anemia, Minamata disease, and even death (Leslee et al., 2023). To reduce the related health risks, the WHO has established a strict limit for mercury (Hg(II)) in drinking water, capping its concentration at 0.001 mg/L (Sharma et al., 2023). Given mercury's health risks and widespread occurrence, extensive research has focused on developing methods for its qualitative and quantitative detection. However, selective recognition of Hg(II) ions remains particularly challenging due to their spectroscopically silent nature and closed-shell d^{10} electronic configuration (Singh et al., 2025).

1.1.6 Iron (Fe)

Iron (Fe) is the most abundant and essential metal for humans and plants, playing a crucial role in numerous biological processes. It facilitates oxygen transport via hemoglobin, drives electron transfer reactions, supports DNA and RNA synthesis, and participates in various enzymatic functions (Heena et al., 2024). Imbalanced iron levels can severely affect enzymatic activity and the immune system, leading to pathological conditions. Iron deficiency is the primary cause of anemia worldwide, while iron overload can result in kidney and liver damage, cardiovascular diseases, and diabetes (Chakraborty et al., 2024). In biological systems, iron primarily exists in ferrous (Fe^{2+}) and ferric (Fe^{3+}) states, forming a critical redox pair. Developing effective methods for detecting Fe^{2+} and Fe^{3+} ions in biological samples is both valuable and challenging. Among established detection techniques- such as inductively coupled plasma mass spectrometry, chemiluminescence, and voltammetry- optical sensors stand out for their simplicity, low cost, and high selectivity for metal ions (Kumar et al., 2023). Furthermore, luminescent supramolecular gels and metal-organic frameworks (MOFs) have been investigated for their ability to recognize Fe^{2+}, offering promising applications in biomedicine and luminescent materials (Zhou et al., 2025). These advancements highlight the ongoing pursuit of innovative and efficient methods for iron detection in biological and clinical research.

1.1.7 Zinc (Zn)

Zinc (Zn) is the second most abundant transition metal in the human body and is critical for various physiological processes, including cell metabolism, metalloenzyme regulation, and neurophysiology (Naithani et al., 2023). It also plays a key role in the formation of β-amyloid, a protein strongly associated with Alzheimer's disease (Singh et al., 2023). During apoptosis, intracellular metalloproteins release zinc, making it essential to develop highly selective and sensitive chemosensors capable of detecting trace amounts of zinc to effectively monitor this process (Alharbi et al., 2023). In addition to its role in apoptosis, Zn is an integral structural component of numerous proteins, contributing significantly to their stability and biological function (Li et al., 2023). Zn(II) ion has a broad spectrum of effects on the immune and nervous

systems, influencing various cellular activities both in vivo and in vitro. These actions are highly dependent on zinc concentration, as imbalances can lead to detrimental outcomes (Behura et al., 2023). Due to zinc's diverse roles in physiological and pathological processes, the ability to detect and study zinc with precision is vital. Advancements in detection technologies will enhance our understanding of zinc's biological significance and its impact on health and disease (Bai et al., 2023).

1.1.8 Copper (Cu)

Copper (Cu), the third most abundant and essential trace element in living organisms, plays a crucial role in a wide range of physiological processes. It is integral to key biological functions such as electron transport, oxidative phosphorylation, and the functioning of various enzymes involved in the synthesis of neurotransmitters, collagen, and melanin (Du et al., 2023). Though the human body has mechanisms to regulate copper levels, both a deficiency and an excess of copper can lead to serious health issues. Copper deficiency has been linked to impaired cell growth, anemia, and neurological disorders, particularly affecting the central nervous system (CNS), leading to conditions such as neurodegeneration and developmental delays (Aruna et al., 2024). On the other hand, an overload of copper ions (Cu^{2+}) has been implicated in a variety of diseases, including Wilson's disease, Alzheimer's disease, and cardiovascular disorders (Sun et al., 2023). Moreover, copper is widely used in industrial, agricultural, and environmental processes, contributing to its presence as a significant contaminant in water systems (Zhou et al., 2025). Excessive copper levels in water sources can pose serious environmental risks, including toxicity to aquatic organisms and disruption of ecosystems, as well as potential health hazards for humans (Leslee et al., 2023).

Due to the related health and environmental implications, there is a strong need for reliable and efficient methods to selectively detect and quantify Cu^{2+} ions. Traditional detection methods, such as inductively coupled plasma mass spectrometry (ICP-MS), ion chromatography, and electrochemical analysis, are highly accurate and sensitive but require expensive instrumentation and extensive sample preparation, making them less accessible for routine monitoring, especially in field applications (Sun et al., 2023). In contrast, optical

detection methods have emerged as a more attractive alternative. These methods offer several advantages, including ease of use, rapid analysis, low cost, and high selectivity for metal ions, particularly copper (Du et al., 2023). Optical sensors can be designed to selectively bind to Cu^{2+} ions, producing a measurable fluorescence signal in response to copper presence. This approach allows for real-time, on-site monitoring with minimal sample preparation, making it ideal for applications in environmental monitoring, water quality assessment, and even biological studies where copper plays a role in cellular processes.

Overall, the development of advanced sensing methods for toxic heavy metals represents a promising approach to enhancing our ability to monitor and manage their toxicity levels. These innovations are crucial for effectively addressing both public health concerns and environmental challenges, allowing for more precise detection, prevention, and remediation strategies in various settings. By improving the sensitivity, selectivity, and accessibility of these sensors, we can better safeguard ecosystems and human health from the detrimental effects of heavy metal contamination.

1.2 Anions: Sources and impact

Researchers across diverse fields have shown growing interest in developing molecular synthetic probes for the selective recognition of anions. This increased focus arises from the crucial roles anions play across biological, aquatic, industrial, and environmental processes (Kataev et al., 2023). Key anionic species such as fluoride (F^-), chloride (Cl^-), cyanide (CN^-), phosphate (PO_4^{3-}), acetate (AcO^-), nitrate (NO_3^-), carbonate (CO_3^{2-}), etc. are essential for various physiological functions. However, their effects on human health and the environment are often dualistic- offering both beneficial and potentially harmful outcomes (Chatterjee et al., 2024) (Table 1.2). For instance, fluoride ion is beneficial for dental and skeletal health when consumed in appropriate amounts, yet excessive intake is linked to diseases such as cystic fibrosis and dental or skeletal fluorosis (Li et al., 2023). Similarly, an imbalance of phosphorus-based ions in the body is associated with conditions like impaired kidney function, abnormal bone mineralization, and muscle weakness (Ma et al., 2023). Among various anions, CN^- stands out as particularly significant due to its extreme toxicity. Adding to the complexity, the fluoridation of tap water remains a

widespread practice in countries like the United Kingdom, the United States, and Australia to promote dental health, despite concerns about potential overexposure (Suna et al., 2023). Furthermore, while deoxyribonucleic acid (DNA) is widely recognized for its role in genetic information storage, its multifunctionality as a binding unit for various analytes, including anions, highlights its intriguing and underexplored potential. Collectively, these factors underscore the significance of anionic species as critical targets for detection and analysis.

Table 1.2. Limits, sources, and effects of anions

Anions	WHO limits (mg L^{-1})	Sources	Effects	References
Cyanide (CN^-)	0.2	Bamboo shoots, spinach, and almonds	Anxiety, coma, lung injury, and	(Hendry-Hofer et al., 2019)
Fluoride (F^-)	1.5	Seafood, tea leaves, and dental products	Cardiovascular problems, reproductive issues, and thyroid dysfunction	(Ghosh et al., 2013)
Chloride (Cl^-)	250	Many vegetables, rye, and tomatoes	Hypertension, and cardiovascular	(Moore et al., 2020)
Bromide (Br-)	0.014-0.2	Seawater, marine algae, and polar regions	Headache, confusion, drowsiness, and memory loss	(Zhang et al., 2023)
Phosphate (PO_4^{3-})	1	Rocks, fertilizers, and dairy	Bone disease, heart disease, and kidney disease	(Wang et al., 2021)

However, detecting anions remains significantly more challenging compared to their cationic counterparts. This difficulty arises partly from the unique characteristics of anions, including their diverse geometries, strong solvation tendencies, and lower charge-to-radius ratios (Naithani et al., 2024). These properties complicate the differentiation of negatively charged anionic species from positively charged counterparts. Consequently, the design of highly selective and sensitive synthetic probes must consider multiple factors, such as the hydrophobic effect, stacking interactions, electrostatic interactions, and hydrogen bonding (H-bonding), among others.

1.2.1 Cyanide (CN^-)

Cyanide ion is of particular concern as an exceptionally toxic inorganic anion with severe impacts on aquatic ecosystems and human health (Naithani et al., 2024). Even at low concentrations, cyanide is highly lethal and can be absorbed through the skin, respiratory system, or digestive tract (Khalid et al., 2024). Mechanistically, cyanide disrupts aerobic respiration by inhibiting cytochrome c oxidase, thereby stopping ATP (adenosine triphosphate) production due to dysfunction of the electron transport chain (Pal et al., 2024). To reduce its risks, the World Health Organization (WHO) has established a maximum permissible cyanide concentration of 1.9 μM in drinking water. Despite its toxicity, cyanide-based compounds find extensive applications in industries such as electroplating, plastics, gum manufacturing, X-ray film recovery, gold and silver leaching, and the synthesis of organic chemicals, pharmaceuticals, and polymers (Naithani et al., 2024). Cyanide contamination can arise from multiple sources, including industrial discharge, structural fires, medical exposures (e.g., sodium nitroprusside), and even certain foods like lima beans and almonds (Jayasudha et al., 2024). Accidental leakage of cyanide-laden wastewater into domestic water supplies is a persistent challenge. Provided that water serves as the primary medium for cyanide trafficking in biological and environmental systems, the development of detection methods specifically designed for CN^- in aqueous environments, rather than organic solvent systems, is paramount.

1.2.2 Fluoride (F^-)

Fluoride (F^-) is an essential ion involved in different physiological processes, particularly in maintaining dental and skeletal health (Roy et al., 2025). Primary sources of fluoride include fluoridated drinking water, toothpaste, mouth rinses, and certain foods like tea, fishes, and those prepared with fluoridated water (Li et al., 2023). Environmental fluoride exposure can also arise from industrial waste, phosphate fertilizers, and some pharmaceuticals (Zheng et al., 2024). Although fluoride is vital for preventing dental cavities and promoting bone strength, an imbalance can lead to severe health issues. Excessive fluoride consumption is associated with dental and skeletal fluorosis, characterized by tooth discoloration and bone deterioration (Paul et al., 2024). Prolonged overexposure may also affect soft tissues, potentially causing thyroid dysfunction, liver damage, and other organ-related diseases. Contextually, the World Health Organization (WHO) has established a maximum allowable fluoride concentration of 1.5 mg L^{-1} in drinking water (Chakraborty et al., 2023). However, regions with naturally high fluoride levels in groundwater and the overuse of fluoride-containing products can lead to toxic effects. Moreover, fluoride, like cyanide, has been historically utilized as a chemical warfare agent and a tool for terrorism, underscoring the importance of rigorous monitoring and regulation (Li et al., 2023).

1.2.3 Phosphate (PO_4^{3-})

Phosphate, an essential nutrient, is derived from various dietary and environmental sources. Common dietary sources include protein-rich foods such as meat, fishes, eggs, dairy products, nuts, legumes, certain vegetables and whole grains (Tsai et al., 2023). Additionally, processed and packaged foods often have added phosphates as preservatives or flavour enhancers, significantly increasing dietary phosphate intake (Li et al., 2024). In agriculture, inorganic phosphate is a key component of fertilizers, aiding plant growth. However, its extensive use can result in environmental runoff, which contributes to water pollution and eutrophication in aquatic ecosystems (Feng et al., 2023). Phosphate is also found in medications, nutritional supplements, and cleaning products, further broadening its potential exposure. Although dietary and supplemental phosphates are crucial for supporting essential physiological

processes, excessive intake or environmental exposure poses health risks. This is particularly concerning for individuals with impaired kidney function or other metabolic disorders, where phosphate regulation is compromised (Xu et al., 2023).

1.2.4 Chloride (Cl^-)

Chloride ions are among the most abundant and vital ions in biological systems. They are commonly found in food additives, organic chemicals, agricultural fertilizers, and are prevalent in various industrial, physiological, environmental, and agricultural processes (Grasso et al., 2023). Chloride ion plays key roles in several physiological functions, such as maintaining osmotic pressure, ensuring electron neutrality, and supporting muscle activity, making up about 70% of the total anion content in the body (Kumar et al., 2023). Chloride ion levels in biological fluids are frequently measured to diagnose a range of disorders, serving as valuable indicators in clinical investigations. Abnormal chloride concentrations can point to issues related to hydration, kidney function, respiratory health, and acid-base balance (Yan et al., 2023). Though chloride is essential for normal bodily functions, both excessive and insufficient levels can lead to health complications. Elevated chloride levels are often associated with dehydration, kidney disease, and metabolic acidosis, where the body becomes overly acidic (Kumar et al., 2023). Conversely, low chloride levels (hypochloremia) can cause symptoms like muscle weakness, respiratory issues, and fluid imbalances (Zhang et al., 2023). Due to a widespread presence of this anion in food and the environment, as well as its crucial biological roles, it is essential to maintain balanced levels to support overall health.

1.2.5 Bromide (Br^-)

Bromide (Br^-) is often recognized as toxic and corrosive to the human body, particularly when exposure occurs over extended periods. Despite its toxicity, bromine and its derivatives are widely used in various industrial applications, including as water purifiers, flame retardants, and pesticides, among others (Zhang et al., 2023). Chronic exposure to bromide ions can lead to a condition known as bromism, which is characterized by a range of neurological symptoms such as headache, confusion, drowsiness, memory loss,

and even hallucinations (Shi et al., 2024). Additionally, prolonged exposure may cause skin eruptions and other dermatological reactions. Bromide is also associated with disturbances in the central nervous system, including symptoms of sedation or depression (Zhang et al., 2023).

In the environment, bromide is found in some drinking water sources due to its use in water treatment processes, and exposure to high levels can pose a risk to public health. Some studies have also indicated that bromide may contribute to the formation of disinfection byproducts, such as brominated trihalomethanes, during the chlorination of drinking water, which are suspected carcinogens (Villarino et al., 2024). Despite being essential to certain chemical processes, its toxicological effects underscore the need for careful regulation of exposure levels in both industrial settings and environmental systems.

1.2.6 Iodide (I^-)

Iodide (I^-) is a biologically important anion that plays a vital role in thyroid and brain functions (Barkale et al., 2024). It is a key component of thyroid hormones, which are essential for regulating metabolism, growth, and development (Bayindir et al., 2023). Iodide also supports cognitive function and plays a crucial role in fetal and early childhood brain development. An imbalance in iodide level- either excess or deficiency- can lead to significant health problems. Iodine deficiency is a leading cause of preventable intellectual disabilities worldwide and can result in conditions such as goiter, hypothyroidism, and developmental delays in children (Deng et al., 2023). Conversely, excessive iodide intake can lead to thyroid dysfunction, including hyperthyroidism, and in rare cases, iodine-induced thyroiditis (Zou et al., 2023). In extreme cases, excessive iodide can also contribute to autoimmune thyroid disease or exacerbate preexisting thyroid conditions. The WHO recommends that individuals consume 150 µg of iodide daily, with a maximum allowable concentration of 18 µg of iodide per litre in drinking water (Barkale et al., 2024).

Ensuring adequate iodide intake through dietary sources such as iodized salt, dairy products, and seafood is essential to prevent iodine deficiency, while managing its levels in the environment and diet is important to avoid overexposure. Excessive iodide levels in drinking water or in the environment can occur in areas where iodine-based disinfectants are used or in regions with

naturally high iodine levels in groundwater. Monitoring iodide concentrations is critical to maintaining public health, particularly in vulnerable populations such as pregnant women and children.

As per the previous discussion, we have outlined several cationic/anionic species and their significant impact on human health. These ions play crucial roles in various biological processes but can also pose serious health risks when present in excess or deficiency. The detrimental effects of these ions on human health underscore the urgent need for reliable detection methods. Accurate and efficient detection is essential for several reasons: it enables the identification of health risks associated with environmental exposure, helps in clinical diagnostics, and ensures compliance with regulatory standards in drinking water, food, and air quality. This has led to the development of various detection approaches including conventional analytical and spectroscopic, optical, as well as electrochemical methods, especially with a focus in complex biological and environmental samples. These methods are important in various fields, including healthcare, environmental monitoring, agriculture, and industrial applications, where precise ion measurements are critical for human safety and environmental protection.

1.3. Some traditional methods to detect metal ions/anions

Traditional methods for detecting metal ions and anions have been widely developed and employed due to their proven analytical reliability and well-established procedures. Techniques such as atomic absorption spectroscopy (AAS), inductively coupled plasma mass spectrometry (ICP-MS), high-performance liquid chromatography (HPLC), and voltammetry play a crucial role in ensuring accurate detection and quantification.

1.3.1 Atomic absorption spectrometry (AAS)

AAS is one of the most widely used techniques for detecting metal ions and anions. It has found extensive application across research laboratories and industries such as food, pharmaceuticals, environmental science, and petroleum (Maharani et al., 2024). However, the optimal approach for detection depends on various factors, including the chemical composition and content of the metal ions/anions, as well as the physical state and chemical makeup of the sample. Unlike liquid samples, AAS requires specialized equipment to directly measure

metal ions/anions in solid samples (Paudel et al., 2024). Despite its many advantages and widespread use, a major limitation of AAS in the past was its inability to perform multi-element analysis. It lacked the capability for sequential or simultaneous measurement of multiple elements.

1.3.2 Inductively coupled plasma mass spectrometry (ICP-MS)

ICP-MS is a highly sensitive and reliable analytical technique used for the qualitative and quantitative identification of trace and ultra-trace elements across various sample matrices. It is extensively employed in fields such as materials research, clinical analysis, environmental science, geochemistry, and food safety (Acker et al., 2023). ICP-MS offers several advantages, including low detection limits, exceptional sensitivity, high accuracy, and the ability to detect multiple elements simultaneously (Bolea et al., 2021). However, despite these benefits, ICP-MS has notable drawbacks, such as the complexity of its instrumentation and high operational and maintenance costs. Additionally, ICP-MS is not suitable for analyzing non-metallic elements, as they may not ionize effectively under typical plasma conditions (Degueldre et al., 2021).

1.3.3 High performance liquid chromatography (HPLC)

HPLC is a highly advanced and widely used analytical technique for identifying, separating, and quantifying compounds in a mixture, commonly employed in chemistry and biochemistry (Engelhardt et al., 1986). By applying high pressure, HPLC forces a liquid sample through a column packed with a solid adsorbent material. The technique offers several advantages, including high sensitivity, efficiency, excellent resolution, quantitative accuracy, and non-destructive analysis (Lough et al., 1997). However, despite its widespread use and sophisticated capabilities, HPLC has notable drawbacks, such as being time-consuming, requiring extensive sample preparation, and having high operational costs (Lindsay et al., 1997). Additionally, it has limitations in analyzing non-volatile and thermally unstable compounds.

1.3.4 Voltammetry

Voltammetry is a widely used electrochemical technique for detecting cations and anions, particularly heavy metal ions (Batchelor-Mcauley et al., 2015). This method involves obtaining a current-voltage curve by measuring the current at various applied potentials, providing valuable information about

the electrochemical properties of the analyte. Voltammetric techniques, such as cyclic voltammetry, differential pulse voltammetry, and square wave voltammetry, are especially effective for detecting trace amounts of metal ions in complex samples (Gulaboski et al., 2022). They offer several advantages, including high sensitivity, low detection limits, and excellent accuracy, making them ideal for detecting heavy metal ions at very low concentrations (Osteryoung et al., 1993). Voltammetry is also appreciated for its cost-effectiveness, simplicity, and ability to perform real-time measurements. However, it is typically limited by interference from other species in the sample, requiring careful optimization of experimental conditions. Despite this, voltammetric methods remain a valuable tool for environmental monitoring, food safety, and clinical applications (Gulaboski et al., 2022).

1.4. Chemosensors

Sensors play an essential role in modern life, ranging from everyday devices to complex industrial systems (Javaid et al., 2021). They are typically designed to detect and respond to certain changes in the environment. Their applications span a wide variety of fields, including medical diagnostics, environmental monitoring, food quality control, and more (Janata et al., 1992). The increasing prevalence of diseases and the rising concerns over environmental contamination due to rapid industrialization highlight the critical need for effective sensors. And thus, developing affordable, fast, and efficient sensors has become a major area of research, driven by the demand to address these challenges and improve quality of life (Principles of Chemical Sensors, 2019). Sensors are typically classified into two main categories: physical sensors and chemical sensors, based on the nature of their inputs. Physical sensors respond to environmental factors such as light, pressure, temperature, or moisture content (Javaid et al., 2021). In contrast, chemical sensors detect chemical information, such as partial pressure, chemical activity, or the concentration of specific elements or ions, depending on the chemical processes or characteristics of the analyte being studied (Wang et al., 2016).

Chemosensors are a specialized class of chemical sensors capable of detecting a wide range of analytes by altering their physicochemical properties, such as emission, absorption, or redox potential. These sensors have gained

significant attention due to their critical roles in environmental monitoring, biological systems, and medical applications (Chemosensors: Principles, Strategies, and Applications, 2011). A large number of researches have focused on developing chemosensors that can selectively identify cations, anions, and small molecules through changes in chromogenic, fluorescent, or electrochemical signals (Jeong et al., 2012). Recent advances in chemosensors have prioritized the detection of ions essential for biological processes and environmental health. Traditional detection methods (as discussed above) have been widely used for accurate detection; however, these methods often suffer from limitations, such as complex instrumentation and labor-intensive sample preparation (Bell et al., 2004).

Among the various chemosensor types, optical sensors, which offer high selectivity for detecting biological and environmental metal ions, have attracted considerable interest (Jeong et al., 2012). These sensors are favored for their advanced features, such as low cost, ease of operation, on-site detection capabilities, fast reaction times, and high selectivity (Martínez-Máñez et al., 2003). As research in this field continues, optical sensors are known to play an increasingly important role in monitoring and addressing global health and environmental concerns (Jung et al., 2013).

1.5 Optical sensors

Optical sensors have gained significant attention for a wide range of analytical applications across chemical industry, biotechnology, and medicine (Wolfbeis et al., 2005). These sensors leverage spectroscopic techniques to obtain valuable information about specific chemical species of interest. This information is derived from the interactions between the target species and recognition ions, which lead to measurable changes in the sensor's response. Colorimetric and fluorogenic sensors are two common types of optical sensors (Shahbaz et al., 2024). Colorimetric sensors detect changes in absorption characteristics, typically resulting in a color shift that corresponds to the concentration or presence of a target analyte (Liu et al., 2020). Fluorogenic sensors, on the other hand, rely on measuring changes in emission characteristics, where the sensor emits light at a different wavelength after interacting with the analyte (Carter et al., 2014).

Among these, fluorescence sensing has emerged as a particularly dynamic and promising area of research. This is due to the related high sensitivity, precision, and ability to detect analytes at low concentrations. The ability to use fluorescence-based methods for detecting specific chemical species with minimal interference has made it a powerful tool in various fields, further enhancing the appeal and application of optical sensors (Guo et al., 2021).

1.5.1. Fluorogenic sensors

Fluorogenic sensors typically produce analytical signals through a photoluminescent process (Wu et al., 2017). Fluorescence sensing is one of the most effective techniques in analytical research due to its high sensitivity, rapid diagnostic capabilities, and ability to quantitatively detect even trace amounts of substances (Brzechwa-Chodzyńska et al., 2021). Additionally, such sensors are ideal for on-site detection and real-time in-vivo monitoring of analytes. Sensing mechanisms can exploit any phenomenon that alters the wavelength, lifetime, or intensity of fluorescence (Gao et al., 2017).

The phenomenon of fluorescence was first discovered by George Gabriel Stokes in 1852, when he observed that fluorite emitted light when exposed to ultraviolet (UV) radiation (Lakowicz, 2006). Fluorescence occurs when photons are emitted from a substance in the nanosecond to picosecond range after it has absorbed energy. The process can be described using the Jablonski diagram, which illustrates the behavior of an excited fluorophore (Jaffé et al., 1966) (Scheme 1.1). This diagram follows the Franck-Condon principle, where transitions occur between electronic states. Specifically, when a fluorophore absorbs appropriate light, it transitions from its ground singlet electronic state to the first singlet excited state, resulting in electronic excitation. The excited molecule then returns to its ground state through either radiative (fluorescence emission) or non-radiative pathways, dissipating the excess energy in the process.

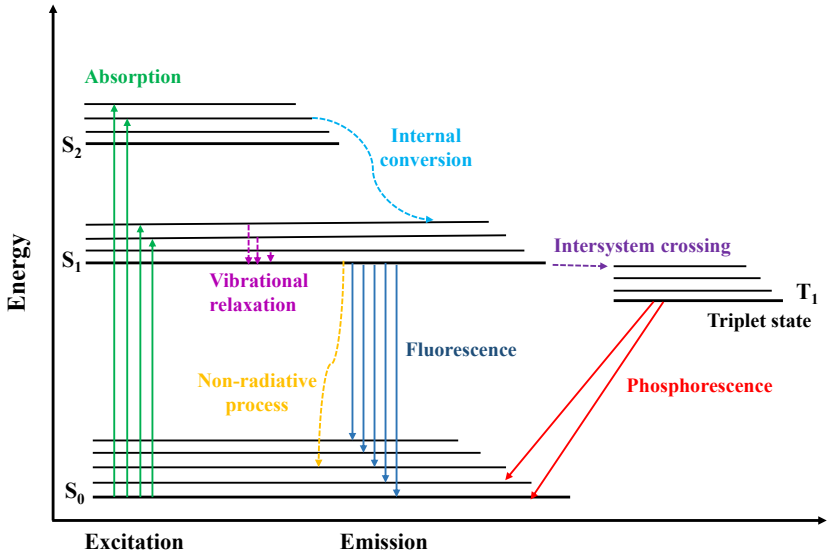

Scheme 1.1. Jablonski diagram.

Some important steps involved in Jablonski's diagram are explained as follows:

Absorption: Absorption is a radiative and very fast process in which a molecule absorbs photon, causing the electronic transition from a lower energy level to a higher energy level. This process excites the molecule to an excited state (Table 1.3).

Vibrational relaxation: This is a non-radiative process that occurs between different vibrational states within the same electronic state. During vibrational relaxation, the excess vibrational energy is dissipated as heat, leading to a relaxation of the molecule to a lower vibrational level.

Internal conversion (IC): IC is a non-radiative transition between two electronic states of the same spin multiplicity (i.e., between singlet states or triplet states). This process allows the molecule to lose energy by transitioning to a lower electronic state without emitting radiation.

Fluorescence: Fluorescence is a radiative transition between two electronic states with the same spin multiplicity, typically from the first singlet excited state (S_1) to the ground singlet state (S_0). This process results in the emission of a photon, and the term "fluorescence" refers to the photon emission associated with this transition.

Intersystem crossing (ISC): Intersystem crossing is a non-radiative process in which a molecule undergoes a change in spin multiplicity, transitioning between

electronic states with different spin states (e.g., from a singlet state to a triplet state or vice versa). This process is crucial for processes like phosphorescence.

Phosphorescence: Phosphorescence is a radiative transition between two electronic states with different spin multiplicities, typically from the triplet excited state (T_1) to the ground singlet state (S_0). This process involves the emission of a photon and is slower than fluorescence due to the spin-forbidden nature of the transition. Phosphorescence is typically observed after intersystem crossing has occurred.

Table 1.3 Average time scale of different transitions.

Transition	Time scale
Absorption	10^{-15} s
Vibrational relaxation	10^{-14} to 10^{-11} s
Internal conversion	10^{-14} to 10^{-11} s
Fluorescence	10^{-9} to 10^{-7} s
Intersystem Crossing	10^{-8} to 10^{-3} s
Phosphorescence	10^{-4} to 10^{-1} s

Fluorescent probes can be broadly classified into two types based on their interaction mechanisms: binding-based probes and reaction-based probes (Kumar et al., 2022). As illustrated in Scheme 1.2(A), a binding-based probe typically consists of a signaling unit (fluorophore) and a binding unit (receptor) designed to interact with a target ion or analyte, sometimes with a spacer between the two components (Ma et al., 2017). Several fluorescent sensors operate through a binding-based mechanism, where a reversible non-covalent interaction between metal ions and the receptor induces a change in the fluorescence intensity or emission wavelength without significantly altering the probe's structure.

In contrast to the reversible nature of binding-based probes, the optical response of reaction-based sensors is typically irreversible when interacting with target analytes (Naithani et al., 2024; Singha et al., 2019). These probes are emerging as a complementary sensing method, addressing some of the synthetic challenges associated with receptor units. Reaction-based probes involve the formation or cleavage of covalent bonds upon ion binding, where the ion acts as a catalyst or reactant to produce a new product after reacting with the receptor (Nan et al., 2021) (Scheme 1.2(B)). Both binding- and reaction-based sensors have distinct advantages and limitations. For instance, reaction-based fluorescent sensors generally offer higher sensitivity and selectivity for analytes compared to binding-based probes (Krämer et al., 2022). However, their irreversible sensing behavior limits their use for monitoring dynamic changes in metal ion concentrations, particularly in environmental and biological samples, where continuous or reversible detection is often required (Nan et al., 2021).

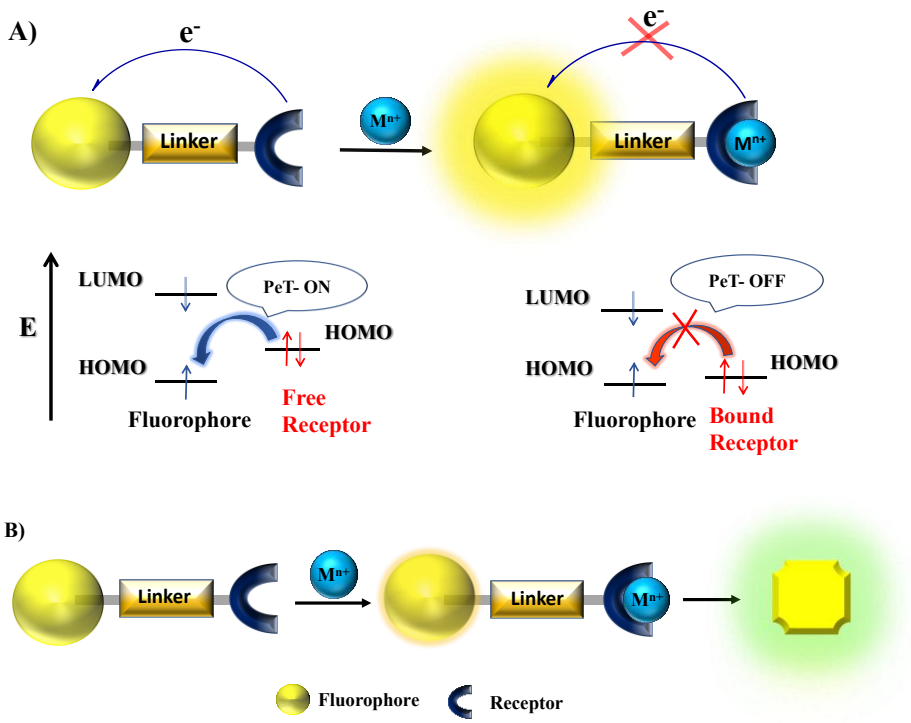

Scheme 1.2. (A) Binding- and (B) reaction-based sensing mechanisms for fluorescent detection of metal ions.

1.5.1.1 Optical probe design: Photoinduced electron transfer (PeT)

There are three fundamental components to a molecular fluorescent sensor (Goswami et al., 2023; Kumar et al., 2021):

(i) Receptor or binding unit (receptor is also known as ionophore which binds with target metal ions or anions).

(ii) Spacer or linker (which communicates electron or energy transfer between the binding unit and fluorophore unit).

(iii) Fluorophore or signal unit (which gives a fluorescent response after binding of target metal ions or anions).

The general approach to develop an ion-responsive fluorescence probe involves combining a fluorophore unit, which can be organic or inorganic (such as a metal complex), with a specific binding unit (Kumar et al., 2020). Typically, ionophores contain electron donor sites (donor atoms such as, N, S, O, P, etc.), while the fluorophore functions as an electron acceptor. In these probes, the presence of metal ions is detected through changes in fluorescence intensity and shifts in the excited-state lifetime, emission, or excitation maxima, which occur upon metal binding to the receptor unit (Lakowicz, 2006). The design of these probes often relies on either intra- or intermolecular interactions between the receptor and signalling units. Various processes have been employed to develop these probes, including photoinduced charge transfer (PCT), fluorescence resonance energy transfer (FRET), and photoinduced electron transfer (PeT) (Guo et al., 2021; Qi et al., 2020; Yoon et al., 2019). In addition, alternative mechanisms such as metal-bound inhibited excited-state intramolecular proton transfer (ESIPT) and aggregation-induced emission (AIE) have also been successfully applied in probe development (Chemistry of the Elements - N. N. Greenwood, A. Earnshaw, 1997; Li et al., 2013).

PeT has been considered as one of the most important sensing mechanisms in the design and development of fluorescent probes to recognize metal ions or anions (Sushma et al., 2024; Varadaraju et al., 2019). In a typical PeT process, an intramolecular electron (e^-) transfer occurs from an electron-rich receptor unit to an electron-acceptor fluorophore in a free probe (with no target analyte) leading to the fluorescence quenching of the probe. The coordination of a target ion to the receptor blocks the PeT process which

eventually results in the restoration of the original fluorescence. Excitation of the fluorophore with an appropriate wavelength enables the promotion of one electron from its HOMO to LUMO. If the energy of the receptor's HOMO is slightly higher than that of the fluorophore's HOMO, the spatial e^- transfer takes place from the HOMO of the receptor to the HOMO of the fluorophore through PeT. As a result, one e^- is locked into the fluorophore's LUMO leading to an emission quenching. The analyte–receptor interaction thus lowers the energy of the receptor's HOMO with respect to that of the fluorophore's HOMO. The reduction in energy level of the receptor's HOMO eventually inhibits the PeT effect and restores the original emission of the probe. The fluorescence recovery is typically linked to $\pi \rightarrow \pi^*$ excited state relaxation of fluorophores, particularly for organic fluorophores. In comparison to fluorescent sensors, colorimetric sensors are even more promising as they allow an obvious naked-eye detection of target analyte based on the color changes produced *via* the interaction between the probe and the target ion. The sensing mechanism is related to the observed electronic transitions in the form of inter- or intramolecular charge transfer (ICT) processes involving either metal-to ligand charge transfer (MLCT) or ligand-to-metal charge transfer (LMCT) process (Kumar et al., 2021; Udhayakumari et al., 2017).

1.5.1.2 Design of the probe's receptor

The selectivity of an optical chemical probe for a target metal ion is a key factor in its efficiency. The receptor pocket, or binding unit, of the probe plays a critical role in achieving high selectivity for a target ion over other competing species (Naithani et al., 2024). The interaction between the receptor and analyte, as well as the selectivity of the probe, can be controlled and enhanced by adjusting several key parameters related to the receptor unit: *(i) size and shape of the receptor's pocket*- the size and shape of the receptor pocket should match the ionic radius and coordination preferences of the target metal ion. For example, a receptor can be tailored to selectively bind ions of a specific size and geometry, excluding other ions with incompatible characteristics; (ii) *number and nature of donor atoms*- the donor atoms in the receptor unit, which provide coordination sites for the metal ion, play a crucial role in determining selectivity. The nature of these donor atoms influences the strength and

specificity of the metal-ion interaction. By adjusting the number and type of donor atoms, the receptor can be designed for high selectivity toward a specific metal ion and *(iii) hard and soft basicity of donor atoms*- the interaction between the cation and the receptor depends on both the properties of the cation and the donor atoms in the receptor. According to the HSAB principle, the interaction strength is influenced by whether the cation is hard or soft. For instance, Ni^{2+} is considered a borderline acid, meaning it can interact with both hard and soft bases. Therefore, incorporating donor atoms like imidazole, pyridine, and tertiary amines into the receptor unit is essential for designing a selective Ni^{2+} probe (Ragavi et al., 2024; Wang et al., 2022). On the other hand, Pd^{2+}, being a soft acid, displays high affinity with soft bases (such as thiols, thioethers (-SH, RSR'), S-bonded thiocyanates, sulfides, carbanions, phosphines (PR_3), cyanides, etc.) (Balamurugan et al., 2018). Therefore, to maximize the probe's selectivity for Pd^{2+}, the probe's receptor must include donor sites.

Additionally, environmental factors such as solvent choice, pH, and the presence of competing species can significantly impact the probe's performance (Naithani et al., 2024). Even slight changes in pH or solvent composition can alter the sensing ability of the probe, highlighting the importance of considering these parameters when designing highly selective metal ion probes.

1.5.1.3 Turn-on, Turn-off, and ratiometric responses in fluorescence sensors

Fluorescence molecular probes are further classified into three main types based on their response to the presence of an analyte i.e., Turn-on, Turn-off, and sratiometric sensors Scheme 1.3 (Du et al., 2012; Gupta et al., 2016; Park et al., 2020). These probes detect changes in photophysical properties, typically due to electron or charge transfer, which results in a fluorescence signal upon analyte binding.

i. **Turn-on (off-on) molecular probes**: In this type of probe, the fluorescence intensity is enhanced after the analyte binds. This increase in fluorescence intensity, often attributed to charge transfer or chelation-enhanced fluorescence (CHEF), signals the presence of the analyte (Aydin, 2020).

ii. **Turn-off (on-off) molecular probes**: Turn-off probes experience a decrease in fluorescence intensity upon analyte binding. This quenching

effect, known as chelation-enhanced quenching (CHEQ), leads to a reduction in the probe's fluorescence emission, effectively "turning off" the signal in the presence of the analyte (Du et al., 2012).

iii. **Ratiometric probes**: Ratiometric probes provide a more quantitative measure by correlating the concentration of the analyte with the ratio of fluorescence intensities at two distinct wavelengths. This dual-emission approach offers enhanced accuracy and reduces the influence of environmental factors, such as changes in probe's concentration or environmental conditions, making it a reliable method for analyte detection (Wang et al., 2022).

Each type of fluorescence probe has distinct advantages, with Turn-on and Turn-off probes offering simpler, binary responses, while ratiometric sensors provide more precise, quantifiable results by monitoring changes in fluorescence at multiple wavelengths.

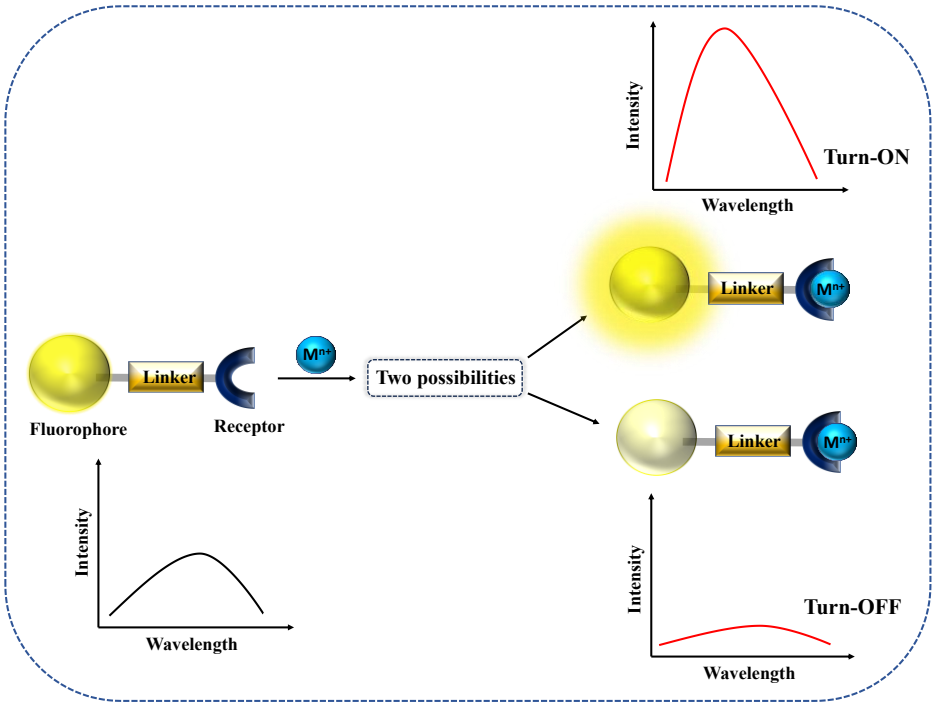

Scheme 1.3. Turn-on and turn-off mechanisms in fluorescent sensors.

1.5.2 Colorimetric sensors

In comparison to the fluorescent sensors, the colorimetric sensors are even more promising among the researchers due to their notable advantages such as simplicity, rapid and on-site detection, as well as negligible capital cost (no need of sophisticated or complex instrumentation) (Liu et al., 2020). Colorimetric sensors allow an obvious naked-eye detection of target analyte based on the color changes produced *via* the interaction between probe and the target ion. The sensing mechanism is related to the observed electronic transitions in the form of inter- or intra-molecular charge transfer (ICT) processes involving either metal-to-ligand-charge-transfer (MLCT) or ligand-to-metal-charge-transfer (LMCT) process (Su et al., 2014).

In general, the colorimetric sensing of metal ions is successfully achieved by using a chemical sensor equipped with D–π–A system which can easily be constructed with the incorporation of e^- donor (i.e., D) and e^- acceptor (i.e., A) units at proper sites in the sensor. The HSAB (hard and soft acids and bases) principle is commonly employed to rationalize the binding of target ions with D or A unit. The metal ion interaction with the donor site (i.e., electron-donating D group) lowers its e^- releasing ability with a virtual conversion of D–π–A system into A–π–A. The reduced π–conjugation of the resultant system ultimately leads to a blue-shift (i.e., hypsochromic shift) in the UV-Vis spectrum of sensor which is usually associated with the LMCT transition (Scheme 1.4) (Naithani et al., 2024).

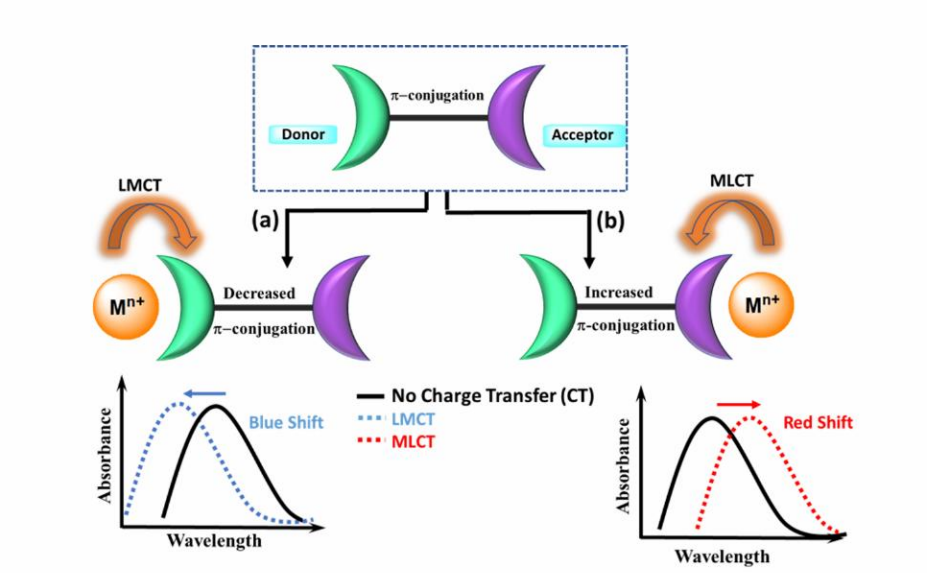

Scheme 1.4. Schematic representation for the binding effect of metal ion on D–π–A system as well as on absorption pattern in colorimetric probes.

On the contrary, metal ion interaction with the acceptor site (i.e., electron withdrawing A group) strengthens the existing D–π–A system (with increased push-pull effect) with a subsequent red-shift (i.e., bathochromic shift) in the absorption spectrum. This red-shift in the absorption spectrum of the probe may be ascribed to the occurrence of MLCT transition. The charge transfer transitions induced by the metal-receptor interaction are directly related to the color changes produced during the colorimetric sensing of metal ions. Concisely, the extended π conjugation leads to the red-shift while the decreased π conjugation leads to the blue-shift in the absorption peak of the probe with respective color changes aiding colorimetric detection of analytes (Chen et al., 2023; Kaur et al., 2018).

1.6. Optical sensors for heavy metal ions

A review of the literature highlights extensive research on detection of various metal ions and anions over the years, driven by the need for sensitive and selective methods to monitor environmental and biological systems (Iftikhar et al., 2023; Li et al., 2022; Wang et al., 2021; Yan et al., 2022). This section emphasizes recent and relevant studies on

the optical detection of metal ions and anions. Particular attention has been given to the detection of aluminum (Al^{3+}), copper (Cu^{2+}), iron (Fe^{2+}/Fe^{3+}), mercury (Hg^{2+}), cyanide (CN^{-}), fluoride (F^{-}), and phosphate (PO_4^{3-}) ions. These ions have garnered significant attention due to their environmental significance, biological roles, and potential toxicity at elevated concentrations (Alam et al., 2021; Chen et al., 2021; Juvekar et al., 2021). Recent advancements in optical sensors have demonstrated high sensitivity and selectivity for these ions, making them valuable tools for environmental monitoring, industrial applications, and health diagnostics (Goswami et al., 2024; Goswami et al., 2024).

1.6.1 Al^{3+} sensors

Kalavathi *et* al. (Kalavathi et al., 2023)synthesized a quinoline-8-ol based Schiff base probe **1**, highly selective for Al^{3+} ions in H_2O: DMSO solution (Fig. 1.1). The sensing behavior of **1** towards different metal ions was examined with the help of fluorescence spectra. The free probe exhibits poor fluorescence at 475 nm when excited at 340 nm; however, in the presence of Al^{3+} ions, the band at 475 nm dramatically enhanced. The binding mechanism was established with the help of Job's plot and DFT analysis, and the binding constant for Al^{3+} was computed as 3.9×10^4 M^{-1} with the help of the Benesi-Hildebrand equation. Job's plot revealed a 1:1 stoichiometry between the probe and Al^{3+} ions. The LoD for Al^{3+} was calculated to be 0.9 μM. This probe could detect Al^{3+} ions in environmental and biological systems. The probe demonstrated efficacy in detecting intracellular Al^{3+} in living HeLa cells. Although the probe exhibited a good LoD however, Fe^{2+} was interfering species in the detection of Al^{3+} ions making its real time application more challenging.

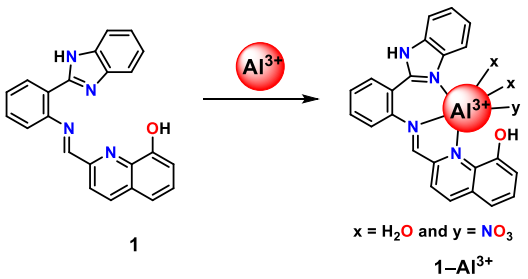

Fig. 1.1. Chemical drawing of probe **1** and its binding mode with Al^{3+} ion in **1**-Al^{3+}.

Samanta *et* al. (Samanta et al., 2023) developed a Schiff base probe **2** by integrating Rhodamine B and quinoline for the detection of Cr^{3+}, HSO_4^-, and Al^{3+} ions in a water-acetonitrile (H_2O-CH_3CN) solution (1:9, *v/v*) (Fig. 1.2). The probe was fully characterized using ^1H NMR, ^{13}C NMR, FT-IR, ESI-MS, and DFT studies. In UV-visible spectroscopic analysis, the probe exhibited distinct absorption bands at 232, 272, 314, and 379 nm. These bands correspond to electronic transitions within the electron-rich aromatic system, specifically π-π* transitions (232, 272, and 314 nm) and an n-π* transition (379 nm). The probe demonstrated excellent selectivity, showing no interaction with other metal ions except for Al^{3+}, Fe^{3+}, Cu^{2+}, and Cr^{3+} ions. Upon binding with Al^{3+} ions, two isosbestic points appeared at 327 nm and 424 nm, accompanied by a visible color change from colorless to orange. However, a similar response was observed for Cr^{3+}, making it challenging to differentiate between Al^{3+} and Cr^{3+} ions using this probe. Fluorescence studies revealed a weak emission band at 567 nm for the free probe. Upon interaction with Al^{3+} ions, a redshifted emission band emerged at 583 nm. The detection limit and binding constant for Al^{3+} were determined to be 2.2×10^{-8} M and 1.79×10^5 M^{-1}, respectively, indicating high sensitivity and strong binding affinity.

To assess the probe's biological applicability, human thyroid cancer cell lines (TPC-1 and HtH-7) were used for cell imaging and cytotoxicity studies. The probe successfully detected Al^{3+} ions within these cells, demonstrating its potential for bioimaging and medical diagnostics.

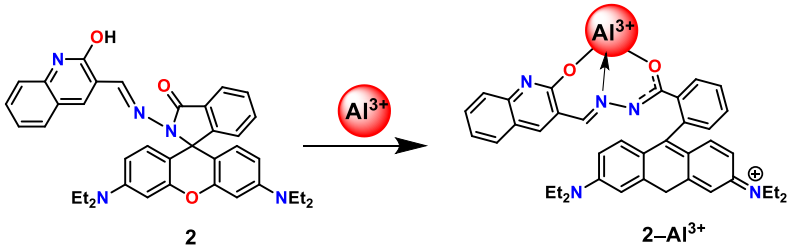

Fig. 1.2. Chemical drawing of probe **2** and its binding mode with Al^{3+} ion in **2**-Al^{3+}.

Huang et al. (Huang et al., 2020) developed a Schiff base probe **3** for the selective detection of Al^{3+} at nanomolar concentrations (Fig. 1.3). UV-visible spectroscopic studies revealed that upon the addition of Al^{3+} ions, the probe

exhibited two distinct absorption bands at 305 nm and 330 nm, which redshifted to 315 nm and 385 nm, respectively. Initially, the probe was non-fluorescent due to the Excited-State Intramolecular Proton Transfer (ESIPT) mechanism involving the phenolic proton. However, in the presence of Al^{3+} ions, the interaction between the deprotonated phenolic group and Al^{3+} inhibited the ESIPT process, leading to a significant fluorescence enhancement with a strong emission band observed at 458 nm. The LoD and binding constant for Al^{3+} were determined to be 8.03×10^{-5} M and 2.78×10^{6} M^{-1}, respectively, indicating high sensitivity and strong binding affinity. The binding mechanism and 1:1 stoichiometry of the interaction has been confirmed using Job's plot, DFT calculations, and Electrospray Ionization Mass Spectrometry (ESI-MS) analyses. Due to its excellent photophysical properties, the probe has shown potential for intracellular imaging of Al^{3+} ions, making it a promising candidate for biological and diagnostic applications.

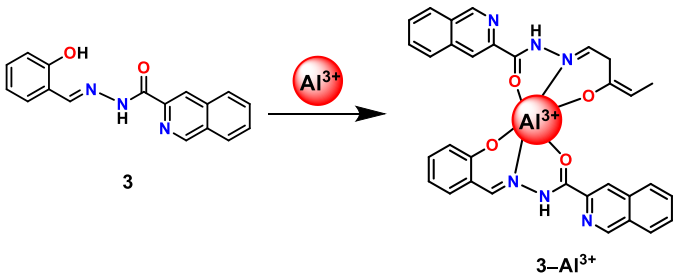

Fig. 1.3. Chemical drawing of probe **3** and its binding mode with Al^{3+} ion in **3**-Al^{3+}.

Fu et al. (Fu et al., 2019) synthesized a quinoline-based Schiff base probe **4** designed as a dual-mode sensor for the colorimetric and fluorescent detection of Al^{3+} and F^{-} ions in a methanol-water (CH_3OH-H_2O) solution (Fig. 1.4). UV-visible studies showed that upon interaction with Al^{3+} ions, the probe's absorption bands at 453 nm and 478 nm underwent a blueshift to 440 nm and 460 nm, respectively, with an isosbestic point observed at 425 nm. In fluorescence studies, excitation at 460 nm revealed a weak emission at 525 nm for the free probe **4**. However, the addition of Al^{3+} ions led to a significant fluorescence enhancement, making the probe highly sensitive for Al^{3+} detection. The limit of detection (LoD) and association constant for Al^{3+} ions were determined to be 0.10 µM and 1.20×10^{2} M^{-2}, respectively, highlighting its high

sensitivity and moderate binding affinity. The probe **4** was further evaluated for biological applications and successfully detected Al^{3+} ions in living PC12 cells. Although it exhibited moderate cytotoxicity, its capability for intracellular imaging suggests its potential for bioimaging and analytical applications.

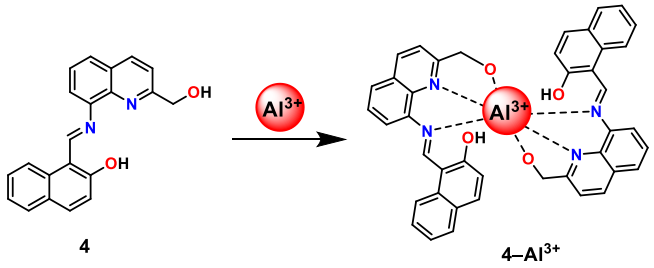

Fig. 1.4. Chemical drawing of probe **4** and its binding mode with Al^{3+} ion in **4**-Al^{3+}.

Naithani et al. (Naithani et al., 2023) developed a naphthalene-based Schiff base probe **5** for the selective detection of Al^{3+} ions in an aqueous acetonitrile solution (Fig. 1.5). The probe was thoroughly characterized using single-crystal X-ray diffraction, ^{1}H NMR, ^{13}C NMR, and ESI-MS analysis. In UV-visible spectroscopy, the probe **5** exhibited two absorption bands at 241 nm and 249 nm. Upon interaction with Al^{3+} ions, three new absorption bands emerged at 248 nm, 265 nm, and 311 nm, accompanied by four isosbestic points at 215 nm, 255 nm, 273 nm, and 291 nm, indicating the formation of a stable complex. Fluorescence studies revealed that the free probe **5** exhibited weak fluorescence due to >C=N– isomerization. However, the addition of Al^{3+} ions resulted in a significant fluorescence enhancement, making it highly sensitive for Al^{3+} detection. The binding constant for Al^{3+} was calculated to be 1.18×10^{6} M^{-1} using the Benesi-Hildebrand equation, with a limit of detection (LoD) of 38.0 nM. The 1:1 binding stoichiometry between the probe and Al^{3+} was confirmed using Job's plot, ESI-MS, and ^{1}H NMR analysis.

Practical applications of this probe were demonstrated through fluorescence detection using filter paper test strips and in real sample analysis, including tap water, distilled water, and soil samples. This versatility highlights its potential for environmental monitoring and analytical applications.

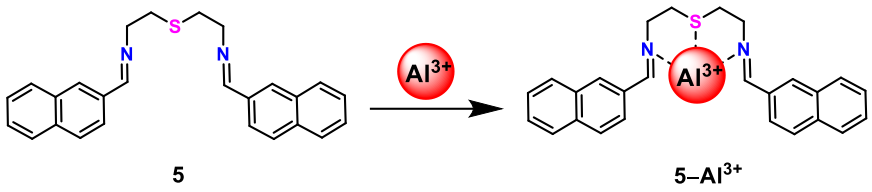

Fig. 1.5. Chemical drawing of probe **5** and its binding mode with Al^{3+} ion in **5**-Al^{3+}.

1.6.2 Ni^{2+} sensors

Ghazali et al. (Ghazali et al., 2019) developed an intramolecular PeT based 'turn-on' fluorescent probe **6** utilizing a diacetyl monoxime moiety for sensing of Ni(II) ions (Fig. 1.6). The probe consisted of 1,8-naphthalimide moiety as fluorophore due to its promising electron-accepting features. Mitochondria-accessing non-fluorescent probe **6** became fluorescent upon introduction of Ni(II) ions. It was reported that the enhancement in the fluorescence intensity was directly proportional (with a linear relation, R^2 = 0.9758) to the concentration of Ni(II) at 497 nm. The results showed a maximum of 160-fold enhancement in the fluorescence intensity (compared to other competing cations), and the LoD for Ni(II) was computed as 21.6 nM. The emission quantum yield of **6** (Φ_{em} = 0.012) was found to be increased upon complexation (Φ_{em} = 0.61) due to photoinduced intramolecular electron transfer. The probe could also effectively detect Ni(II) over a wide pH range of 5.0–12.0. Successful live cell imaging of oral carcinoma KB cells and HeLa cells was also investigated in this study. The addition of 1.0 mM $NiCl_2$ in cells incubated with probe **6** resulted in noticeable enhancement in the emission intensity. Probe **6** has also been used to determine Ni(II) levels in the mitochondria of living cell.

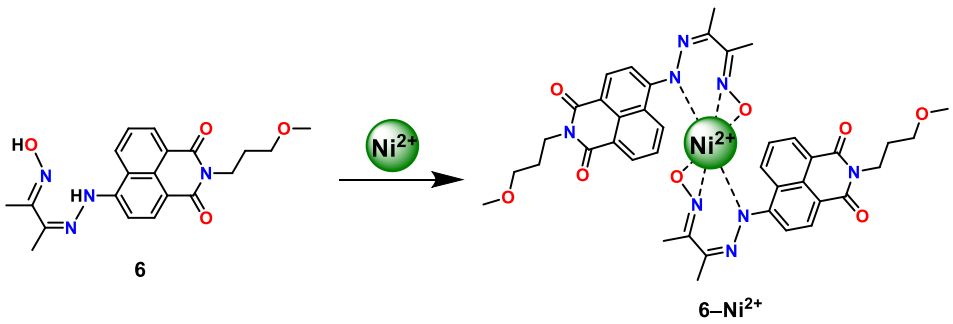

Fig. 1.6. Chemical drawing of probe **6** and its binding mode with Ni^{2+} ion in **6**-Ni^{2+}.

Manna et al. (Manna et al., 2019) synthesized a N′-(2-hydroxybenzylidene)-2-(benzamido)benzohydrazide-derived Schiff base as colorimetric probe **7** to detect Ni(II) in a methanol–Tris buffer (Fig. 1.7). UV–visible analysis of probe **7** clearly showed its absorption maximum centred at 310 nm most likely due to the S0 → S1 transition. The metal ion sensing ability of **7** was investigated using 2.0 equiv. of assorted metal ions such as Fe (III), Ni(II), Ag(I), Zn(II), Cu(II), Co(II), Cd(II), Hg(II), Cr(III), Al(III), Fe(II), and Mn(II). Amongst them, only Ni(II) ion could produce a redshift in the absorption band from 310 nm to 375 nm with an isosbestic point near 353 nm. The colorless solution of the probe also turned yellow in the presence of Ni(II) due to the formation of **7**-Ni(II) complex. Besides this, the addition of Cu (II) resulted in a pale yellow-colored solution; however, the spectroscopic changes were nominal. The LoD value for Ni(II) was calculated to be 1.8 μM. A Benesi–Hildebrand (B–H) linear fitting plot was used to calculate the association constant toward Ni(II) and the resultant value was 1.45×10^3 $M^{-1/2}$ with a 2 : 1 binding stoichiometry. The spectroscopic changes and the colorimetric changes were reversed upon addition of EDTA. The probe exhibited a weak emission at 450 nm because of >C=N– isomerization and photoinduced electron transfer processes. The addition of Ni(II) ions resulted in fluorescence enhancement along with a slight redshift of the emission band from 450 nm to 465 nm. This enhancement effect has been ascribed to a CHEF effect. A pH effect study indicated that the H^+ ions compete with metal binding in high acidic conditions (below pH 4.0). Moreover, the >C=N– functionality was also found susceptible to cleavage under highly acidic conditions. Probe **7** could successfully be utilized for the detection of Ni(II) in environmental materials, imaging of living cells, and the construction of logic gates of the INHIBIT type.

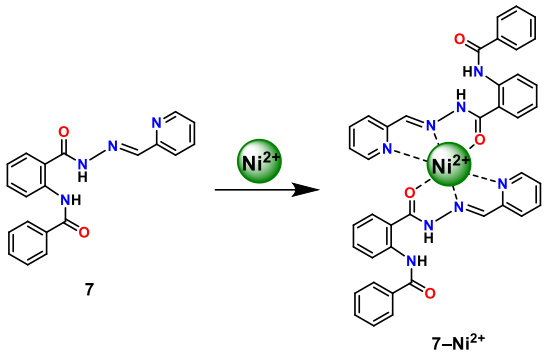

Fig. 1.7. Chemical drawing of probe **7** and its binding mode with Ni^{2+} ion in **7**-Ni^{2+}.

A Schiff base-derived colorimetric probe **8** was developed by Sahu et al. (Sahu et al., 2020) for selective and rapid recognition of Ni(II) in methanol–Tris-HCl buffer (1 : 1 *v/v*, 10.0 mM, pH = 7.2) (Fig. 1.8). Probe **8** displayed three absorption maxima near 295 nm, 330 nm and 358 nm which could be attributed to the probe-centered π → π* and n → π* transitions. However upon Ni(II) addition, a red-shifted absorption was observed at 408 nm, together with a distinct color change from colorless to yellow. Besides, the well-defined isosbestic point near 373 nm clearly indicated the existence of dynamic equilibrium between the free probe and **8**-Ni(II) adduct. Upon excitation at 390 nm, **8** showed an intense emission band near 460 nm which has been attributed to its structural rigidity. The introduction of 2.0 equiv. of Ni(II) produced a significant fluorescence quenching behavior. It was anticipated that this quenching occurred due to the presence of a photoinduced electron/energy transfer process. The detection limit and the binding constant values of **8** for Ni(II) have been computed as 7.4×10^{-7} M and 1.7×10^{4} M^{-1} , respectively. Job's plot analyses indicated a 1 : 1 binding for Ni(II) ions based on the maximum absorption intensity at 0.5 mole fraction of probe **8**. The interaction of **8** with Ni(II) and the formation of complex **8**-Ni(II) were validated with the help of DFT (density functional theory) and TD-DFT (time-dependent DFT) studies.

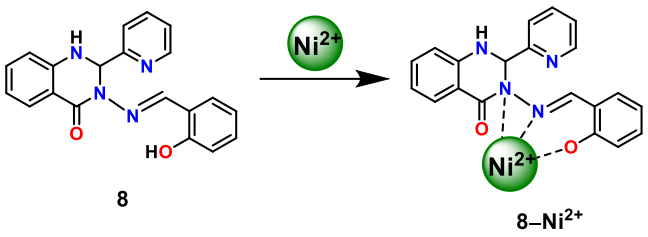

Fig. 1.8. Chemical drawing of probe **8** and its binding mode with Ni^{2+} ion in **8**-Ni^{2+}.

Liu et al. (Liu et al., 2018) synthesized probe **9** based on acylhydrazone scaffold to detect Ni(II) ions in DMF solution (Fig. 1.9). Probe **9** showed two absorption peaks centered at 266 nm and 413 nm. Upon addition of Ni(II), the absorption intensity of the above bands showed a drastic quenching behavior. When excited at 300 nm, **9** showed an emission peak at 503 nm, and the intensity of this peak was found to be lower in ethanol and water as compared to DMF and DMSO. The difference in peak intensity could be attributed to the lower deprotonation tendency of the probe in protic solvents. Addition of Ni(II) resulted in a decrease in the fluorescence intensity with the most decrease in DMF solution. However, an enhancement in the fluorescence intensity could be noticed with the increase in pH of the medium. A 2 : 1 binding stoichiometry between the probe and Ni(II) was determined using Job's plot analysis, and the LoD value was calculated to be 60.0 nM in this study. Mechanistic investigation showed the formation of bis-complex **9**-Ni(II) upon coordination of Ni(II) with **9**. DFT studies further revealed that Ni(II) binding resulted in the lowering of the energy gap making the electronic transition more feasible.

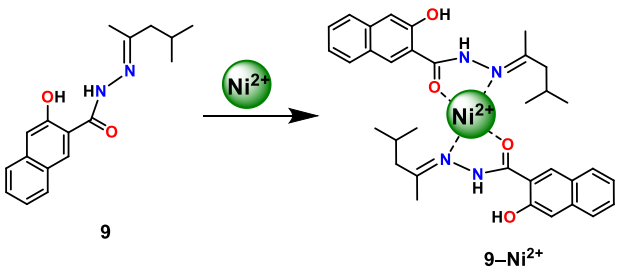

Fig. 1.9. Chemical drawing of probe **9** and its binding mode with Ni^{2+} ion in **9**-Ni^{2+}.

Kumar and co-workers (Kumar et al., 2022) presented two rationally designed fluorescent probes **10** and **11** based on naphthalimide derivatives (Fig.

1.10). These probes displayed a 'turn-on' emissive response for both Ni(II) and Zn(II) ions. Ni(II) binding with **10** and **11** resulted in prominent changes in their emission as well as absorption spectra. Comparable binding profiles, LoD and binding constant values clearly illustrated a notable sensing ability of both **10** and **11** for Ni(II) ions. Job's plot analysis along with HR-MS (high-resolution mass spectroscopy) and NMR titrations of probes with Ni(II) and Zn(II) ions suggested a 1 : 1 binding stoichiometry which was also corroborated by DFT analyses. For practical applications in real samples, the sensing ability of probes was also exploited using paper strips and polystyrene films including colorimetric sensing in aqueous solution.

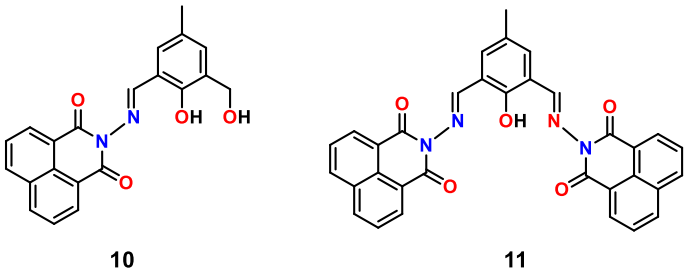

Fig. 1.10. Chemical drawing of probes **10** and **11**.

1.6.3 Pd^{2+} sensors

Feng et al. (Feng et al., 2018) synthesized a FRET-based probe **12** having a phthalimide-rhodol scaffold (Fig. 1.11). The 3-amino phthalimide unit acts as an energy donor and a rhodamine-fluorescein hybrid acts as the energy acceptor which are linked by rigid piperazine. Probe **12** exhibited both ESIPT and FRET processes. The probe was initially colorless and exhibited blue fluorescence under UV light illumination (λ_{max} = 365 nm). The probe exhibited a weak absorption; however, after the addition of 20 µM of $Pd(PPh_3)_4$, the peak intensity at 500 nm dramatically increased. Similarly, in the fluorescence study, the emission band at 490 nm diminished upon Pd(0) addition and a new emission band emerged at 547 nm along with a clear iso-emissive point at 520 nm. Under UV light illumination, the solution color turned yellow-green from blue. These results were found in agreement with mass spectrometry. These spectral changes were attributed to the Tsuji-Trost reaction induced by Pd(0) cleaving the allyl carbonate moiety where the final product **12** promoted the

FRET process. As a result, the rhodol unit exhibited ESIPT-based emission of phthalimide. The fluorescence quantum yield of the product was 0.81, i.e., higher than that of the original probe without guest analyte (*ca.* 0.11). Probe **12** was stable over a wide range of pH from 2.0 to 10.0; however, the best response was observed at pH 7.0–9.0. The LoD value was determined to be 31.0 nM. The probe was highly selective for Pd(0), and no other cations, anions, biothiols and protein could exhibit a change similar to that of palladium. This probe showed almost no direct response for Pd(II) and Pd(IV) ions. The detection of these ions was achieved by in situ generation of Pd(0) using an appropriate reducing agent such as PPh_3. The probe was also applied in live cell imaging of Pd(0), Pd(II) and Pd(IV) ions (in the presence of PPh_3) and exhibited very low cytotoxicity even at 50 μM concentration.

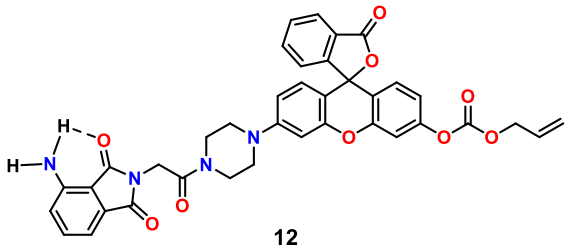

Fig. 1.11. Chemical drawing of probe **12.**

Feng's group (Kuhana et al., 2018) developed probe **13** with an allyl carbonate moiety as the reaction site and a commercially available semi-naphthorhodafluor (SNARF) dye as the fluorophore (Fig. 1.12). The probe exhibited a weak absorption band and negligible fluorescence in PBS buffer. However, the addition of $Pd(PPh_3)_4$ led to the appearance of a new absorption band at 558 nm which was also accompanied by a color change from colorless to pink. Meanwhile, an intense peak was observed in the emission spectrum of **13** at 636 nm after the addition of $Pd(PPh_3)_4$. The probe further employed Tsuji–Trost reaction mediated by Pd(0) restoring the fluorophore which is responsible for the changes in UV–visible and emission spectra. Probe **13** was also investigated against Ca(II), Mg(II), Zn(II), Cu (II), Ni(II), Ag(I), Ce(III), Co(II), Cd(II), Al(III), Fe(II), Sr(II), Mn(II), Li (I), K(I), Na(I), Hg(II) and Ba(II); however, these metal ions were unable to produce any drastic changes in the

spectra. Furthermore, this probe was able to detect Pd(II) and Pd(IV) in the presence of PPh_3 which acts as a reducing agent by generating Pd(0) in situ. The LoD value was as low as 1.6 nM and this probe was capable of detecting palladium species in the range of pH 6.0–9.0. The potential applications of **13** have also been explored in live-cell Pd imaging.

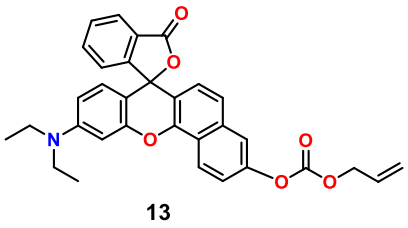

13

Fig. 1.12. Chemical drawing of probe **13.**

Zhao, Dong and coworkers (Zhou et al., 2019) synthesized two BODIPY-based probes **14a** and **14b** for palladium detection in aqueous solution (Fig. 1.13). These probes used propargyl carboxylate groups as palladium binding site. In DMSO solutions, both the probes displayed weak fluorescence and a low emission quantum yield (Φ_{em} < 0.01). However, in water, the fluorescence intensity of **14a** and **14b** was significantly enhanced, ascribed to J-aggregation (λ_{ex} = 480 nm). The fluorescence intensity of **14a** was slightly higher than that of **14b**. UV– visible spectra displayed absorption maxima for **14a** and **14b** at 516 and 587 nm, respectively, in PBS buffer (pH 7.4, 1% DMSO) solution. Interestingly, the addition of $Pd(PPh_3)_4$ to **14** induced a blue-shift in the absorption maxima to 495 nm. This probe was excited at 480 nm to give bright orange fluorescence at 591 nm. The addition of $Pd(PPh_3)_4$ to **14a** resulted in significant enhancement of the emission band where saturation was reached within 6.0 minutes. In the presence of Pd salt, the emission band of **14a** also exhibited a hypsochromic shift, and a new band could be seen at 513 nm. Furthermore, the initial pink color of **14a** turned to colorless in the presence of Pd(0). Similarly, probe **14b** could detect Pd(0); however, the fluorescence enhancement was comparatively less than that of **14a**, indicating weaker AIE in this case. Metal ions such as Fe(III), Ag(I), Cu(II), Hg (II), Co(II), Mg(II), Ca(II), Ni(II), Zn(II), Na(I), Mn(II), Li(I), Na(I), K(I), Pb(II), Al(III), Au(III) and Ba(II) did not interfere in the sensing process and failed to produce any

remarkable spectral changes in **14a** and **14b**. Both probes were found capable of detecting other palladium species such as Pd(II) and Pd(IV) but only in the presence of a reductant such as $NaBH_4$. The LoD for **14a** was 7.4 nM whereas for **14b** it was 20.3 nM. The probe functioned well in the pH range of 6.0–9.0. HeLa cells were incubated with 20 μM of **14a** and exhibited strong red fluorescence. The red fluorescence turned to green in the presence of Pd(0) suggesting the suitability of the probe for Pd imaging in live cells.

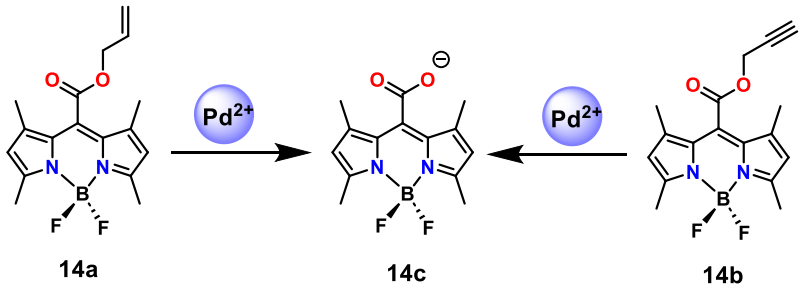

Fig. 1.13. Chemical drawing of probes **14a** and **14b** and their binding modes with Pd^{2+} ion in **14c**.

Soares-Paulino et al. (Soares-Paulino et al., 2020) constructed probe **15** based on selenide and rhodamine scaffolds (Fig. 1.14). UV-visible study of **15** in EtOH-H_2O (1 : 1, *v/v*) solution displayed two absorption bands at 272 nm and 315 nm, attributed to the $\pi \rightarrow \pi^*$ transitions. With a low emission quantum yield ($\Phi_{em} < 0.01$), a weak fluorescence band could be noticed at 451 nm for this probe. The addition of Pd(II) caused remarkable changes in the fluorescence and UV-visible spectra of **15**. The reason behind the resultant spectral changes was the opening of the spirolactam ring, as evidenced by the appearance of a characteristic band at 565 nm. Moreover, Pd(II) addition induced a new intense emission at 558 nm with higher emission quantum yield ($\Phi_{em} = 0.17$) as compared to the original probe. Meanwhile, the color of probe solution also turned intense pink from colorless. Job's plot analyses confirmed a 1:1 stoichiometry for **15**-Pd(II) which was in full agreement with the ESI-MS data. Interestingly, the cation sensing behavior of **15** was found reversible as the addition of EDTA quenched the fluorescence intensity. Studies of pH effect clearly indicated that the Pd imaging can be screened in pH range 6.0 to 10.0.

The sensing ability of **15** was also explored for Pd(0) that produced negligible changes in the spectra. The binding constant (log K = 6.1) and LoD (32.0 nM) values clearly suggested the high affinity and selectivity of **15** for Pd(II) ions.

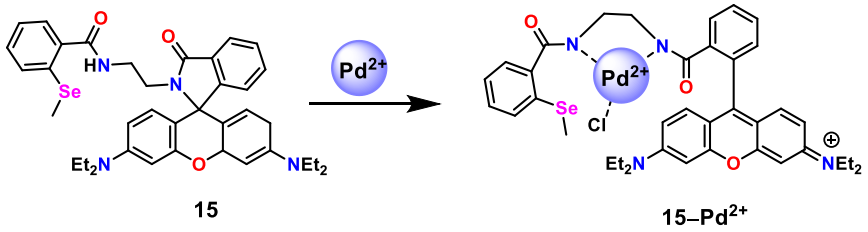

Fig. 1.14. Chemical drawing of probe **15** and its binding mode with Pd^{2+} ion in **15**-Pd^{2+}.

Murale et al. (Murale et al., 2021) synthesized another BODIPY-based probe **16** with pyridinyl pyrazole moiety (Fig. 1.15). This probe exhibited a narrow Stokes shift with an absorption maximum at 510 nm and emission maximum at 523 nm in PBS buffer with 1% DMSO solution. Probe **16** was non-fluorescent in water but displayed high quantum yield in ethanol (i.e., 40.2%). In PBS buffer, the emission quantum yield was 5.53% which decreased further upon addition of 100 µM of Pd (II) ions. Other studied cations such as Ca(II), Cu(II), Cd(II), Cu (I), Fe(II), Hg(II), Fe(III), Sn(II), Mg(II), Sn(II), and Zn(II) led to minor or no changes in the spectra of **16**, and failed to interfere with the selective detection ability of **16** for Pd(II) ions. The response time of the probe for Pd(II) was nearly 30 min with the respective LoD and binding constant values of 1.0 µM and 4.89×10^{-6} M^{-1}, respectively. The probe displayed a 1:1 binding stoichiometry between Pd(II) and **16** as evidenced by HR-MS and Job's plot analyses. HeLa cells incubated with 10 µM of probe were used for live-cell Pd imaging. In the presence of Pd(II), the fluorescence in the cells was significantly reduced. As per the cytotoxicity results, probe **16** was found to be non-toxic and showed remarkable biocompatibility under physiological conditions.

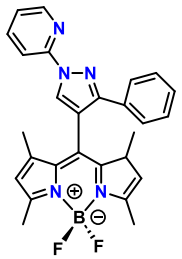

16

Fig. 1.15. Chemical drawing of probe **16**.

1.6.4 Pt^{2+} sensors

Kim et al. (Kim et al., 2010) synthesized a rhodamine-based probe **17** for fluorescent detection of Pt(II) in aqueous medium (Fig. 1.16). A click reaction was carried out to convert the propargyl-tethered rhodamine 6G hydroxamate into the corresponding triazole moiety. Rhodamine hydroxamate containing the triazole moiety offered the target metal ions a structured platform for coordination. Probe **17** exhibited almost no color or fluorescence in water (DMSO 1%, *v/v*), attributed to it predominantly existing in spirocyclic form. Upon addition of Pt(II) to probe **17**, the color changed from colorless to pink-red, and the probe displayed intense fluorescence at 562 nm. As per Job's plot analysis, probe **17** displayed a 1 : 1 binding with Pt(II) and afforded **17**-Pt(II). The binding constant (log K = 5.2 ± 0.7) estimated in aqueous (DMSO 1%, *v/v*) solution using fluorescence titration demonstrated a significant binding ability of probe **17** with Pt(II). This fluorescent probe has also been utilized to monitor the cisplatin concentrations in aqueous solutions. The authors reported a negligible fluorescence intensity change for other ions such as Pd(II), Mn(II), Cr(II), Hg(II), Fe(III) and Rh(II) when performing a comparative study.

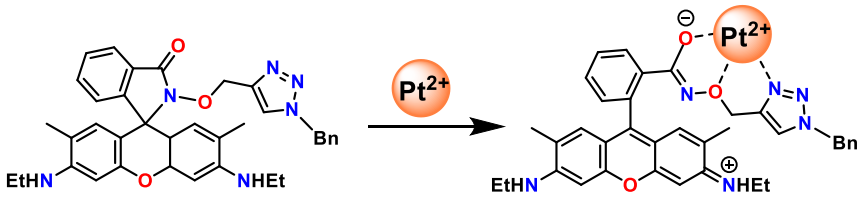

17 **17–Pt^{2+}**

Fig. 1.16. Chemical drawing of probe **17** and its binding mode with Pt^{2+} ion in **17**-Pt^{2+}.

Zhou et al. (Zhou et al., 2012) synthesized a series of organic probes **18a-18d** based on salen-type Schiff bases (Fig. 1.17). The probes exhibited quenching of fluorescence due to complexation with Pt(II). The absorption bands for probes **18a-18d** were observed between 315 and 331 nm corresponding to the $\pi \rightarrow \pi^*$ transition between the benzene ring and >C=N moiety. In addition, lower intensity bands were observed in the range 380-420 nm which were attributed to $n \rightarrow \pi^*$ transition. The probes exhibited strong fluorescence caused by ILCT ($\pi \rightarrow \pi^*$) with a quantum yield of 0.057 for **18a**, 0.097 for **18b**, 0.19 for **18c**, and 0.56 for **18d** in DMF solution. The emission for probes **18a–18d** was measured at 420, 428, 497 and 457 nm, respectively. Amongst them, probe **18c** displayed the best Pt(II)- responsive behavior. The colorimetric response of **18c** was investigated against other cations such as Pt(II), Sr(II), Pb(II), Sn (II), Cr(III), Al(III), Mn(II), Ce(III), Fe(III), Li(I), Ag(I), Na(I), Mg(II), Cu(II), Cd(II), Zn(II), Ca(II), K(I), Zn(II), Ni(II), Co(II), Au(III), Ir(III) and Pd(II) by incubating the probe solution and metal ion at 70 °C for 3 hours. An obvious color change from yellow to red was observed (visible to the naked eye) in the case of Pt(II) ions while other metal ions did not produce considerable changes. UV-visible studies revealed the appearance of new bands at 450 nm and 525 nm upon addition of Pt(II) ions. Complex **18c** exhibited a red phosphorescence and the yellow-green fluorescence was found to decrease after addition of 1–2 equiv. of Pt(II). The red phosphorescence was more pronounced in the case of degassed DMF as oxygen could quench it. The stoichiometry of the probe was 1:1 as evidenced by Job's plot data. The lowest LoD value was reported as 2.31 ppb when the solution was degassed. Moreover, fluorescence quenching could be observed at 497 nm in the case of Pd(II), Ni(II) and Cu (II), and enhancement in the case of Sr(II), Cd(II) and Mg(II); however, the band at 608 nm was unique in the case of Pt(II). Even in the presence of other cations, the red fluorescence was not affected. The probe was also able to detect K_2PtCl_4, cisplatin and Pt(1,5-cyclooctadiene)Cl_2 but the reaction and the subsequent fluorescence enhancement were directly linked to the presence of bulky group, and therefore, cisplatin had much slower response. Interestingly, a sulphonate group assisted in the water solubility of probe **18d** and it was tested

against Pt(II) in aqueous solution. A red phosphorescence enhancement was seen at 585 nm; however, the detection limit was 180 ppb.

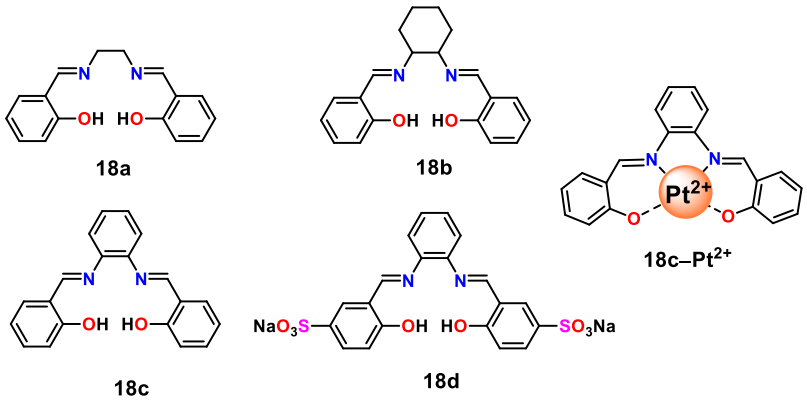

Fig. 1.17. Chemical drawing of probes **18a-18d** and representative binding modes with Pt^{2+} ion in **18c**-Pt^{2+}.

Tang et al. (Tang et al., 2020) designed a BODIPY-based probe **19** to mimic methionine for the recognition of Pt(II) and Pt-based drugs in water (Fig. 1.18). The water solubility of this probe was improved by terminal carboxylate groups, and the thioether moiety acted as the binding unit for the platinum species. UV–visible spectra showed no significant changes when Pt(II) was introduced to the probe solution in DMF/HEPES (3 : 7, *v/v*) solution; however, a strong emission band was noticed at 520 nm with an incubation time of 6 hours. Sensing and interference experiments were also performed in water with cations including Na(I), Li(I), K(I), Ca(II), Mg(II), Cr(III), Al(III), Fe(III), Mn (II), Fe(II), Ni(II), Co(II), Zn(II), Cu(II), Pd(II), Cd(II), Ag(I), Hg(II), Pb(II) and Au(III), with none of them interfering in the sensing experiment except Ag(I) that exhibited a slight 'turn-on' response. Probe **19** could also identify K_2PtCl_4 and $PtCl_2$ in aqueous media, but the intensity of the band was much lower because of the low solubility of the target species. Nedaplatin and cisplatin have also been successfully detected with 14-fold and 22-fold enhancement in the emission band, respectively. Notably, this probe was unable to detect carboplatin, oxaliplatin, and Pt(IV) complex. Furthermore, probe **19** was capable of detecting Pt(II) ions in the range of pH 5.0–10. The binding ratio of 1 : 1 was confirmed by Job's plot analysis and mass spectrophotometry as well

as NMR analyses. This probe was initially non-fluorescent most likely due to the PeT effect. Pt(II) binding with **19** inhibited the PeT event, and consequently, a remarkable fluorescence enhancement could be observed due to the formation of **19**-Pt(II). For cellular imaging experiments, the cell viability of **19** was tested against A-549 cells which was markedly high even at 20 μM concentration. The cells incubated with **19** were weakly fluorescent; however, in the presence of Pt species such as cisplatin, nedaplatin, and K_2PtCl_4, the cells displayed strong green fluorescence when excited at 488 nm.

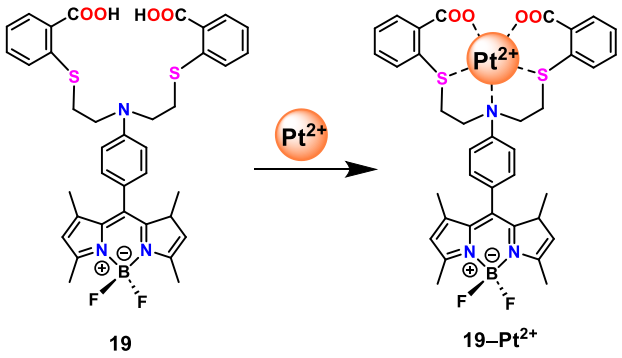

Fig. 1.18. Chemical drawing of probe **19** and its binding mode with Pt^{2+} ion in **19**-Ni^{2+}.

1.6.5 Hg^{2+} sensors

Bera *et* al. (Bera et al., 2014) synthesized a rhodamine B-based probe **20** to detect Hg^{2+} through cyclization and spirolactam ring opening mechanism (Fig. 1.19). The CAN bond breaking provides the probe **20** the ability of a turn-on sensor by restoring the repressed rhodamine's intense fluorescence. Rapid response in fluorescence and color could result from the irreversible reaction caused by the introduction of 3-amino rhodamine, which effectively increases the affinity for Hg^{2+}. Additionally, it can be utilized to identify the biomolecules and nanoparticles in various cells, including vertebrates, primary and differentiated cells, and mammalian cells, to monitor Hg^{2+}. Specifically, it can readily use basic fluorescence confocal imaging technology to obtain the high-resolution real-time distribution map of Hg^{2+} deposits in the zebrafish brain.

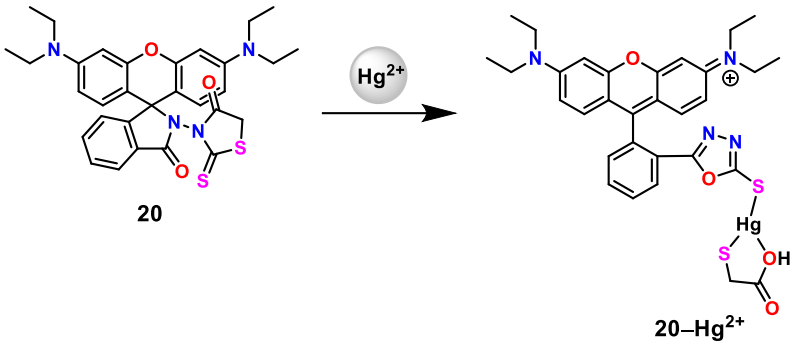

Fig. 1.19. Chemical drawing of probe **20** and its binding mode with Hg^{2+} ion in **20**-Hg^{2+}.

Atta *et* al. (Atta et al., 2013) developed an acetylene-based fluorescent molecular probe **21**, which was synthesized by coupling it with ethynyl phenol and malononitrile derivative (Fig. 1.20). Furthermore, this is the first report of an efficient synthesis of a Hg^{2+} probe **21** via the intramolecular cyclization reaction of ethynyl phenols at room temperature in a semi-aqueous medium. When the reaction conditions were optimized, the sensitive indicator probe was used for fast reaction Hg^{2+} detection. The probe **21** showed a noticeable color shift from blue to pale yellow in the DMSO/H_2O solution when Hg^{2+} was present. The LoD for Hg^{2+} was calculated to be 0.13 μM.

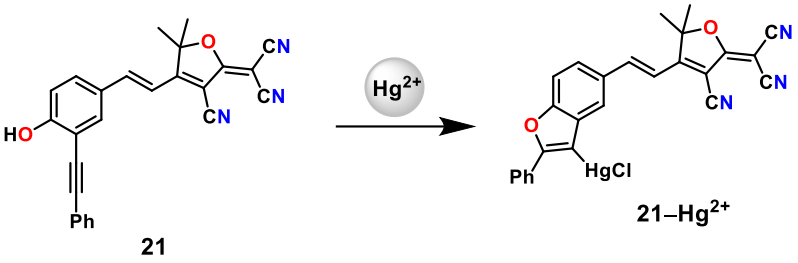

Fig. 1.20. Chemical drawing of probe **21** and its binding mode with Hg^{2+} ion in **21**-Hg^{2+}.

1.6.6 Zn^{2+} sensors

Kumar *et* al. (Kumar et al., 2020) developed a fluorescent probe **22** containing quinoline as a fluorophore for detecting Zn^{2+} ions in aqueous acetonitrile solution (Fig. 1.21). When the probe was excited at 310 nm, the probe displayed turn-on fluorescence at 496 nm in the presence of Zn^{2+} ions. The probe **22** is non-fluorescent due to PeT-induced quenching of the lone pair of electrons on nitrogen in the quinoline ring system and an excited state

intramolecular proton transfer (ESIPT) reaction linked to the amide's keto-enol tautomerism. All three nitrogen atoms align with the metal ion upon interaction with Zn^{2+}, blocking PeT and ESIPT. Furthermore, CHEF rises also. The fluorescence turns off when the compound **22**–Zn^{2+} reacts with H_2PO_4.

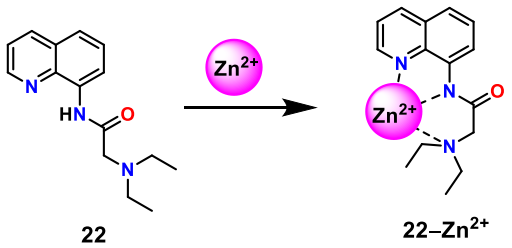

Fig. 1.21. Chemical drawing of probe **22** and its binding mode with Zn^{2+} ion in **22**-Zn^{2+}.

Wu *et* al. (Wu et al., 2018) synthesized a fluorescent molecular probe **23** containing a coumarin and quinoline ring system for detecting Zn^{2+} ions in an acetonitrile solution (Fig. 1.22). In this probe **23**, the triazole and quinoline groups bind to Zn^{2+} ligands and electron acceptors, while the coumarin groups act as an electron-rich fluorophore. When **23** was excited at 380 nm, only the probe **23** displayed bright green fluorescence in the buffer solution. Due to the increase of ICT from the coumarin moiety to the quinoline and triazole groups, the fluorescence of this probe changed from green to yellow in the presence of Zn^{2+} ions. On the other hand, **23** displayed no change with other metal ions. The LoD of this probe **23** was determined to be 48.1 nM. Using a probe **23**, Zn^{2+} ions were identified in real samples, including drinking, pond, and river water. The probe has been used to fluorescence image Zn^{2+} ions in living MCF-7 cells because of its high cell membrane permeability and low biotoxicity.

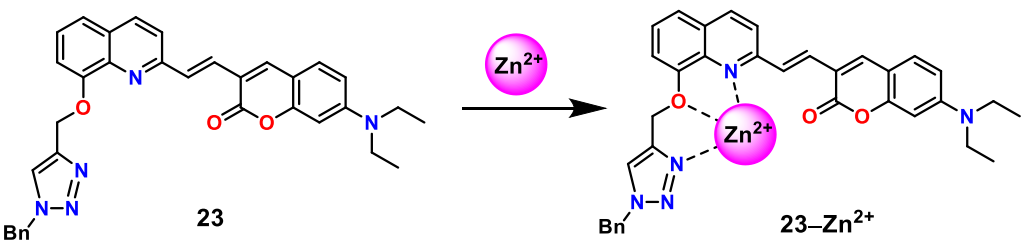

Fig. 1.22. Chemical drawing of probe **23** and its binding mode with Zn^{2+} ion in **23**-Zn^{2+}.

A coumarin-based probe **24** was synthesized by Bhattacharyya *et* al. (Bhattacharyya et al., 2019). This probe **24** detects Zn^{2+} ions in a methanol solution (Fig. 1.23). Only the probe **24** showed an emission band at 506 nm, but in the presence of Zn^{2+} ions, **24** displayed an emission band at 535 nm, and the color of this probe changed from green to yellow under UV light. However, the probe **24** has a ketoimine moiety as an acceptor and a diethylamino group as a donor. It participates in charge transfer electronically, and the ICT process is partially quenched by electron donation from the thiosemicarbazone linkage corresponding to the imine moiety. On the other hand, charge transfer from the diethylamino moiety to the ketoimine moiety is facilitated by the imine, thiosemicarbazone, and coumarin's interaction with Zn^{2+} ions. As a result, when the ICT process became more efficient, the probe's emission maximum shifted following complexation with Zn^{2+} ions.

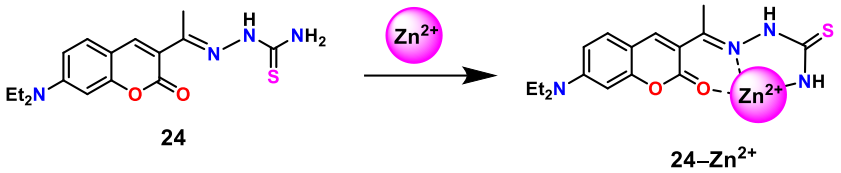

Fig. 1.23. Chemical drawing of probe **24** and its binding mode with Zn^{2+} ion in **24**-Zn^{2+}.

Pradhan et al. (Pradhan et al., 2015) developed a quinoline-based molecular probe **25** to detect Zn^{2+} ions (Fig. 1.24). When the probe was excited at 461 nm, **25** showed an emission band at 576 nm. The intensity of the absorption band of the probe **25** at 339 nm decreased with increasing Zn^{2+} concentration, whereas a new absorption band at 461 nm was noticed. It undergoes a redshift in fluorescence to 594 nm accompanied by a significant rise in emission intensity when complexed with Zn^{2+} ions. The LoD of this probe **25** was calculated to be 1.3×10^{-7} M. Job's plot revealed a 2:1 stoichiometry between the probe and Zn^{2+} ions.

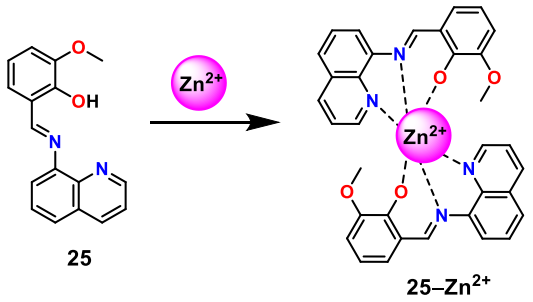

Fig. 1.24. Chemical drawing of probe **25** and its binding mode with Zn^{2+} ion in **25**-Zn^{2+}.

1.7. Optical sensors for anions

1.7.1 CN^- sensors

Nandhini *et* al. (Nandhini et al., 2021) developed an imine-based fluorescent molecular probe **26** to detect CN^- ions in solid and solution states (Fig. 1.25). The free probe **26** showed absorption bands at 361 and 412 nm and a broad band at 610 nm in the DMSO medium, which have been caused by significant intramolecular charge transfer (ICT) transitions. Upon the addition of CN^- ions to **26**, the absorbance band at 412 nm continuously decreased, and another absorbance band at 610 nm increased. This was accompanied by change in probe **26**'s color from pale yellow to intense blue color in the DMSO medium. When treated with CN^- ions in 30% DMSO solutions, the absorption peak of the probe at 412 nm decreased, and a new absorption band appeared at 540 nm. The solvatochromism noticed in these two media confirmed the nature of these transitions as ICT transitions. In the fluorescence study, the probe was excited at 415 nm in a 30% aqueous DMSO solution and displayed a poor broad band at 595 nm. The probe **26** showed an emission band at 640 nm on adding CN^- ions. The probe displayed an emission band at 658 nm in the presence of cyanide ions in pure DMSO. The limit of detection of the probe for CN^- ions is calculated to be 0.5 μM. The binding constant for the interaction of CN^- ions with the probe was determined at 2.23×10^5 M^{-1} using the Benesi-Hildebrand equation. The deprotonation of the -OH proton by the CN^- ion is the mechanism by which the receptor senses cyanide, and the phenolate ion that results from this process ultimately causes the receptor's fluorescence changes. The practical application

of probe **26** was extended to food products. Moreover, Color Picker app on a smartphone has been effectively integrated with the detectable color shift of the probe **26** upon binding with cyanide ions to estimate CN^- ions.

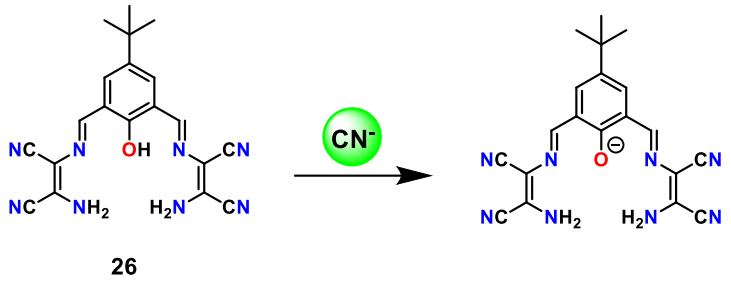

Fig. 1.25. Chemical drawing of probe **26** and its binding with CN^- species.

Naithani *et* al. (Naithani et al., 2024) developed a pyridyl-benzimidazole-based probe **27**, which is highly selective for cyanide ions in water (Fig. 1.26). UV-visible spectrum of **27** showed absorption ligand centred band at 285 nm and characteristic MLCT band at 460 nm. CN^- ions were added gradually, resulting in the probe's MLCT band to significantly redshift from 460 to 487 nm. Three isosbestic points were also observed at 324, 402, and 477 nm. These spectral changes were followed by colorimetric response of probe from light brown to dark brown. The probe **27** displayed an emission band at 625 nm in water which was significantly quenched exclusively in the presence of CN^- ions. Job's plot revealed a 1:1 stoichiometry between the probe and CN^- ions. The limit of detection was calculated to be 12.8 nM. The probe **27**'s anion-sensing ability was also investigated using an acetonitrile solution when the probe was treated with anions. The MLCT band of the probe **27** exhibited remarkable redshift (from 457 to 497 nm) in the presence of AcO^-, F^-, and CN^- ions, while other competing anions showed no change. There are three isosbestic points at 322, 411, and 474 nm. The probe **27** displayed an emission band at 622 nm in acetonitrile solution when **27** was excited at 460 nm. The probe **27** was quenched upon adding F^-, AcO^-, $H_2PO_4^-$, and CN^- ions. The Limit of detection values of the probe **27** for F^-, CN^-, and AcO^- ions were calculated to be 2.26 nM, 1.30 nM, and 1.90 nM, respectively. The reason behind cyanide selectivity in water was its higher deprotonating ability and lesser energy of hydration value as compared to F, AcO and H_2PO_4 anion. The probe was also able to detected

CN^- in human breast cancer MCF-7 cell lines and natural food sources (such as apple seeds and sprouting potatoes).

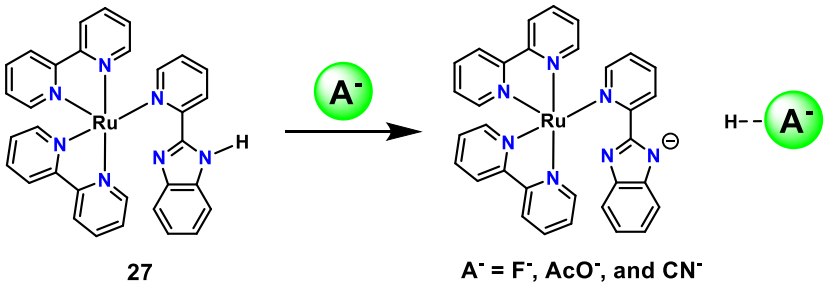

Fig. 1.26. Chemical drawing of probe **27** and its binding mode with F^-, AcO^-, or CN^- species.

A new unsymmetrical azine derivative-based probe **28** was synthesized by Sun et al. (Sun et al., 2016) to recognize cyanide ions in aqueous DMSO solution (Fig. 1.27). When CN^- ions were added, the probe's color changed considerably from colorless to yellow. Additionally, the fluorescence of this probe **28** at 530 nm enhanced by 50 folds when CN^- ions were added. The binding affinity was computed based on the fluorescence enhancement studies. The calculated binding constant using **28** was 1.5×10^4 M^{-1} for CN^- ions. The LoD of the probe for CN^- ions was computed to be 6.17×10^{-8} M. The probe **28**'s pH dependence was further investigated, and it performs well in the range of 8.0 to 12.0. The binding mechanism of **28**-CN^- was based on the ^1H NMR spectroscopic experiments. When CN^- ions were added, it caused deprotonation, which broke the hydrogen bond and released energy through radioactive decay. Filter paper test strips are a cost-effective and efficient CN^- test kit to detect CN^- ions in aqueous solution.

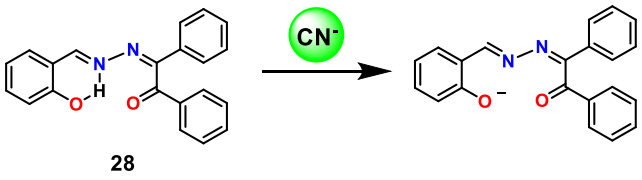

Fig. 1.27. Chemical drawing of probe **28** and its binding mode with CN^- species.

Chao *et* al. (Chao et al., 2016) synthesized a benzothiazolium-based fluorescent probe **29** to detect CN^- and HSO_3^- ions in a DMSO solution (Fig.

1.28). The probe **29** displayed a croci color to colorless in the presence of CN^- and HSO_3^- ions via colorimetric experiments. When the probe **29** was treated with CN^- ions, the absorption peak at 468 nm slowly disappeared, a new band appeared from around 260 to 300 nm, and an isosbestic point was observed at 330 nm. The remarkable ICT effect of the water-soluble probe from the electron donor carbazole group to the electron acceptor benzothiazole moiety was responsible for its intense fluorescence into CN^- ions. A band at 450 nm decreases with the gradual addition of HSO_3^-, and a new band at 276 nm emerges with a distinct isosbestic point at 281 nm (orange to non-fluorescent). The CN^- and HSO_3^- ion detection limits were determined to be 0.94 μM and 0.53 μM, respectively. The probe **29** can be used to detect CN^- and HSO_3^- ions in living cells, respectively, and function as excellent cell membranes.

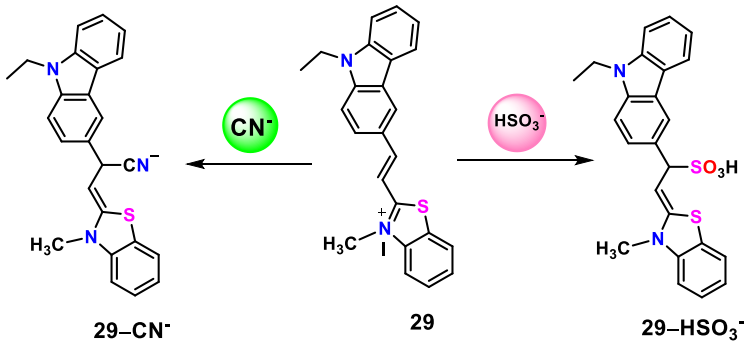

Fig. 1.28. Chemical drawing of probe **29** and its binding modes with CN^- and HSO_3^- ions in **29**-CN^- and **29**-HSO_3^- species.

Gupta et al. (Gupta et al., 2016) developed a benzimidazole-based probe **30** for the detection of CN^- ions in aqueous methanol solution (Fig. 1.29). In absorption experiments, a new band appeared at 380 nm, and the absorbance peak at 340 nm diminished with the addition of CN^- ions. It displays the limit of detection value of 1 μM and the binding constant of 0.45×10^3 M^{-1}. The ESIPT emission at 485 nm is restricted when CN^- ions are added to the probe because of H-bonding interactions between OH and the nitrogen of the benzimidazole molecule, which release its enol emission. In CH_3OH:H_2O solutions, the probe **30**'s ability to detect different metal ions was also examined. Absorption spectra revealed the probe **30**'s distinct behavior when

Cu^{2+} and Hg^{2+} ions were present. The LoD was calculated to be 1 µM and the binding constant was 3.28×10^6 M^{-1}.

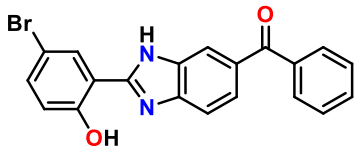

30

Fig. 1.29. Chemical drawing of probe **30.**

1.7.2 F^- sensors

Gupta *et* al. (Gupta et al., 2017) developed a tetraphenylethylene-based molecular probe **31** to detect Cu^{2+} and F^- ions in aqueous acetonitrile solution (Fig. 1.30). The emission band changed when water was added to the probe **31** dissolved in acetonitrile. When the solution's water content increased, a new band appeared at 450 nm. The planar geometry of the deprotonated probe was considered to cause this aggregation-induced emission. The ability of this AIEgen to recognize F^- and Cu^{2+} ions in acetonitrile solution was examined. The colorless solution of the probe **31** turned dark yellow when F^- ions were present. The probe containing Cu^{2+} and F^- ions emitted fluorescence at 490 and 565 nm, respectively. The conjugation to increase the fluorescence intensity was actually promoted by the Cu-complex generated in the solution, surpassing the opposing quenching behavior of the paramagnetic Cu^{2+} ions. The emission of the probe was at a different wavelength from the original probe because the F^- ions deprotonated it.

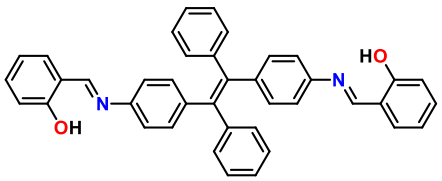

31

Fig. 1.30. Chemical drawing of probe **31**.

Mohanasundaram *et* al. (Mohanasundaram et al., 2020) synthesized a loutonin-based probe **32** to detect F^- ions in an aqueous DMSO solution (Fig.

1.31). The probe **32** displayed a broad absorption peak at 418 nm in the presence of F^- ions. This probe **32** is highly selective for F^- ions. Due to the addition of F^- ions, the colorless **32** solution became yellow. Additionally, the outcomes might be explained by the interaction between the F^- ions and an -OH group during the intermolecular hydrogen bonding. There are two isosbestic points at 340 and 380 nm. They attribute the observed red shift of the absorption band to the alteration of the intramolecular charge transfer band, indicating that fluoride deprotonated the -OH group in the probe. Job's plot revealed a 1:1 stoichiometry between the probe and F^- ions. The LoD of this probe **32** for F- ions was calculated to be 5.41×10^{-7} M. The Binding constant was determined to be 1.95×10^5 M^{-1} with the help of the Benesi-Hildebrand equation. The probe **32**'s ability to detect anions successfully may result in the development of test kits and silica gel plates with high selectivity for identifying, monitoring, and detecting F^- ions in an aqueous solution.

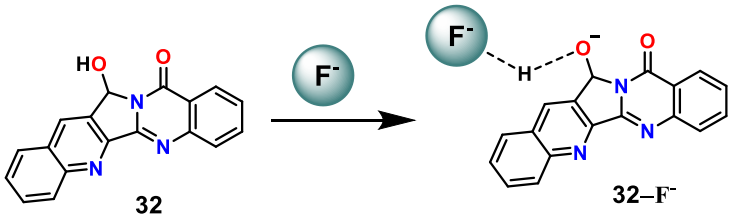

Fig. 1.31. Chemical drawing of probe **32** and its binding mode with F^- ion in **32**-F^- species.

1.7.3 ClO_4^- sensors

Naithani et al. (Naithani et al., 2025) reported a luminescent probe **33** containing pyridyl-benzimidazole for detecting ClO_4^- ions in an aqueous acetonitrile solution (Fig. 1.32). The probe **33** displayed an absorption band at 307 nm in the UV-visible studies due to π-π* transition. When **33** was excited at 300 nm, the probe showed an enhancement of the fluorescence intensity at 363 nm in an acetonitrile solution. The ClO_4^- ion and N-H units also form a hydrogen bond that promotes the probe **33**'s structural stiffness and could be responsible for the adduct's increased fluorescence. The LoD and the binding constant values were calculated to be 0.121 μM and 2.6×10^5 M^{-1}, respectively. Job's plot analysis showed a clear 1:1 binding stoichiometry for adduct. ClO_4^-

ions were successfully traced with this probe **33** in actual samples, including soil, groundwater, and tap water, with good to exceptional recovery values.

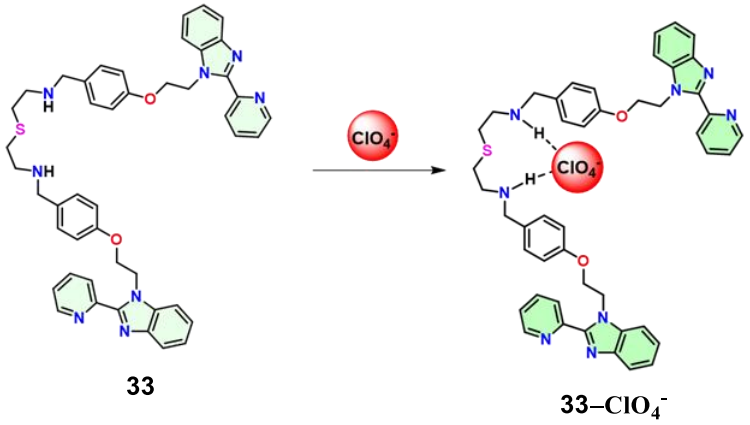

Fig. 1.32. Chemical drawing of probe **33** and its binding mode with ClO_4^- ion in **33**-ClO_4^- species.

1.8. Objectives

The current study has explored all relevant previously done studies and then found some related research gaps. We conducted our study with the aim to accomplish following research objectives:

1. To design and develop new molecular probes acting as fluorescent chemosensors
2. To investigate the photophysical and redox behavior of these probes using UV-visible and fluorescence studies
3. To explore the potential of resultant probes towards fluorescent detection of metal ions and anions

The research gaps, particularly in the area of fluorescent molecular probes, are addressed in this thesis through a novel approach. The structure of this thesis is categorized into seven chapters:

Chapter 1: *Introduction*

This chapter offers a comprehensive introduction to various optical sensors, focusing on the fundamentals, probe design for fluorescence, and fluorescent molecular probes. It highlights research gaps, provides an insightful literature

review, and sets the stage for the work detailed in subsequent chapters. Additionally, the objectives of the thesis are thoroughly outlined.

Chapter 2: *Materials, methods and instrumentation*

This chapter outlines the materials and methodologies employed in the development of fluorescent sensors. It includes detailed discussions on sample preparation, methods for detecting metal ions, cell imaging experiments, and the diverse instruments used for characterization and analysis.

Chapter 3: *A quinoline-derived Schiff base as a highly selective 'turn-on' probe for fluorogenic recognition of Al^{3+} ion*

In this chapter, a quinoline-derived Schiff base, **QnSb**, has been synthesized for fluorescent and colorimetric detection of Al^{3+} ions in a semi-aqueous medium. Characterized by elemental analysis, FT-IR, NMR, UV-Vis, and fluorescence spectra, its crystal structure was confirmed *via* single-crystal X-ray diffraction (SC-XRD). **QnSb**, initially non-fluorescent, exhibited a significant fluorescence increase at 422 nm when excited at 310 nm upon Al^{3+} binding. It showed high selectivity for Al^{3+} over other metal ions in CH_3CN/H_2O (4:1, *v/v*), with a low detection limit of 15.8 nM, below the WHO's drinking water standard for Al^{3+}. A 1:1 **QnSb**-Al^{3+} binding stoichiometry was confirmed by Job's plot, ESI-MS, NMR, and DFT analyses. The probe was further applied in molecular logic gates and fluorescence-based detection on filter paper test strips.

Chapter 4: *Turn-on detection of Al^{3+} ion by quinoline-based tripodal probe: Mechanistic investigation and live cells imaging applications*

This chapter introduces **TQSB**, a Schiff base probe with a quinoline fluorophore, as a turn-on optical sensor for Al^{3+} ions in a semi-aqueous medium (CH_3CN/water, 4:1, *v/v*). Absorption, emission, and colorimetric studies revealed that TQSB exhibits high selectivity for Al^{3+}, with a detection limit of 7.0 nM. Though **TQSB** was nearly non-fluorescent initially, Al^{3+} binding induced strong fluorescence at 414 nm, likely due to chelation-enhanced fluorescence (CHEF) and restricted PET effects. The sensing mechanism was confirmed using Job's plot, ESI-mass, and DFT analyses. **TQSB**'s sensing ability was demonstrated in real-world samples, including soil and Al^{3+}-containing Digene tablets, as well as on low-cost filter paper strips.

Fluorescence microscopy further showed its potential as a non-cytotoxic probe for detecting intracellular Al^{3+} in live cells.

Chapter 5: *Isolation and characterization of the labile tetrahedral gem-diol intermediate in the Al(III)-catalyzed hydration of aromatic aldehydes*

In this chapter, we demonstrated a robust synthetic design of the Lewis acid catalysed nucleophilic reaction of aromatic aldehydes. While typically energetically disfavoured, the Lewis acid co-ordination to the carbonyl group induces here the effective hydration of the aldehyde substrates and ensures the recurring occurrence of *gem*-diol as an isolable reaction intermediate. Interestingly, these labile and transient species are stabilized in solid state by the *in situ* generated HCl and unambiguously characterized by X-ray crystallography. These results highlight that the structural analysis of *in situ* chemical species are important and aids to accomplish mechanistic understandings of chemical transformations occurring in biomimetic reactions.

Chapter 6: *Imidazo-phenanthroline based optical sensing platform for cyanide and fluoride ions: Experimental and theoretical investigations*

This chapter presents a fluorogenic imidazo-phenanthroline-based probe (**bpmpip**) for the selective detection of fluoride (F^-) and cyanide (CN^-) in a semi-aqueous medium. Probe **bpmpip** exhibits a ratiometric fluorescence response upon interacting with these anions, driven by hydrogen bonding with the N-H group of the imidazole moiety. **bpmpip** distinctly discriminates CN^- from other anions, causing a color change from pale yellow to light green, with a detection limit in the nanomolar range. Paper-based strips embedded with **bpmpip** were developed for detecting CN^- and F^- under UV light. The probe's high sensitivity and selectivity are attributed to the N-H proton's strong acidity, promoting hydrogen bonding and deprotonation. The binding mechanism was analyzed using Job's plot, NMR, and DFT studies. Additionally, **bpmpip** was successfully applied to detect cyanide and fluoride ions in soil samples and to identify fluoride ions in live MCF-7 cells *via* blue fluorescence imaging.

Summary of the thesis*:* This section provides the concluding remark and main output of the thesis along with the possible future works that can be explored.

CHAPTER 2

Materials, methods and instrumentation

This chapter details the materials used in this research, including chemicals and solvents, highlighting their sources and key properties. It describes the methods for synthesizing different compounds, focusing on the procedures and reaction conditions. Additionally, it discusses advanced analytical techniques such as spectroscopy, spectrometry, and diffraction, used to analyze and confirm the structure and composition of the synthesized compounds. The chapter also emphasizes the principles, equipment, and applications of these methods to ensure accurate and reliable characterization. Experimental techniques used to investigate the analyte sensing behavior of as-synthesized compounds have also been described.

2.1 Materials

A variety of chemicals and solvents used in this study were sourced from commercial suppliers and utilized without further purification unless stated otherwise. Quinoline-2-aldehyde, tris-(2-amino)ethylamine, terephthaldehyde, and 2,2′-thiobis(ethylamine) were obtained from Sigma-Aldrich. Other reagents, including sodium borohydride, sodium bicarbonate, potassium bromide (KBr), ammonium acetate (NH_4OAc), sodium sulfate (Na_2SO_4), di-(2-picolyl)amine (DPA), 1,10-phenanthroline, and triethylamine (Et_3N), were also purchased from Sigma-Aldrich. Common metal salts were procured from Alfa Aesar. Solvents such as ethanol, acetonitrile, dichloromethane, methanol, and ethyl acetate were employed in various experimental procedures. Stock solutions of metal ions (Ca^{2+}, Cu^{2+}, Cd^{2+}, Zn^{2+}, Co^{2+}, Cr^{3+}, Hg^{2+}, Ni^{2+}, Mg^{2+}, Pb^{2+}, Fe^{3+}, Sn^{2+}, In^{3+}, Mn^{2+}, and Al^{3+}) were prepared from their corresponding chloride or nitrate salts. Similarly, stock solutions of anions (AcO^-, Br^-, ClO_4^-, CN^-, F^-, CO_3^{2-}, $Cr_2O_7^{2-}$, PO_4^{3-}, SO_4^{2-}, and CrO_4^{2-}) were prepared using their tetrabutylammonium (TBA) salts before conducting recognition experiments.

1,10-phenanthroline-5,6-dione was synthesized following a previously reported procedure (Arora et al., 2019). Most of the synthetic manipulations were performed under an inert nitrogen atmosphere using the Schlenk line

technique, with solvents thoroughly purified and dried prior to use. Reaction solvents were evaporated under reduced pressure using a rotary evaporator, and all solvents used in reactions and workup procedures were distilled and dried to ensure high purity.

2.2 Methods

2.2.1 Calculation of detection limit (LoD) and binding constant (K_b)

The limit of detection (LoD) for metal ions/anions has been calculated by using the formula LoD = 3σ/S based on emission titration profiles (where σ is the standard deviation arising from 10 blank emission scans and S is the slope) (Goswami et al., 2024).

On the other hand, the binding constant (K_b) for the probe towards metal ions/anions has been calculated using the Benesi–Hildebrand equation (Naithani et al., 2023):

$$1/(F-F_0) = 1/(F_{max}-F_0) + 1/(F_{max}-F_0)(1/K_b)(1/[A]) \quad (1)$$

Where, A stands for target analyte (i.e., metal ion or anion), F_{max} = fluorescence intensity of probe in the presence of analyte at saturation point; F_0 = fluorescence intensity of free probe; F = fluorescence intensity of probe at any intermediate concentration of target metal ions/anions. The K_b value can be determined using the slope of the straight line in the plot of $1/(F - F_0)$ against 1/[analyte].

2.2.2 Calculation of quantum yield

The fluorescence quantum yields of the probes were determined using the slope method, with anthracene (Φ = 27%) dissolved in ethanol as the standard reference (Sharma et al., 2024). The procedure involved preparing solutions of the probe and anthracene at various concentrations, ensuring the absorbance remained below 0.1, and setting a fixed excitation wavelength. Fluorescence spectra were recorded for each solution, and the emission maxima were plotted against the absorbance. The quantum yield was then calculated using the following equation:

$$\boldsymbol{\phi_X} = \phi_{std} \times \frac{Grad_x}{Grad_{std}} \times \frac{\eta_x^2}{\eta_{std}^2}$$

where $Grad_x$ = slope of the sample, $Grad_{std}$ = slope of the reference ϕ_X = Quantum yield of reference, ϕ_{std} = Quantum yield of sample, η_x^2 = refractive index of sample solution, and η_{std}^2 = refractive index of reference solution.

2.2.3 Low-cost detection methods: Paper strips and colorimetric assay

For the test strip sensing studies, Whatman filter paper strips were first immersed in a stock solution containing the probe and allowed to air-dry. After drying, the treated strips were placed in separate beakers containing aqueous solutions of various metal ions. Visual changes were observed under both UV and visible light illumination, enabling the detection and differentiation of metal ions based on the colorimetric response. This method provides a simple, rapid, and cost-effective approach for real-time sensing of metal ions, with the fluorescence or color change serving as a clear indicator of the presence and concentration of specific ions (Kumar et al., 2013).

2.2.4 MTT assay

The cell viability of MCF-7 cell lines in response to the probe was evaluated using the 3-(4,5-dimethylthiazol-2-yl)-2,5-diphenyl tetrazolium bromide (MTT) assay. Initially, 0.5×10^4 cells per well were seeded into a 96-well plate. Once the cells reached approximately 70% confluency, they were treated with varying concentrations of the probe (10-100 μM). After 24 hours of exposure, 0.2 mg/mL MTT solution was added to each well and incubated for 4 hours. The resulting formazan crystals were dissolved in DMSO, and the absorbance was measured at 570 nm using a multilabel plate reader (Fluostar Optima, BMG Labtech, Ortenberg, Germany). Cell viability was then calculated using the appropriate equation:

$$\textbf{\textit{Percentage cell viability}} = \frac{Mean\ absorbance\ of\ drug\ treated\ cells}{Mean\ absorbance\ of\ vehicle\ treated\ cells} \times 100$$

This assay allows for the assessment of cytotoxic effects and provides valuable insights into the biological activity of the probe, helping to determine its potential as a therapeutic agent (Melhuish, 1961).

2.2.5 Cell culture and imaging

The cell lines were cultured in DMEM-HG (Dulbecco's Modified Eagle's Medium with high glucose) supplemented with 10% heat-inactivated fetal bovine serum (FBS). The cells were seeded at a density of 0.05×10^6 cells per well in a 24-well plate and incubated at 37°C with 5% CO_2 for 24 hours. Following this, the cells were treated with varying concentrations of the probe for 4 hours, then gently washed with PBS buffer. The probe-incubated cells at a concentration of 40 μM were further exposed to different concentrations of metal ions (40-100 μM) for 2-3 hours, followed by a gentle wash with PBS to remove any excess metal ions. Imaging of the cells was performed using an inverted fluorescence microscope (EVOS FLOID, Thermo Fisher, USA), capturing images in green, blue, and red fluorescence channels. This approach enables the visualization and assessment of probe interactions with metal ions in living cells.

2.2.6 Analysis in real samples

The practical application of the probe was validated by testing it with a soil sample and a Digene gastric tablet. For the soil sample, 0.5 mg was thoroughly mixed with 10 mL of CH_3CN and then centrifuged at 5000 rpm for 30 minutes. The resulting mixture was filtered using Whatman Grade 1 filter paper. The gastric tablet was finely ground, sonicated, and left overnight in CH_3CN solution, followed by filtration through Whatman Grade 1 filter paper. The filtered solution was then diluted to a final volume of 50 mL. Both the soil and gastric tablet samples were spiked with known concentrations of metal ions and then mixed with the probe solution. After incubating for 10 minutes, the fluorescence spectra were recorded and compared to a calibration curve. This method demonstrated the probe's ability to detect metal ions in complex environmental and pharmaceutical matrices (Suryawanshi et al., 2020).

2.3 Instrumentation

In this thesis work, various instruments have been utilized to characterize and detect metal ions and anions using fluorescent molecular probes. The necessary instruments for the proposed approach are listed below:

2.3.1 Melting point apparatus

The melting points of the synthesized compounds have been measured using an electrically heated apparatus. The samples were enclosed in sealed glass capillaries, with one end sealed off. Measurements were then taken with an accuracy of ± 2°C and reported accordingly.

2.3.2 Fourier transform infrared spectroscopy (FT-IR)

FT-IR spectroscopy is the most commonly used technique for infrared analysis due to its superior sensitivity, accuracy, and precision compared to dispersive spectrometers. It is non-destructive to samples and can collect spectral data across a wide range. In FTIR analysis, infrared radiation is passed through a sample, and the absorbed radiation is recorded. The molecules in the sample absorb the radiation, converting the energy into vibrational or rotational energy. The resulting signal is a spectrum that serves as the molecular fingerprint of the material. Since each molecule has a unique spectral fingerprint, FTIR is a valuable method for chemical identification. FT-IR spectra in this study were obtained using a Shimadzu IR-Spirit instrument with KBr pellets.

Principle

The fundamental principle of FTIR involves the absorption of infrared light by the sample. Infrared light with a high wavelength is transmitted through the sample, and the FTIR instrument measures the wavelengths of light that are absorbed. This absorption provides valuable information about the sample's molecular structure, as different bonds within the molecules absorb specific wavelengths of infrared radiation. The resulting data is used to create a spectrum that reflects the chemical composition of the sample.

Instrumentation

FTIR instrumentation consists of several key components:

- **Source**: The infrared source generates the radiation used for analysis. The energy incident on the sample is regulated by a slit, which controls the amount of infrared light directed toward the sample.
- **Interferometer**: The interferometer performs spectral encoding when the radiation enters it. This combines all the infrared frequency components into the output signal.

- **Sample**: The sample interacts with the infrared beam, either transmitting or reflecting the radiation depending on the type of study being conducted. The sample absorbs energy at frequencies that are specific to its molecular structure.

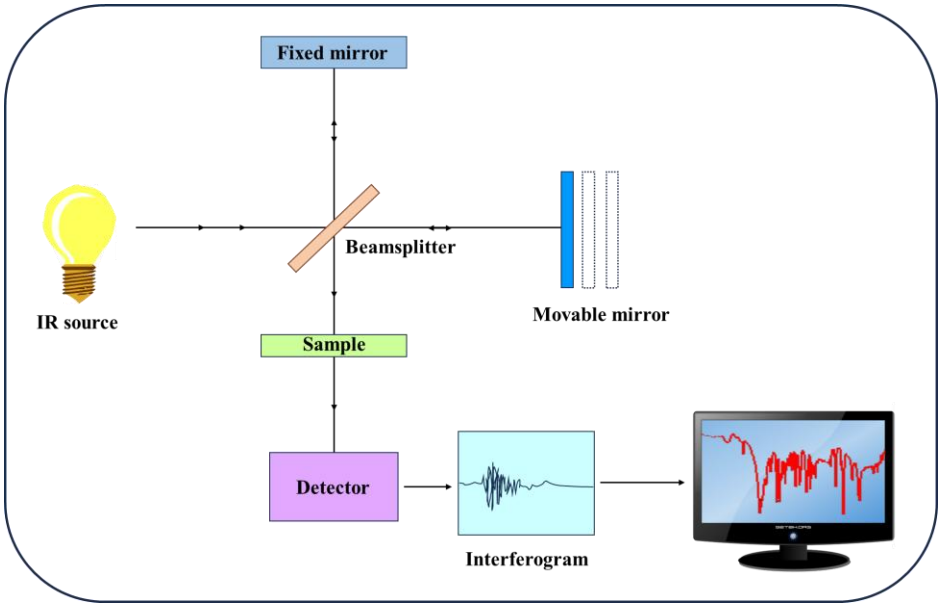

Fig. 2.1 Schematic diagram of FT-IR spectrometer.

- **Detector**: The detector measures the interferogram signal, which contains the information needed to create the infrared spectrum.
- **Computer**: The computer performs the Fourier transform on the signal to produce the final infrared spectrum, which is then analyzed.

2.3.3 Nuclear magnetic resonance (NMR) spectroscopy

NMR spectroscopy was employed extensively to characterize the synthesized compounds and monitor reaction progress. ^{1}H and ^{13}C NMR spectra were recorded on Bruker AVANCE 500 MHz (ECX 500) spectrometer in $CDCl_3$ and DMSO-d_6 solutions with TMS (i.e., tetramethyl silane) as internal standard. This high-precision instrument provided detailed spectral data, crucial for the structural and compositional analysis of the synthesized compounds and complexes.

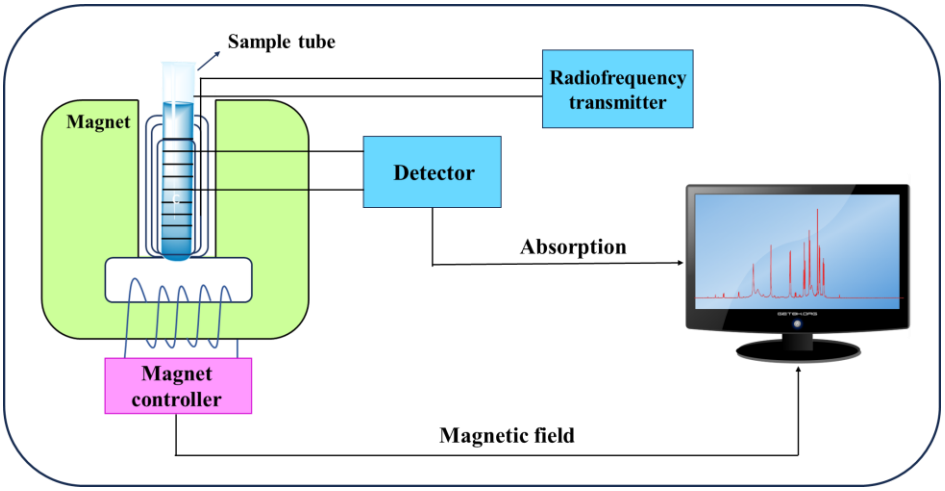

Fig. 2.2 Schematic diagram of NMR spectrometer.

2.3.4 Single crystal X-ray diffraction

X-ray diffraction data for the synthesized compounds were obtained using a Rigaku Oxford diffractometer, equipped with graphite-monochromated Mo-Kα radiation (λ = 0.71073 Å). The resulting data were processed with *CrysAlisPro* software, which included a multi-scan absorption correction to enhance data accuracy and precision. Cell refinement and data reduction were performed using the SAINT program (Petříček et al., 2016). Crystal data were collected using φ and ψ scans. Anisotropic refinement was applied to non-hydrogen atoms, while hydrogen atoms were positioned in idealized locations and refined using riding models. Absorption corrections and data scaling were carried out with SADABS (Sheldrick, 1990). The crystal structure solution and refinement were performed using direct methods, followed by full-matrix least-squares refinements against F2 (all data in HKLF 4 format) with the SHELXT software package (Sheldrick, 1990). These procedures allowed for the accurate determination of the molecular geometry, bond lengths, angles, and the overall crystal structure, providing a comprehensive characterization of the compounds.

2.3.5 UV-visible absorption spectroscopy

UV-visible absorption spectra of the synthesized materials were recorded at ambient temperature in a 1.0 cm path length quartz cuvette using a Shimadzu UV240 spectrophotometer. This technique provided critical insights into the electronic transitions and optical properties of the compounds.

This spectroscopy is based on the absorption, reflectance, and transmission of photons through samples within the UV-visible region, encompassing both liquids and transparent or opaque solids. It utilizes photons from the visible (400–800 nm) and ultraviolet (200–400 nm) portions of the electromagnetic spectrum. In this range, atoms and molecules undergo electronic transitions. Absorption spectroscopy specifically measures the intensity of electromagnetic radiation absorbed by a sample as a function of wavelength or frequency. This process relies on detecting the light that passes through the sample, with the absorption spectra revealing the sample's color in the visible spectrum. The Beer-Lambert law, which forms the foundation of UV-visible spectroscopy, states that the amount of light absorbed is directly related to both the concentration of the sample and the path length of the sample cell.

Principle

The basis of UV-visible spectroscopy is the interaction of light and matter. A molecule may vibrate due to light passing through it or being absorbed by it. The absorption maximum is the wavelength of light that a molecule can absorb the most strongly.

Instrumentation

UV-visible spectrophotometer is composed of several essential components, including a light source, monochromator, sample cells, and a detector. These components work together to measure the absorption of light by a sample, providing detailed information about its electronic transitions and optical properties.

(i) Light Source

The light source in a UV-visible spectrophotometer is responsible for emitting the radiation required for the analysis. Common light sources include deuterium lamps for ultraviolet light, tungsten-halogen lamps for visible and near-infrared light, and Xenon flash lamps, which offer high intensity and broad spectral range. These sources produce continuous light across a wide range of wavelengths, with each being selected based on the wavelength region under investigation.

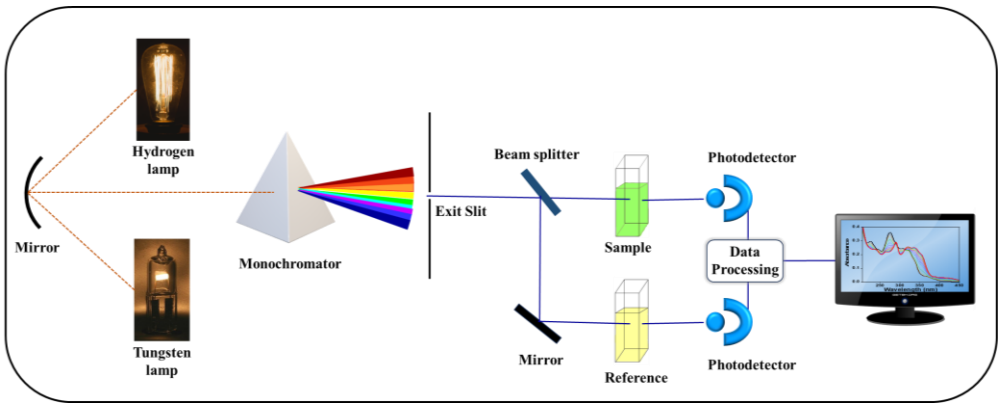

Fig. 2.3 Schematic diagram of UV-visible spectrophotometer.

(ii) Monochromator

The monochromator is used to isolate specific wavelengths from the broad-spectrum light emitted by the source. It disperses the light using a prism or diffraction grating and selects a narrow band of wavelengths through an exit slit. The chosen wavelengths then pass through the sample, enabling absorption measurement at particular points within the UV-visible spectrum.

(iii) Sample Cells

The sample compartment is where the sample is placed, and it typically consists of a black, non-reflective interior to minimize stray light interference. The sample is positioned so that the monochromatic beam passes through it, with cuvettes made from materials like glass, plastic, or quartz, depending on the wavelength range being measured. Quartz cuvettes are typically used for UV measurements due to their transparency in that range.

(iii) Detector

The detector in a UV-visible spectrophotometer converts the transmitted light passing through the sample into an electrical signal. Photodiodes and photomultiplier tubes are commonly used as detectors due to their sensitivity and low noise levels. The detector must have a broad wavelength response and high accuracy to measure the amount of light absorbed by the sample, providing the necessary data for analysis.

2.3.6 Fluorescence spectroscopy

Fluorescence studies were performed at ambient temperature using a Perkin Elmer LS45 spectrophotometer. This technique was employed to investigate the photoluminescent properties of the synthesized compounds, including their emission spectra and intensity at various wavelengths.

A spectrofluorometer is the specialized instrument designed to record and measure the fluorescence emitted by a sample when excited by light. The measurements are made by scanning the excitation, emission, or both wavelengths. A schematic diagram of the fluorescence spectrophotometer is shown in Fig. 2.4. Fluorescence spectrophotometers typically utilize laser sources for sample illumination, and they consist of several key components including detectors, monochromators, and light sources. The light source is typically an ozone-free xenon arc lamp. The emitted light is directed by a diamond-shaped elliptical mirror to the entry slit of the excitation monochromator. There are two types of monochromators in these instruments: excitation and emission monochromators. The grating, an essential part of the monochromator, disperses the incident light by passing it through grooves. The monochromator is equipped with flexible slits at both the entrance and exit points to allow for precise wavelength selection. The detectors used in the fluorescence spectrophotometer include signal detectors for measuring fluorescence and reference detectors for monitoring light intensity during the analysis.

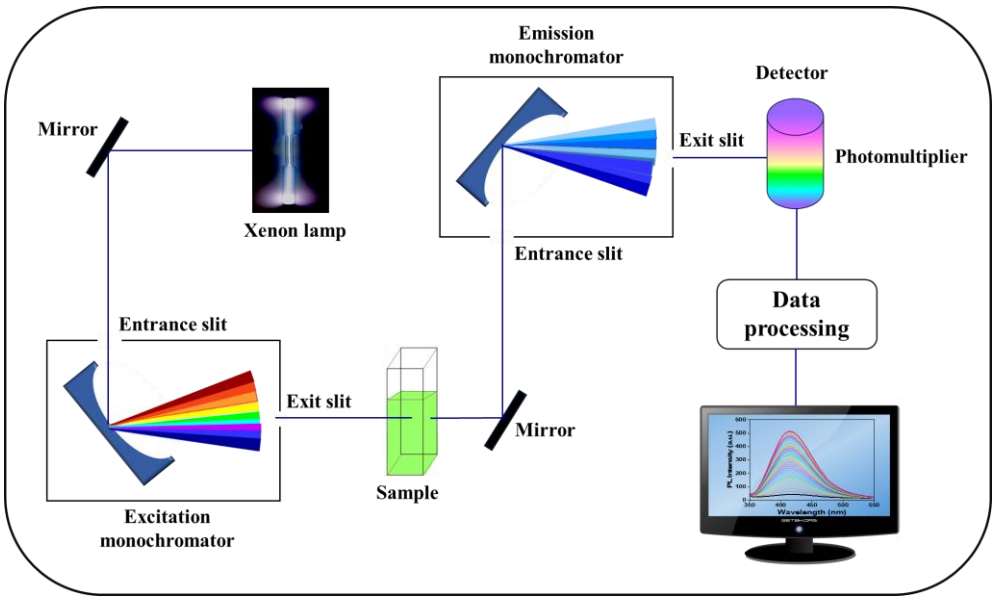

Fig. 2.4 Schematic diagram of fluorescence spectrophotometer.

2.3.7 Electrospray ionization mass spectrometry (ESI-MS)

ESI-MS analysis was performed using an Agilent Waters Q-TOF Premier-HAB213 mass spectrometer. Acetonitrile and methanol were used as solvents for sample preparation. This technique facilitated the determination of the molecular weight, fragmentation patterns, and provided valuable structural insights into the synthesized compounds.

2.3.8 *Elemental analysis*

Elemental analyses were conducted using a 2400 Series-II CHN analyzer from Perkin Elmer, USA. This method allowed for the precise determination of the carbon, hydrogen, and nitrogen content of the synthesized compounds, offering critical information regarding their elemental composition.

CHAPTER 3

A QUINOLINE-DERIVED SCHIFF BASE AS HIGHLY SELECTIVE 'TURN-ON' PROBE FOR FLUOROGENIC RECOGNITION OF Al^{3+} ION

3.1 State of the art

Although aluminium (Al) can occur naturally, anthropological reasons also contribute to its increase in the environment. Aluminium is the most abundant metal in the Earth's crust and the 3rd most abundant element in the lithosphere (*ca.* 8.0 % of total mineral substances). Al^{3+} ion is widely applied in different essential aspects of human social life, industries, material science, and biology (Gui et al., 2015; Han et al., 2011; Krewski et al., 2007; Lee et al., 2014; Liu et al., 2022). It has been typically employed in various household products, electrical and electronic components, building construction materials, sophisticated medical devices, to name but a few (Liu et al., 2023; Wang et al., 2023; Xie et al., 2023; Xu et al., 2022; Yang et al., 2023). Due to its extensive usage, more and more Al^{3+} ions get into the environment, leading to detrimental impact and alteration to human life. Excessive intake of Al^{3+} in humans has been linked to many inimical neurodegenerative disorders such as Parkinson's disease, Alzheimer's disease, as well as dialysis encephalopathy (Fasman, 1996; Nayak, 2002; Samanta et al., 2023; Shen et al., 2023; Xu et al., 2021). Therefore, it has been categorised as a neurotoxic agent to humans (Xia et al., 2022; Zhang et al., 2022). A high degree of Al^{3+} deposition causes the soil to become highly acidic which is deadly to the flora and aquatic fauna. Furthermore, other physiological dysfunctions such as gastrointestinal issues, interruption with Ca^{2+} metabolism, reduced kidney and liver functioning can be caused by Al^{3+} toxicity (Baral et al., 2008; Gupta et al., 2007; Kim et al., 2010; Sorenson et al., 1974). Due to a close relationship between Al and human health, WHO (World Health Organisation) has limited a daily intake of Al^{3+} ion ranging from 3.0 to 10.0 mg/day while a limit of only 7.41 μM (200 μg/L) is allowed in the drinking water (Berhanu et al., 2019). Hence, there is an urgent need to develop selective and efficient methods for detection and/or diagnosis of Al^{3+}, particularly in the

environmental and biological settings. Among the various metal ion detection techniques known so far (Bankaji et al., 2023; Berhanu et al., 2019; Sharma et al., 2023; Merten et al., 2023; Majidian et al., 2023; M'hamdi et al., 2023; Goswami et al., 2023; Jreije et al., 2022; Karasiński et al., 2020; Karch et al., 2022; Karimi-Maleh et al., 2023; Kumar et al., 2021; Sharma et al., 2023; Shen et al., 2022; Tian et al., 2023; Vallejo et al., 2022; Vivier & Orazem, 2022), the optical detection (fluorescent/colorimetric) methods have been the major focus of exploration as they offer a convenient, selective as well as sensitive metal ion recognition properties (Alizada et al., 2021; Bayrakcı et al., 2013; Kaur et al., 2018; Long & Yu, 2016; Meng et al., 2023; Saleem et al., 2017; Wang et al., 2020). In particular, the fluorescent sensors display the advantages of easy sample preparation, rapid response, easy operation, good sensitivity, and selectivity. Indeed, several fluorescent sensors have seen a gradual growth in high efficacy along with microscopic imaging and real-time analysis. Although a large number of fluorescent/colorimetric organic molecular probes have been reported for Al^{3+} detection either *in-vitro* or *in-vivo* (Silva et al., 2023; Huang et al., 2020; Kursunlu et al., 2022; Bilgic et al., 2022; Patil et al., 2019; Samanta et al., 2023; Kalavathi et al., 2023; Strianese et al., 2023; Yuan et al., 2023; Zhou et al., 2020), many of them suffer from laborious synthetic procedures (Anu et al., 2021). Additionally, the interference caused by Zn^{2+}, Fe^{3+}, and Cu^{2+} ions and the moderate limits of detection (LoD) are serious concerns for a majority of the optical sensors (Anu et al., 2021; Patil et al., 2019; Wang et al., 2021). Therefore, the sensors, selective for a specific metal ion, with relative ease of synthesis and structural simplicity are rapidly being produced and are still on high demand. In this context, Schiff base derived probes have emerged as viable alternatives for selective detection of metal ions (Kalavathi et al., 2023; Samanta et al., 2023). This is due to their advantageous features such as facile synthetic route (often one-step reaction), air- and moisture-insensitivity, and robust metal ion coordination capability. Notably, the optical (absorption and/or emission) features of Schiff base compounds can easily be modulated *via* facile incorporation of an appropriate fluorophore in their molecular scaffolds (Hou et al., 2020; Wang et al., 2018). Although various fluorescent Schiff bases have already been demonstrated for highly selective Al^{3+} monitoring, only a few

contain quinoline as a fluorophore. Quinoline-based probes have some remarkable advantages over other derivatives which include good water solubility, significant Stokes shift and good biocompatibility (Jakovljević et al., 2013; Zhou et al., 2018). Quinoline, as an important construction motif, has been widely noticed in drug discovery, natural products, and advanced functional materials (Fan et al., 2020). As a part of our ongoing efforts in the development of metal ion responsive optical sensors (Goswami et al., 2023.; Kumar et al., 2021; Sharma et al., 2023), herein, we present a quinoline-containing Schiff base probe (**QnSb**) for a highly selective detection of Al^{3+} in semi-aqueous medium (Fig. 3.1). The quinoline moiety acts as a fluorophore in the probe **QnSb**. Typically, Al^{3+} exhibits a hard-acid behavior and preferentially accommodates the coordination sphere holding hard-base donor sites (e.g., O and N atoms) (Balasubramanian et al., 2023; Naithani et al., 2023; Zeng et al., 2019). The incorporation of the hard donor quinoline and imine N atoms in the receptor pocket results in the exhaustive selectivity of **QnSb** for Al^{3+} ions. The probe **QnSb** displays a 'turn-on' fluorescence response for Al^{3+} that can be attributed to the inhibition of >C=N- isomerization and chelation-enhanced-fluorescence (i.e., CHEF) processes (Wang et al., 2018). The originally non-fluorescent probe **QnSb** strongly emits at 422 nm in the presence of Al^{3+} when excitation wavelength is 310 nm. The sensing ability of **QnSb** has been scrutinized by fluorescence and UV-Vis studies, and the binding mechanism has been established with the help of ^{1}H NMR, ESI-MS (electrospray ionisation mass spectrometry), and DFT (density functional theory) analyses.

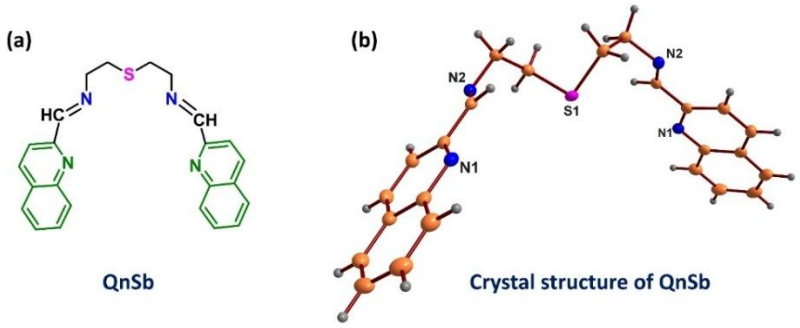

Fig. 3.1. (a) Chemical drawing of the probe **QnSb** and (b) ORTEP diagram for **QnSb**.

3.2 Experimental section

3.2.1 Synthesis of the probe QnSb

Schiff base probe **QnSb** has been synthesized *via* a one-step condensation reaction between quinoline-2-aldehyde and 2,2′-thiobis (ethylamine) in 2:1 ratio in ethanol (Scheme 3.1). Briefly, quinoline-2- aldehyde (0.31 g, 2.0 mmol) and 2,2′-thiobis(ethylamine) (0.12 g, 1.0 mmol) were taken in 25 mL ethanol, and the reaction mixture was stirred at room temperature for 2–3 h. The obtained off-white precipitate was filtered out, washed thrice with cold EtOH and diethyl ether, and then dried at 70° C for 2 h to give an off-white solid. Anal. Calcd. for $C_{24}H_{22}N_4S$: C, 72.33; H, 5.56; N, 14.06; Found: C, 72.26; H, 5.68; N, 13.98. FT-IR (KBr disk): 3442, 3049, 2925, 2883, 2835, 1645 ($\nu_{C=N}$), 1494, 1046, 837, 752, 613 cm^{-1}. UV-Vis (CH_3CN/water = 4:1; *v/v*): $\lambda_{max/nm}$ ($\varepsilon/M^{-1}cm^{-1}$) = 242 ($15.2 \times 10^4$), 287 ($4 \times 10^4$), 245 ($2.18 \times 10^4$) and 292 ($6.6 \times 10^3$). ^1H NMR ($CDCl_3$, 500 MHz, TMS), δ (ppm): 8.57 (s, 2H), 8.16 (d, 2H), 8.11 (d, 4H), 7.82 (d, 2H), 7.74 (t, 2H), 7.57 (t, 2H), 3.98 (t, 4H, -CH_2-N) and 3.01 (t, 4H, -CH_2-S). ^{13}C NMR ($CDCl_3$, 500 MHz, TMS), δ (ppm): 163.69, 154.53, 147.80, 136.62, 129.82, 129.67, 128.80, 127.71, 127.49, 118.42, 61.41, 33.30.

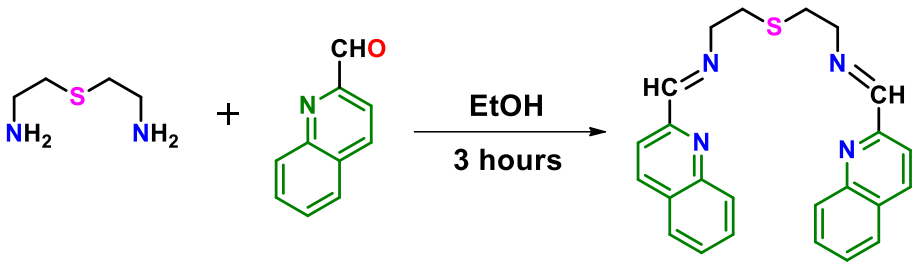

Scheme 3.1. Synthetic route to prepare Schiff base probe **QnSb.**

3.2.2 Crystal structure determination

Suitable single crystals of **QnSb** for X-ray analysis were obtained within two days *via* slow evaporation of its solution in a dichloromethane-methanol (8:2, v/v) mixture. The crystallographic data of **QnSb** has been collected on Oxford Diffraction Gemini diffractometer equipped with CrysAlis Pro at 150 K using the monochromatic Cu-Kα radiation source (λ 1.5416Å). The crystal structure of **QnSb** was solved by direct method

(SHELXL-97) and refined against all the data by full-matrix least squares on F^2 using anisotropic displacement parameters for all non-hydrogen atoms (Sheldrick, 1990; Sheldrick, 1997). All the H atoms were refined with a riding model. The MERCURY software package and ORTEP-3 for Windows program have been used to generate the structure (Bruno et al., 2002; Farrugia, 1997).

3.2.3 Absorption and emission spectra

All the absorption and emission experiments have been measured in semi-aqueous (CH_3CN/water = 4:1; *v/v*) medium. The emission spectra were measured in the range 320-580 nm with an excitation wavelength of 310 nm. The stock solution of **QnSb** (4.0×10^{-4} M) and the target metal ions (~10^{-2} M) were prepared in CH_3CN-H_2O (4:1, *v/v*) solution. Double distilled de-ionised water was thoroughly used to perform the UV-Vis and fluorescence experiments.

3.2.4 Job's plot analysis

Using Job's plot, the fluorescence spectroscopic measurements were used to determine the complexation ratio of **QnSb** with Al^{3+}. For analysis, the measurements were done using 1.0 μM of **QnSb** with various Al^{3+} molar ratios between 0.1 and 0.9. The emission intensity was measured at 422 nm. The resultant complex **QnSb-**Al^{3+} had a 1:1 binding stoichiometric ratio, which coincides with colorimetric and fluorometric titration data, the maximum emission intensity was precisely reached on the mole fraction of 0.5 (Arora et al., 2019; Yue et al., 2015).

3.2.5 Test strips experiments

The test strip sensing experiments have been performed by immersing Whatman filter paper strips into CH_3CN solution (4×10^{-4} M) of **QnSb** and then air-dried. The solutions of different metal ions (approx. 10^{-2} M) were separately prepared in different beakers, and the dried filter paper strips were immersed into them. The optical changes have been monitored under UV light illumination.

3.3 Results and discussion

The probe **QnSb** has been synthesized by condensation of 2,2′-thiobis (ethylamine) with quinoline-2-aldehyde in ethanol in 1:2 ratio (Scheme 3.1) (Fu et al., 2019; A. Kim et al., 2018; Arora et al., 2021) and characterized using various spectroscopic techniques such as elemental analysis, $^{1}H/^{13}C$ NMR, FT-IR, UV-Vis, and photoluminescence analyses. The structure of the probe **QnSb** was confirmed by single-crystal X-ray diffraction (SC-XRD) analysis. This probe was soluble in most of the organic solvents including dichloromethane, chloroform, tetrahydrofuran, acetonitrile etc. with relatively very less solubility in ethanol and water. The characteristic infrared (IR) bands of **QnSb** provided important information of the functionalities present in its framework (Annexure I, Fig. A1).

An intense IR peak corresponding to azomethine group ($\nu_{CH=N}$) appeared at 1645 cm^{-1} whereas the methylene ($-CH_2-$) groups displayed vibrational frequencies near 2930–2800 cm^{-1} (Fu et al., 2019). The ^{1}H and ^{13}C NMR spectra of **QnSb** have been recorded in $CDCl_3$ at room temperature with the frequency of 500 MHz (Annexure I, Figs. A2 and A3). In ^{1}H NMR spectrum, a singlet near 8.57 ppm could be attributed to the azomethine (-CH=N-) proton (Kaushal et al., 2022; Arora et al., 2021; Sun et al., 2018; Tian et al., 2019; Zhu et al., 2017). Additionally, two adjacent methylene ($-CH_2-$) groups displayed two triplets centred at 3.98 ppm and 3.01 ppm, respectively, for $=N-CH_2-$ and $-S-CH_2-$ moieties (Annexure I, Fig. A2). ^{13}C NMR spectrum of **QnSb** displayed a resonance at 163.69 ppm corresponding to the carbon atom of -CH=N- group. The methylene carbon atoms of $=N-CH_2-$ and $-S-CH_2-$ appeared at 61.41 and 33.30 ppm, respectively, while other resonances in the region 154.53-118.42 were attributed to the aromatic carbon atoms (Annexure I, Fig. A3). In order to depict the exact structure of **QnSb**, X-ray diffraction analyses have been performed (Fig. 3.1(b)). The probe **QnSb** crystallized in a monoclinic system with the space group -I 2ya. The crystallographic data, selected bond lengths and bond angles have been listed in Tables 3.1-3.2. The bond lengths of S(1)-C(12) i.e., 1.8111(15) and N(1)-C(1) i.e., 1.323(2) were found consistent with the single and double bond characters of -S-C- and >C=N- groups, respectively. The molecular structure of **QnSb** was stabilized by both inter- and intra-

molecular hydrogen bonding interactions which is clearly visible in Fig. A4 (Annexure I).

Table 3.1. Selected bond lengths [Å] and angles [°] in the single crystal of probe **QnSb**.

Bond Length (Å)		**Bond Angle (°)**	
S(1)–C(12)	1.8111(15)	C(12)-S(1)-C(12)	98.67(10)
N(1)–C(1)	1.323(2)	C(1)-N(1)-C(9)	117.71(12)
C(1)-C(2)	1.421(2)	N(1)–C(1)–C(10)	115.59(12)
C(9)-C(4)	1.416(2)	N(2)-C(10)-H(10)	119.2

Table 3.2. Crystallographic data and structural refinement parameters for **QnSb**.

	QnSb
Formula	$C_{24}H_{22}N_4S$
Formula weight ($gmol^{-1}$)	398.52
Space group (hall)	-I 2ya
Temperature/K	150(2)
λ (Å) (Cu-Kα)	1.54184
Crystal system	Monoclinic
a (Å)	12.0955(5)
b (Å)	4.7505(2)
c (Å)	34.7922(15)
α(˚)	90
β (˚)	97.067(4)
γ (˚)	90
V ($Å^3$)	1983.96(15)
Z	4
ρ_{calc}(gcm^{-3})	1.334
Crystal size (mm)	0.48 x 0.09 x 0.04
F(000)	840.0
Index ranges	-14 <*h*<14

	-5 <k< 5
	-38 <l< 42
Reflns/restraints/para.	1859/0/132
GOF on F^2	1.085
$R1^a$ [$I > 2\sigma(I)$]	0.0412
*R*1[all data]	0.0436
$wR2^b$ [$I > 2\sigma(I)$]	0.1126
*wR*2 [all data]	0.1172

$^a R1 = \Sigma||Fo|-|Fc||/\Sigma|Fo|$; $^b wR2 = |\Sigma w(|Fo|^2 - |Fc|^2)|/\Sigma|w(Fo)^2|^{1/2}$

3.3.1 Detection of Al^{3+} ions by fluorescence spectral studies

The sensing ability of **QnSb** for various metal ions was investigated by fluorescence spectral titrations (Fig. 3.2(a)). The emission spectra of **QnSb** were measured at different excitation wavelengths ranging from 290 nm to 340 nm; however, it gave best response only when excited at 310 nm. **QnSb** probe alone exhibited a very weak emission at 422 nm (λ_{ex} 310 nm) in CH_3CN-H_2O (4:1, *v/v*) solution that may be ascribed to lower ICT (intramolecular charge transfer) as well as >C=N- isomerization processes. However, the addition of 4.0 equiv of Al^{3+} induced a significant fluorescence enhancement (upto 20-fold) of **QnSb** at 422 nm. At this stage, a distinct color change also occurred from off-white to light purple under UV light illumination which was obvious to the naked eyes. In contrast, the presence of other metal ions such as Mg^{2+}, Pb^{2+}, Zn^{2+}, Cd^{2+}, Co^{2+}, Cu^{2+}, Ca^{2+}, Ni^{2+}, Fe^{3+}, Fe^{2+}, Cr^{3+}, Mn^{2+}, Sn^{2+} and Hg^{2+} showed nearly no fluorescence intensity enhancement. In^{3+} belongs to the same group in the periodic table, we thus tested the effect of In^{3+} on the fluorescence intensity of **QnSb**. As shown in Fig. A5 (Annexure I), the probe **QnSb** exhibited no substantial selectivity for In^{3+} ion as compared to Al^{3+} ion. These observations suggested a highly selective response of **QnSb** towards Al^{3+} and the formation of a new complex between Al^{3+} and **QnSb** during the recognition process. We have also studied the effect of concentration variation of Al^{3+} ions on the emission intensity of **QnSb** (Fig. 3.2(b)). From the plot of concentration variation, the extent for Al^{3+} binding could be measured *via* determination of

the LoD and the binding constant (K_b). The emission titration experiment revealed the significant enhancement in the fluorescence band upon sequential addition of Al^{3+} ions (01.2 equiv). The spectrophotometric titrations and the Job's plot analysis supported a 1:1 binding stoichiometry for the formation of complex **QnSb**-Al^{3+} (Fig. 3.7). The K_b and LoD values were depicted as 2.3 × 10^5 M^{-1} (Annexure I, Fig. A8) and 15.8 nM, (Fig. 3.3) respectively, with the help of emission titration profiles.

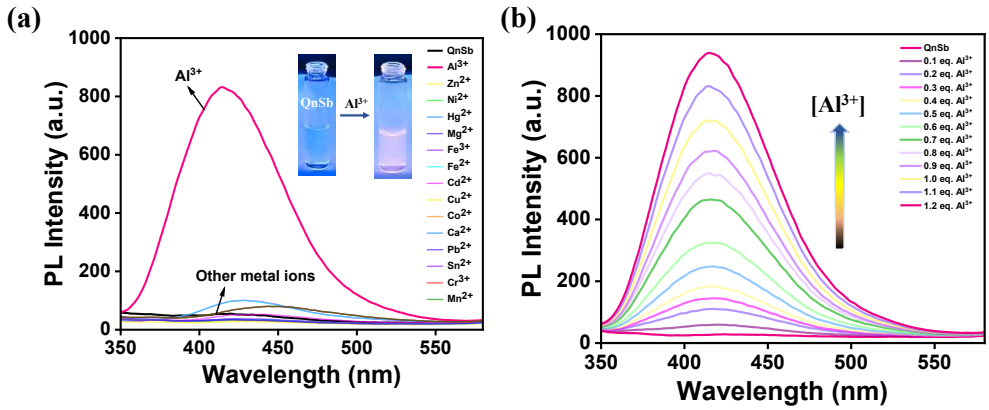

Fig. 3.2. (a) Fluorescence spectra of **QnSb** (*ca.* 10^{-6} M) in CH_3CN/H_2O (4:1; *v/v*) solution in the presence of 4.0 equiv of various metal ions (e.g., Mg^{2+}, Pb^{2+}, Zn^{2+}, Cd^{2+}, Co^{2+}, Cu^{2+}, Ca^{2+}, Ni^{2+}, Fe^{3+}, Fe^{2+}, Cr^{3+}, Mn^{2+}, Sn^{2+}, Hg^{2+} and Al^{3+}) and (b) Fluorescence spectral changes of **QnSb** with different concentrations of Al^{3+} (0 to 1.2 equiv) in CH_3CN/H_2O (4:1; *v/v*) solution. λ_{ex} = 310 nm.

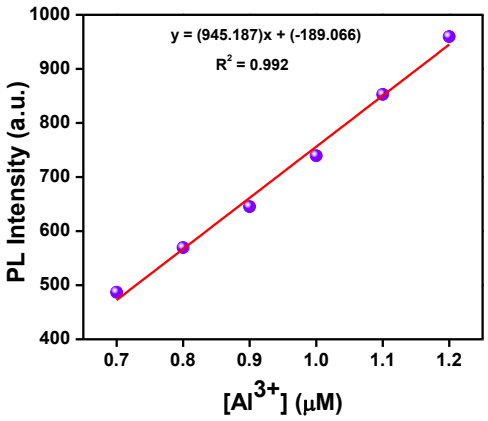

Fig. 3.3. Calibration curve obtained for determination of Al^{3+} by **QnSb** in CH_3CN/H_2O (4:1; *v/v*) solution.

The selectivity of the probe towards Al^{3+} ion was further investigated in the presence of different investigated metal ions. The emission spectra of Al^{3+} were recorded in the presence of 10.0 equiv of other interfering metal ions. The probe exhibited an excellent anti-interference performance and no metal ion including competing Cu^{2+}, $Fe^{2+/3+}$, Cr^{3+}, Mn^{2+}, Sn^{2+}, and Zn^{2+} interfered with the detection of Al^{3+} ion by **QnSb**, and the enhancement in the emission intensity was observed only due to the formation of stable **QnSb**-Al^{3+} complex (Fig. 3.4).

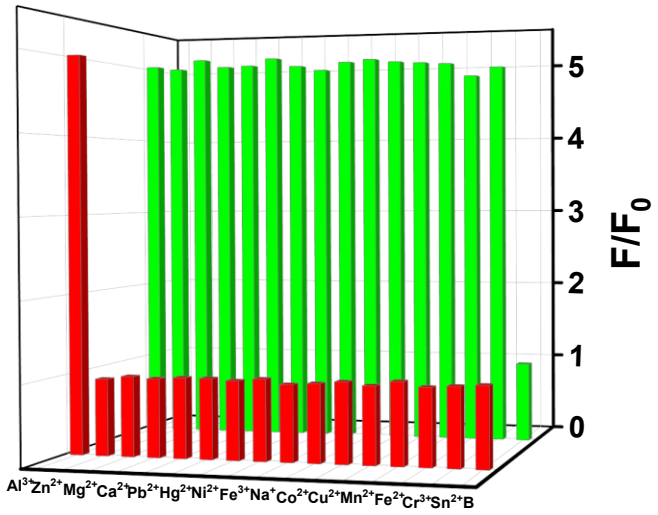

Fig. 3.4. Selectivity of probe **QnSb** for Al^{3+} ion in the presence of assorted metal ions in CH_3CN/H_2O (4:1; v/v) solution. **QnSb** + other metal ions (green pillars); **QnSb** + other metal ions + Al^{3+} (red pillars) at λ_{em} 422 nm.

3.3.2 Detection of Al^{3+} ions by UV-Vis spectral studies

The molecular interactions of probe **QnSb** with various metal ions were further investigated using UV-Vis spectroscopy. The electronic absorption spectrum of **QnSb** displayed two bands with their maxima centred at 242 nm (ε = 15.2 × 10^4 $M^{-1}cm^{-1}$) and 287 nm (ε = 4 × 10^4 $M^{-1}cm^{-1}$) in organic-aqueous (CH_3CN/H_2O = 4:1; *v/v*) solution (Fig. 3.5). These peaks have been ascribed to π-π* and n-π* electronic transitions of electronically rich aromatic probe, **QnSb**. After addition of 4.0 equiv of different metal ions, only slight perturbations could be observed in electronic spectra of **QnSb**. The spectrophotometric titrations of probe **QnSb** were performed with varied concentrations of Al^{3+} ions. Upon addition of Al^{3+} (0 to 1.3 equiv), the

absorption bands centred at 242 nm and 287 nm exhibited small redshifts to 245 nm and 292 nm, respectively. Along with these changes, two clear and distinct isosbestic points appeared at 209 nm and 302 nm (Dong et al., 2017; Goshisht et al., 2022; Liu et al., 2018) (Fig. 3.5). Furthermore, the absorption changes were accompanied by a slight color change in probe's solution from off-white to purple-red color which was obvious to the naked eyes under visible light illumination.

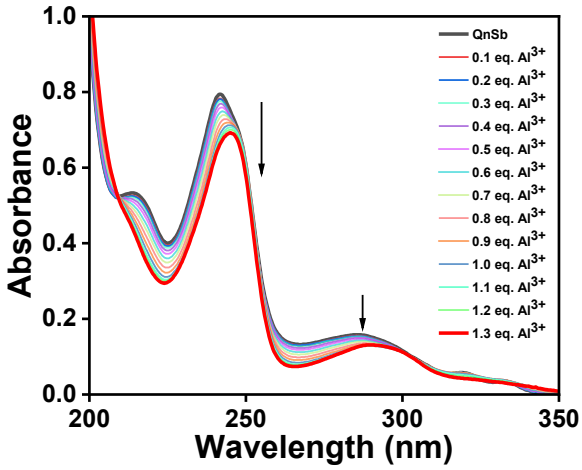

Fig. 3.5. UV-Vis spectral changes of **QnSb** with varied concentration of Al^{3+} ions (0-1.3 equiv).

3.3.3 Response time and pH effect

The coordination behaviour of probe was further investigated by monitoring the response time of **QnSb** towards Al^{3+} ions at different times from 0 to 30 mins (Fig. 3.6(a)). The addition of 1.5 equiv of Al^{3+} to the probe's solution resulted in gradual increase of the emission band because of complexation between **QnSb** and Al^{3+}. After 20 mins, a steady state was reached which did not change further with time. Moreover, the effect of pH on **QnSb** and **QnSb**-Al^{3+} was investigated in the range of pH 2.0-12.0 (Fig. 3.6(b)). The probe **QnSb** was almost pH-independent and non-fluorescent with only a slight increase in emission at pH 2.0. On the contrary, **QnSb** in the presence of Al^{3+} ion was substantially sensitive to both acidic as well as the basic pH. The emission intensity remained unchanged with addition of Al^{3+} ions at pH 4.0–2.0, most likely due to the competition between the H^{+} and Al^{3+} ions. On further increase of the pH, significant fluorescence increment was observed upto pH 9.0. As the

pH increased from 10.0 to 12.0, the emission intensity quenched to a considerable amount. The decrease in emission intensity at a higher pH could be ascribed to the formation of Al $(OH)_3$ that leads to the increased concentration of free **QnSb** in solution. Significant response of **QnSb** emission intensity over a pH range of 5.0 to 8.0 indicates the pH independence of **QnSb**, which is applicable to biological processes (pH 7.4).

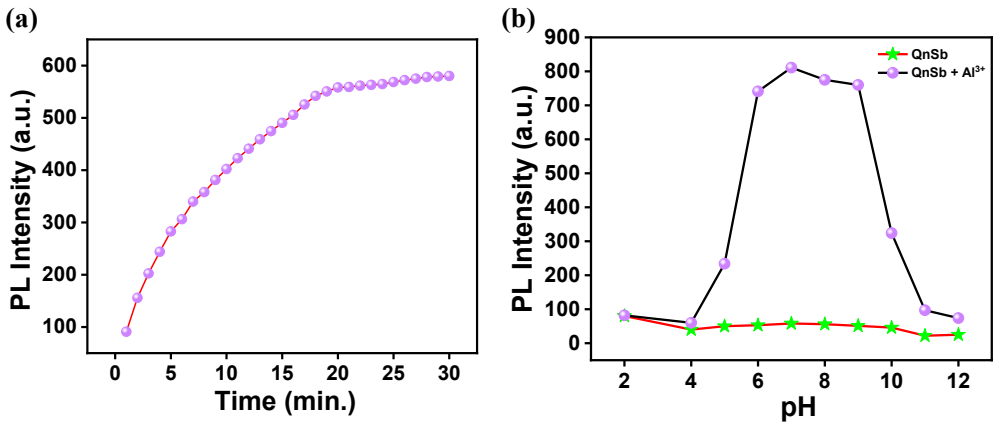

Fig. 3.6. (a) Response time of probe **QnSb** with Al^{3+} ions and (b) Effect of pH on probe **QnSb** and **QnSb** + Al^{3+} ions.

3.3.4 Binding mechanism

The binding and sensing mechanism have been established with the help of Job's plot, NMR, ESI-MS and DFT analyses. Job's plot data revealed a 1:1 stoichiometry between **QnSb** and Al^{3+} indicating the formation of **QnSb**-Al^{3+} adduct (Fig. 3.7). This was further supported by ESI-MS studies where the peak at *m/z* 554.1699 corresponds to the species [**QnSb** + Al^{3+} + Cl^- + $3CH_3OH$] which matches well with the theoretical mass value (Annexure I, Fig. A6). The ^1H NMR study of **QnSb**-Al^{3+} suggested that the azomethine (-CH=N-) proton peak at 8.56 ppm slightly shifted to downfield at 8.63 ppm after the gradual addition of Al^{3+} (upto 0.75 equiv) to **QnSb** in DMSO-d_6 solution. Other quinoline ring protons were also little de-shielded and downfield shifted upon complexation (Annexure I, Fig. A7).

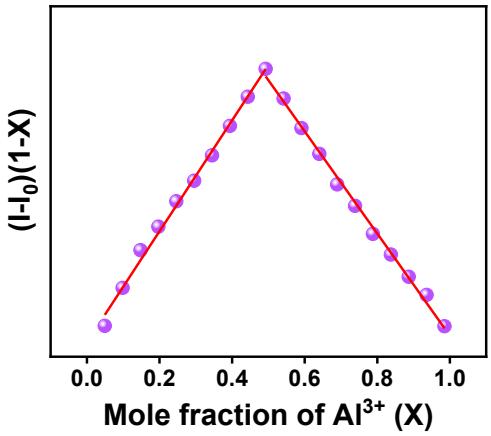

Fig. 3.7. Job's plot of **QnSb** for Al^{3+} determined by the fluorescence method indicating 1:1 stoichiometry.

DFT calculations have also been carried out to establish the binding mechanism between **QnSb** and Al^{3+} ion. The optimized structures of free probe **QnSb** and its Al^{3+} adduct (i.e., **QnSb**-Al^{3+}) are presented in Fig. 3.8. DFT based optimizations have been measured on the conformations based on ESI-mass analyses. The mass peak at *m/z* 554.1699 corresponds to 1:1 binding stoichiometry. In complex **QnSb**-Al^{3+}, metal ion occupies five coordination sites from **QnSb**. For **QnSb**-Al^{3+}, the computed Al-N_{imine} and Al-$N_{quinoline}$ bond distances were found to be 2.1120 Å and 2.0988 Å, respectively (Annexure I, Table A1). The HOMO-LUMO energy data of **QnSb** and its complex **QnSb**-Al^{3+} are shown in Fig. 3.8. The deep-red colored lobes represent the positive phases while the green ones represent the negative phases of *pi* molecular orbitals. As shown in Fig. 3.8, the HOMO-LUMO gap in free **QnSb** is 3.7152 eV; however, this energy gap is substantially reduced to 2.6928 eV after complexation. Therefore, the binding mechanism underlying the probe's ability to detect Al^{3+} is supported by this data. Based on all these findings, the following mechanistic pathway for interaction between **QnSb** and Al^{3+} has been proposed (Scheme 3.2). The Al^{3+} ion coordinates to the S atom in (thiobis)ethylamine moiety, two N atoms of the imine group and two N atoms of the quinoline moieties. The fluorescence enhancement in the presence of Al^{3+} has been attributed to CHEF effect and inhibited >C=N- isomerization due to the

formation of the stable **QnSb**-Al^{3+} complex (Dutta et al., 2017.; Kumar et al., 2019; Sheet et al., 2012).

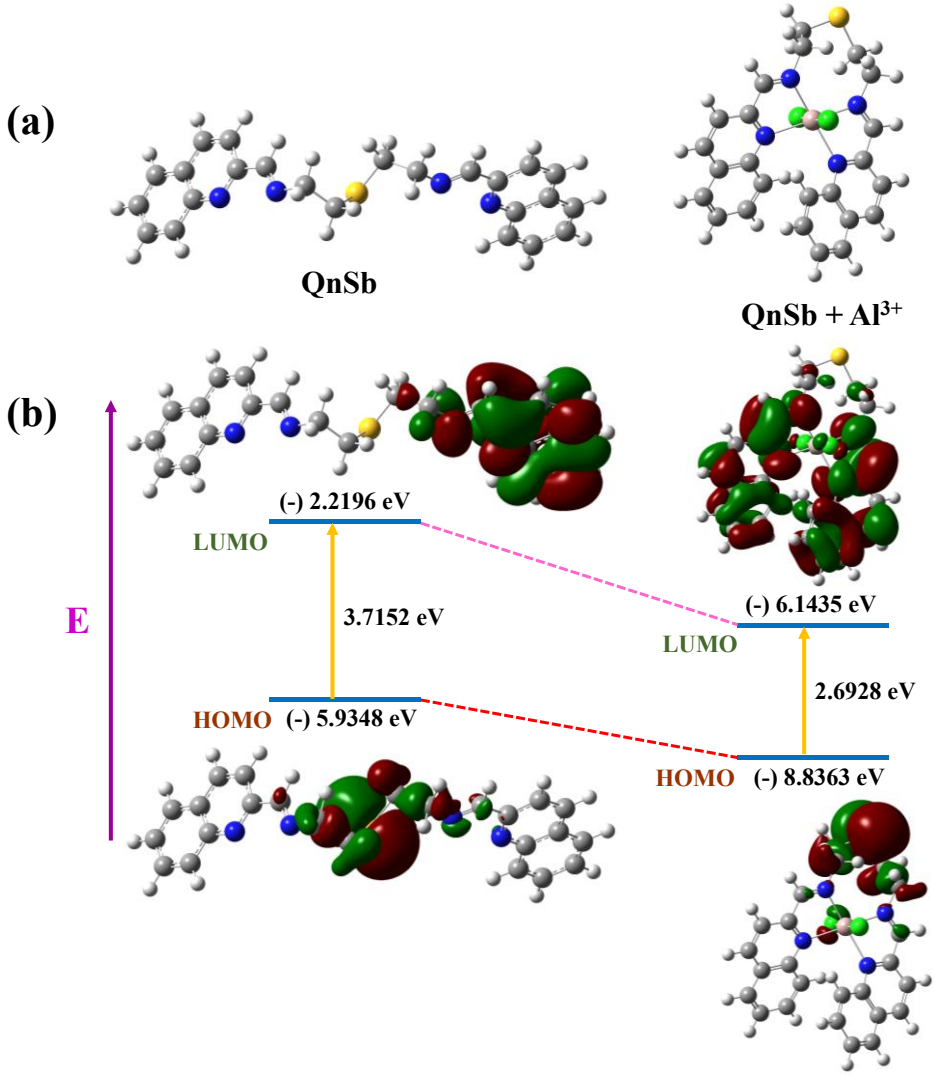

Fig. 3.8. The frontier molecular orbitals and the optimized geometries of **QnSb** and **QnSb**-Al^{3+} complex.

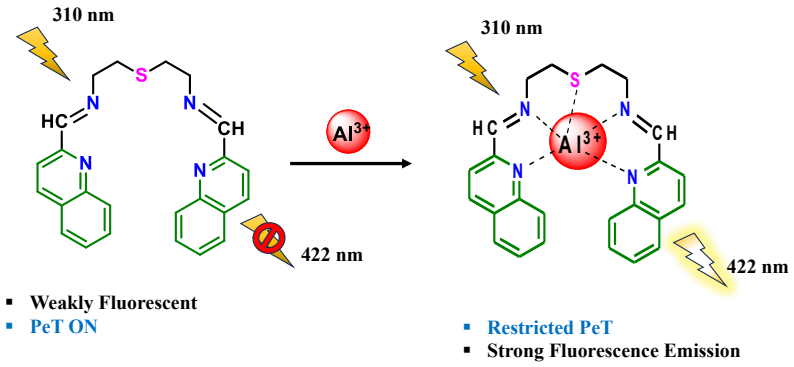

Scheme 3.2. Proposed binding mode of **QnSb** with Al^{3+} ion.

3.3.5 Reversibility and logic gate analysis

The reversibility, sustainability and reusability of a fluorescent sensor are essential components in terms of its real time applications. The reversibility of fluorescence spectral reaction of **QnSb**-Al^{3+} has been examined using a strong chelating agent i.e., EDTA (ethylenediaminetetraacetate) ion. The EDTA ion displays preferential binding with Al^{3+} to afford a highly stable Al^{3+}-EDTA complex (Lu et al., 2020). As shown in Fig. 3.9(a), Al^{3+} ion exhibits enhancement in the fluorescence intensity of **QnSb**; however, the addition of Na_2EDTA resulted in the fluorescence quenching and restored the original fluorescence of **QnSb** (almost non-fluorescent) up to 3 cycles (Annexure I, Fig. A9). The addition of 3.0 equiv EDTA had no effect on the emission band of free probe **QnSb** which indicated that the quenching was due to the decomplexation of **QnSb**-Al^{3+} (Annexure I, Fig. A10). The fluorogenic sensing of **QnSb** for Al^{3+} was also studied in a molecular logic circuit in which Al^{3+} and EDTA ions were used as two inputs (IN 1 for Al^{3+} and IN 2 for EDTA), and the obtained fluorescence at 422 nm served as one output. The threshold emission intensity was fixed at 500 for the detection of Al^{3+} ion (Fig. 3.9(b)). The emission above and below this threshold value was allocated as "ON" and "OFF" for "on" and "off" output signals, respectively. A simple symbolic representation of INHIBIT logic gate with two input lines is shown in Fig. 3.9(b). Al^{3+} input line goes into a single-input OR gate and EDTA input line goes into NOT gate while output from the NOT gate goes into the OR gate. In this case, OR gate output is the emission intensity of probe **QnSb** at 422 nm. Such a logic gate analysis suggests

that this single fluorogenic probe can perform arithmetic operations like a signal transmission computer.

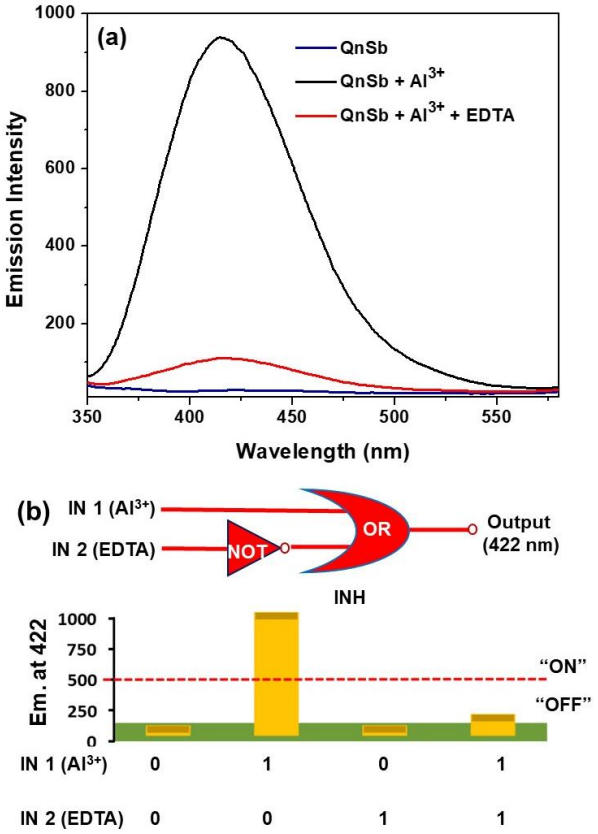

Fig. 3.9. Fluorescence outputs of probe **QnSb** at 422 nm in presence of chemical inputs *viz*. IN 1 = Al^{3+} and IN 2 = EDTA and the corresponding two-input combinational logic circuit.

3.3.6 Low-cost recognition: Colorimetric and paper strips experiments

The detection of Al^{3+} was also investigated *via* low-cost colorimetric and filter paper strips experiments due to their practicality, affordability, convenience, portability, and disposable features. At low concentrations in CH_3CN-H_2O solution (*ca.* 10^{-4} M), the probe **QnSb** displayed off-white color under visible and UV light illumination. The addition of Al^{3+} induced a detectable solution color change from off-white to light purple (obvious to naked eye) under UV region; however, other metals produced negligible visual changes (Fig. 3.10). For Al^{3+} monitoring on the paper strips, the finely shaped Whatman filter paper strips have been dipped into the CH_3CN solution of probe

QnSb, and then dried. These dried strips could be directly used for a rapid detection of metal ions by their immersion into the aqueous solutions of various metal ions. Like colorimetric analyses, a substantial fluorescence enhancement could be realized only in case of Al^{3+} among all the tested metal ions. Hence, it is feasible to selectively recognise Al^{3+} ion by probe **QnSb** in solution as well as solid-state under UV region, and this probe can be utilized for practical applications.

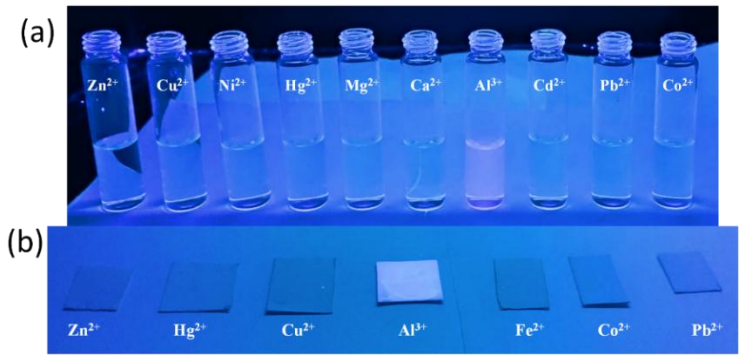

Fig. 3.10. Fluorogenic and chromogenic changes in **QnSb** upon addition of different metal ions under UV light (λ_{max}= 365 nm) (a) in CH_3CN-H_2O solution and (b) on paper strips.

3.4. Conclusions

In summary, a simple quinoline-based fluorescent sensor **QnSb** has been synthesized and characterized using various spectral techniques, and the structure of **QnSb** was depicted by SC-XRD analysis. **QnSb** exhibited strong 'turn-on' fluorescence response toward Al^{3+} over other competing metal ions in semi-aqueous medium. The high selectivity of **QnSb** for Al^{3+} was attributed to the chelation-enhanced-fluorescence effect and restricted >C=N- isomerization. The solution of **QnSb** exhibited a color change from pale-yellow to purple-red under visible light enabling this probe a naked eye indicator for Al^{3+} ions. A 1:1 binding stoichiometry was established for **QnSb**-Al^{3+} complex with the help of job's plot, ^{1}H NMR, ESI-mass and DFT analyses. Addition of Na_2EDTA to the solution of **QnSb**-Al^{3+} induced an 'on-off' type fluorescence response, suggesting the reversibility and reusability of probe **QnSb**. Furthermore, an INHIBIT type logic gate was created using **QnSb**- Al^{3+} and EDTA as inputs and the emission intensity at 422 nm as output.

CHAPTER 4

TURN-ON DETECTION OF Al^{3+} ION BY QUINOLINE-BASED TRIPODAL PROBE: MECHANISTIC INVESTIGATION AND LIVE CELLS IMAGING APPLICATIONS

4.1 State of the art

The development of efficient methods for the rapid and selective detection of metal ions is an extremely important research area, particularly in environmental and biological settings. This is due to the extensive use of metal ions in various essential fields of human social life, materials science, industries, medicine, and biology (Alam et al., 2021; Li et al., 2022; Pak et al., 2021; Qiao et al., 2021; Xu et al., 2022; Zhou et al., 2017). Among the pool of metals, aluminium (Al) is of great interest considering its significant role in our day-to-day life. Aluminium is the 3rd most abundant metallic element (about 8.0% by mass) found in the Earth's crust (He et al., 2019; Singh et al., 2013; Zhao et al., 2020). Al-based food additives, pharmaceuticals, cooking utensils, containers and contaminated drinking water are the key sources allowing the entry of this metal in living beings (Gui et al., 2015; Islam et al., 2024; Krewski et al., 2007; Liu et al., 2022; Dathees et al., 2024). Though Al is a non-essential element to humans; anthropogenic activities result in increased Al^{3+}-based pollution causing adverse health effects, e.g., Alzheimer's disease, Parkinson's disease, and even breast cancer (Nayak et al., 2002; Fasman et al., 1996; Samanta et al., 2023; Shen et al., 2023; Xu et al., 2021). The permissible limit for aluminium intake in humans is 3-10 mg per day, as set by the World Health Organization (WHO) (Li et al., 2021). Consequently, there is an increasing interest in the research focusing on detecting low concentrations of Al^{3+} ions in chemical, environmental and biological samples (Sharma et al., 2024).

Among the various other metal ion detection approaches, fluorescence-based methods offer substantial advantageous features such as short reaction

time, simple operation, and high sensitivity/selectivity without the need for any sophisticated instrumentation (Guo et al., 2021; Singha et al., 2019). However, the development of Al^{3+}-responsive fluorescent molecular probes is a challenge due to the poor coordination ability and strong hydrophilicity of this metal ion. A high charge-to-radius ratio makes Al^{3+} a hard acid in nature, and thus, fluorescent probes integrated with hard donor atoms (N, O, etc.) must display strong binding affinity towards Al^{3+} ions (Balasubramanian et al., 2023; Naithani et al., 2023; Zeng et al., 2019). In the recent past, a large number of small molecules-based fluorescent probes (both organic and inorganic probes) have been developed; however, many of them suffer from tedious synthetic routes. In addition, other interfering metal ions such as Fe^{3+}, Zn^{2+} and Cu^{2+} have become real concerns for many fluorescent probes to be exhaustively selective for Al^{3+} ions. Hence, the development of easily synthesizable fluorescent probes with selective response to a particular metal ion is always on high demand (Anu et al., 2021; Patil et al., 2019; Wang et al., 2021). In this effort, Schiff base compounds have seen gradual growth owing to their essential features, including synthetic ease, less or no sensitivity toward air and moisture, optical tunability, and strong metal binding ability (Samanta et al., 2023; Kalavathi et al., 2023). Contextually, a diverse panel of Schiff base probes have been employed for fluorescence-based detection of various analytes such as cations (Wang et al., 2019; Shellaiah et al., 2024; Shellaiah et al., 2013, 2022), anions (Fu et al., 2019), pesticides (Kateshiya et al., 2023; Kumar et al., 2024), and antibiotics/drugs (Afrin et al., 2023; Goshisht et al., 2022; Lu et al., 2024; Zhou et al., 2022); nevertheless, only a few demonstrate the use of quinoline as a fluorophore (Goswami et al., 2024; Jun et al., 2018). Distinctive from other derivatives, the quinoline-based molecular probes display significant advantages such as good solubility in water, remarkable Stokes shift, and high biocompatibility (Zhou et al., 2018). Several medicinally active compounds and advanced functional materials involve quinoline as an important motif for their construction (Fan et al., 2020).

Considering all these facts, we herein demonstrate a quinoline-derived Schiff base, **TQSB** (Scheme 4.1), acting as a highly selective and sensitive

fluorescent and colorimetric Al^{3+}-responsive probe. Al^{3+} is a hard acid that preferentially coordinates with the receptors comprising hard donor bases such as imine-N, amine-N, and -OH (Goswami et al., 2023; Kumar et al., 2021; Sharma et al., 2023). Along these lines, the probe **TQSB** has been integrated with the hard donor quinoline, imine and amine nitrogen atoms to provide an extraordinary coordination sphere for the selective detection of Al^{3+} ions over other metal ions (Balasubramanian et al., 2023; Zeng et al., 2019). The coordination of Al^{3+} with the probe restricts the PET effect and >C=N- isomerization and displays a typical CHEF effect to eventually provide a turn-on fluorescence response (Wang et al., 2018). The metal ion sensing ability of **TQSB** was investigated using UV-Vis and fluorescence spectral techniques, while the binding mechanism was established using job's plot, ^{1}H NMR spectroscopy, mass spectrometry, and DFT analyses. An advanced level logic gate was constructed using a strongly chelating EDTA ligand. For onsite Al^{3+} detection, this probe was applied onto filter paper strips as well as in gastric tablets. Moreover, we investigated the practical application of our sensing system to image Al^{3+} in real-life matrices such as soil samples and live cells.

4.2 Experimental section

4.2.1 Synthesis of the probe TQSB

Schiff base probe **TQSB** was easily synthesized *via* a one-step condensation reaction between quinoline 2-carboxaldehyde and tris(2-aminoethyl)amine. Briefly, a batch of quinoline 2- carboxaldehyde (0.471 g, 3.0 mmol) and tris(2-aminoethyl) amine (0.149 g, 1.0 mmol) was taken in 30 mL absolute ethanol, and the reaction mixture was stirred at room temperature for three hours. The color of the solution turned brown from light yellow. A brown precipitate was obtained upon addition of 25 mL of diethyl ether, following by cooling in an ice bath for 2 hours. The obtained precipitate was filtered out, washed a few times with diethyl ether, and dried under vacuum for 3 hours to give a brown solid in 44% yield. Anal. Calcd for $C_{36}H_{33}N_7$: C, 76.71; H, 5.90; N, 17.39; Found: C, 72.26; H, 5.68; N, 14.98. FT-IR (KBr disk): 2841, 1956, 1636 (>C=N-), 1498, 836, 753 and 614 cm^{-1}. UV-Vis (CH_3CN: H_2O, 4:1; *v/v*): $\lambda_{max/nm}$ ($\varepsilon/M^{-1}\ cm^{-1}$) = 245 ($9.8 \times 10^4\ M^{-1}\ cm^{-1}$), 291 ($1.8 \times 10^4\ M^{-1}\ cm^{-1}$), 240 ($9.0 \times 10^4\ M^{-1}\ cm^{-1}$) and 302 ($1.7 \times 10^4\ M^{-1}\ cm^{-1}$). ^{1}H NMR ($CDCl_3$, 500 MHz,

TMS), δ (ppm): 8.51 (s, 3H, imine), 8.04 (s, 6H), 8.01 (d, 3H), 7.72 (dd, 3H), 7.68 (t, 3H), 7.51 (t, 3H), 3.89 (t, 6H, -CH_2-N_{imine}), 3.09 (t, 6H, -CH_2- N_{amine}). ^{13}C NMR ($CDCl_3$, 500 MHz, TMS), δ (ppm): 163.39, 154.61, 147.61, 136.50, 129.67, 129.51, 128.62, 127.63, 127.26, 118.30, 59.86, 55.17. HR-MS (ESI-TOF) *m/z* Calcd. for $C_{36}H_{33}N_7$ = 563.2797; Found m/z = 586.2690 [**TQSB** + Na]$^+$.

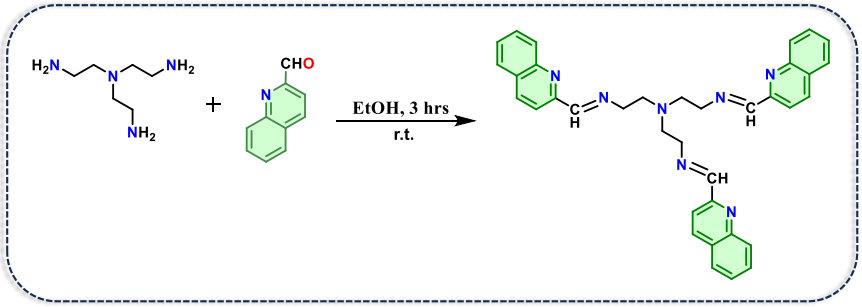

Scheme 4.1 Synthetic route to prepare Schiff base probe **TQSB**.

4.2.2 Absorption and emission spectra

Fluorescence and UV-Vis spectroscopy experiments were conducted at room temperature in an organic-aqueous (CH_3CN: H_2O = 4:1; *v/v*) solvent mixture due to the poor solubility of the probe in pure water. All emission spectral data for **TQSB** were measured from 340 nm to 560 nm at an excitation wavelength of λ_{ex} = 310 nm. The stock solutions of **TQSB** (2.0×10^{-4} M) and assorted metal ions (1.0×10^{-4} M) were prepared in CH_3CN and distilled water, respectively.

4.2.3 DFT studies

DFT calculations were performed without symmetry constraints using the Gaussian09W software package. The geometries of the probe **TQSB** and its complex **TQSB**-Al^{3+} were derived *via* a semi-empirical PM3 level molecular framework. Their geometries were then optimized by employing B3LYP with the G-311G++(d,p) basis set for C, N, and O atoms. Moreover, the LANL2DZ basis set was utilized for Al^{3+} with an effective core potential. The relevant bond parameters and energy levels obtained from the optimized geometries are listed in Tables A2 and A3 (Annexure I).

4.2.4 Analysis in real samples

The practical applicability of the probe was validated by using soil samples and Digene gastric tablets. A batch of 0.5 mg of soil sample was vigorously mixed in 10 mL CH_3CN followed by its centrifugation at 5000 rpm for 30 min. Thereafter, the sample was filtered using Whatman Grade 1 filter paper. The gastric tablet was finely crushed, sonicated and left overnight in a CH_3CN solution, followed by filtration using Whatman filter paper. The solution was then diluted to 50 mL. The prepared soil and gastric tablet samples were spiked with known concentrations of Al^{3+} ions and were mixed with the **TQSB** solution. The fluorescence spectra were recorded after 10 min incubation and compared with the calibration curve.

4.3 Results and discussion

4.3.1 Syntheses and characterization of TQSB

To synthesize the compound **TQSB**, an equimolar mixture of tris-(2-aminoethyl)amine and quinoline 2-carboxaldehyde was condensed in absolute ethanol at room temperature. **TQSB** was characterized by standard spectroscopic and analytical techniques such as FT-IR, ^{1}H NMR, ^{13}C NMR, UV-Vis, photoluminescence, elemental, and ESI-MS (electrospray ionisation mass spectrometry) analyses. **TQSB** exhibited a very low solubility in ethanol and water but was found appreciably soluble in most of the organic solvents including dichloromethane, chloroform, tetrahydrofuran, acetonitrile, dimethyl sulfoxide, and dimethyl formamide.

^{1}H NMR spectrum of **TQSB** exhibited all the aliphatic as well as aromatic resonances in the expected regions (Annexure I, Fig. A11). A singlet near 8.51 ppm could be assigned to the imine -CH=N- protons, whereas two triplets for methylene protons were noticed at 3.88 ppm ($-N_{imine}-CH_2-$) and 3.09 ppm ($-N_{amine}-CH_2-$), respectively. ^{13}C NMR spectrum of **TQSB** further displayed a clear signal near 163 ppm corresponding to the C atom of imine. In addition, the aromatic carbon atoms showed resonances ranging from 154.60 to 118.31 ppm, whereas the methylene carbon atoms of $-N_{imine}-CH_2-$ and $-N_{amine}-CH_2-$ appeared at 59.83 ppm and 55.14 ppm, respectively (Annexure I, Fig. A12). The infrared spectrum of **TQSB** revealed a stretching frequency around 2930 cm^{-1} due to the presence of methylene ($>CH_2$) groups, while an intense

peak near 1640 cm^{-1} could be attributed to the azomethine (>C=N-) groups (Fu, Li, et al., 2019). Moreover, the ESI-MS analysis of **TQSB** yielded the exact mass of *m/z* 586.2723 matching well with its theoretical mass of 586.2690 (Annexure I, Fig. A13).

4.3.2 Optical sensing of Al^{3+} ions

Both emission and absorption studies were employed to examine the sensing ability of **TQSB** for various metal ions such as Ca^{2+}, Cu^{2+}, Cd^{2+}, Zn^{2+}, Co^{2+}, Cr^{3+}, Hg^{2+}, Ni^{2+}, Mg^{2+}, Pb^{2+}, Fe^{3+}, Sn^{2+}, In^{3+}, Mn^{2+}, and Al^{3+} ions. Probe **TQSB** (3.0 μM) exhibited a very weak fluorescence intensity near 414 nm (probably due to >C=N- isomerization process) when excited at 310 nm in an acetonitrile-water (4:1, *v/v*) solvent mixture. Other metal ions including Ca^{2+}, Cu^{2+}, Cd^{2+}, Zn^{2+}, Co^{2+}, Cr^{3+}, Hg^{2+}, Ni^{2+}, Mg^{2+}, Pb^{2+}, Fe^{3+}, Sn^{2+}, In^{3+}, and Mn^{2+} (1.4 equiv) produced negligible changes in the fluorescence behavior of the probe; however, Al^{3+} induced a significant fluorescence enhancement when added to the probe (Fig. 4.1). The emission titration experiments conducted *via* sequential addition of Al^{3+} (0-1.4 equiv) clearly exhibited a gradual enhancement in the fluorescence intensity of **TQSB**. The probe **TQSB** also showed a drastic increase in the quantum yield after the addition of Al^{3+} ions from Φ_{TQSB} = 0.058 to $\Phi_{TQSB\text{-}Al3+}$ = 0.464. At nearly 1.3 equiv of Al^{3+}, the enhanced fluorescence reached saturation, suggesting a 1:1 binding stoichiometry. Furthermore, UV-Vis analysis was performed to investigate the sensing ability of **TQSB** for Al^{3+} ions. The probe **TQSB** displayed two absorption bands centred at 245 nm ($\varepsilon = 9.8 \times 10^4$ $M^{-1}cm^{-1}$) and 291 nm ($\varepsilon = 1.8 \times 10^4$ $M^{-1}cm^{-1}$). Significant absorption changes could be observed in the spectral profile of **TQSB** when treated with Al^{3+} in a semi-aqueous medium. The absorption band centred at 245 nm exhibited a blue shift to 240 nm, while the band near 291 nm red-shifted to 302 nm. Two clear isosbestic points could also be noticed at 243 nm and 254 nm, indicating a newly formed species between **TQSB** and Al^{3+} ions (Fig. 4.2). The absorption changes of **TQSB** in the presence of Al^{3+} were also associated with a solution color change from brown to pale yellow. The free probe **TQSB** exhibited significant Stokes shift (*ca.* 124 nm) effectively separating the excitation and emission bands. Furthermore, **TQSB**-Al^{3+} exhibited a Stokes shift of 119 nm. This is an

extremely desirable feature for a fluorescent probe for accurate and sensitive fluorescence detection of analytes (Annexure I, Fig. A14).

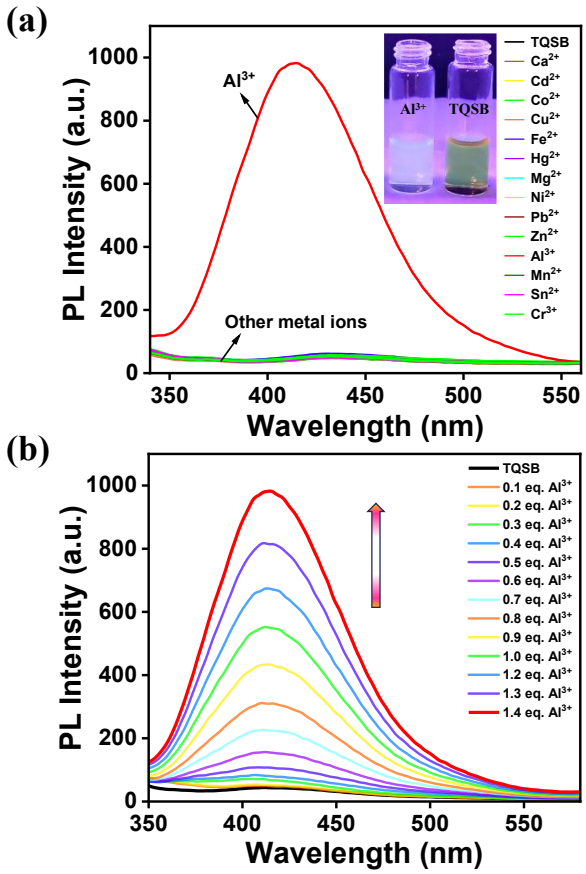

Fig. 4.1 (a) Emission changes in **TQSB** (3.0 μM) in an organic-aqueous (CH_3CN: H_2O = 4:1; *v/v*) solvent mixture with different metal ions (1.4 equiv) and (b) Emission titration profile for **TQSB** (3.0 μM) after successive addition of Al^{3+} ions (0-1.4 equiv).

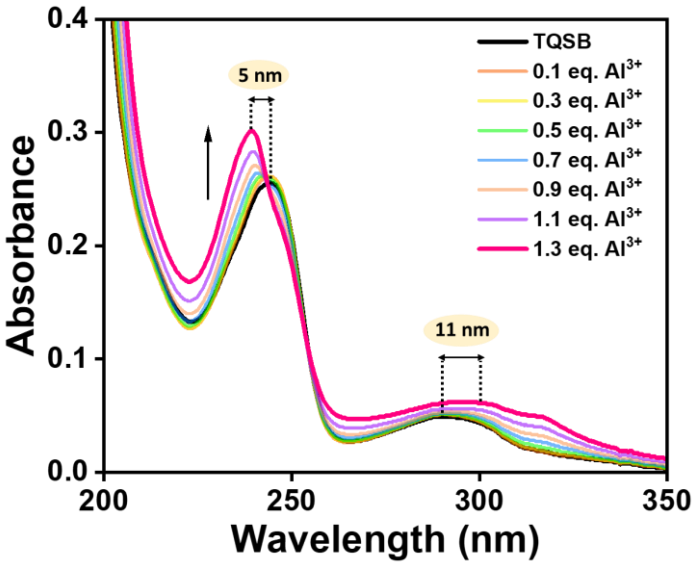

Fig. 4.2 Absorption spectral changes in **TQSB** (3.0 μM) upon successive addition of Al^{3+} ions (0-1.3 equiv.) in an organic–aqueous (CH_3CN: H_2O = 4:1; *v/v*) solvent mixture.

4.3.3 Competitive binding studies

The selective response of **TQSB** for Al^{3+} ions was further evaluated in the presence of other metal ions by a competitive binding assay (Gong et al.; 2022). We have measured the emission of **TQSB** at 414 nm with Al^{3+} ions in the presence of equal quantities of other competing metal ions (Fig. 4.3). The ability of the probe **TQSB** to detect Al^{3+} ions was not significantly impacted by the competing metal ions. Because of this, the probe **TQSB** can be used as an efficient probe to sense Al^{3+} in complex environmental and biological media. To measure the extent of metal ion binding, the detection limit (LoD) (Fig. 4.4) and the binding constant (K_b) (Annexure I, Fig. A15) values were computed using emission titration profiles which were depicted as 7.0 nM and 3.8×10^6 M^{-1}, respectively. The analytical performance of the probe was also compared with the previously reported probes as shown in Table 4.1.

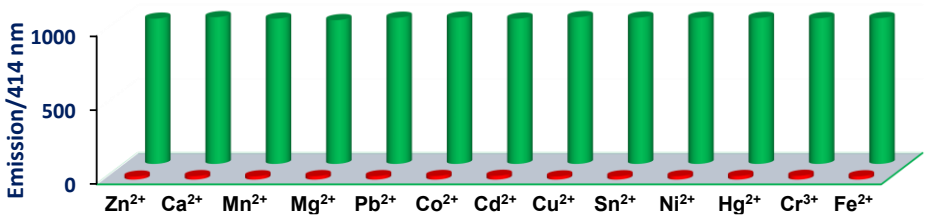

Fig. 4.3 Selectivity studies of probe **TQSB** towards Al^{3+} ions over other metal ions; **TQSB** + metal ion (red bars) and **TQSB** + metal ion + Al^{3+} (green bars).

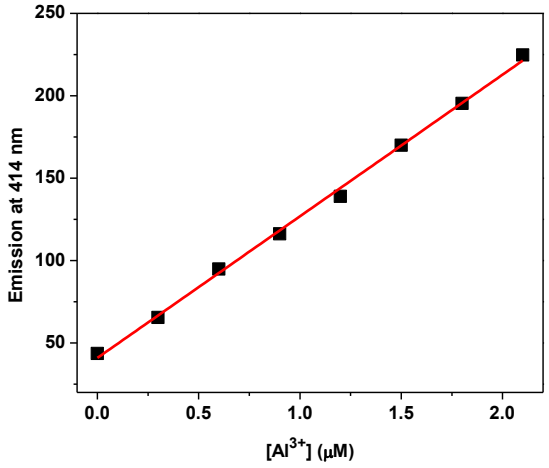

Fig. 4.4 Calibration curve obtained for the determination of Al^{3+} by **TQSB** in CH_3CN/H_2O (4:1; *v/v*) solution.

4.3.4 pH effect and response time

The effect of pH on the fluorescence intensity of **TQSB** and its **TQSB**-Al^{3+} adduct was investigated over a range of pH from 2.0 to 12.0. At pH 2.0, the free probe exhibited considerable fluorescence response; however, it was almost pH independent in the range of pH from 3.0 to 12.0. The enhanced fluorescence in the acidic region can be ascribed to the protonation of N atoms available with tris-(2-aminoethyl)amine and quinoline moieties. In case of **TQSB**-Al^{3+}, the original fluorescence significantly quenched under both highly acidic and basic conditions. At acidic pH (2.0-4.0), Al^{3+} may display competition with H^+ ions, while a highly basic medium (pH 10.0-12.0) may favour the generation of $Al(OH)_3$, ultimately leading to restoration of free probe. As a result, **TQSB**-Al^{3+} exhibited a poor emissive response in strong acidic and basic media. In contrast, a remarkable fluorescence enhancement of **TQSB**-Al^{3+} was observed at pH 5.0-10.0, which clearly indicates that **TQSB** can be potentially applied to recognize

Al^{3+} in real-time applications (Annexure I, Fig. A16). The time required for the detection of Al^{3+} ions by **TQSB** was also depicted using time-dependent studies up to 45 minutes, suggesting an instantaneous enhancement response (Annexure I, Fig. A17).

4.3.5 Binding mechanism studies

The binding mechanism between **TQSB** and Al^{3+} was established using Job's plot, ESI-mass spectrometry, and DFT analyses. Job's plot study exhibited a 1:1 binding stoichiometry for the formation of complex **TQSB**-Al^{3+}, as shown in Fig. 4.5. ESI-mass spectrometry study further supported the formation of a **TQSB**-Al^{3+} adduct as *m/z* peaks at 718.3420 and 734.3414 could be ascribed to the presence of [**TQSB** + Al^{3+} + Na^+ + $3Cl^-$]$^+$ and [**TQSB** + Al^{3+} + K^+ + $3Cl^-$]$^+$ species, respectively (Annexure I, Fig. A18). ^{1}H NMR analysis of **TQSB**-Al^{3+} clearly indicated that the imine proton of free **TQSB** resonating at 8.51 ppm shifted downfield at 8.55 ppm upon addition of 1.0 equiv of Al^{3+} to **TQSB**. Furthermore, other aromatic protons were found slightly shifted upon complexation (Annexure I, Fig. A19). The enhanced fluorescence in **TQSB** can be attributed to the strong complexation between **TQSB** and Al^{3+} ions to give a **TQSB**-Al^{3+} adduct, leading to the chelation-enhanced fluorescence effect. Initially, **TQSB** was almost non- fluorescent due to the related >C=N- isomerization process in its excited state (Park et al., 2014; Yang et al., 2024) together with the photoinduced electron transfer (PeT) arising from the N atom of the imine group (donor) to the excited-state fluorophore (acceptor) (Kshirsagar et al., 2020; Li et al., 2020; Liu et al., 2013; Wang et al., 2015; Wang et al., 2017; Yang et al., 2024; Zhou et al., 2020; Zhu et al., 2023). Three imine-N atoms along with three quinoline-N atoms act as hard donor sites to preferentially bind with hard Al^{3+} ions. Such a strong binding results in restricted >C=N- isomerization and subsequently N6 binding to Al^{3+} blocks the PET process- both the effects combinedly become conducive to enhanced fluorescence of **TQSB** in complex **TQSB**-Al^{3+}. (Bu et al., 2020; Kumar et al., 2019; Bhatta et al., 2017; Gupta et al., 2016; Jung et al., 2010; Li et al., 2010; Ray & Bharadwaj, 2008; Wu et al., 2007; Wu et al., 2007; Zhao et al., 2011)

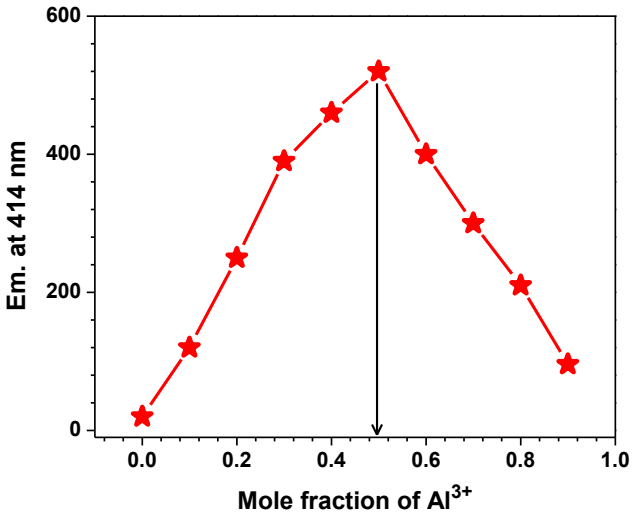

Fig. 4.5 Job's plot of **TQSB** for Al^{3+} determined using the fluorescence method indicating 1:1 stoichiometry.

The binding mechanism between **TQSB** and Al^{3+} was further assessed *via* DFT analysis using the Gaussian-09 program. The LANL2DZ (B3LYP level) and 6-31G+(d,p) basis sets were used for Al and other atoms, respectively (Prabha et al., 2021). The optimized geometries of the probe **TQSB** and complex **TQSB**-Al^{3+} are shown in Fig. 4.6, together with their frontier molecular orbitals, i.e., HOMO (highest occupied molecular orbital) and LUMO (lowest unoccupied molecular orbital). In complex **TQSB**-Al^{3+}, the metal ion is coordinated with six nitrogen atoms (all quinoline and imine N atoms), and the bond parameters are found consistent with the previously reported data (Al-N_{imine} = 2.04638-2.15962 Å and Al-$N_{quinoline}$ = 2.04614-2.15956 Å) (Annexure I, Table A2) (Goswami et al., 2024; Goyal et al., 2023). The electrostatic potential maps (ESP) are typically used to recognize the active sites in a host for guest analyte binding. The red regions are areas of high charge density and correspond to electrophilic attack (Huang et al., 2020). As observed in Fig. A20 (Annexure I), the red region is located over the N atom of the imine and quinoline groups, and therefore, these are preferred metal ion binding sites. The HOMO in the free probe was primarily located over the tris-(2-aminoethyl)amine unit, while its LUMO was majorly distributed over one of the quinoline moieties. Notably, the HOMO was found to significantly stabilize after complexation (−5.4017 eV in **TQSB**; −13.7156 eV in **TQSB**-Al^{3+}),

suggesting a very strong binding between **TQSB** and Al^{3+} ions. In **TQSB**, the free electron from the HOMO of the donor group is transferred to the low-lying HOMO of the acceptor, indicating quenching response in the free probe. The complexation results in a drastic decrease in the HOMO level of the donor, thereby restricting the electron transfer and ultimately resulting in the fluorescence enhancement. These results support the existing PET mechanism as reported earlier (Ganguly et al., 2015).

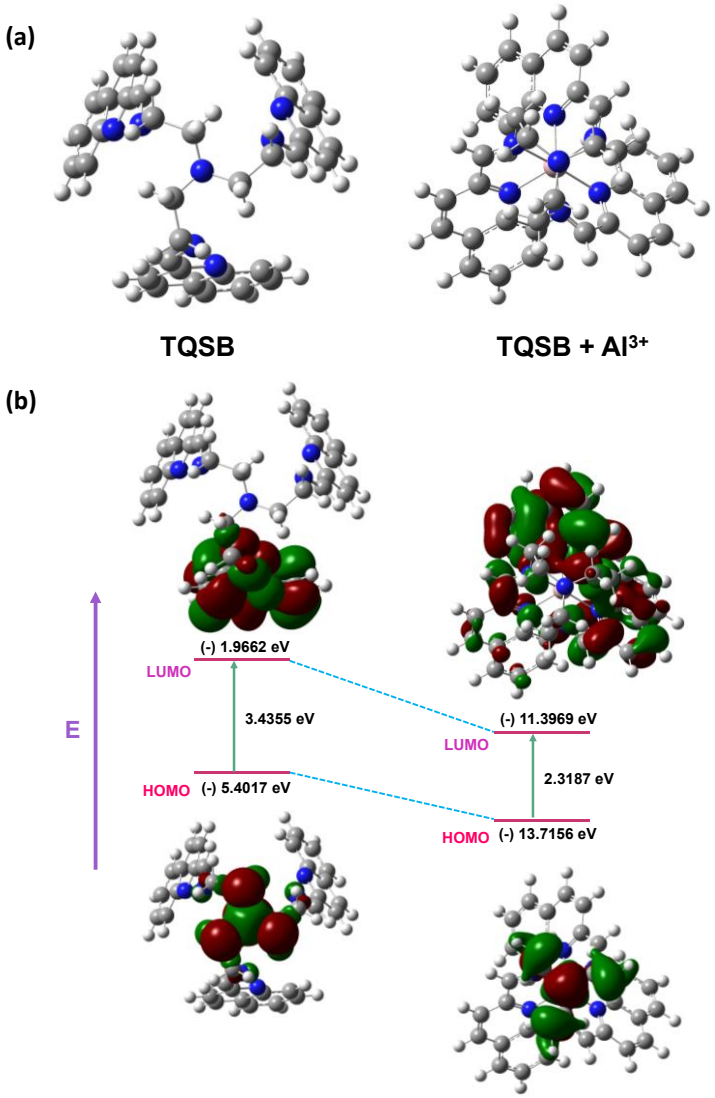

Fig. 4.6 (a) Optimized geometries and (b) frontier molecular orbitals of probe **TQSB** and complex **TQSB**-Al^{3+}.

Furthermore, the HOMO-LUMO energy gap (ΔE) of the **TQSB**-Al^{3+} adduct was found to be considerably lower (2.3187 eV) than that of the free

probe (3.4355 eV), which clearly suggests that the electronic/photophysical characteristics of **TQSB** are markedly influenced upon complexation (Annexure I, Table A3). These findings also aligned with the red-shift observed in the absorption spectrum of **TQSB** upon Al^{3+} chelation (Fig. 4.2). Based on these findings from Job's plot data, ESI-mass spectrometry and DFT analyses, a probable binding mode between **TQSB** and Al^{3+} is presented in Scheme 4.2.

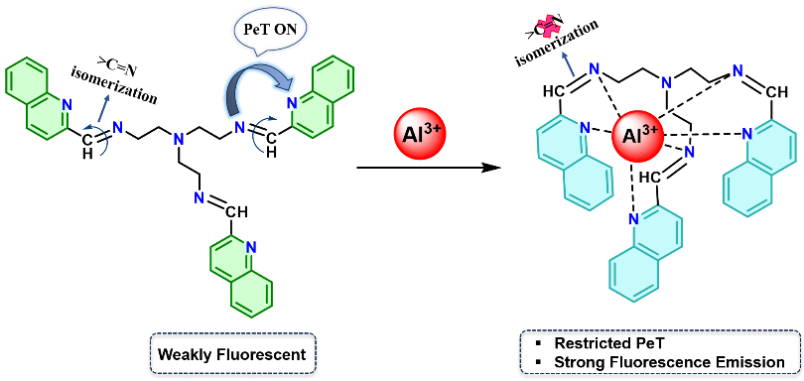

Scheme 4.2 Proposed binding mode of **TQSB** with Al^{3+} ions.

4.3.6 Reversibility studies and logic gate

The reversibility, sustainability, and reusability of a sensor play crucial roles in its real-time applications. The reversible performance of **TQSB**-Al^{3+} could be successfully attained by using a potent chelating agent, i.e., ethylenediamine tetraacetate (EDTA). The Al^{3+} ion, a hard acid, displays a very strong affinity towards EDTA (a hard base), leading to the formation of a highly stable Al^{3+}-EDTA complex. As depicted in Fig. 4.7(a), the introduction of Al^{3+} ions led to an enhanced fluorescence intensity of **TQSB** at 414 nm; however, upon adding Na_2EDTA to **TQSB**-Al^{3+}, the original weakly fluorescence state of **TQSB** revived. Further addition of Al^{3+} ions to the **TQSB** + Al^{3+} + Na_2EDTA mixture caused the fluorescence intensity to reactivate. This outcome demonstrated that the reversible cycle could be repeated at least three times by alternating addition of EDTA and Al^{3+} ions (Annexure I, Fig. A21), and the corresponding INHIBIT logic gate was thus developed based on Boolean logic operations (Fig. 4.7(b)). The logic circuit and the truth table for **TQSB** were built using IN 1 = Al^{3+} and IN 2 = EDTA, while the emission intensity of **TQSB** at 414 nm served as an output. The emission intensities above and below the

threshold value (dotted line on bar diagram) were assigned as "ON" (1) and "OFF" (0) for "on" and "off" outputs, respectively. A symbolic representation of the INHIBIT logic gate having two inputs is presented in Fig. 4.7(b), where IN 1 (Al^{3+}) line leads to a single input OR gate and IN 2 (EDTA) line leads to a NOT gate, while the output from the NOT gate approaches the OR gate.

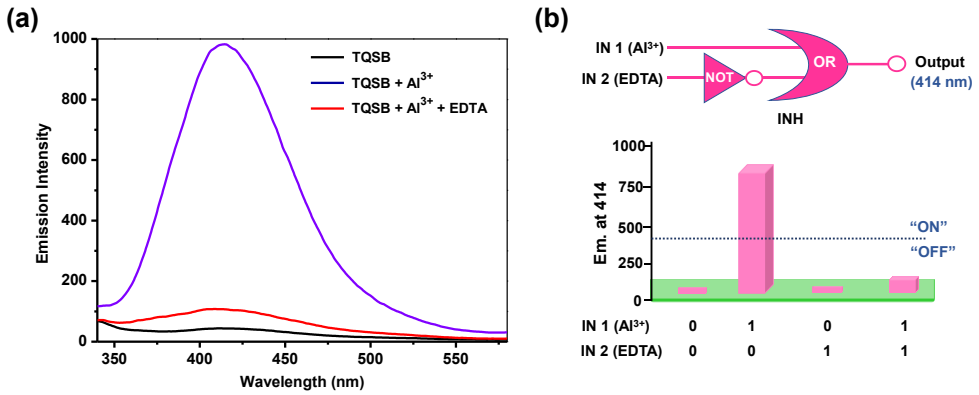

Fig. 4.7 (a) Reversibility studies for probe **TQSB** using EDTA for the detection of Al^{3+} ions. (b) Fluorescence outputs of probe **TQSB** at 414 nm in the presence of chemical inputs viz. IN 1 = Al^{3+} and IN 2 = EDTA, and the corresponding two-input combinational logic circuit.

4.3.7 Colorimetric and paper strip detection

We have also carried out the low-cost colorimetric as well as paper strip experiments for Al^{3+} detection using **TQSB**. To achieve better visualization, the stock solution of tested metal ions (*ca.* 10^{-2} M) was introduced to the solution of probe **TQSB** in different glass vials. Amongst the various metal ions studied, only Al^{3+} displayed enhanced fluorescence when exposed to UV light (Fig. 4.8); however, only nominal changes were observed in normal visible light. Test strips were prepared by finely cutting the Whatman filter paper. The strips were then immersed in a 10^{-2} M stock solution of **TQSB** for 30 minutes to attain uniform adsorption. The strips wet with **TQSB** were then dried and subsequently dipped into stock solutions (10^{-2} M) of assorted metal ions. A significant 'turn-on' emissive response could be observed in the presence of Al^{3+} under UV light illumination (Fig. 4.8), further illustrating the selective recognition ability of **TQSB** for Al^{3+} ions.

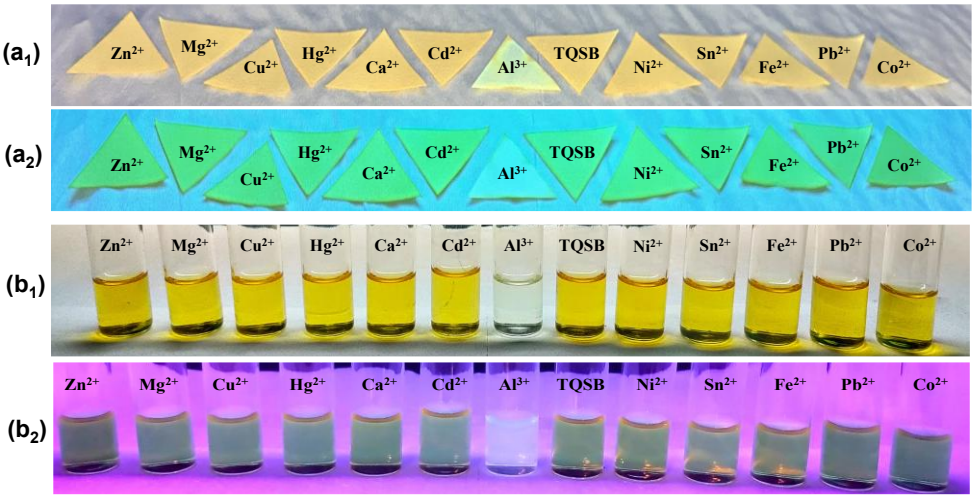

Fig. 4.8 Fluorogenic and chromogenic changes in **TQSB** upon addition of various metal ions (λ_{ex}= 310 nm) (a_1-a_2) on paper strips and (b_1-b_2) in CH_3CN-H_2O solution under visible and UV light, respectively.

4.3.8 Analysis of real samples

The use of gastric tablets as an Al^{3+}-rich medication is widely recognized to control gastrointestinal function. As a result, gastric tablets were selected as real samples to assess the sensing ability for Al^{3+} ion. Moreover, spiked soil samples were prepared to validate the sensing performance of **TQSB**. The standard addition recovery method was used to examine the Al^{3+} spike recovery in the extract (Annexure I, Table A4). The observations are displayed in Fig. 4.9, indicating strong fluorescence emission at 414 nm in the Al^{3+} spiked samples. These findings were consistent with earlier titration tests and indicated that **TQSB** has a great on-site detection ability for Al^{3+} in real samples via an easy-to-follow process with good recovery values.

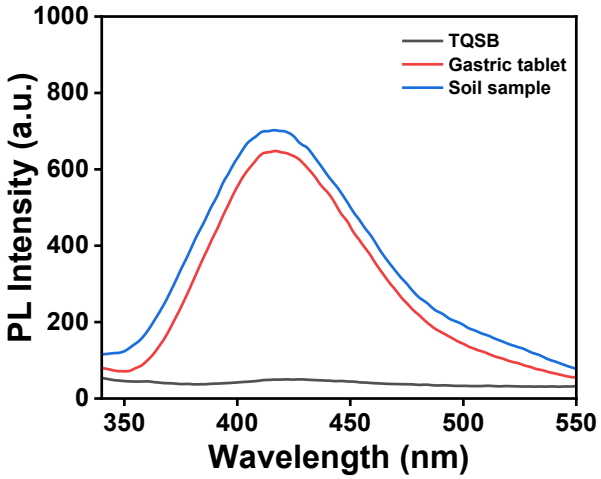

Fig. 4.9 Fluorogenic detection of Al^{3+} by **TQSB** in gastric tablets and soil samples.

4.3.9 Live cell imaging

The practical applicability of probe **TQSB** was validated for Al^{3+} imaging in biological media. Initially, the MTT assay revealed that the probe **TQSB** exhibited a low cytotoxicity at 10 μM and hence can be used for bioimaging applications (Annexure I, Fig. A22). The breast cancer MCF-7 cell lines were employed and incubated at 20 μM to 60 μM concentration of probe **TQSB**. As shown in Fig. A23 (Annexure I), no fluorescence response was observed even at higher concentrations after 4 hours due to the non-fluorescence nature of **TQSB**. In contrast, the incubation of **TQSB** labelled cells with different concentrations of Al^{3+} (40-100 μM) resulted in a drastic enhancement of fluorescence (Fig. 4.10). Therefore, the present results are in agreement with in vitro experiments, and demonstrate the potential of **TQSB** to selectively detect Al^{3+} ions.

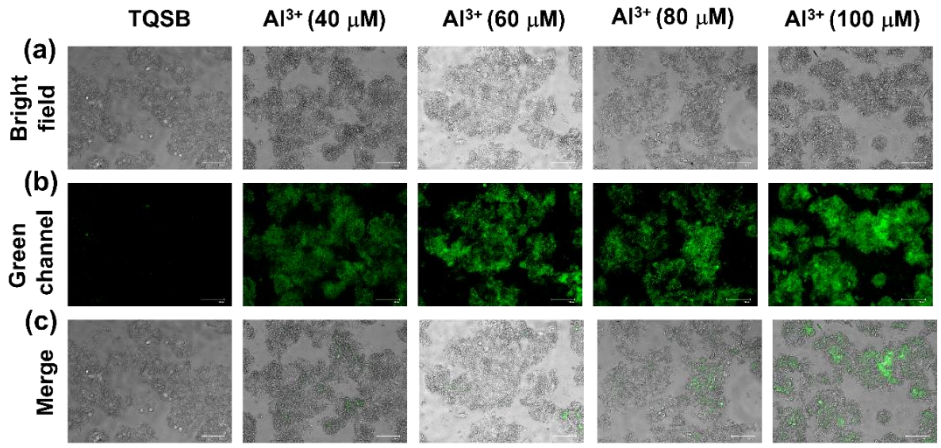

Fig. 4.10 Live cell imaging experiment for **TQSB** with Al^{3+} ions. (a) Brighfield images; (b) fluorescence images and (c) the overlap images.

Table. 4.1 Comparison of sensing parameters of probe **TQSB** with some previously reported probes.

S.No.	Probe	Target ions	LoD (μM)	Application	Ref.
1.	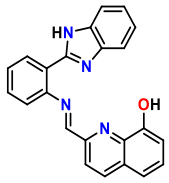	Al^{3+}	0.9	Bore water, drinking water, tap water, Live cell imaging	(Kalavathi et al., 2023)
2.	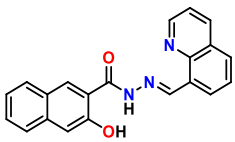	Al^{3+}, Fe^{3+}	0.0122 0.104	Tap water, bottled water	(Ding et al., 2021)
3.	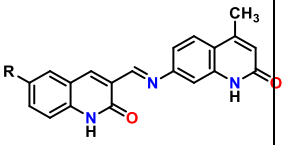	Al^{3+}, ClO^-	0.0298 0.025	Real water samples and Live cell imaging	(Zhang et al., 2023)

4.	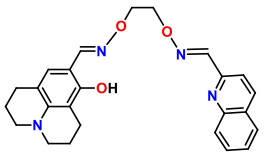	Al^{3+}, Zn^{2+}	0.097 0.21	Real water samples	(Man et al., 2024)
5.	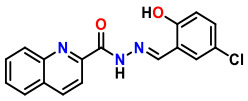	Al^{3+}	1.25	Bioimaging in living cells, plants and zebrafish	(Lu et al., 2021)
6.	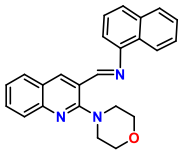	Al^{3+}, HSO_3^-	0.0021 0.0023	Drinking water and food samples	(David et al., 2022)
7.	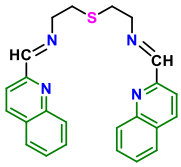	Al^{3+}	0.0158	Test paper strips	(Goswami et al., 2024)
8.	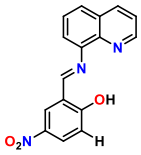	Al^{3+}	0.0235	Cell imaging	(Ghorai et al., 2020)
9.	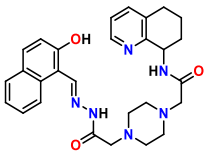	Al^{3+}	3.67×10^{-2}	Cell imaging	(Zeng et al., 2018)
10.	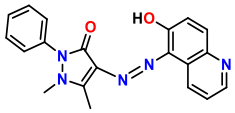	Al^{3+}	0.01	-	(Bartwal et al., 2020)
11.	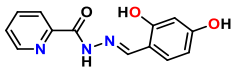	Al^{3+}	2.14×10^{-2}	Real water samples	(Peng et al., 2020)

12.	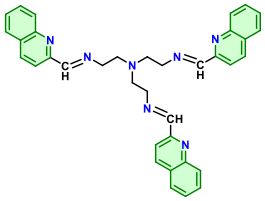	Al^{3+}	0.007	Live cell imaging, test paper strips, and digene tablet	This work

4.4 Conclusions

In this study, a quinoline-derived probe, **TQSB**, having N6 donor sites was demonstrated to specifically detect Al^{3+} ions in a semi-aqueous medium. Interestingly, the almost non-fluorescent probe **TQSB** served as a 'turn-on' sensor by emitting at 414 nm in the presence of Al^{3+} over other metal ions. The **TQSB** exhibited an appreciable detection limit of 7.0 nM for Al^{3+}, and was found highly selective for Al^{3+} even in the presence of other competing metal ions. The enhanced fluorescence response of **TQSB** for Al^{3+} could be ascribed to the CHEF effect together with the inhibition of both PeT and >C=N- isomerization processes. Job's plot, ESI-mass spectrometry, NMR spectroscopy and DFT analyses firmly supported a 1:1 binding between **TQSB** and Al^{3+} ions. This sensing behaviour of **TQSB** was found reversible when the adduct **TQSB**-Al^{3+} was treated with the chelating EDTA agent, and the respective logic gate and truth table were developed. In terms of its applied potential, **TQSB** was utilized to image Al^{3+} in real samples such as soil samples and gastric tablets. The low-cost colorimetric and paper-strip experiments were demonstrated for the fluorescence detection of Al^{3+} ions. Moreover, **TQSB** has been successfully used for fluorescence imaging of Al^{3+} in live cells, indicating that this simple and easily synthesizable sensor can be potentially applied for Al^{3+} detection in complex biological systems. In this endeavour, current efforts in our lab are directed towards the optimization of its applications in vivo, allowing for a real-time tracking of Al^{3+} distribution within live organisms.

CHAPTER 5

ISOLATION AND CHARACTERIZATION OF THE LABILE TETRAHEDRAL GEM-DIOL INTERMEDIATE IN THE AL(III)-CATALYZED HYDRATION OF AROMATIC ALDEHYDES

5.1 state of the art

The generation of geminal diols (gem-diols) is an example of nucleophilic addition type of reactions via covalent addition of water to the carbonyl compound (Crespi et al., 2018). This reaction is typically energetically unfavourable and reversible, favouring the regeneration of parent carbonyl compound. However, the formation of gem-diol from aldehydes is intriguing due to their crucial role in various physiological processes involving enzymes such as aldehyde dehydrogenases (ALDHs), HIV-protease, etc. ALDHs represents a key class of enzymes involving gem-diol during the catalytic conversion of aldehyde to carboxylic acid (Crespi et al., 2023). Similarly, gem-diols are employed by HIV-protease enzyme to facilitate peptide bond hydrolysis which is a vital step in HIV lifecycle. Therefore, stabilizing gem-diol is vital for accomplishing high catalytic efficiency in such enzymatic reactions. However, implementing these transformations in laboratory remains challenging due to less stability of aldehyde hydrate generated in situ (Crespi & Lázaro-Martínez, 2023).

As a result, numerous efforts have been spent for developing alternative synthetic approaches for stabilizing aldehyde hydrate by emulating the function of ALDHs (Crespi et al., 2016). In a notable study, Hamada's group demonstrated aldehyde hydrate formation in solution utilizing heteroaromatic aldehydes as substrates. This finding suggests strong hydrogen bond accepting solvents and intra-ring nitrogen promotes the generation of aldehyde-water adduct. Additionally, the covalent hydration is directly impacted by the position of carbonyl group within the pyridine species. Later, Hirota group investigated the solvents effect and reported that DMSO was the most effective hydrogen bond acceptor whereas CH_3CN was the least effective among investigated

solvents. This was further extended by Lazaro-Martinez group, which reported the stabilization of transient gem-diols in acidic medium therefore enhancing the hydration. Finally, Stark group demonstrated efficient stabilization of aldehyde-water adduct via *N*-morpholine-*N*-oxide (NMO) during the transformation of primary alcohol to carboxylic acid. Interestingly, even after utilization of a strong co-oxidant and stabilizing agent, ~33% of aldehyde-water adduct was observed when CH_3CN was solvent. To date, such adducts have been characterized via NMR spectroscopy in solution and validation by X-ray crystallography is rare (Kawamichi et al., 2009).

Although isolation of gem-diol is possible when a highly electron-deficient carbon is attached to the carbonyl group, the factors governing this process remains poorly understood. Specifically, there is limited clarity regarding the variables involved such as pH, choice of solvent, and catalytic conditions impacting the equilibrium of reversible nucleophilic addition of water to carbonyl compound. Therefore, further examination is vital for optimizing and exploring new strategies for efficient isolation of gem-diols.

This work highlights three aspects (i) a novel approach involving Al(III) catalysed hydration of aromatic aldehyde for the isolation of gem-diol; (ii) a detailed investigation of the photophysical property of gem-diol; (iii) an assessment of stability of the synthesized intermediate by altering H-bond accepting anions in solution. To the best of author's knowledge this is the first study demonstrating $AlCl_3.6H_2O$ activating the carbonyl group and facilitating aldehyde-water adduct formation while stabilizing the gem-diol species (**Q2G**) through in situ generation of HCl. Notably, the gem-diol species derived from quinoline-2-aldehyde (**Q2A**) exhibited high photostability and fluorogenic behaviour.

5.2 Experimental section

5.2.1 Synthesis of *gem*-diol (Q2G)

The gem-diol **Q2G** was synthesized through a straightforward one-pot reaction involving quinoline-2-aldehyde and $AlCl_3 \cdot 6H_2O$ in a 1:1 stoichiometric ratio, using methanol as the solvent at room temperature (Scheme 5.1). Specifically, quinoline-2-aldehyde (0.157 g, 1.0 mmol) and $AlCl_3 \cdot 6H_2O$ (0.48 g, 2.0 mmol) were dissolved in 15-20 mL of methanol, and

the reaction mixture was stirred for 2-3 hours at room temperature. The resulting crude product, initially obtained as a liquid, was recrystallized in methanol to yield fine block-shaped crystals. FT-IR (KBr disk): 1635, 1527, 1179, 1077, 848 cm^{-1}. UV-Vis (CH_3CN): $\lambda_{max/nm}$ ($\varepsilon/M^{-1}cm^{-1}$) = 237 ($17.8 \times 10^4$), 316 ($39.8 \times 10^3$). ^1H NMR (DMSO, 500 MHz, TMS), δ (ppm): 8.63, 7.89, 7.87, 7.77, 7.75, 7.44, 7.42, 7.37, 7.35, 7.34, 7.30, 7.28, 7.17,7.16, 7.14, 4.99, and 4.73. ^{13}C NMR (DMSO, 500 MHz, TMS), δ (ppm): 139.07, 131.24, 128.79, 128.44, 128.11, 119.49, 105.18, 97.82, 54.70, 118.42, 61.41, and 33.30.

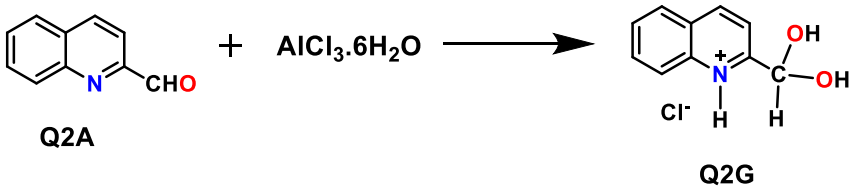

Scheme 5.1 Synthetic route to prepare *gem*-diol (**Q2G**).

5.2.2 Crystal structure determination

The wine-red colored crystals of **Q2G** were obtained in methanol via slow evaporation. The crystallographic data of **Q2G** has been collected on Oxford Diffraction Gemini diffractometer equipped with CrysAlis Pro at 150 K using the monochromatic Cu-Kα radiation source (λ 1.5416Å). The crystal structure of **Q2G** was solved by direct method (SHELXL-97) and refined against all the data by full-matrix least squares on F^2 using anisotropic displacement parameters for all non-hydrogen atoms (Sheldrick, 1990; Sheldrick, 1997). All the H atoms were refined with a riding model. The MERCURY software package and ORTEP-3 for Windows program have been used to generate the structure (Bruno et al., 2002; Farrugia, 1997).

5.2.3 Absorption and emission spectra

Fluorescence and UV-Vis spectroscopy experiments were performed at room temperature in CH_3CN solution. The emission spectra were recorded over a wavelength range of 340-560 nm, with the excitation wavelength set at 310 nm.

5.3 Result and discussion

5.3.1 UV-Vis and fluorescence analysis

Compound **Q2A** was chosen as a model substrate due to its propensity to form a moderately stable gem-diol moiety, a characteristic attributed to the position of its carbonyl group relative to the intra-ring nitrogen atom. To provide experimental evidence for the formation of a gem-diol in solution, the absorption spectral behavior of **Q2A** in the presence of $AlCl_3 \cdot 6H_2O$ was investigated using CH_3CN as the solvent. Gradual addition of $AlCl_3 \cdot 6H_2O$ (0–2.0 equiv) to **Q2A** (~10^{-5} M) induced significant spectral changes, including the appearance of four distinct isosbestic points at 226 nm, 240 nm, 300 nm, and 340 nm. These observations indicate the stoichiometric conversion of **Q2A** into a new species. Specifically, the original absorption peak of **Q2A** at 289 nm exhibited a red shift to 316 nm, while the band at 244 nm underwent a blue shift to 237 nm. The saturation point was reached with the addition of approximately 2.0 equiv. of $AlCl_3 \cdot 6H_2O$, at which the final spectral profile closely resembled that of **Q2G** crystals dissolved in CH_3CN. This strong similarity supports the formation of the gem-diol species.

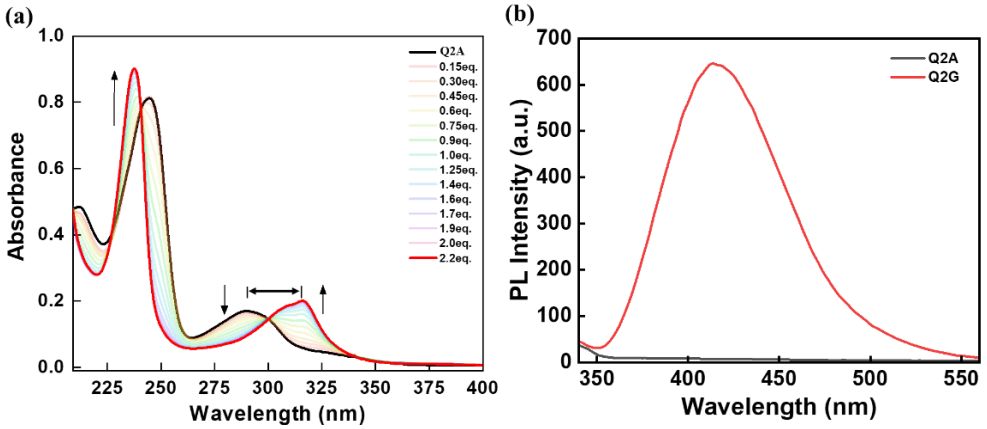

Fig. 5.1. (a) UV-Vis analysis of **Q2A** with $AlCl_3.6H_2O$ and (b) Emission spectra of **Q2A** and **Q2G** in acetonitrile solution.

The absorption spectral changes of various aromatic aldehyde analogues, including pyridine-2-aldehyde (**P2A**), 6-bromo-pyridine-2-aldehyde (**BP2A**),

2-naphthaldehyde (**N2A**), furfuraldehyde (**F2A**), and thiophene-2-aldehyde (**T2A**), were examined in the presence of $AlCl_3 \cdot 6H_2O$.

P2A, when titrated with $AlCl_3 \cdot 6H_2O$, exhibited significant spectral changes. The initial UV-Vis spectrum showed two absorption bands at 233 nm and 268 nm. With the incremental addition of $AlCl_3 \cdot 6H_2O$, the band at 233 nm diminished, while the band at 268 nm blue-shifted to 259 nm. Saturation occurred after the addition of approximately 2.0 equiv. of $AlCl_3 \cdot 6H_2O$, leaving a single absorption band at 259 nm. Clear isosbestic points were observed at 215 nm, 246 nm, 268 nm, and 294 nm, indicating the formation of a new species.

BP2A displayed moderate-intensity absorption bands at 236 nm and 282 nm. Upon the addition of $AlCl_3 \cdot 6H_2O$, the band at 236 nm decreased, while the band at 282 nm blue-shifted to 270 nm, accompanied by a shoulder at 282 nm. Three distinct isosbestic points were observed at 227 nm, 247 nm, and 274 nm. These spectral changes suggest the possible formation of a gem-diol species, although attempts to obtain crystals were unsuccessful.

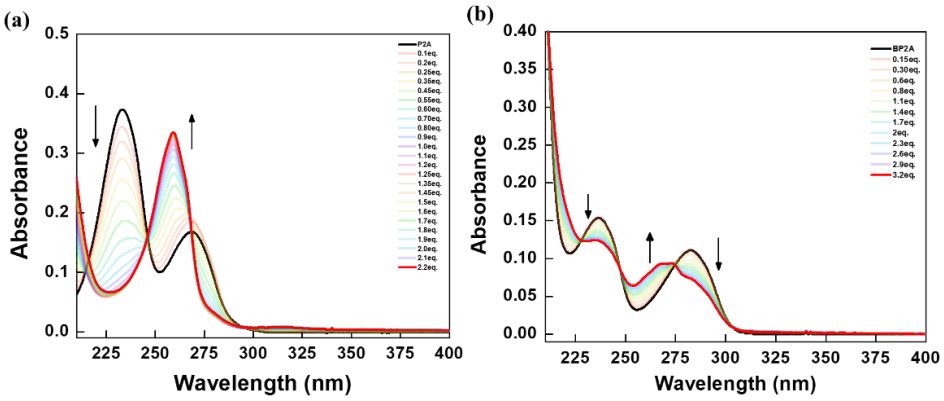

Fig. 5.2. (a) Absorption spectral variations in **P2A** at different concentrations of $AlCl_3.6H_2O$ and (b) Absorption spectral variations in **BP2A** at different concentrations of $AlCl_3.6H_2O$.

In contrast, **N2A** exhibited no spectral changes, even after the addition of 1.5 equiv. of $AlCl_3 \cdot 6H_2O$, underscoring the critical role of the nitrogen atom in the ring (Annexure I, Fig. A24). Similarly, no spectral changes were observed for **F2A** and **T2A** upon the addition of $AlCl_3 \cdot 6H_2O$ in CH_3CN, further

confirming the importance of nitrogen in facilitating gem-diol formation (Annexure I, Fig. A25).

For 2-acetyl-pyridine (**A2P**), the UV-Vis spectrum displayed two distinct absorption bands at 229 nm and 266 nm (Annexure I, Fig. A25). Upon the addition of Al^{3+} ions, the intensity of the band at 229 nm decreased, while the band at 266 nm exhibited significant enhancement with only a slight shift. Two isosbestic points could be observed at 216 nm and 243 nm, indicating the formation of a new species. Saturation occurred at a lower concentration, with approximately 1.4 equiv. of Al^{3+} ions. These changes, along with the observed isosbestic points, suggest the interaction between **A2P** and Al^{3+} ions, likely leading to a structural transformation.

The response of other Lewis salts was also examined. Slight spectral alterations could be noticed with $ZnCl_2$ and $FeCl_3$; however, no isosbestic points or significant red or blue shifts were detected (Annexure I, Fig. A26). Similarly, the response to $InCl_3$, a salt in Al family, was investigated. The addition of 2.5 equiv. of $InCl_3$ to **Q2A** resulted in a drastic decrease in the intensity of the band at 289 nm. Additionally, the band at 289 nm diminished while a red shift to 310 nm was observed, indicating weaker interaction compared to $AlCl_3 \cdot 6H_2O$.

The emission spectra of **Q2A** revealed that it was initially non-fluorescent. However, the addition of 2 equiv. of $AlCl_3 \cdot 6H_2O$ led to a significant enhancement of a fluorescence band at 414 nm in CH_3CN solution. This fluorescence response closely resembled the behavior observed when crystals of **Q2G** were dissolved in CH_3CN, further confirming that the two species are identical.

The response of **Q2G** to different anions, including Br^-, ClO_4^-, F^-, CN^-, I^-, PF_6^-, and CF_3COO^- (TFA), was also evaluated. Strong fluorescence quenching was observed in the presence of CN^- and TFA ions. Interestingly, UV-Vis spectral analysis of **Q2G** with TFA and CN^- revealed significant changes: the band at 316 nm decreased drastically, and a broad band appeared in the range of 250–300 nm, indicating substantial interactions with these anions.

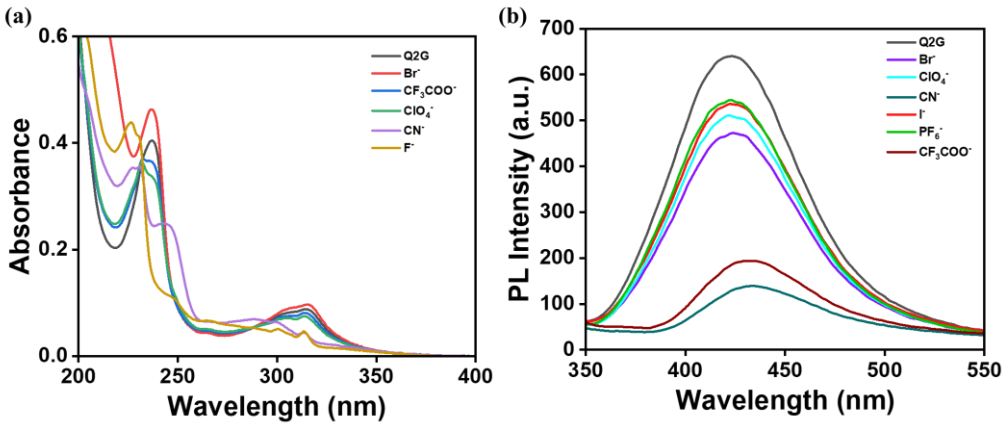

Fig. 5.3 (a) UV-Vis spectra of the **Q2G** with various anions in acetonitrile and (b) Emission spectra of **Q2G** with various anions in acetonitrile.

5.3.2 X-ray analysis of *gem*-diol

After completion, the product was completely dried and redissolved in methanol solution for purification or recrystallization. After several days, diffraction quality, block shaped single crystals were observed in the methanolic solution, we performed low temperature X-ray analysis of these crystals. These crystals were found to be the hydrochloride salt of **Q2G** with the crystallographic parameters (*P*-1, a = 6.749, b = 8.7632, c = 9.2419, α = 103.648, β = 110.623, γ= 103.021, V = 467.707). Fig. 5.4(a) depicts the crystal structure which contains one molecule of **Q2G** and one molecule of the *in-situ* generated hydrochloric acid in the crystalline lattice. The nature of this intermediate chemical species is depicted in Fig. 5.4(b). Here, the C–O and O–H bond lengths are of nearly 1.41Å and 0.86Å respectively which are analogous to the previously reported structures in literature. The F_o electron density from Fourier map establishes the unambiguous tetrahedral nature of the intermediate based on their tetrahedral angles, like O_1-C_{10}-O_2 (111.41º), O_1-C_{10}-C_1 (109.92º), O_2-C_{10}-C_1 (109.33º), O_2-C_{10}-H_{1O} (108.73º), C_1-C_{10}-H_{1O} (108.71º), and O_1-C_{10}-H_{1O} (108.68º) respectively (Fig. 5.4(d)).

Fig. 5.4c demonstrates that the quinoline group is protonated while chloride anion (Cl^-) is used in several hydrogen bonds like O–H···Cl^-, N^+–H···Cl^- and C–H···Cl^- to stabilize the *gem*-1,1-diol intermediate in the solid state. Here, the O–H···Cl^- (d, θ : 2.213Å, 167.23º and 2.277Å, 163.17º)

hydrogen bond is particularly important which plays a significant role in stabilizing this chemical species. Moreover, the Cl^- anions further stabilized by the supplementary N^+–H···Cl^- (*d*, θ : 2.718Å, 131.83º) and C–H···Cl^- (*d*, θ : 2.968Å, 116.99º) hydrogen bonds.

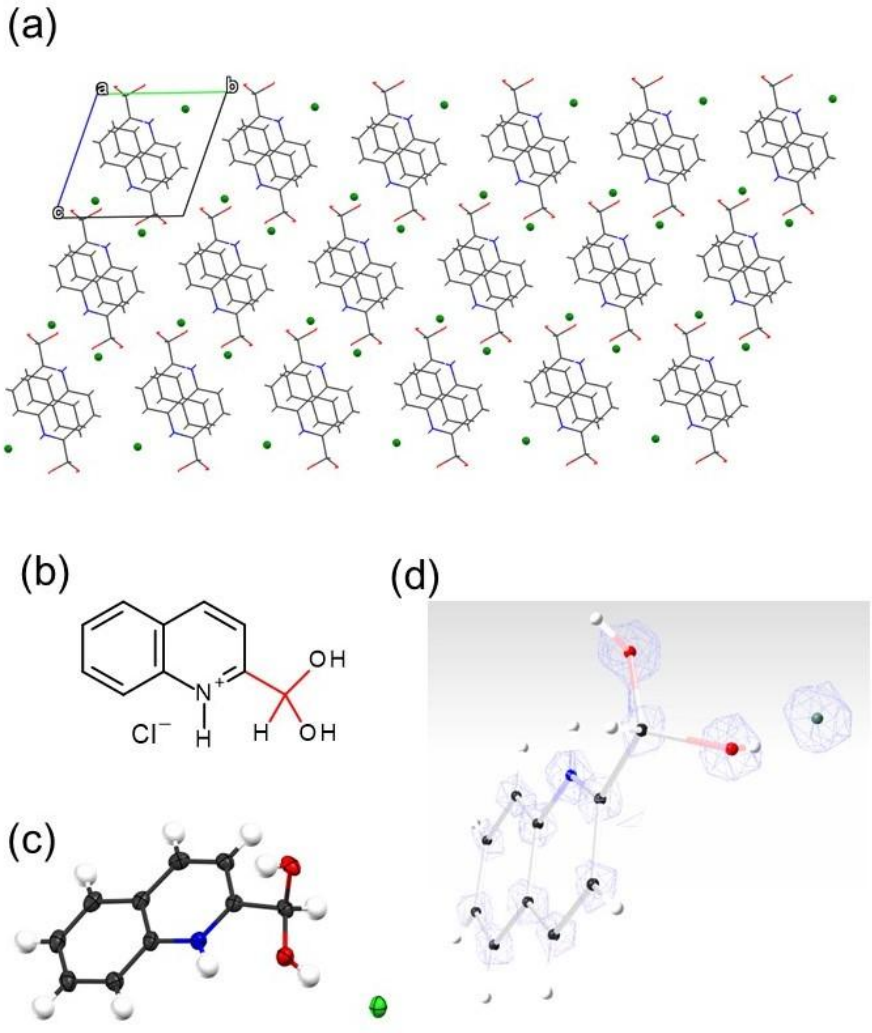

Fig. 5.4. X-ray analysis of the tetrahedral intermediate, *gem*-1,1-diol, of **Q2G** (a) Crystal structure of **Q2G** (carbon, nitrogen, oxygen, and chlorine are depicted in grey, blue, red, and green respectively); (b) Molecular scaffold of **Q2G**, the tetrahedral geometry is highlighted in red); (c) ORTEP drawing of **Q2G** where ellipsoid drawn in 50% probability and (d) Electron density map *Fo* (cut off at 2.50 e/Å^3).

5.3.3 FT-IR studies

The characteristic vibrational band of **Q2A** at 1708 cm^{-1} completely disappeared in **Q2G**, which strongly indicated the absence of the >C=O

functionality in **Q2G**. This change was further confirmed by the appearance of a C-O stretching band at 1090 cm^{-1}, along with the deformation of the C-O-H out-of-plane bending band at 1290 cm^{-1}. These new bands are consistent with the conversion of the >C=O group into a gem-diol species, confirming the structural transformation. In a separate experiment, **P2A** was stirred with $AlCl_3 \cdot 6H_2O$ for 3 hours. After the reaction, the final product was dried and characterized by FT-IR analysis. The characteristic absorption band at 1711 cm^{-1}, which corresponds to the >C=O functionality in **P2A**, vanished upon conversion to **P2G**. This disappearance of the carbonyl stretch in **P2G** mirrors the behavior observed with **Q2A**, further supporting the formation of the gem-diol species in both cases. These results provide compelling evidence for the successful transformation of the aldehyde into a gem-diol in the presence of $AlCl_3 \cdot 6H_2O$.

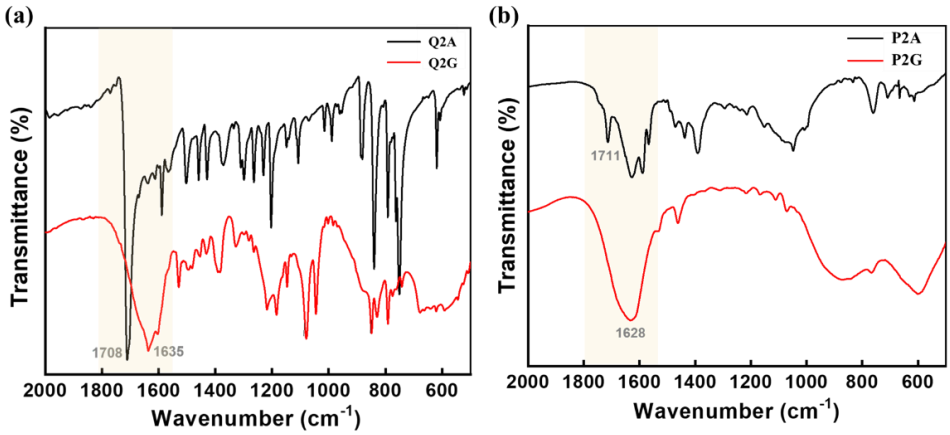

Fig. 5.5. FT-IR spectra of **Q2G** and **P2G**.

5.3.4 NMR studies

^{1}H and ^{13}C NMR analyses provided further confirmation of the presence of the gem-diol species in solution. In the ^{1}H NMR spectrum of **Q2G**, a singlet near 4.99 ppm was observed, which could be assigned to the methyne proton ($C\underline{\mathbf{H}}(OH)_2$) of the gem-diol moiety. However, the -OH proton of the gem-diol $CH(OH)_2$ group was not visible in the spectrum due to the high degree of exchange in the solution. Notably, the signal at 194.17 ppm, which corresponds to the carbonyl group in **Q2A**, was absent in the ^{13}C NMR spectrum of **Q2G**,

further indicating the conversion of the carbonyl group into the gem-diol. Additionally, a new resonance peak appeared at 54.70 ppm, which was assigned to the carbon atom of the gem-diol (**C**-H$(OH)_2$ moiety). These NMR findings strongly support the formation of the gem-diol species in solution, consistent with the spectroscopic evidence obtained from other techniques (Fig. 5.6). On the basis of these observation a proposed mechanism for the formation of gem-diol species has been provided in Fig. 5.7.

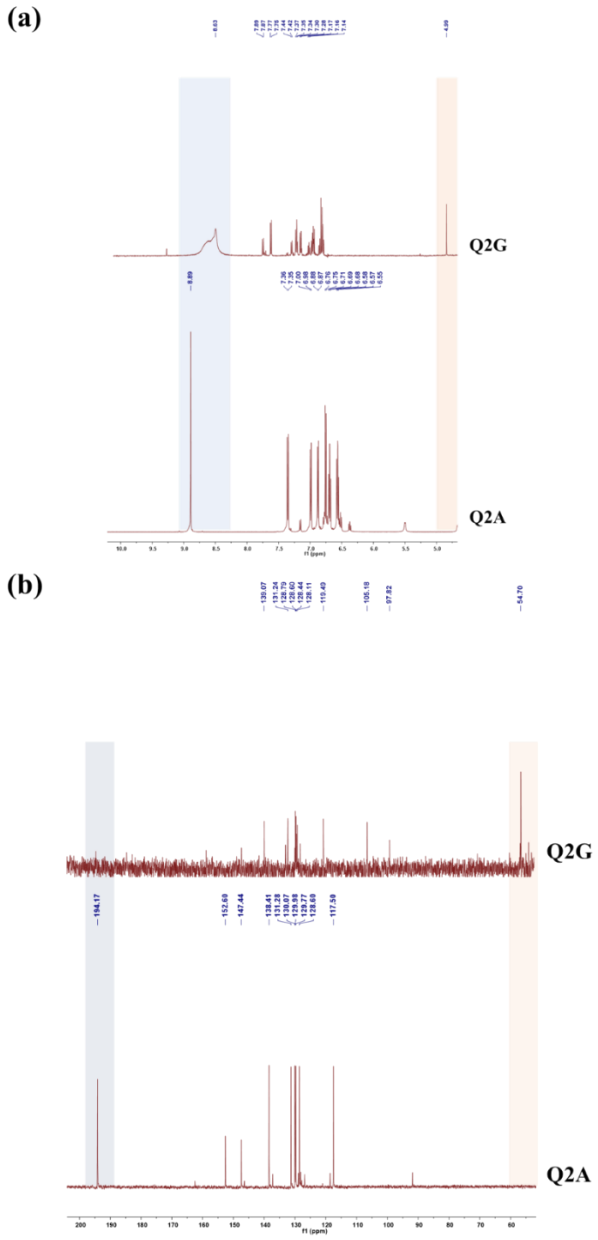

Fig. 5.6. (a) ^{1}H NMR spectra of **Q2A** and **Q2G** in DMSO at room temperature and (b) ^{13}C NMR spectra of **Q2A** and **Q2G** in DMSO at room temperature.

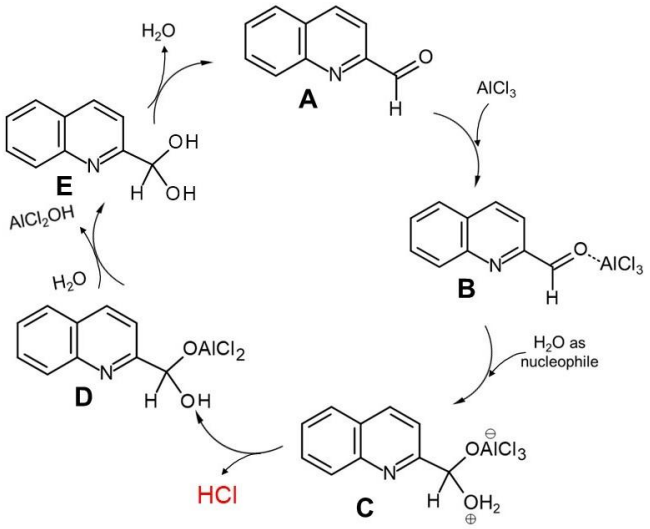

Fig. 5.7 Proposed mechanism to the formation of gem-diol **Q2G** species when **Q2A** is treated with $AlCl_3.6H_2O$.

5.6 Conclusions

In this work, we present a novel approach for the isolation of aldehyde hydrates through Al(III)-catalyzed hydration of heteroaromatic aldehydes, using quinoline-2-aldehyde as the model substrate. The resulting aldehyde hydrate species was successfully stabilized in both solution and solid state. Structural analysis revealed that the intermediate was stabilized by in situ generated HCl, which facilitated O-H···Cl hydrogen bonding interactions. Notably, this transient species exhibited strong fluorescence emission at 419 nm in acetonitrile solution-an observation that has not been reported for such rare and unstable reaction intermediates. To the best of our knowledge, this is the first documented instance of fluorogenic behavior in aldehyde hydrate intermediates, providing valuable insights into their properties and potential applications.

CHAPTER 6

IMIDAZO-PHENANTHROLINE BASED OPTICAL SENSING PLATFORM FOR CYANIDE AND FLUORIDE IONS: EXPERIMENTAL AND THEORETICAL INVESTIGATIONS

6.1 State of the art

Over the preceding years, selective recognition of anions using optical chemosensors has gained considerable attention due to their crucial roles in various chemical, biological, and environmental processes (Chatterjee et al., 2024; Gale et al., 2018; Martínez-Máñez & Sancenón, 2003; Wu et al., 2020). However, designing a specific chemosensory probe for anions remains a huge challenge because of the related diverse shapes, sizes, and strong solvation characteristics (Chang et al., 2015; Naithani et al., 2023). Among illustrations, cyanide (CN^-) ion stands out as an extremely toxic anion, capable of causing histotoxic anoxia and leading to death in humans and marine lives, even at very low concentrations (Jaszczak et al., 2017; Malahom et al., 2023; Wood, 2016). CN^- ion potentially interferes with aerobic respiration by inhibiting cytochrome-*c*-oxidase, a crucial enzyme in the electron transport chain. This disruption prevents the production of ATP, eventually leading to the energy depletion and cellular dysfunctions (Manoj et al., 2020; Naithani et al., 2024). Despite being so non-innocent to living organisms, this anion is being extensively utilized in many industrial and metallurgical processes such as metal extraction, mining, jewellery manufactures, electroplating, and the recovery of X-ray films (Kaushik et al., 2016; Padghan et al., 2024; Pal et al., 2021; Pervaiz et al., 2024; Wang et al., 2014). Cyanide containing salts, especially those soluble in water, are considered as the most detrimental and poisoning agents to human health. Similarly, fluoride (F^-) ion is found to be involved in various physiological processes and largely contributes to the health of teeth and bones (Lacson et al., 2020; Manna et al., 2022). However, an imbalance in fluoride levels can lead to severe human health problems, including thyroid and liver disorders, damage to other organs, as well as dental and skeletal fluorosis (Solanki et al., 2022; Wu et al., 2022). Consequently, World Health Organization (WHO) has set the

permissible limits for CN^- and F^- in drinking water as 0.07 mg L^{-1} and 1.5 mg L^{-1}, respectively (Chilton et al., 2006; Organization, 2022; World Health Organization, 2003).

Although several conventional methods have been developed for the detection of CN^- or F^- ions, many of them are notably time-consuming and typically require trained and sophisticated operations (Jackson et al., 2017; Randviir et al., 2015). In this regard, selective and sensitive optical molecular sensors, encompassing both colorimetric and fluorogenic sensors, have seen gradual growth during the recent past (David et al., 2024; Xu et al., 2010). Optical sensors offer several attractive advantages over traditional methods such as excellent sensitivity/selectivity, rapid and visual detection, optical imaging and on-site field applications (Krämer et al., 2022; Naithani et al., 2024; Naithani et al., 2025). Therefore, a diverse range of fluorescent small molecular probes have been developed for targeted F^- and CN^- detection based on the interaction of these anions with electron-deficient receptor sites such as imidazole, pyridinium, acridinium, salicylaldehyde, trifluoro-acetophenone, oxazine, to name but a few (Chakraborty et al., 2021; Chung et al., 2006; Emandi et al., 2018; Jamuna et al., 2023; Sukato et al., 2016; Tomasulo et al., 2005; Yang et al. 2006). The anion sensing approaches typically rely on hydrogen bonding interactions, deprotonation, single electron transfer, and/or nucleophilic addition reactions, inducing detectable changes in the optical characteristics of the probe.

Most of the reported F^- and CN^- responsive probes exhibit a single emission feature, such as Turn-on or Turn-off, when interacting with these anions (Chakraborty et al., 2021; Han et al., 2015; David et al., 2024; Jo et al., 2013; Manickam et al., 2020; Thanayupong et al., 2017; Wang et al., 2014). These methods are prone to interference during analysis, as minor changes in the microenvironment, fluctuations in probe concentration, or photobleaching can sometimes lead to false positive results. To address these challenges, ratiometric probes are often preferred, as they rely on distinct changes in the intensity of multiple emission bands during probe-anion interactions (Huang et al., 2018; Park et al., 2020). The concentration of the anion is directly correlated with the ratio of emission intensities at two different wavelengths, offering a

built-in mechanism to mitigate environmental influences and improve sensitivity. In this study, we introduce a ratiometric fluorogenic probe, **bpmpip**, based on an imidazo-phenanthroline moiety, for a selective detection of cyanide and fluoride ions in aqueous-acetonitrile solution. Though this probe has been previously reported by our group (Arora et al., 2019), it has not yet been applied for anion sensing purposes. One of the key advantages of such systems is that their photophysical properties can be easily and precisely tuned by introducing substitutions at various positions on the imidazo-phenanthroline moiety, allowing for the optimization of chemosensing capabilities for the target anions (Kumar et al., 2022; Naithani et al., 2023).

6.2 Experimental section

6.2.1 Synthesis of the probe bpmpip

Probe **bpmpip** has been prepared following the procedure reported earlier by our group (Arora et al., 2019). Briefly, a mixture of 1,10-phenanthroline-5,6-dione (0.52 g, 2.5 mmol) and ammonium acetate (5.8 g, 75 mmol) was prepared in hot glacial acetic acid (30 mL) under inert atmosphere, protected from light. To this, bpmp-CHO (0.79 g, 2.5 mmol) was added, and the solution was refluxed at 70-80 °C for 3 hours. Thereafter, the reaction mixture was cooled in an ice bath and neutralized with 1.0 N NaOH to pH 7.0. The crude product precipitated as a light brown solid, was filtered, washed with distilled water, and then dried under vacuum (Scheme 6.1). The product has been purified using silica-gel column chromatography with a CH_2Cl_2-MeOH mixture (9:1, *v/v*). ^{1}H NMR [(500 MHz, DMSO, TMS, δ (ppm)]: 13.88 (s, 1H, NH-imidazole), 8.96 (s, 4H), 8.53 (s, 2H), 8.04 (d, 2H), 7.66 (t, 2H), 7.53 (d, 3H), 7.27-7.32 (m, 3H), 7.17 (t, 2H), 3.78 (s, 4H, -CH_2-pyridine), 3.59 (s, 2H, -CH_2-phenyl), HR-MS (ESI-TOF) *m/z* Calcd. for $C_{32}H_{25}N_7$ = 508.2244; Found *m/z* = 508.2247 [**bpmpip** + Na]$^+$.

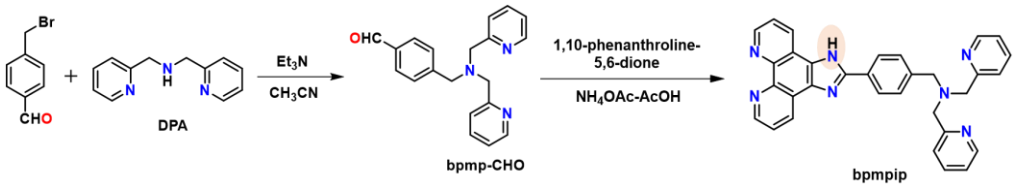

Scheme 6.1. Synthetic route to prepare the probe **bpmpip**.

6.2.2 Calculation of limit of detection and binding constant

The detection limits (LoD) for both the anions were calculated using the formula: LoD = 3σ/S, where σ represents the standard deviation derived from ten blank emission spectra, and S is the slope obtained from the emission titration profiles. Additionally, the binding constant (K_b) for target anions was determined using the Benesi-Hildebrand equation (Goswami et al., 2024; Naithani et al., 2023):

$$\frac{1}{\Delta FI} = \frac{1}{\Delta FI_{max}} + \left(\frac{1}{\Delta FI_{max} K_b}\right)\frac{1}{[A^-]}$$

Where, ΔFI = change in the fluorescence intensity of **bpmpip** in the presence and absence of anion A^- (A = CN or F); ΔFI_{max} = maximum change in the fluorescence intensity of **bpmpip** upon addition of CN^- or F^- ions, while the value of K_b was determined using the slope and the intercept of the plot of 1/ΔFI against 1/[A^-].

6.2.3 Job's plot analysis

Job's plot analysis was performed by utilizing a series of aqueous-acetonitrile solutions (CH_3CN-H_2O; 4:1, *v/v*) containing **bpmpip** and A^- to maintain a total concentration of 0.5 μM. The mole fraction was then varied from 0 to 1.0 and the emission spectra were recorded. A graph was plotted between [I_0-I] × [1-X] and the mole fraction of A^- ion (Goswami et al., 2024).

6.3 Results and discussion

Probe **bpmpip** has been prepared following the procedure reported earlier (Arora et al., 2019), and notably characterized using standard spectroscopic and analytical techniques such as UV-Vis, fluorescence, infrared (IR), NMR, mass, elemental analyses, etc. UV-Vis studies of **bpmpip** in acetonitrile revealed two absorption bands at 276 nm and 308 nm, attributed to π→π* and n→π* transitions, respectively (Arora et al., 2019) (Fig. 6.1). The emission spectra of **bpmpip** were measured at different excitation wavelengths ranging from 290 nm to 340 nm; however, it gave the best emission response at 425 nm in CH_3CN-H_2O (4:1, *v/v*) solvent mixture, when excited at 320 nm. ^{1}H NMR spectrum of **bpmpip** in DMSO showed all the expected resonances (Annexure I, Fig. A27). The N-H proton of imidazole moiety appeared as a broad singlet

near 15.34 ppm. The methylene protons of phenyl-CH_2 and pyridine-CH_2 groups were observed at 3.74 ppm and 3.77 ppm, respectively. Additionally, the resonances ranging 7.17-8.96 ppm have been attributed to all the aromatic protons. ESI-mass spectrum of the probe showed an intense peak at 508.2247 (calcd 508.2244) corresponding to [**bpmpip**+ Na]$^+$ (Annexure I, Fig. A28).

6.3.1 Optical sensing of CN^- and F^- ions

UV-Vis spectroscopy was utilized to evaluate the sensing capability of probe **bpmpip** toward various anions. A 3.9 × 10^{-4} M solution of **bpmpip** in CH_3CN-H_2O (4:1, *v/v*) was tested against selected anions, including AcO^-, Br^-, ClO_4^-, CN^-, F^-, CO_3^{2-}, $Cr_2O_7^{2-}$, PO_4^{3-}, SO_4^{2-}, and CrO_4^{2-} (Fig. 6.1(a)). Among these, noticeable spectral changes could be observed only for CN^- and F^- ions. Upon progressive addition of CN^- (0-1.8 equiv), the absorption bands of **bpmpip** at 276 nm and 308 nm underwent substantial red shifts to 290 nm and 319 nm, respectively, accompanied with two isosbestic points at 240 nm and 313 nm (Fig. 6.1(b)). The clear isosbestic points indicated the stoichiometric formation of some new species from **bpmpip** upon interaction with CN^- ions. These spectral alterations were also associated with an obvious visible color change in probe's solution from colorless to light green. A similar trend was noted for F^- ions, although the spectral changes were less pronounced as compared to cyanide ions (Annexure I, Fig. A29).

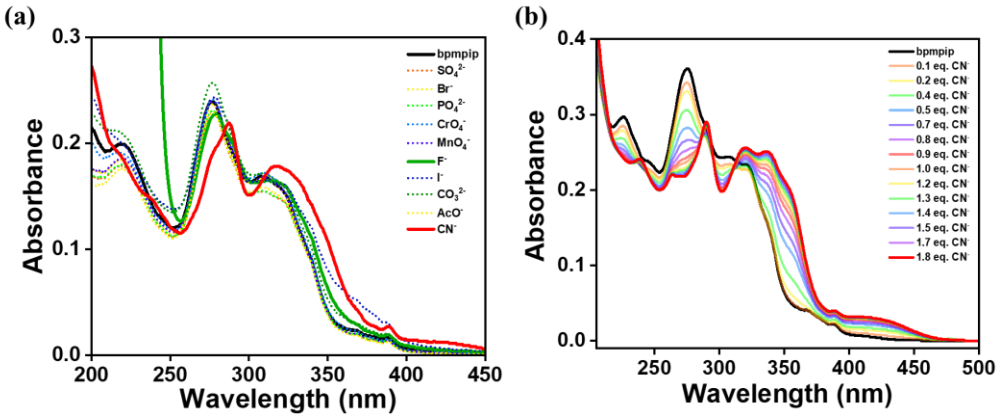

Fig. 6.1 (a) UV-Vis spectra of the probe **bpmpip** (*ca.* 4.0 μM) with various anions in semi-aqueous (CH_3CN-H_2O; 4:1, *v/v*) medium and (b) Absorption spectral variations in **bpmpip** at different concentrations of cyanide ion (0-1.8 equiv). Inset: Color changes in semi-aqueous solution occurring when **bpmpip** was treated with CN^- ions.

The fluorescence studies further provided confirmation to the obtained sensing results. As illustrated in Fig. 6.2(a), the fluorescence intensity of **bpmpip** at 425 nm underwent significant changes exclusively in the presence of CN^- and F^- ions (1.0 equiv) in CH_3CN-H_2O (4:1, *v/v*) solution, while other anions showed negligible impact (λ_{ex} 320 nm). Upon incremental addition of CN^-, the emission intensity at 425 nm markedly declined, accompanied by the appearance of a new emission peak near 518 nm and an iso-emissive point at 485 nm. This red-shift in the emission was visually evident with a distinct color change from colorless to pastel green under UV light illumination. Similarly, the addition of F^- ions resulted in a decrease in the emission intensity at 424 nm, the formation of a new emission band at 516 nm, and the appearance of an iso-emissive point at 482 nm. Notably, F^- and CN^- can be distinguished clearly due to their slightly distinct emission responses. The ratio of emission intensities at the two wavelengths (I_{425}/I_{520}) highlights the ratiometric sensing behavior of the probe.

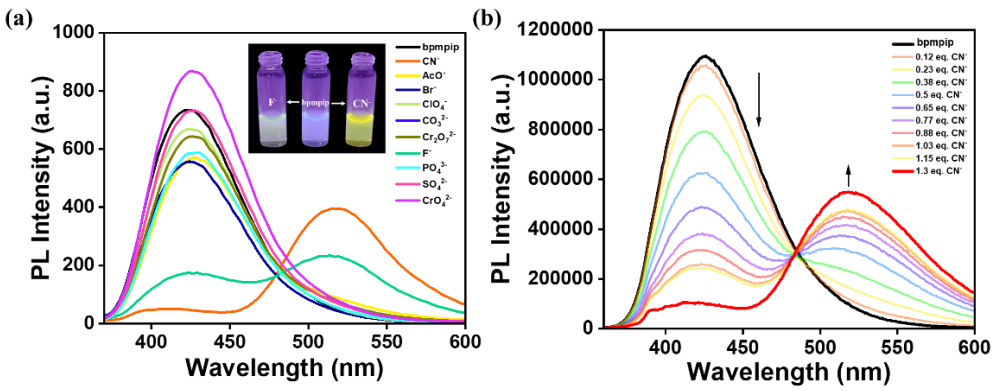

Fig. 6.2 (a) Emission spectra of the probe **bpmpip** (*ca.* 4.0 μM) with various anions in semi-aqueous media and (b) Emission spectral variations in **bpmpip** at different concentrations of cyanide ions (0-1.3 equiv). Inset: Color changes in semi-aqueous solution when **bpmpip** was treated with CN^- ion (right-side glass vial).

Job's plot analysis revealed a 1:1 stoichiometric ratio between **bpmpip** and CN^-/F^- ions (Annexure I, Fig. A30). The calculated detection limits for CN^- and F^- ions, derived from emission titration profiles, were 32.26 nM and 899 nM, respectively (Fig. 6.3). Notably, the detection limit for cyanide ions is much lower than the permissible CN^- concentration in drinking water, as regulated by

the U.S. EPA (*Cyanide, Free CASRN 57-12-5 | IRIS | US EPA, ORD*, n.d.). To further illustrate its sensing performance, a comparative analysis of the sensing parameters with previously reported CN^--responsive imidazo-phenanthroline-based fluorescent probes was conducted (see Table 6.1). The results demonstrate a superior LoD, although the binding constants were generally similar, ranging from 10^{-5} to 10^{-6} M^{-1} across most studies (Gosi et al., 2021; Malkondu et al., 2020). Remarkably, the addition of CN^- to **bpmpip** induced a more pronounced emission shift compared to other ratiometric probes in the literature (Table 6.1). Interestingly, the addition of OH^- resulted in similar ratiometric changes in the spectra when compared to CN^- or F^- ions.

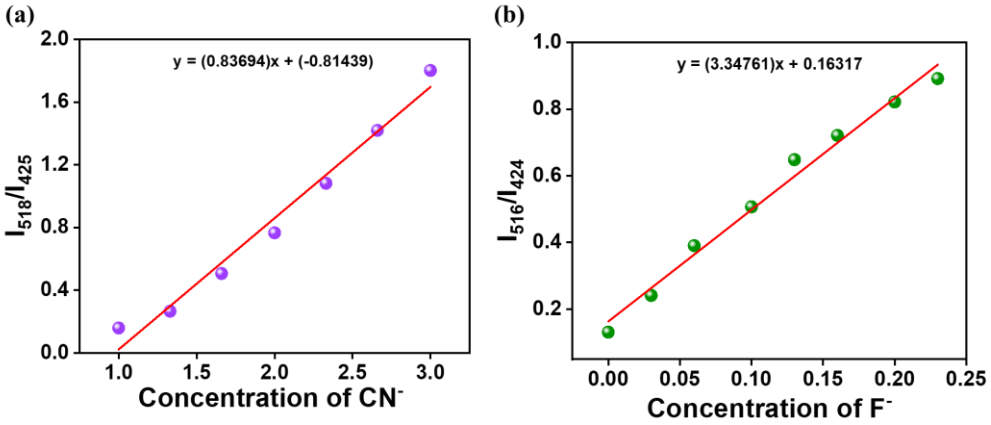

Fig. 6.3 Calibration curve obtained for determination of CN^- and F^- by **bpmpip** in semi-aqueous CH_3CN-H_2O solution.

Therefore, the observed spectral changes in **bpmpip** can be attributed to the strong hydrogen bonding interaction between the anion (A^-, where A = CN or F) and the N-H functionality of the imidazole moiety, resulting in the formation of N-H----A^- bonds. At higher concentrations of anions, this interaction may cause the N-H bond to elongate and eventually break due to a proton transfer process, where hydrogen bonding initially occurs, followed by the deprotonation process. This mechanism was further supported by ^{1}H NMR titration experiments, in which the broad signal at 15.34 ppm, corresponding to the N-H group, initially shifted upfield to 13.7 ppm and then disappeared with the gradual addition of fluoride ions (0-1 equiv) (Annexure I, Fig. A31). Additionally, slight changes in the chemical shifts of aromatic protons, ranging from 0.28 to 0.92 ppm, further support this interaction. The observed red-shift

in absorption bands is likely due to the increased electron density on the imidazole moiety, which facilitates intramolecular charge transfer between the phenanthroline and imidazole units.

Interference studies were performed in a CH_3CN-water (4:1, *v/v*) mixture to evaluate the selectivity of **bpmpip** in the presence of various competing anions. Remarkably, no noticeable change in the fluorescence of **bpmpip** was observed when exposed to competing anions such as AcO^-, Br^-, ClO_4^-, CN^-, F^-, CO_3^{2-}, $Cr_2O_7^{2-}$, PO_4^{3-}, SO_4^{2-}, and CrO_4^{2-}, even at concentrations as high as 5 equiv. In contrast, the addition of even a small amount of CN^- resulted in an immediate shift in the emission spectrum. This suggests that **bpmpip** exhibits an excellent selectivity for CN^-, unaffected by the presence of other anions in a semi-aqueous environment (Annexure I, Fig. A32). Additionally, the probe demonstrated reversible behavior in the presence of acetic acid. Upon treatment with acetic acid, the dark-red color of the **bpmpip**-CN^- species faded, and the original emission and absorption profiles of **bpmpip** were fully restored, likely due to protonation of the imidazole moiety.

6.3.2 DFT studies

Density functional theory (DFT) calculations were performed to further elucidate the anion binding mechanism. The optimized ground-state geometries of probe **bpmpip** and its anion-bound species (**bpmpip**-CN^- or **bpmpip**-F^-) are illustrated in Fig. 6.4. A strong agreement could be noticed between experimental and theoretical findings. For probe **bpmpip**, the highest occupied molecular orbital (HOMO) was predominantly localized on the imidazo-phenanthroline unit, with a minor contribution from the phenyl linker. Conversely, the lowest unoccupied molecular orbital (LUMO) was distributed less uniformly across the imidazo-phenanthroline moiety. Upon binding with anions, the HOMO of the anion complexes (**bpmpip**-CN^- or **bpmpip**-F^-) was primarily associated with the DPA moiety, while the LUMO remained centred on the imidazo-phenanthroline unit, similar to the HOMO of the free probe. The energy gap between the frontier molecular orbitals of probe **bpmpip** was calculated to be 4.064 eV. Following hydrogen-bonding interactions, this gap was significantly reduced to 0.823 eV and 0.832 eV for CN^- and F^- ions,

respectively (Fig. 6.4). The reduction in the energy gap between the HOMO and LUMO of the **bpmpip**-CN^- and **bpmpip**-F^- adducts aligns well with the red-shifted absorptions observed in their experimental UV-Vis spectra (*vide-supra*).

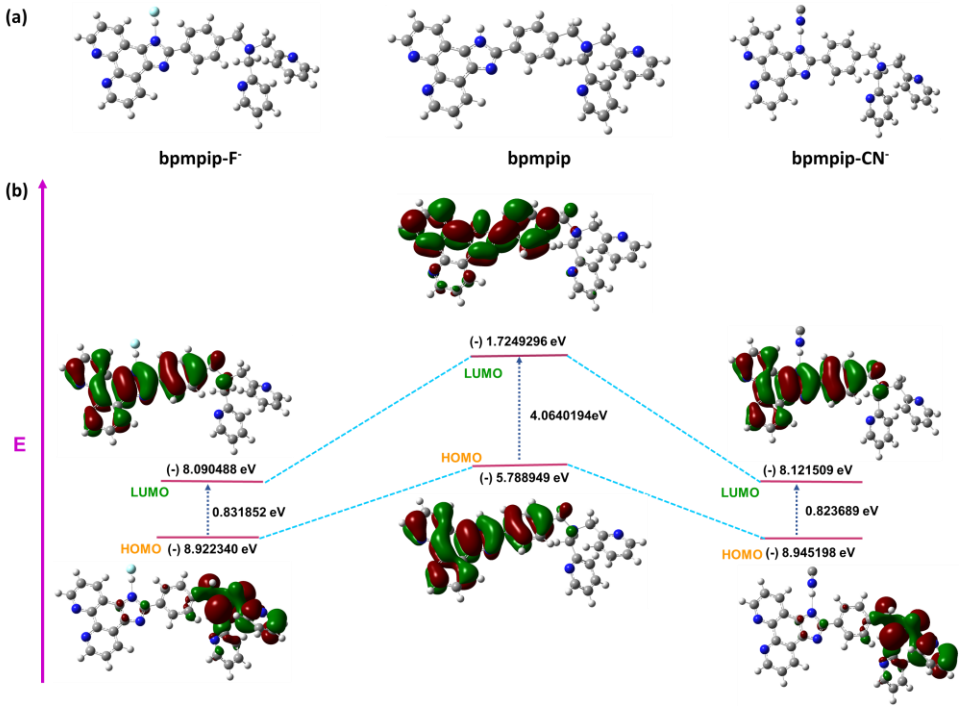

Fig. 6.4 DFT analysis of probe **bpmpip** and its adducts with CN^- and F^- ions.

6.3.3 Detection of anions in real samples

The practical applicability of the probe was demonstrated using real-world samples, including mouthwash (for F^- detection) and soil samples (for both F^- and CN^- detection). Mouthwash samples were analyzed without any pretreatment, while soil samples were first processed by vigorous mixing in acetonitrile, followed by filtration and centrifugation at 6000 rpm for 15 minutes. As depicted in Fig. 6.5, the fluorescence bands of **bpmpip** were quenched upon the addition of either sample. The response to fluoride was moderate, whereas the probe displayed relatively better sensitivity to cyanide, showing a distinct ratiometric response with good recovery values. Consistent changes were also observed in the UV-Vis spectra upon the addition of real samples (Fig. 6.5), highlighting the probe's effectiveness for real-world sensing applications.

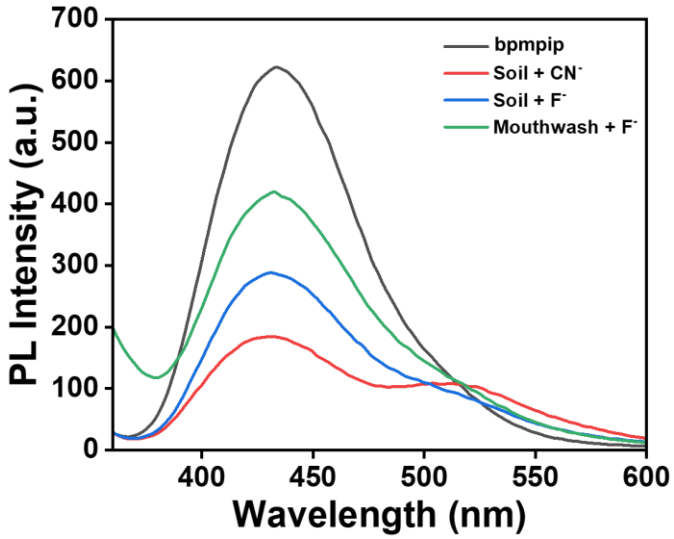

Fig. 6.5 Emissive response of probe **bpmpip** in different real samples. Detection for CN^- (red line) and F^- (red line) in corresponding anion-spiked soil samples, as well as for F^- in commercially available mouthwash (olive green line).

6.3.4 Low-cost test strip experiments

For its applied potential, the colorimetric and fluorogenic sensing performance of **bpmpip** has been further examined onto low-cost Whatman grade filter paper strips. The strips were finely cut into desired shapes, soaked in a semi-aqueous solution of probe **bpmpip** (~ 10^{-3} M), and air-dried. These prepared strips were then sprayed with solutions containing various anions, including CrO_4^{2-}, SO_4^{2-}, NO_3^-, AcO^-, F^-, CN^-, Br^-, I^-, CO_3^{2-}, and MnO_4^-, to assess their selectivity. Notably, only F^- and CN^- induced a visible color change, as shown in Fig. 6.6, turning from off-white to pastel green, with the response to fluoride being slightly less intense. Under UV light illumination, the probe exhibited a distinct color transition from light blue to yellow specifically in the presence of F^- and CN^-, demonstrating its dual-mode sensing capability.

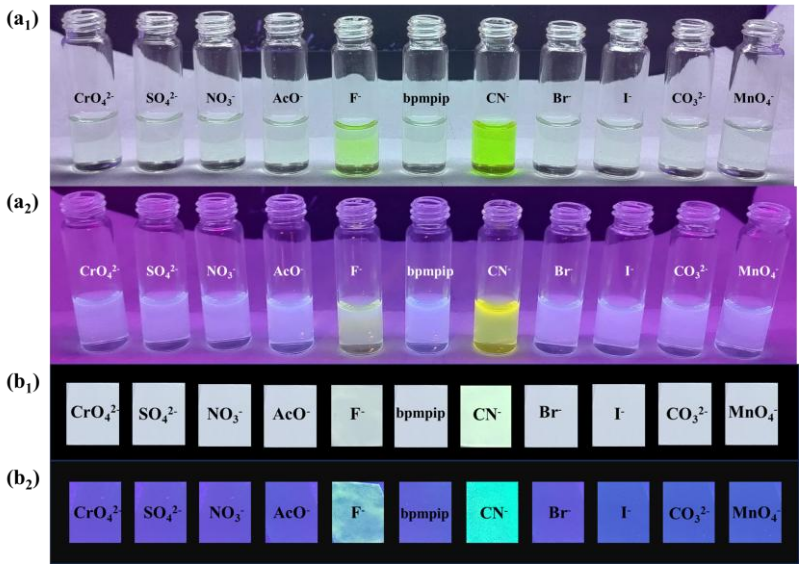

Fig. 6.6 Photographs of CH_3CN-H_2O solutions of **bpmpip** in presence of different metal ions captured under (a_1) visible light and (a_2) UV light illumination. Test strips of **bpmpip** treated with different anions under (b_1) visible light and (b_2) UV light illuminations.

6.3.5 Cell imaging study

To explore its practical applications in biological settings, probe **bpmpip** was evaluated for intracellular anion detection in living MCF-7 cell lines. Before bioimaging studies, the cytotoxicity of **bpmpip** was assessed using an MTT assay, which demonstrated its low cytotoxicity, confirming its suitability as a fluorescence-based probe for intracellular anion imaging. For the experiments, the cell lines were incubated with **bpmpip** (25 μM) for 3 hours, followed by treatment with fluoride ions (0-2.0 equiv) for next 1 hour. As depicted in Fig. 6.7, the probe was initially non-fluorescent in the blue channel. However, upon the addition of fluoride ions, a marked fluorescence enhancement was observed, with the intensity increasing proportionally to the fluoride ion concentration. In contrast, the probe exhibited a much weaker response to cyanide in live cells. These results establish that **bpmpip** is a promising candidate for the *in-vivo* detection of fluoride ions.

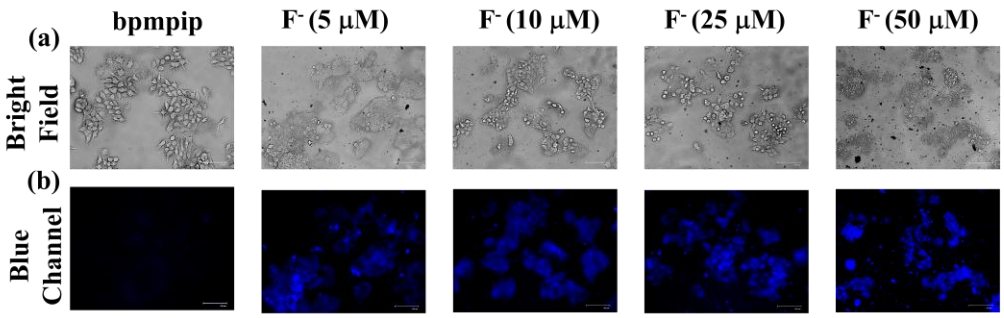

Fig. 6.7 Fluorescence imaging of MCF-7 cells incubated with 25 μM of probe **bpmpip** for 3 h, and then introduced 5-50 μM of F^- ions for 1 h. (a) Brightfield images and (b) fluorescence images in blue channel.

Table. 6.1 Comparison of sensing parameters of probe **bpmpip** with some previously reported probes.

S.N.	Probe	Target ions	LoD (μM)	Application	Ref.
1.	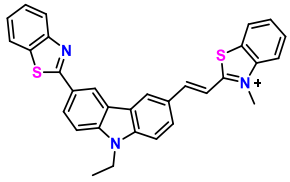	CN^-	0.09	Live cell imaging	(Sun et al., 2016)
2.	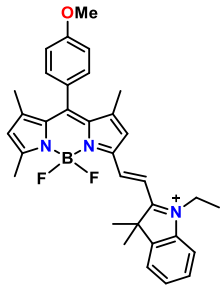	CN^-	2.41	Live cell imaging	(Kang et al., 2019)
3.	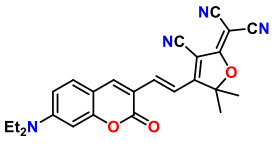	CN^- S^{2-}	- -	Live cell imaging	(Li et al., 2017)

4.	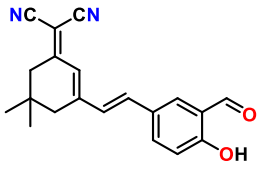	CN^-	0.27	Live cell imaging	(Huo et al., 2017)
5.	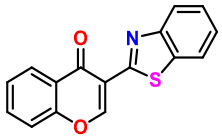	CN^-	0.0057	Live cell imaging	(Lohar et al., 2018)
6.	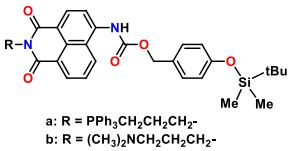 a: R = $PPh_3CH_2CH_2CH_2$- b: R = $(CH_3)_2NCH_2CH_2CH_2$-	F^-	a. 0.067 ppm b. 0.073 ppm	Live cell imaging	(Wu & Tang, 2015)
7.	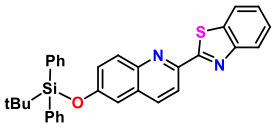	F^-	0.5	Live cell imaging	(Hu et al., 2016)
8.	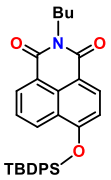	F^-	-	Live Cell and tissue imaging	(Zhu et al., 2015)
9.	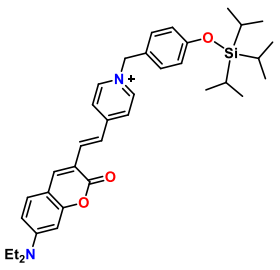	F^-	12×10^{-3}	Cell imaging	(Shen et al., 2018)

10.	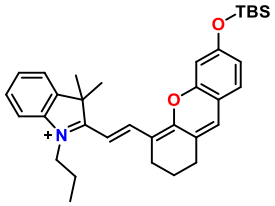	F^-	0.2	Drinking water, white flour, and cell imaging	(Tian et al., 2018)
11.	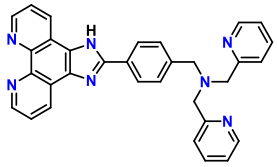	CN^-, F^-	0.032 0.899	Live cell imaging, test paper strips, and real samples (soil and mouthwash)	This work

6.4 Conclusions

We have successfully demonstrated that probe **bpmpip** can ratiometrically detect fluoride and cyanide ion by H-bonding interaction followed by deprotonation. The deprotonation of N-H group in the imidazole-phenanthroline ring was supported by NMR titration and DFT analysis. The aforementioned ions also exhibited a visual colour change from colourless to bright yellow-green which was visible to the naked eye. Low-cost test paper strips were also employed to detect cyanide and fluoride ions. The probe was able to successfully detect cyanide and fluoride in soil sample however recovery values were much better for cyanide ion. Moreover, **bpmpip** could successfully detect F^- in MCF-7 cancer cell lines as revealed by live cell imaging assessment.

SUMMARY OF THE THESIS

Title: Fluorescent Molecular Probes to Detect Metal Ions/Anions

This thesis presents the development of novel organic luminophores for the highly selective detection of metal ions and anions. The focus was given to design structurally simple luminophores with easy synthesis and purification processes. Ratiometric or "turn-on" sensors were prioritized due to their reliability over quenching-based sensors. Among various analytes, the detection of Al^{3+} was emphasized due to their widespread use, toxic effects on human health (e.g., neurodegenerative diseases, gastrointestinal issues), and detrimental environmental impacts, such as soil acidification and harm to aquatic ecosystems. The findings from this research have been published in prestigious journals, as listed below:

1. **Nidhi Goswami**, Sudhanshu Naithani, Tapas Goswami, Pankaj Kumar, Pramod Kumar, Sushil Kumar "Turn-on detection of Al^{3+} ions by quinoline based tripodal probe: Mechanistic investigation and live cells imaging applications" ***Anal. Methods*** **2024**, *16*, 5022-5031.
2. **Nidhi Goswami**, Sudhanshu Naithani, Tapas Goswami, Pankaj Kumar, Sushil Kumar "A quinoline derived Schiff base as highly selective 'turn-on' probe for fluorogenic recognition of Al^{3+} ion" ***Spectrochim. Acta A Mol. Biomol. Spectrosc.*** **2024**, *310*, 123971.
3. **Nidhi Goswami**, Sudhanshu Naithani, Jimmy Mangalam, Tapas Goswami, Ritesh Dubey, Pramod Kumar, Pankaj Kumar, Sushil Kumar "Fluorescent and chromogenic organic probes to detect group 10 metal ions: Design strategies and sensing applications" ***Dalton Trans.*** **2023**, *52,* 14704-14732.

In this thesis, a series of structurally simple compounds have been developed for their potential applications in optical sensing of metal ions and/or anions. The thesis has been divided into six chapters:

- **Chapter 1:** Introduces different types of optical sensors, fluorescence probes, and research gaps, alongside the thesis objectives.

- **Chapter 2:** Details materials, methods, and techniques for sensor development, metal ion detection, cell imaging, and characterization.
- **Chapter 3:** Discusses **QnSb**, a quinoline-based probe, for selective Al^{3+} detection. Characterized by spectroscopic techniques, **QnSb** exhibits a turn-on fluorescence response (422 nm) with high binding affinity (K_b: 2.3 × 10^5 M^{-1}) and a low detection limit (15.8 nM). DFT studies and Job's plot confirm a 1:1 binding stoichiometry. Practical applications include colorimetric and paper-strip tests for Al^{3+}.
- **Chapter 4:** Presents **TQSB**, a modified probe with N6 donor sites, enhancing sensitivity (LoD: 7.0 nM) for Al^{3+} in real samples (e.g., soil, gastric tablets) and intracellular imaging in MCF-7 cells. The CHEF effect and inhibition of PeT and >C=N- isomerization contribute to its performance.
- **Chapter 6:** Describes **bpmpip**, an imidazo-phenanthroline-based probe for selective CN^- and F^- detection. Characterized by ^1H NMR and ESI-MS, **bpmpip** detects these ions via H-bonding and deprotonation, with LoDs of 32.26 nM (CN^-) and 233 nM (F^-). Applications include soil, mouthwash, and cancer cell imaging.

ANNEXURE I

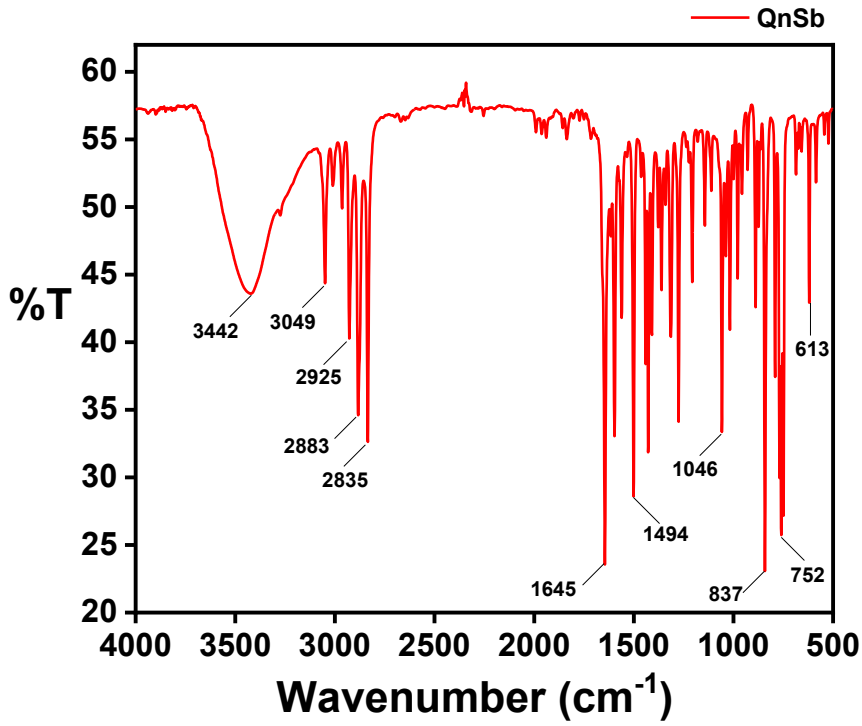

Fig. A1. Infrared spectrum of **QnSb**.

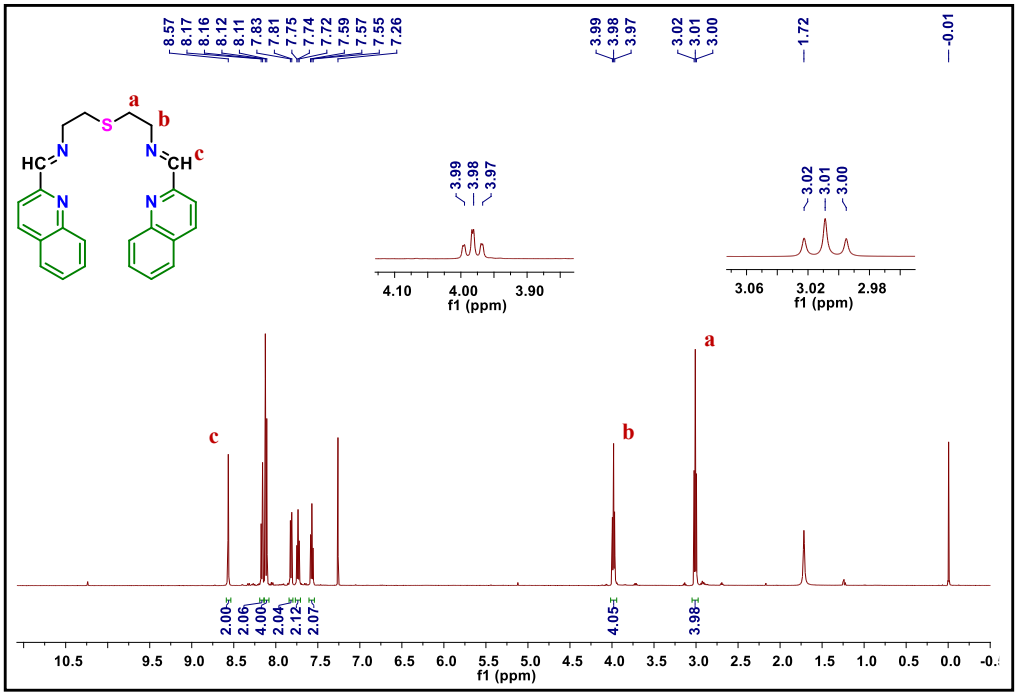

Fig. A2. ^{1}H NMR spectrum of **QnSb** in $CDCl_3$ at room temperature.

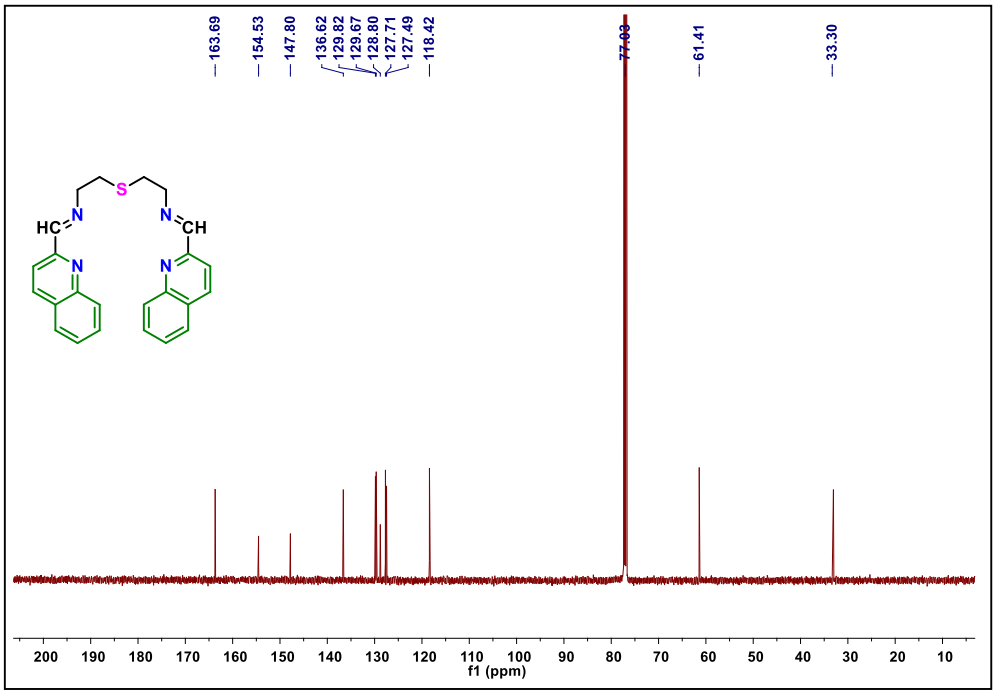

Fig. A3. ^{13}C NMR spectrum of **QnSb** in $CDCl_3$ at room temperature.

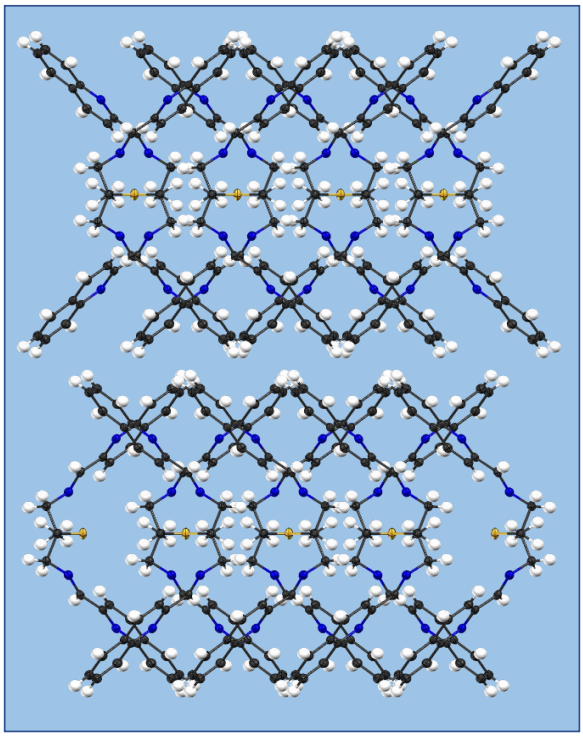

Fig. A4. Intermolecular hydrogen bonding interactions in the crystal structure of probe **QnSb**.

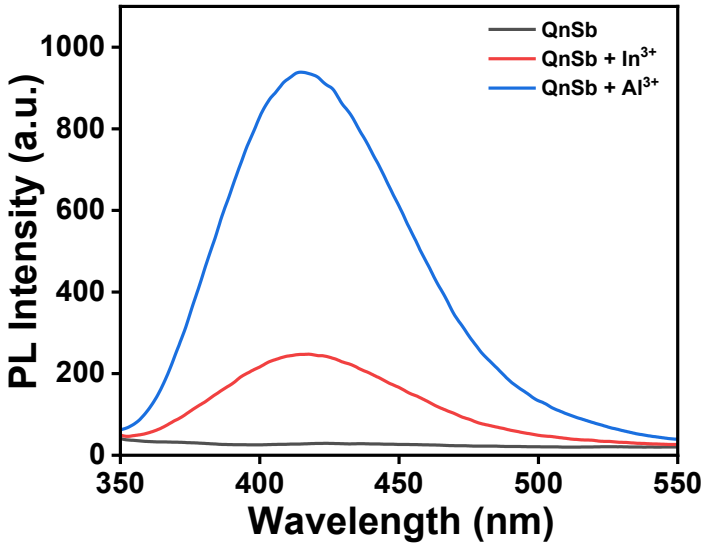

Fig. A5. Steady-state fluorescence spectra of **QnSb** in presence of In^{3+} and Al^{3+} ions.

Table A1. Optimized bond distances obtained from DFT calculations.

	Bond length (Å)
Al-N1	2.11208
Al-N2	2.15694
Al-N3	2.17668
Al-N4	2.09885
Al-Cl	2.25364

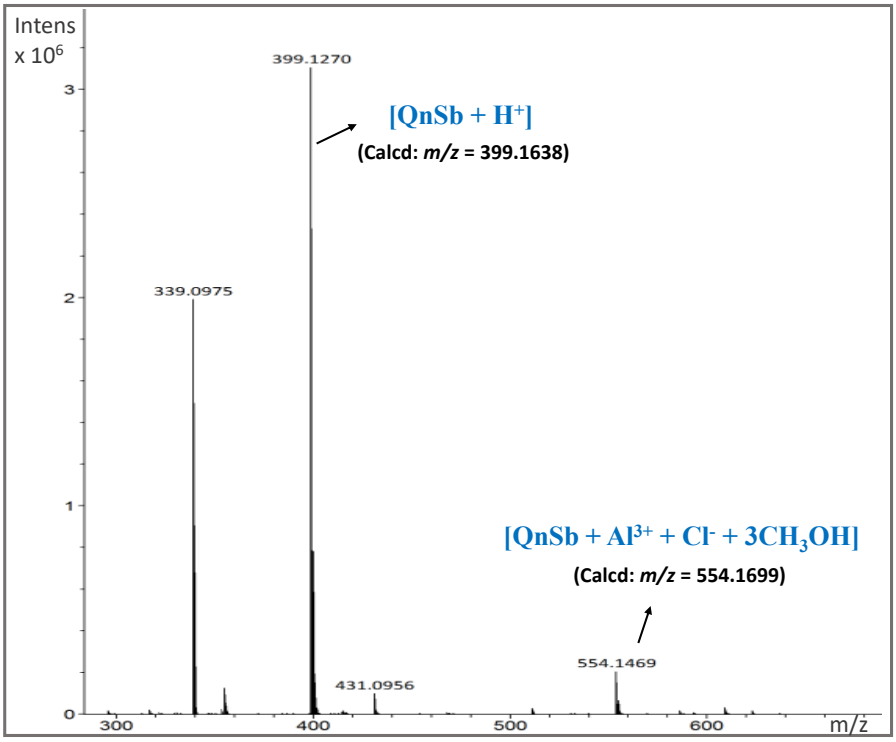

Fig. A6. ESI-MS analysis of **QnSb** in the presence of Al^{3+} ions in methanol at room temperature.

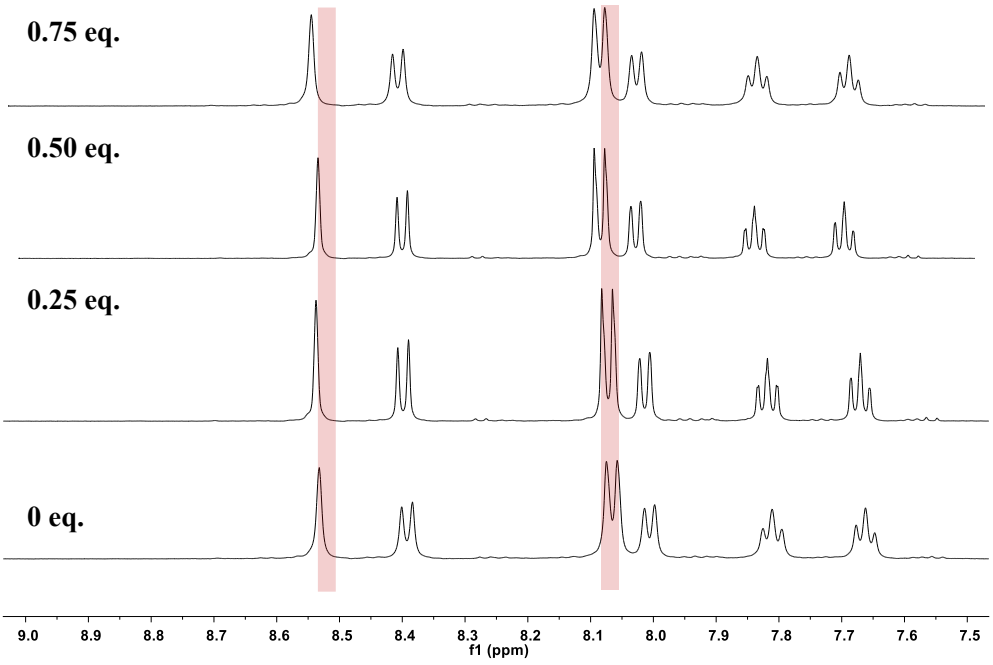

Fig. A7. ^{1}H NMR analysis of **QnSb** with varied concentration of Al^{3+} ions in DMSO-d_6 at room temperature.

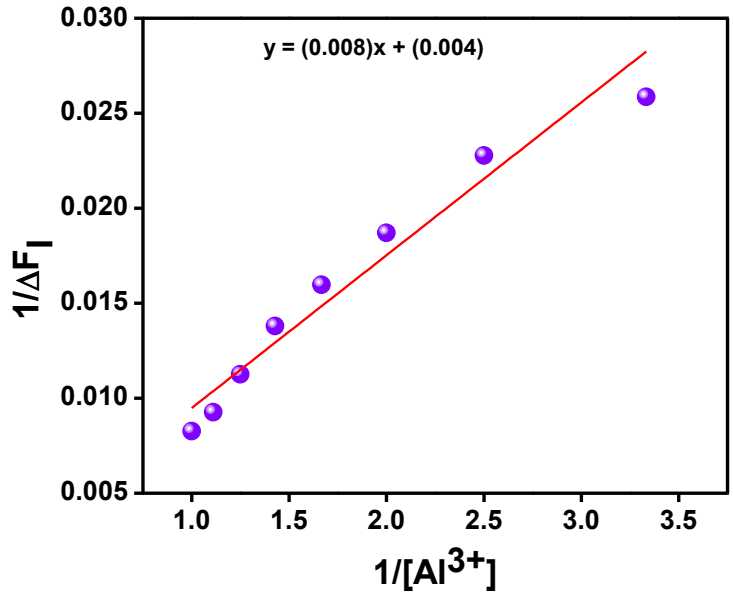

Fig. A8. Benesi-Hildebrand plot for determination of binding constant.

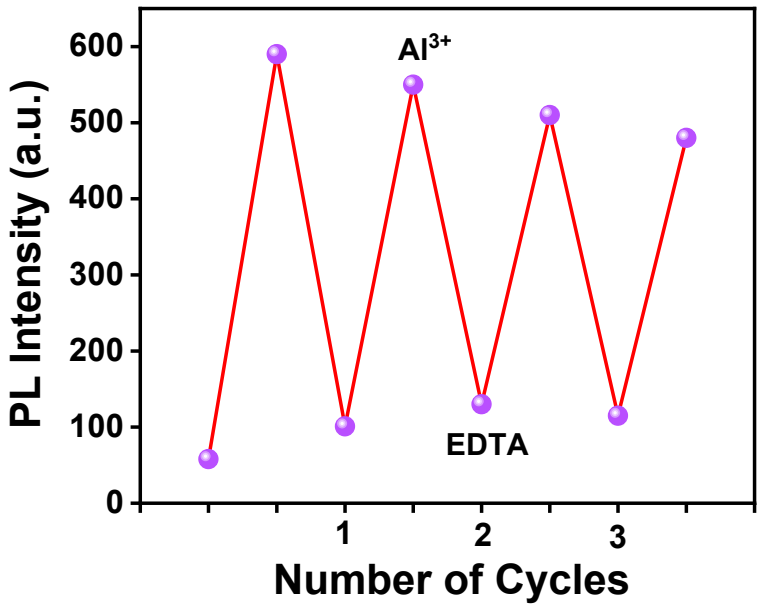

Fig. A9. Fluorescence intensity of **QnSb** at 422 nm upon alternate addition of a varied amount of Al^{3+} and EDTA ions.

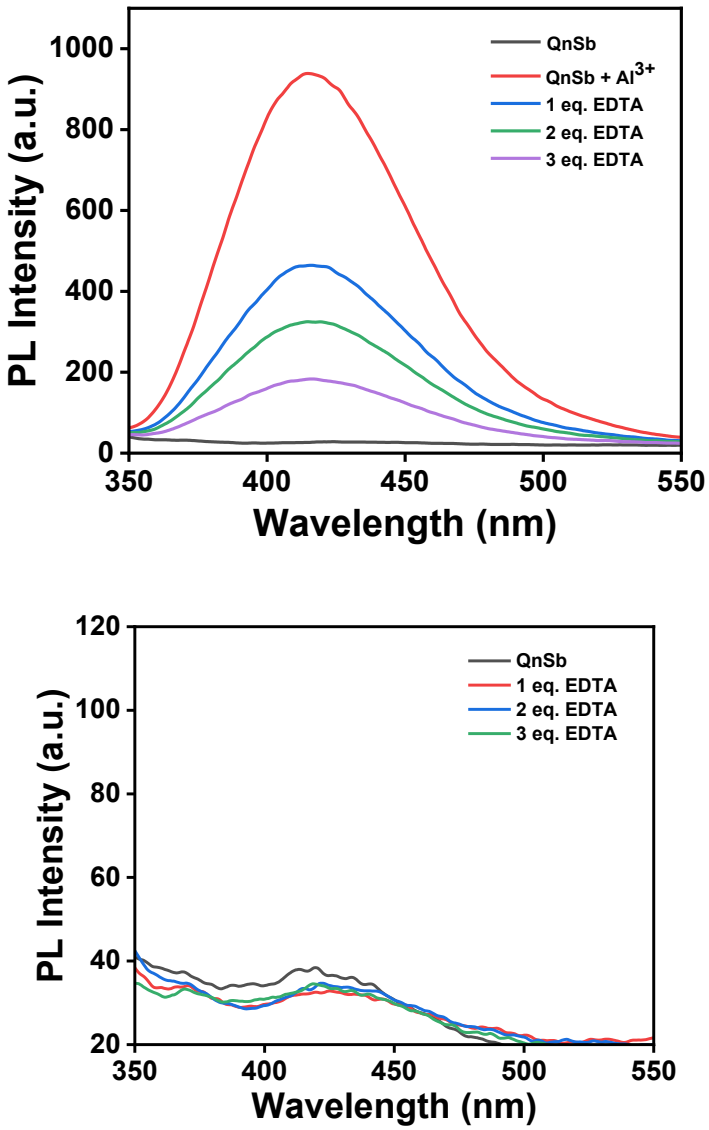

Fig. A10. Fluorescence intensity of **QnSb** at 422 nm addition of a particular amount of Al^{3+} with varied concentrations of EDTA ions (1 eq. to 3 eq.)

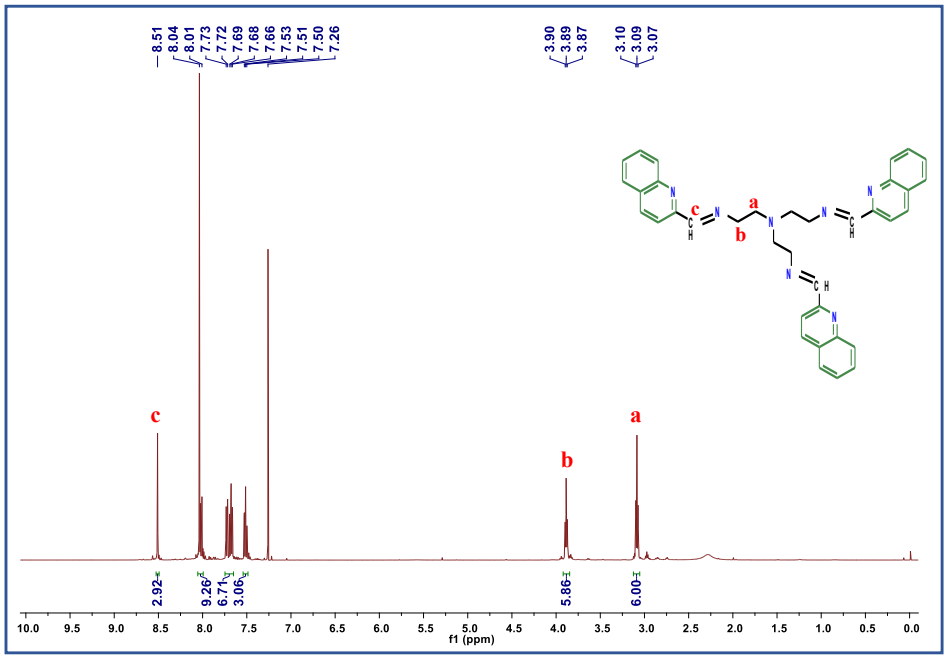

Fig. A11. ^{1}H NMR spectrum of **TQSB** in $CDCl_3$ at room temperature.

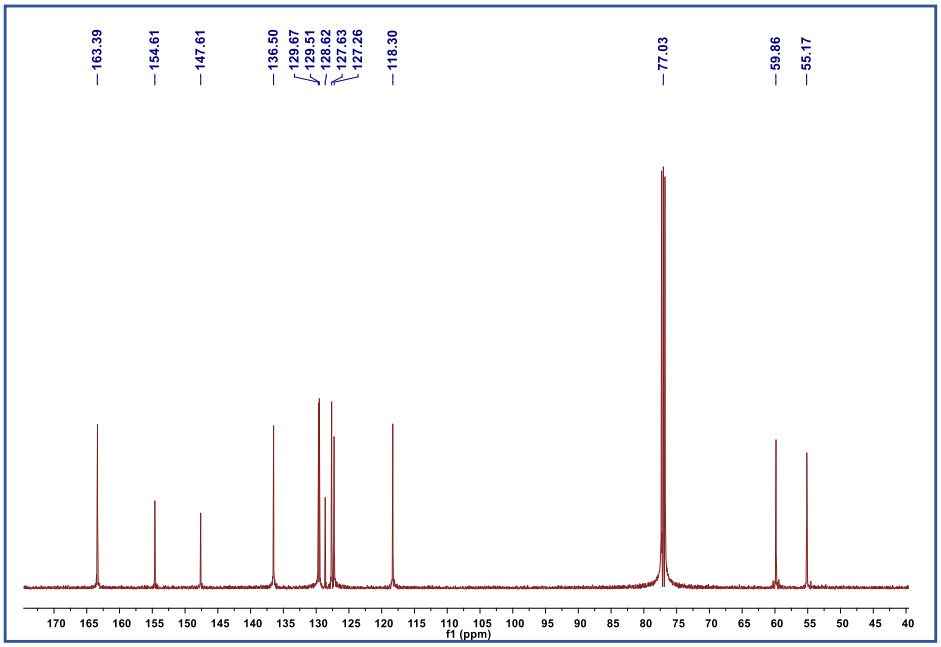

Fig. A12. ^{13}C NMR spectrum of **TQSB** in $CDCl_3$ at room temperature.

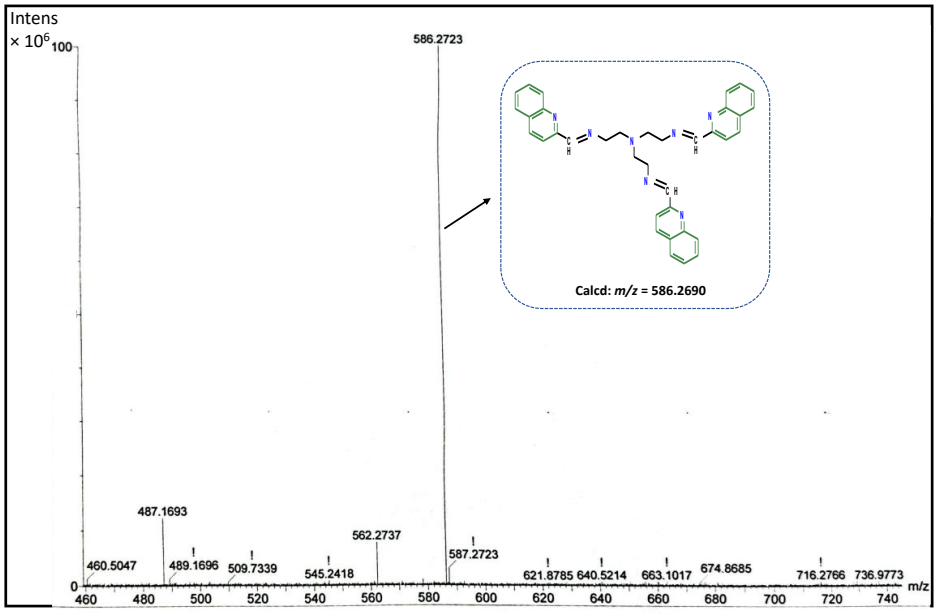

Fig. A13. ESI-MS analysis of **TQSB** in methanol at room temperature.

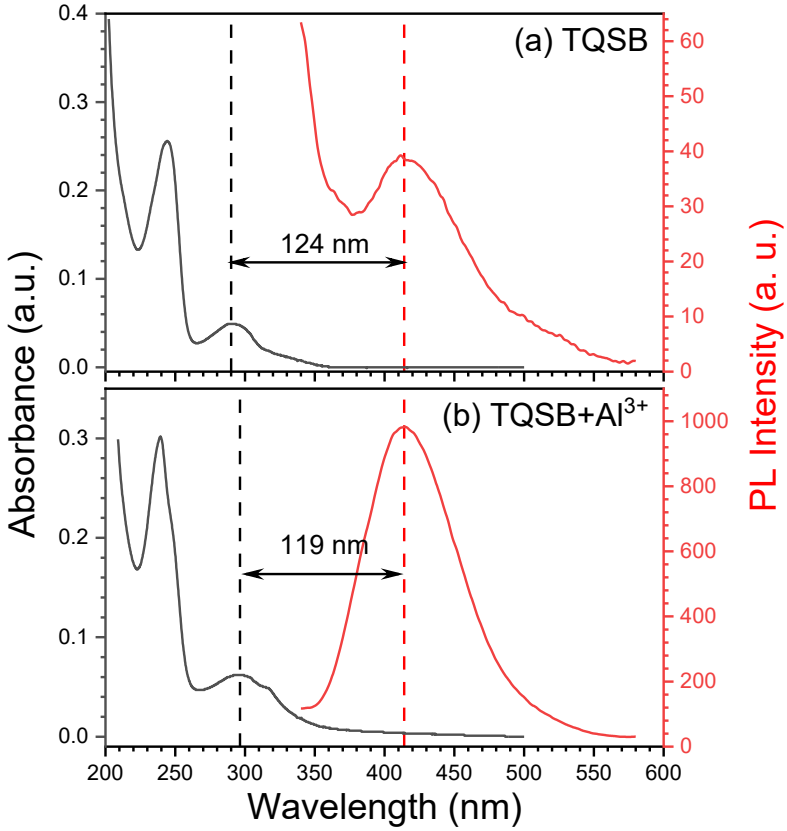

Fig. A14. UV-Vis and emission spectra for (a) **TQSB** and (b) **TQSB**-Al^{3+} in acetonitrile solution along with their Stokes shift values.

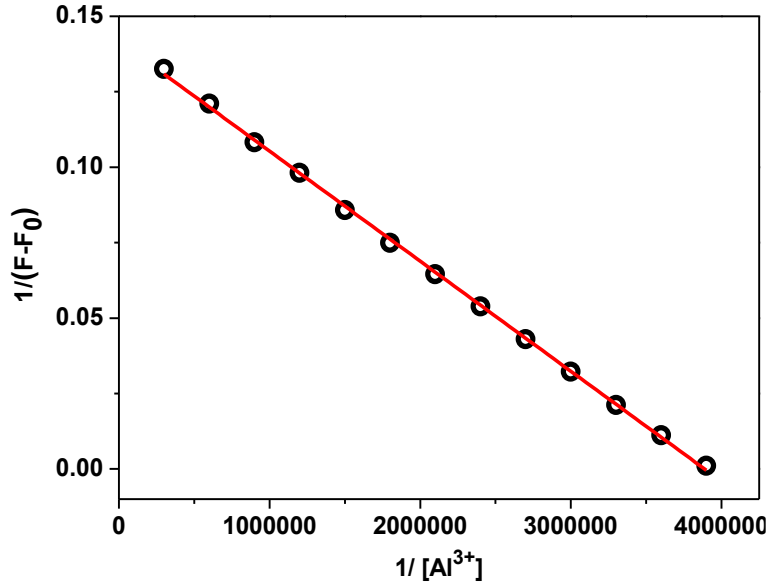

Fig. A15. Benesi-Hildebrand plot for determination of binding constant.

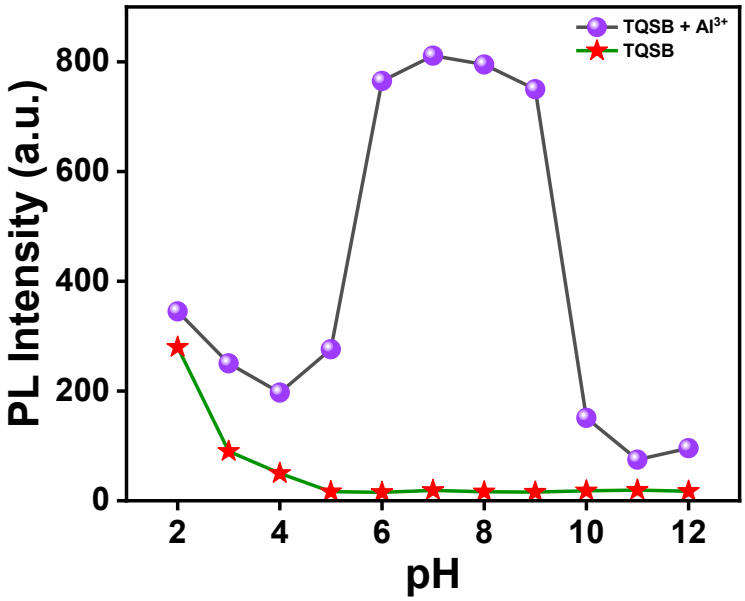

Fig. A16. Effect of pH on probe **TQSB** and **TQSB**-Al^{3+} complex.

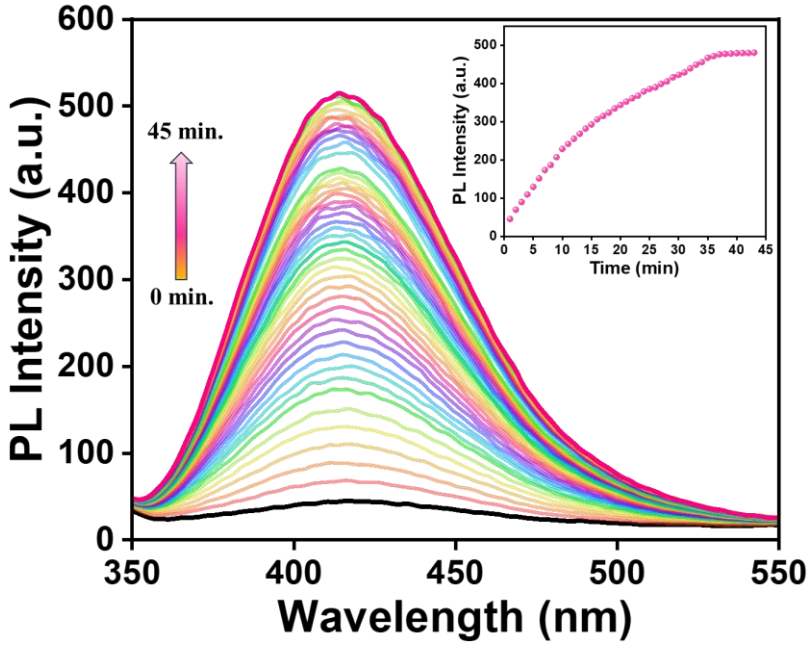

Fig. A17. Response time of probe **TQSB** with Al^{3+} ions.

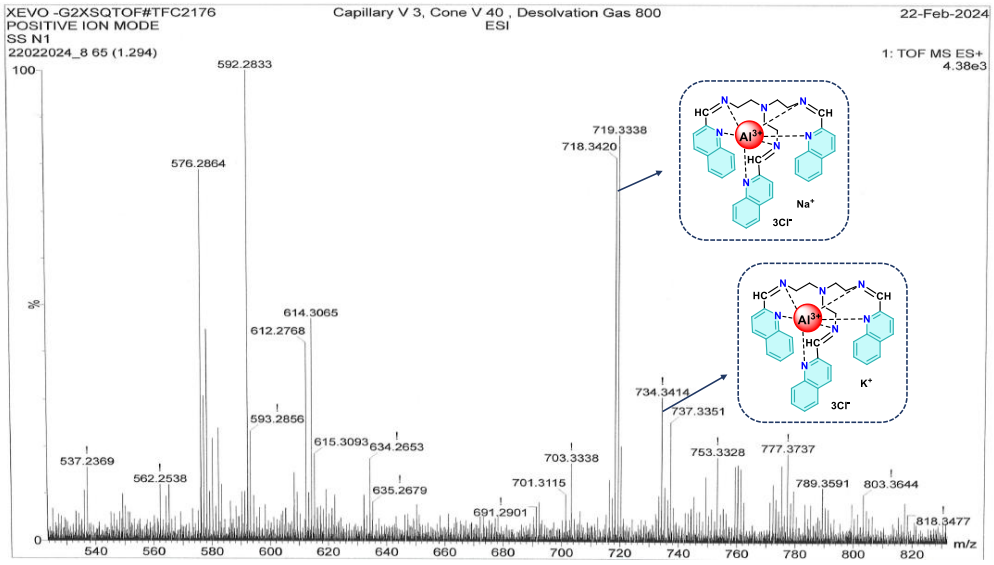

Fig. A18. ESI-MS analysis of **TQSB**-Al^{3+} in methanol at room temperature.

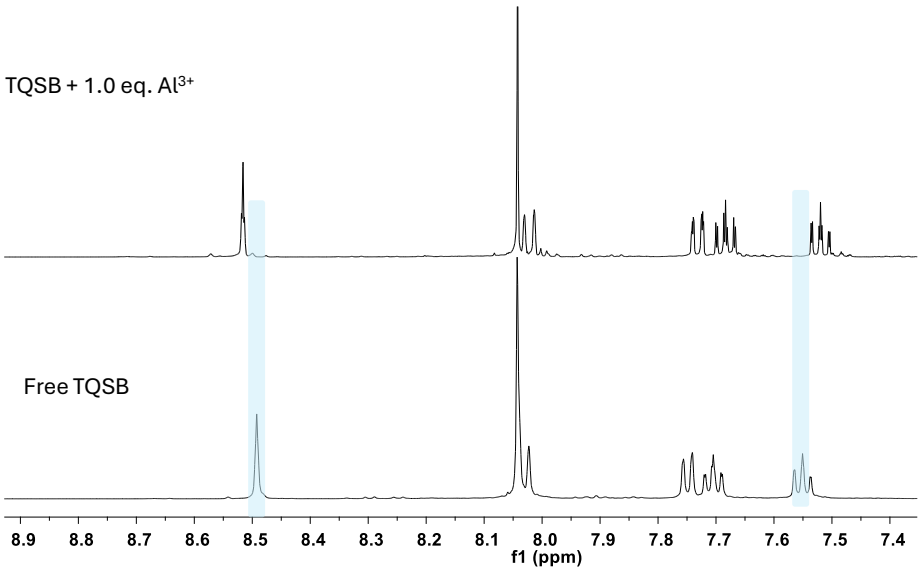

Fig. A19. ^{1}H NMR analysis of probe **TQSB** in absence and presence of Al^{3+} at room temperature.

Table A2. Optimized bond distances obtained from DFT calculations.

	Bond length (Å)
Al-N11	2.15927
Al-N12	2.04614
Al-N21	2.15956
Al-N22	2.04639
Al-N31	2.15962
Al-N32	2.04638

Table A3. Fluorescence quantum yield values and HOMO/LUMO energies of **TQSB** and **TQSB**-Al^{3+}.

	TQSB	**TQSB-Al^{3+}**
Quantum yield	0.058	0.464
HOMO (E_1)	(-) 5.4017 eV	(-) 13.7156 eV
LUMO (E_2)	(-) 1.9662 eV	(-) 11.3969 eV
ΔE (E_1-E_2)	3.4355 eV	2.3187 eV

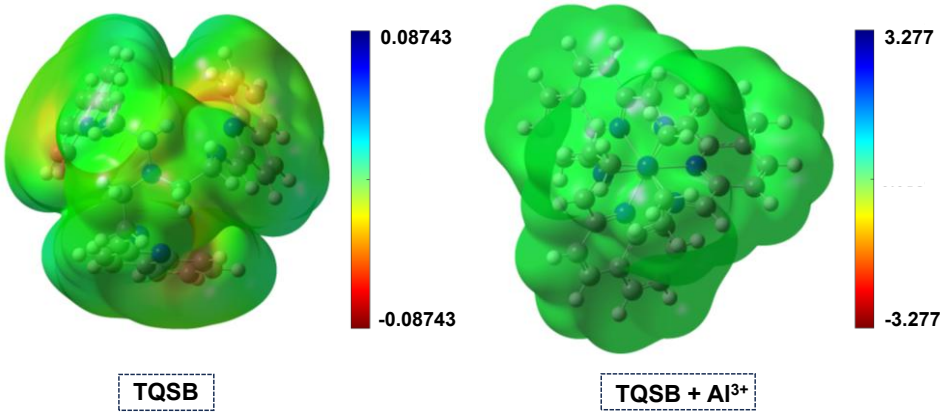

Fig. A20. The electrostatic potential (ESP) of **TQSB** (-0.08743 to + 0.08743) and **TQSB**-Al^{3+} (-3.277 to + 3.277).

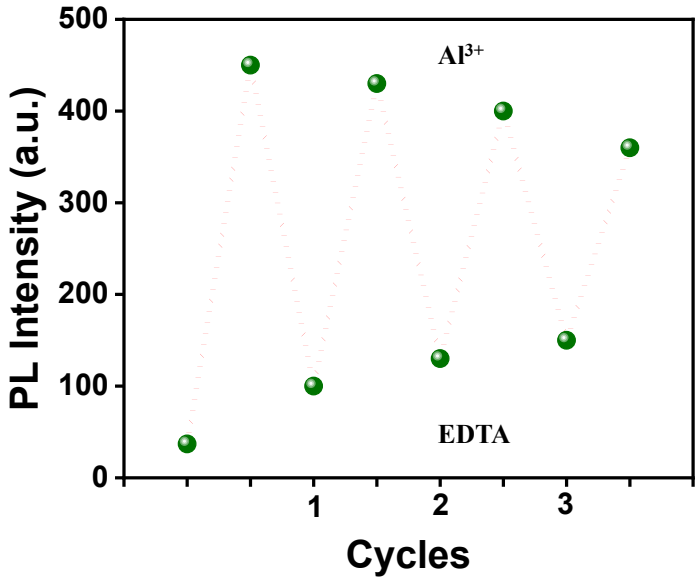

Fig. A21. Fluorescence intensity of **TQSB** at 414 nm upon alternate addition of a varied amount of Al^{3+} and EDTA ions.

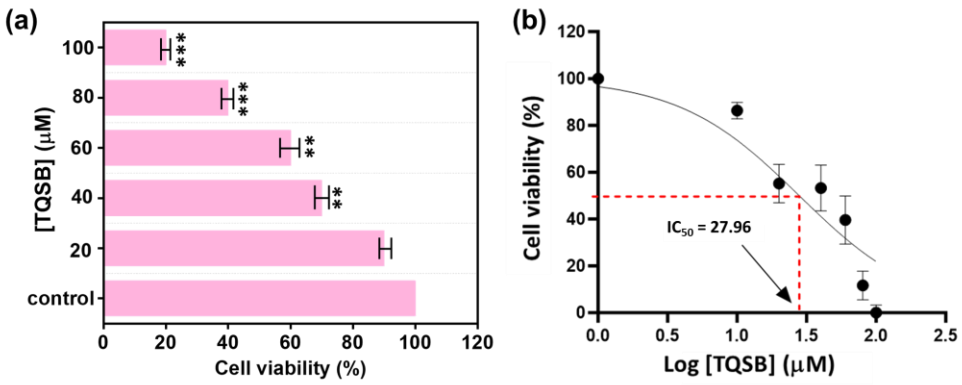

Fig. A22. (a) MTT assay of **TQSB**, $Al^{3+,}$ and **TQSB**-Al^{3+} complex on MCF7 cancer cell lines and **(b)** Cell viability of **TQSB** at different concentrations (IC_{50} value was 27.96 μM).

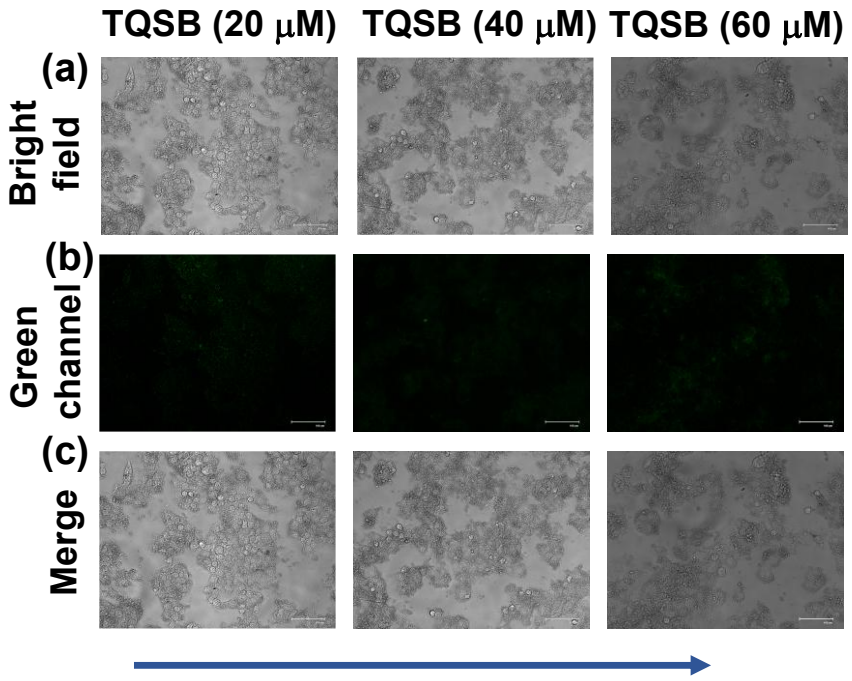

Fig. A23. Confocal imaging of human breast cancer MCF-7 cell lines incubated with variable concentrations (20-60 μM) of **TQSB**.

Table. A4. Detection of Al^{3+} in real samples.

Sample	Al^{3+} spiked / Present (μM)	Al^{3+} calculated (μM)	Al^{3+} calculated from ICP-MS (μM)	% Recovery
Soil samples				
	0.4	0.38	0.39	95.0
	0.8	0.77	0.81	96.25
	1.0	1.04	1.02	104
Gastric Tablet				
	0.4	0.39	0.38	97.5
	0.8	0.82	0.81	102.5
	1.0	0.97	0.99	97

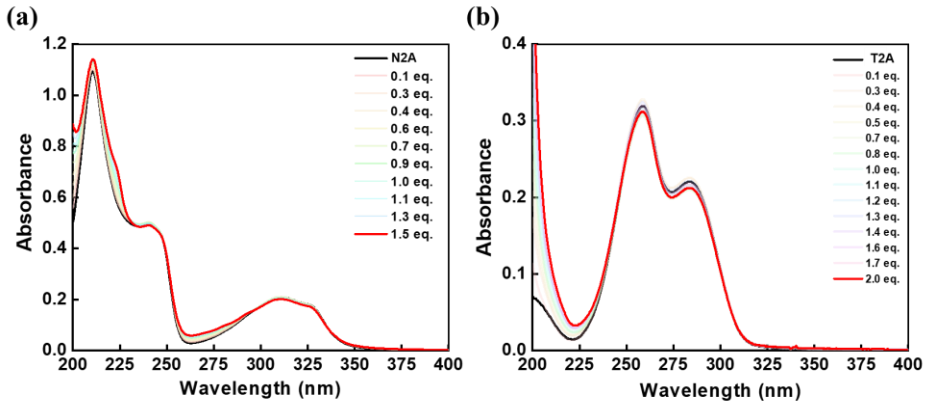

Fig. A24. (a) Absorption spectral variations in **N2A** at different concentrations of $AlCl_3.6H_2O$ and (b) Absorption spectral variations in **T2A** at different concentrations of $AlCl_3.6H_2O$.

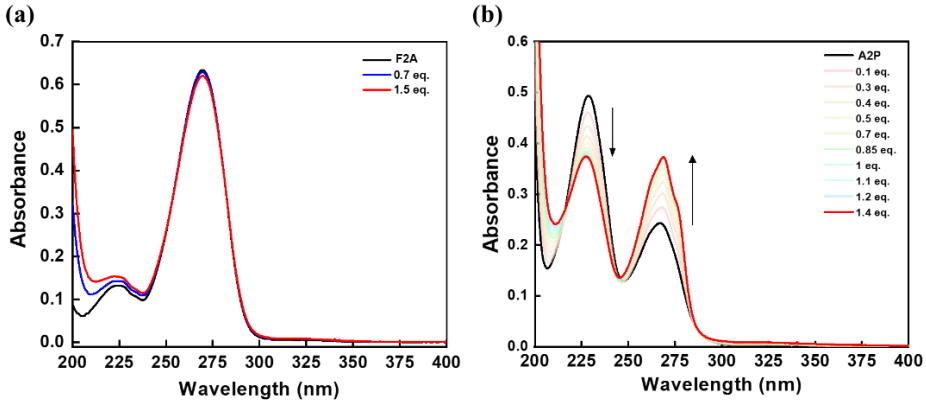

Fig. A25. (a) Absorption spectral variations in **F2A** at different concentrations of $AlCl_3.6H_2O$ and (b) Absorption spectral variations in **A2P** at different concentrations of $AlCl_3.6H_2O$.

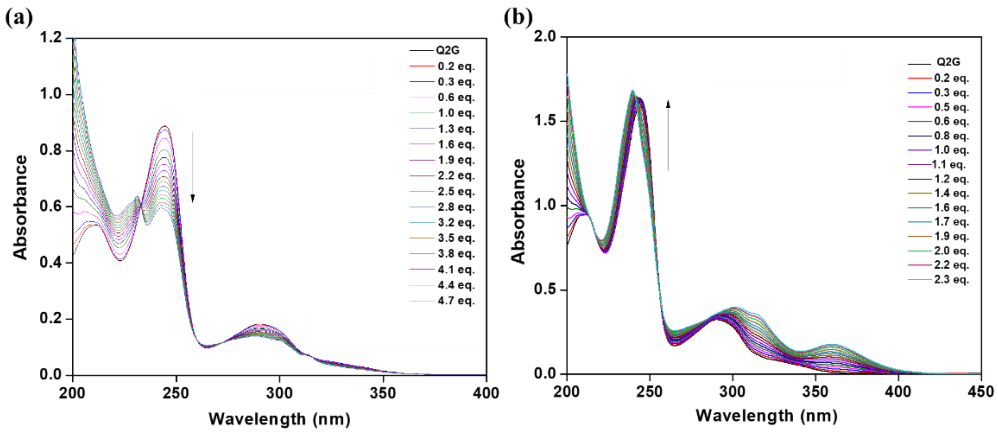

Fig. A26. (a) Absorption spectral changes in **Q2G** upon addition of $ZnCl_2$ in acetonitrile and (b) Absorption spectral changes in **Q2G** upon addition of $FeCl_3$ in acetonitrile.

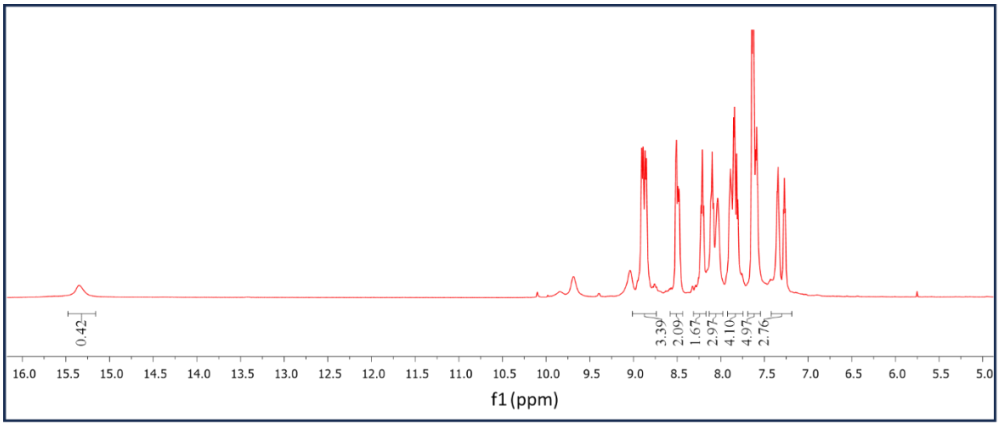

Fig. A27. ^1H NMR spectrum of **bpmpip** in $CDCl_3$ at room temperature.

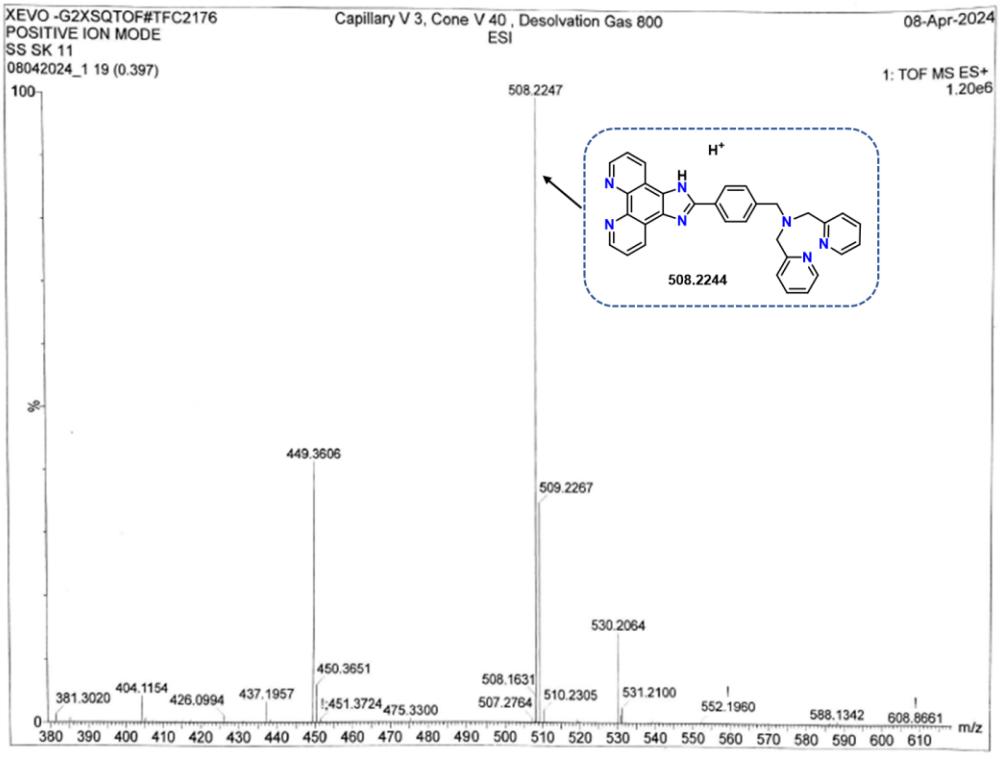

Fig. A28. ESI-MS analysis of **bpmpip** in methanol at room temperature.

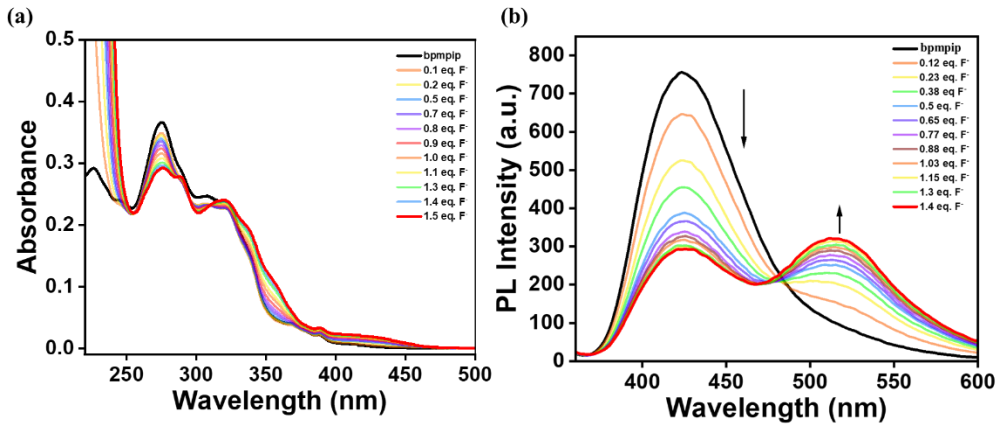

Fig. A29. (a) Absorption spectral variations in **bpmpip** at different concentrations of fluoride ion (0-1.5 eq) and (b) Emission spectral variations in **bpmpip** at different concentrations of fluoride ions (0-1.4 eq).

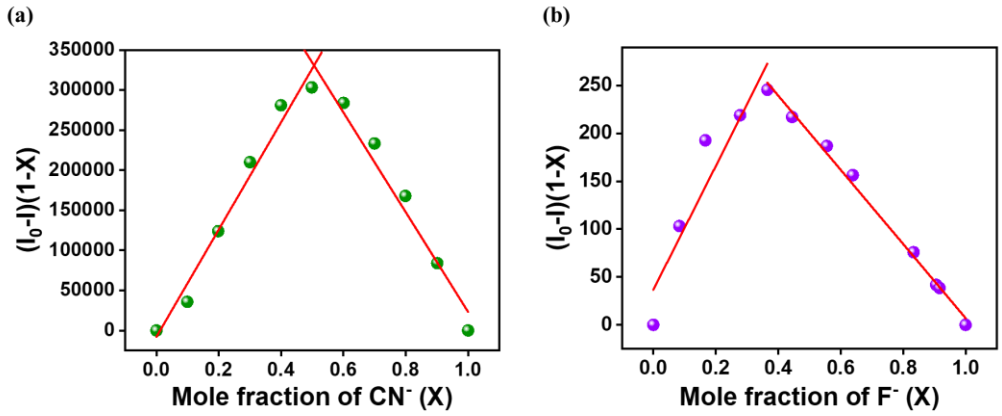

Fig. A30. Job's plot of **bpmpip** for CN^- and F^- determined by the fluorescence method indicating 1:1 stoichiometry.

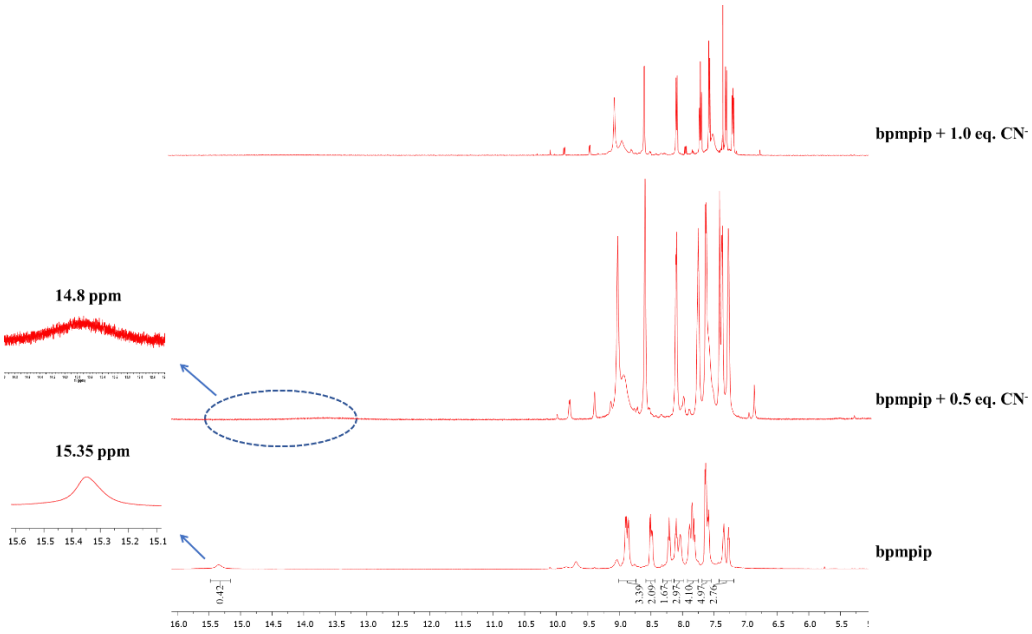

Fig. A31. ^1H NMR titration of probe **bpmpip** in presence of CN^- ions at room temperature.

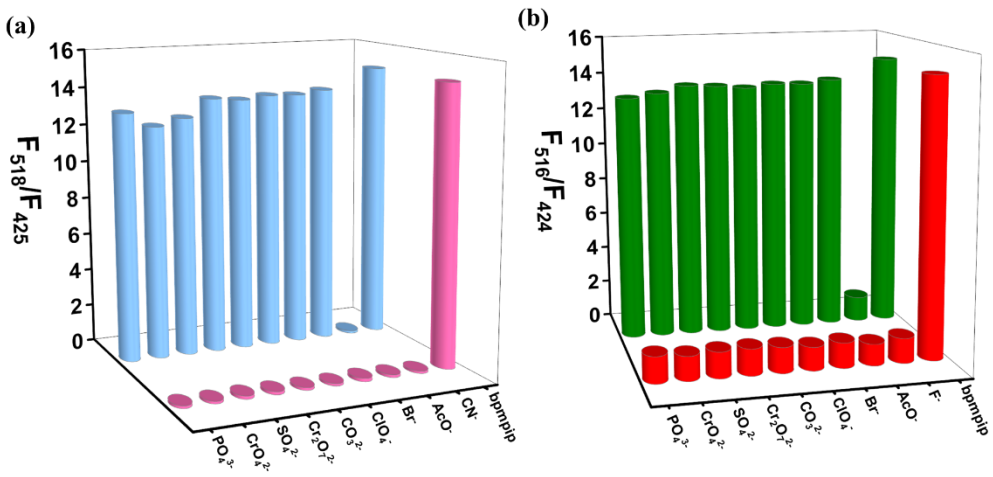

Fig. A32. (a) Selectivity studies of probe **bpmpip** towards CN^- ion over other anions; **bpmpip** + anions (skyblue bars) and **bpmpip** + anion + CN^- (pink bars); (b) Selectivity studies of probe **bpmpip** towards F^- ion over other anions; **bpmpip** + anions (green bars) and **bpmpip** + anion + F^- (red bars).

REFERENCES

A new ’turn-on’and reversible fluorescent sensor for Al 3+ detection and live cell imaging. (n.d.). *Pubs.Rsc.OrgJH Wang, LH Feng, JB Chao, Y Wang, SM ShuangAnalytical Methods, 2019•pubs.Rsc.Org*. Retrieved December 23, 2024, from https://pubs.rsc.org/en/content/articlehtml/2019/ay/c9ay01438a

A novel AIE-active camphor-based fluorescent probe for simultaneous detection of Al 3+ and Zn 2+ at dual channels in living cells and zebrafish. (n.d.). *Pubs.Rsc.OrgS Gong, Y Zhang, A Qin, M Li, Y Gao, C Zhang, J Song, X Xu, Z Wang, S WangAnalyst, 2022•pubs.Rsc.Org*. Retrieved December 30, 2024, from https://pubs.rsc.org/en/content/articlehtml/2001/va/d1an01733k

A novel quinoline derivative as dual chemosensor for selective sensing of Al3+ by fluorescent and Fe2+ by colorimetric methods. (n.d.). *Elsevier*. Retrieved January 2, 2025, from https://www.sciencedirect.com/science/article/pii/S002228602100096X

A photoswitchable “turn-on” fluorescent chemosensor: Quinoline-naphthalene duo for nanomolar detection of aluminum and bisulfite ions and its multifarious. (n.d.). *ElsevierCI David, H Jayaraj, G Prabakaran, K Velmurugan, DP Devi, R Kayalvizhi, A AbiramFood Chemistry, 2022•Elsevier*. Retrieved January 2, 2025, from https://www.sciencedirect.com/science/article/pii/S0308814621021361

Afrin, A., & Chinna Ayya Swamy, P. (2023). Novel Schiff base derivatives for the detection of one-to-multi metal ions and tracking the live cell imaging. *Coordination Chemistry Reviews*, *494*, 215327. https://doi.org/10.1016/J.CCR.2023.215327

Afrin, A., Reviews, P. S.-C. C., & 2023, undefined. (n.d.). Novel Schiff base derivatives for the detection of one-to-multi metal ions and tracking the live cell imaging. *ElsevierA Afrin, PCA SwamyCoordination Chemistry*

Reviews, 2023•Elsevier. Retrieved December 23, 2024, from https://www.sciencedirect.com/science/article/pii/S0010854523003168

AIE-based luminescence probes for metal ion detection. (n.d.). *ElsevierP Alam, NLC Leung, J Zhang, RTK Kwok, JWY Lam, BZ TangCoordination Chemistry Reviews, 2021•Elsevier*. Retrieved December 23, 2024, from https://www.sciencedirect.com/science/article/pii/S0010854520309383

Alam, P., Leung, N. L. C., Zhang, J., Kwok, R. T. K., Lam, J. W. Y., & Tang, B. Z. (2021). AIE-based luminescence probes for metal ion detection. *Coordination Chemistry Reviews*, *429*, 213693. https://doi.org/10.1016/J.CCR.2020.213693

Alharbi, K. H. (2023). A Review on Organic Colorimetric and Fluorescent Chemosensors for the Detection of Zn(II) Ions. *Critical Reviews in Analytical Chemistry*, *53*(7), 1472–1488. https://doi.org/10.1080/10408347.2022.2033611

Alizada, M., Gul, A., Oguz, M., Kursunlu, A. N., & Yilmaz, M. (2021). Ion sensing of sister sensors based-on calix[4]arene in aqueous medium and their bioimaging applications. *Dyes and Pigments*, *184*, 108741. https://doi.org/10.1016/J.DYEPIG.2020.108741

Alqarni, S. A. (2024a). A Review on Conducting Polymers for Colorimetric and Fluorescent Detection of Noble Metal Ions (Ag+, Pd2+, Pt2+/4+, and Au3+). *Critical Reviews in Analytical Chemistry*, *54*(2), 389–400. https://doi.org/10.1080/10408347.2022.2079945

Alqarni, S. A. (2024b). A Review on Conducting Polymers for Colorimetric and Fluorescent Detection of Noble Metal Ions (Ag+, Pd2+, Pt2+/4+, and Au3+). *Critical Reviews in Analytical Chemistry*, *54*(2), 389–400. https://doi.org/10.1080/10408347.2022.2079945

An AIE active anthracene-based Schiff base probe for “turn-on” detection of Cu2+ ions: Demonstrations with nanostructural investigations, DFT,

cellular imaging, and. (n.d.). *Elsevier*. Retrieved December 23, 2024, from https://www.sciencedirect.com/science/article/pii/S0022286023024353

An ESIPT characteristic “turn-on” fluorescence sensor for Hg2+ with large Stokes shift and sequential “turn-off” detection of S2–as well as the application in living cells. (n.d.). *Elsevier*. Retrieved December 30, 2024, from https://www.sciencedirect.com/science/article/pii/S1010603019315758

An, Y., Li, B., Yu, Y., Zhou, Y., Yi, J., Li, L., Sun, Y., Qiang, Z., Liu, Y., & Wang, P. (2024). A rapid and specific fluorescent probe based on aggregation-induced emission enhancement for mercury ion detection in living systems. *Journal of Hazardous Materials*, *465*, 133331. https://doi.org/10.1016/J.JHAZMAT.2023.133331

Anu, D., Naveen, P., and, R. R.-J. of P., & 2021, undefined. (n.d.). Development of hydrazide based fluorescence probe for detection of Al3+ ions and application in live cell image. *Elsevier*. Retrieved December 23, 2024, from https://www.sciencedirect.com/science/article/pii/S1010603020307188

Arora, A., Kaushal, J., Kumar, A., Kumar, P., & Kumar, S. (2019a). Ruthenium(II)-Polypyridyl-Based Sensor Bearing a DPA Unit for Selective Detection of Cu(II) Ion in Aqueous Medium. *ChemistrySelect*, *4*(20), 6140–6147. https://doi.org/10.1002/SLCT.201900682

Arora, A., Kaushal, J., Kumar, A., Kumar, P., & Kumar, S. (2019b). Ruthenium(II)-Polypyridyl-Based Sensor Bearing a DPA Unit for Selective Detection of Cu(II) Ion in Aqueous Medium. *ChemistrySelect*, *4*(20), 6140–6147. https://doi.org/https://doi.org/10.1002/slct.201900682

Arora, A., Oswal, P., Rao, G. K., Kaushal, J., Kumar, S., Singh, A. K., & Kumar, A. (2019). Chalcogen (S/Se) Ligated Palladium(II) Complexes of Bulky Ligands: Application in O-Arylation of Phenol. *ChemistrySelect*, *4*(36), 10765–10769. https://doi.org/10.1002/SLCT.201901834

Aruna, Verma, V. P., Singh, A. P., & Shrivastava, R. (2024a). Recent advancement in development of fluorescein based molecular probes for analytes sensing. *Journal of Molecular Structure*, *1295*, 136549. https://doi.org/10.1016/J.MOLSTRUC.2023.136549

Aruna, Verma, V. P., Singh, A. P., & Shrivastava, R. (2024b). Recent advancement in development of fluorescein based molecular probes for analytes sensing. *Journal of Molecular Structure*, *1295*, 136549. https://doi.org/10.1016/J.MOLSTRUC.2023.136549

Atta, A. K., Kim, S. B., Heo, J., & Cho, D. G. (2013). Hg(II)-mediated intramolecular cyclization reaction in aqueous media and its application as Hg(II) selective indicator. *Organic Letters*, *15*(5), 1072–1075. https://doi.org/10.1021/OL4000873/SUPPL_FILE/OL4000873_SI_002.CIF

Aydin, D. (2020). A novel turn on fluorescent probe for the determination of Al3+ and Zn2+ ions and its cells applications. *Talanta*, *210*, 120615. https://doi.org/10.1016/J.TALANTA.2019.120615

Bai, Q., Xia, Y., Liang, G., Wang, C., Redshaw, C., & Xiao, X. (2023). Novel fluorescent probe for sequential recognition of Zn2+ and pyrophosphate in aqueous based on aggregation-induced emission. *Spectrochimica Acta Part A: Molecular and Biomolecular Spectroscopy*, *295*, 122585. https://doi.org/10.1016/J.SAA.2023.122585

Balamurugan, R., Liu, J. H., & Liu, B. T. (2018). A review of recent developments in fluorescent sensors for the selective detection of palladium ions. *Coordination Chemistry Reviews*, *376*, 196–224. https://doi.org/10.1016/J.CCR.2018.07.017

Balasubramanian, K., Ramaraj, S., … C. K.-I. C., & 2023, undefined. (n.d.-a). A novel Schiff base derived quinoline moieties as a selective fluorophore for Sn2+ ion sensing. *Elsevier*. Retrieved December 22, 2024, from https://www.sciencedirect.com/science/article/pii/S1387700323006810?c

asa_token=F0CGb5ORU-EAAAAA:nmo1ZeT2eru4V19k_1tBPwhl-4119tLToOY36Nsg0NmwjYcAQ0vO_XrUDE3DVXKFZoPxPG9nVbgk

Balasubramanian, K., Ramaraj, S., … C. K.-I. C., & 2023, undefined. (n.d.-b). A novel Schiff base derived quinoline moieties as a selective fluorophore for Sn2+ ion sensing. *Elsevier*. Retrieved December 23, 2024, from https://www.sciencedirect.com/science/article/pii/S1387700323006810?casa_token=Sd3o9P-TzUUAAAAA:PI4iQp53gVYTEoc8l1hjcWCKrLhV4hRJz1Mvf4i40A1QSxyqd5Mz_5tzM6BUFK_YyfRQ4F7766YV

Balasubramanian, K., Ramaraj, S., … C. K.-I. C., & 2023, undefined. (n.d.-c). A novel Schiff base derived quinoline moieties as a selective fluorophore for Sn2+ ion sensing. *Elsevier*. Retrieved December 23, 2024, from https://www.sciencedirect.com/science/article/pii/S1387700323006810?casa_token=FYyVeL9dX9oAAAAA:HKLB_8dpvpORnCJE5KV06xSSD3mbkJwR6xuvFwTyxbkE7aHI4Vjz5S5V9zgqYqz146IMjFUwIHia

Bankaji, I., Kouki, R., Dridi, N., Ferreira, R., Hidouri, S., Duarte, B., Sleimi, N., & Caçador, I. (2023). Comparison of digestion methods using atomic absorption spectrometry for the determination of metal levels in plants. *Mdpi.ComI Bankaji, R Kouki, N Dridi, R Ferreira, S Hidouri, B Duarte, N Sleimi, I CaçadorSeparations, 2023•mdpi.Com*. https://doi.org/10.3390/separations10010040

Baral, M., Sahoo, S. K., & Kanungo, B. K. (2008). Tripodal amine catechol ligands: A fascinating class of chelators for aluminium(III). *Journal of Inorganic Biochemistry*, *102*(8), 1581–1588. https://doi.org/10.1016/J.JINORGBIO.2008.02.006

Barkale, H. V., & Dey, N. (2024). Phenazine-based fluorescence probes for simultaneous sensing of silver and iodide ions. *Journal of Molecular Structure*, *1303*, 137427. https://doi.org/10.1016/J.MOLSTRUC.2023.137427

Bartwal, G., Aggarwal, K., and, J. K.-J. of P., & 2020, undefined. (n.d.). Quinoline-ampyrone functionalized azo dyes as colorimetric and fluorescent enhancement probes for selective aluminium and cobalt ion detection in semi-aqueous. *Elsevier*. Retrieved January 2, 2025, from https://www.sciencedirect.com/science/article/pii/S1010603020302914

Batchelor-Mcauley, C., Kätelhön, E., Barnes, E. O., Compton, R. G., Laborda, E., & Molina, A. (2015). Recent Advances in Voltammetry. *ChemistryOpen*, *4*(3), 224–260. https://doi.org/10.1002/OPEN.201500042

Bayindir, S., Hussein, A. S., Lafzi, F., & Toprak, M. (2023). The switchable fluorescent detection of mercury, copper, and iodine in real water samples using bola-amphiphilic-tetraphenylethene. *Journal of Molecular Liquids*, *382*, 121939. https://doi.org/10.1016/J.MOLLIQ.2023.121939

Bayrakcı, M., Kursunlu, A., Güler, E., Pigments, Ş. E.-D. and, & 2013, undefined. (n.d.). azacrown ether based boradiazaindacene (Bodipy): Selective fluorescence changes towards trivalent lanthanide ions. *ElsevierM Bayrakcı, AN Kursunlu, E Güler, Ş ErtulDyes and Pigments, 2013•Elsevier*. Retrieved December 22, 2024, from https://www.sciencedirect.com/science/article/pii/S0143720813001964?casa_token=9qOEfS9shNIAAAAA:2z9kFTZLMRkYRVLg4tyaYoC_IslkH2mu2WgXGr62pbf_-wDotmZVKS_XRK2-Y5nadv_5DLu8RbtT

Behura, R., Mohanty, P., Sahu, G., Dash, P. P., Behera, S., Dinda, R., Hota, P. R., Sahoo, H., Bhaskaran, R., Barick, A. K., Mohapatra, P., & Jali, B. R. (2023). A highly selective Schiff base fluorescent sensor for Zn2+, Cd2+ and Hg2+ based on 2,4-dinitrophenylhydrazine derivative. *Inorganic Chemistry Communications*, *154*, 110959. https://doi.org/10.1016/J.INOCHE.2023.110959

Bell, T. W., & Hext, N. M. (2004). Supramolecular optical chemosensors for organic analytes. *Chemical Society Reviews*, *33*(9), 589–598. https://doi.org/10.1039/B207182G

Bera, K., Das, A. K., Nag, M., & Basak, S. (2014). Development of a rhodamine-rhodanine-based fluorescent mercury sensor and its use to monitor real-time uptake and distribution of inorganic mercury in live zebrafish larvae. *Analytical Chemistry*, *86*(5), 2740–2746. https://doi.org/10.1021/AC404160V/SUPPL_FILE/AC404160V_SI_008.AVI

Berhanu, A. L., Gaurav, Mohiuddin, I., Malik, A. K., Aulakh, J. S., Kumar, V., & Kim, K. H. (2019a). A review of the applications of Schiff bases as optical chemical sensors. *TrAC Trends in Analytical Chemistry*, *116*, 74–91. https://doi.org/10.1016/J.TRAC.2019.04.025

Berhanu, A. L., Gaurav, Mohiuddin, I., Malik, A. K., Aulakh, J. S., Kumar, V., & Kim, K. H. (2019b). A review of the applications of Schiff bases as optical chemical sensors. *TrAC Trends in Analytical Chemistry*, *116*, 74–91. https://doi.org/10.1016/J.TRAC.2019.04.025

Bhat, A., Hara, T. O., Tian, F., & Singh, B. (2023). Review of analytical techniques for arsenic detection and determination in drinking water. *Environmental Science: Advances*, *2*(2), 171–195. https://doi.org/10.1039/D2VA00218C

Bhatta, S. R., Mondal, B., Vijaykumar, G., & Thakur, A. (2017). ICT-Isomerization-Induced Turn-On Fluorescence Probe with a Large Emission Shift for Mercury Ion: Application in Combinational Molecular Logic. *Inorganic Chemistry*, *56*(19), 11577–11590. https://doi.org/10.1021/ACS.INORGCHEM.7B01304

Bhattacharyya, A., Makhal, S. C., & Guchhait, N. (2019). Evaluating the merit of a diethylamino coumarin-derived thiosemicarbazone as an intramolecular charge transfer probe: Efficient Zn(II) mediated emission swing from green to yellow. *Photochemical and Photobiological Sciences*, *18*(8), 2031–2041. https://doi.org/10.1039/C9PP00108E/METRICS

Bolea, E., Jimenez, M. S., Perez-Arantegui, J., Vidal, J. C., Bakir, M., Ben-Jeddou, K., Gimenez-Ingalaturre, A. C., Ojeda, D., Trujillo, C., & Laborda, F. (2021). Analytical applications of single particle inductively coupled plasma mass spectrometry: a comprehensive and critical review. *Analytical Methods*, *13*(25), 2742–2795. https://doi.org/10.1039/D1AY00761K

Bruno, I. J., Cole, J. C., Edgington, P. R., Kessler, M., Macrae, C. F., McCabe, P., Pearson, J., & Taylor, R. (2002). New software for searching the Cambridge Structural Database and visualizing crystal structures. *Acta Crystallographica Section B: Structural Science*, *58*(3 PART 1), 389–397. https://doi.org/10.1107/S0108768102003324

Brzechwa-Chodzyńska, A., Drożdż, W., Harrowfield, J., & Stefankiewicz, A. R. (2021). Fluorescent sensors: A bright future for cages. *Coordination Chemistry Reviews*, *434*, 213820. https://doi.org/10.1016/J.CCR.2021.213820

Carter, K. P., Young, A. M., & Palmer, A. E. (2014). Fluorescent sensors for measuring metal ions in living systems. *Chemical Reviews*, *114*(8), 4564–4601. https://doi.org/10.1021/CR400546E/ASSET/IMAGES/LARGE/CR-2013-00546E_0002.JPEG

Chakraborty, A., Rajana, V. K., Saritha, C., Srivastava, A., Mandal, D., & Das, N. (2024). A new Eosin Y-based 'turnon' fluorescent sensor for ratiometric sensing of toxic mercury ion (Hg2+) offering unaided eye detection and its antibacterial activity. *Journal of Hazardous Materials*, *470*, 134207. https://doi.org/10.1016/J.JHAZMAT.2024.134207

Chakraborty, S. (2023). Detection of fluoride ion by chemosensing and fluorosensing technology. *Results in Chemistry*, *6*, 100994. https://doi.org/10.1016/J.RECHEM.2023.100994

Chakraborty, S., Paul, S., Roy, P., & Rayalu, S. (2021). Detection of cyanide ion by chemosensing and fluorosensing technology. *Inorganic Chemistry*

Communications, *128*, 108562. https://doi.org/https://doi.org/10.1016/j.inoche.2021.108562

Chang, K.-C., Sun, S.-S., Odago, M. O., & Lees, A. J. (2015). Anion recognition and sensing by transition-metal complexes with polarized NH recognition motifs. *Coordination Chemistry Reviews*, *284*, 111–123. https://doi.org/https://doi.org/10.1016/j.ccr.2014.09.009

Chao, J., Li, Z., Zhang, Y., Huo, F., Yin, C., Liu, Y., Li, Y., & Wang, J. (2016). A single fluorescent probe for multiple analyte sensing: efficient and selective detection of CN − , HSO 3 − and extremely alkaline pH. *Journal of Materials Chemistry B*, *4*(21), 3703–3712. https://doi.org/10.1039/C6TB00119J

Chatterjee, S., Liu, B., & Peng, H. (2024a). Chelation strategies in spiropyran-based chemosensors for colorimetric and fluorescent sensing of metal ions and anions. *Coordination Chemistry Reviews*, *508*, 215779. https://doi.org/https://doi.org/10.1016/j.ccr.2024.215779

Chatterjee, S., Liu, B., & Peng, H. shang. (2024b). Chelation strategies in spiropyran-based chemosensors for colorimetric and fluorescent sensing of metal ions and anions. *Coordination Chemistry Reviews*, *508*, 215779. https://doi.org/10.1016/J.CCR.2024.215779

Chemistry of the Elements - N. N. Greenwood, A. Earnshaw - Google Books. (n.d.). Retrieved December 17, 2024, from https://books.google.co.in/books?hl=en&lr=&id=EvTI-ouH3SsC&oi=fnd&pg=PP1&dq=N.+N.+Greenwood+and+A.+Earnshaw,+Chemistry+of+the++Elements,+2012&ots=pR6XTAiqHa&sig=TRBAvhtpf86t8_qhpAy6fQG1ygE&redir_esc=y#v=onepage&q=N.%20N.%20Greenwood%20and%20A.%20Earnshaw%2C%20Chemistry%20of%20the%20%20Elements%2C%202012&f=false

Chemosensors: Principles, Strategies, and Applications - Google Books. (n.d.). Retrieved December 17, 2024, from

https://books.google.co.in/books?hl=en&lr=&id=8KZyhdWdWhcC&oi=fnd&pg=PP13&dq=chemosensors&ots=rMzUh8Gstm&sig=sS2NUweJMZF8o4vej0v6eSI9dOQ&redir_esc=y#v=onepage&q=chemosensors&f=false

Chen, S. Y., Li, Z., Li, K., & Yu, X. Q. (2021). Small molecular fluorescent probes for the detection of lead, cadmium and mercury ions. *Coordination Chemistry Reviews*, *429*, 213691. https://doi.org/10.1016/J.CCR.2020.213691

Chen, Z., Zhang, Z., Qi, J., You, J., Ma, J., & Chen, L. (2023). Colorimetric detection of heavy metal ions with various chromogenic materials: Strategies and applications. *Journal of Hazardous Materials*, *441*, 129889. https://doi.org/10.1016/J.JHAZMAT.2022.129889

Chilton, J., Dahi, E., Lennon, M., & Jackson, P. (2006). *Fluoride in Drinking-water: Background document for development of WHO Guidelines for Drinking-water Quality*.

Choudhury, A. R., & Dey, N. (2023). Molecular Amplification as an Affordable Strategy for Trace-Level Detection of Ionic Analytes with Fluorimetric or Colorimetric Readout. *ChemPhotoChem*, *7*(6), e202200306. https://doi.org/10.1002/CPTC.202200306

Christopher Leslee, D. B., Venkatachalam, U., Gunasekaran, J., Karuppannan, S., & Kuppannan, S. B. (2023). Synthesis of a quinoxaline–hydrazinobenzothiazole based probe—single point detection of Cu2+, Co2+, Ni2+ and Hg2+ ions in real water samples. *Organic & Biomolecular Chemistry*, *21*(19), 4130–4143. https://doi.org/10.1039/D3OB00298E

Chung, Y., & Ahn, K. H. (2006). N-Acyl Triazenes as Tunable and Selective Chemodosimeters Toward Cyanide Ion. *The Journal of Organic Chemistry*, *71*(25), 9470–9474. https://doi.org/10.1021/jo061798t

Crespi, A. F., Byrne, A. J., Vega, D., Chattah, A. K., Monti, G. A., & Lázaro-Martínez, J. M. (2018). Generation and Stability of the gem-Diol Forms in

Imidazole Derivatives Containing Carbonyl Groups. Solid-State NMR and Single-Crystal X-ray Diffraction Studies. *Journal of Physical Chemistry A*, *122*(2), 601–609. https://doi.org/10.1021/ACS.JPCA.7B12390

Crespi, A. F., & Lázaro-Martínez, J. M. (2023). Can a gem-Diol Moiety Be Isolated? A Reaction Study by NMR and X-ray Spectroscopies. *Journal of Chemical Education*, *100*(11), 4536–4542. https://doi.org/10.1021/ACS.JCHEMED.3C00446

Crespi, A. F., Vega, D., Pérez, A. L., Rodríguez-Castellón, E., & Lázaro-Martínez, J. M. (2023). Gem-diol Generation in Copper and Zinc N-methyl-2-imidazolecarboxaldehyde Complexes: Solid-state NMR, EPR and Single-Crystal X-ray Studies. *European Journal of Inorganic Chemistry*, *26*(9). https://doi.org/10.1002/EJIC.202200737

Crespi, F., Vega, D., Karina Chattah, A., Alberto Monti, G., Yolanda Buldain, G., Manuel La, J., & Allende, M. (2016). gem-Diol and Hemiacetal Forms in Formylpyridine and Vitamin-B6-Related Compounds: Solid-State NMR and Single-Crystal X-ray Diffraction Studies. *ACS PublicationsAF Crespi, D Vega, AK Chattah, GA Monti, GY Buldain, JM Lázaro-MartínezThe Journal of Physical Chemistry A, 2016•ACS Publications*, *120*(39), 7778–7785. https://doi.org/10.1021/acs.jpca.6b07898

Cyanide, free CASRN 57-12-5 | IRIS | US EPA, ORD. (n.d.). Retrieved January 2, 2025, from https://iris.epa.gov/ChemicalLanding/&substance_nmbr=31

D., A., P., N., R., R., & M., V. K. (2021). Development of hydrazide based fluorescence probe for detection of Al3+ ions and application in live cell image. *Journal of Photochemistry and Photobiology A: Chemistry*, *405*, 112921. https://doi.org/10.1016/J.JPHOTOCHEM.2020.112921

da Silva, G., Pang, Y., Meng, D., Liu, J., Duan, S., Fan, J., Gao, L., & Long, X. (2023). Schiff Base Compounds as Fluorescent Probes for the Highly Sensitive and Selective Detection of Al3+ Ions. *Mdpi.ComY Pang, D*

Meng, J Liu, S Duan, J Fan, L Gao, X LongMolecules, 2023•mdpi.Com. https://doi.org/10.3390/molecules28073090

Das, B., & Gupta, P. (2024). Multimetallic transition metal complexes:Luminescent probes for biomolecule sensing, ion detection, imaging and therapeutic application. *Coordination Chemistry Reviews*, *504*, 215656. https://doi.org/10.1016/J.CCR.2024.215656

Degueldre, C. (2021). Single virus inductively coupled plasma mass spectroscopy analysis: A comprehensive study. *Talanta*, *228*, 122211. https://doi.org/10.1016/J.TALANTA.2021.122211

Deng, L., Xiong, J., Liu, W., Wu, L., Hu, H., Wu, J., Liu, Y., Yu, L., Zhou, Y., Gao, W., He, H., & Yin, W. (2023). A Novel Fluorescence Sensor for Iodide Detection Based on the 1,3-Diaryl Pyrazole Unit with AIE and Mechanochromic Fluorescence Behavior. *Molecules*, *28*(20), 7111. https://doi.org/10.3390/MOLECULES28207111/S1

Development of low-cost copper nanoclusters for highly selective “turn-on” sensing of Hg2+ ions. (n.d.). *ElsevierP Sharma, S Naithani, S Layek, A Kumar, R Rawat, S Kaja, A Nag, S Kumar, T GoswamiSpectrochimica Acta Part A: Molecular and Biomolecular Spectroscopy, 2023•Elsevier*. Retrieved December 22, 2024, from https://www.sciencedirect.com/science/article/pii/S1386142523003827

Dong, W., Akogun, S., Zhang, Y., Chemical, Y. S.-… and A. B., & 2017, undefined. (n.d.). A reversible “turn-on” fluorescent sensor for selective detection of Zn2+. *ElsevierWK Dong, SF Akogun, Y Zhang, YX Sun, XY DongSensors and Actuators B: Chemical, 2017•Elsevier*. Retrieved December 22, 2024, from https://www.sciencedirect.com/science/article/pii/S0925400516310826?casa_token=MagWY6E4du4AAAAA:m5F5xAlnUIxX2jK0YyQc11GAVf9vrUzGgMsLo-zl-W6e3MnnlnRG8wdRmM2viLtaq9fPJ1yqvEKI

Du, B., Li, Q., Huang, K., & Liang, L. (2023). A quinoline-fluoran hybrid fluorescent probe for selectively and sensitively sensing copper ions and fluorescence imaging application. *Journal of Molecular Structure*, *1271*, 134015. https://doi.org/10.1016/J.MOLSTRUC.2022.134015

Du, J., Liu, M., Lou, X., Zhao, T., Wang, Z., Xue, Y., Zhao, J., & Xu, Y. (2012a). Highly sensitive and selective chip-based fluorescent sensor for mercuric ion: Development and comparison of turn-on and turn-off systems. *Analytical Chemistry*, *84*(18), 8060–8066. https://doi.org/10.1021/AC301954J/SUPPL_FILE/AC301954J_SI_001.PDF

Du, J., Liu, M., Lou, X., Zhao, T., Wang, Z., Xue, Y., Zhao, J., & Xu, Y. (2012b). Highly sensitive and selective chip-based fluorescent sensor for mercuric ion: Development and comparison of turn-on and turn-off systems. *Analytical Chemistry*, *84*(18), 8060–8066. https://doi.org/10.1021/AC301954J/SUPPL_FILE/AC301954J_SI_001.PDF

Dutta, M., Chemistry, D. D.-T. T. in A., & 2012, undefined. (n.d.). Recent developments in fluorescent sensors for trace-level determination of toxic-metal ions. *ElsevierM Dutta, D DasTrAC Trends in Analytical Chemistry, 2012•Elsevier*. Retrieved December 22, 2024, from https://www.sciencedirect.com/science/article/pii/S0165993611003177

Emandi, G., Flanagan, K. J., & Senge, M. O. (2018). Fluorescent imidazole-based chemosensors for the reversible detection of cyanide and mercury ions. *Photochemical & Photobiological Sciences*, *17*(10), 1450–1461. https://doi.org/10.1039/C8PP00226F

Fan, L., Qin, J. can, Li, C. rui, & Yang, Z. yin. (2020). Two similar Schiff-base receptor based quinoline derivate: Highly selective fluorescent probe for Zn(II). *Spectrochimica Acta. Part A, Molecular and Biomolecular Spectroscopy*, *236*, 118347–118347. https://doi.org/10.1016/J.SAA.2020.118347

Fan, L., Qin, J., Li, C., and, Z. Y.-S. A. P. A. M., & 2020, undefined. (n.d.). Two similar Schiff-base receptor based quinoline derivate: Highly selective fluorescent probe for Zn (II). *ElsevierL Fan, J Qin, C Li, Z YangSpectrochimica Acta Part A: Molecular and Biomolecular Spectroscopy, 2020•Elsevier*. Retrieved December 22, 2024, from https://www.sciencedirect.com/science/article/pii/S1386142520303255

Farrugia, L. J. (1997). ORTEP-3 for Windows - a version of ORTEP-III with a Graphical User Interface (GUI). *Journal of Applied Crystallography*, *30*(5–1), 565–565. https://doi.org/10.1107/S0021889897003117

Fasman, G. D. (1996). Aluminum and Alzheimer's disease: model studies. *Coordination Chemistry Reviews*, *149*, 125–165. https://doi.org/10.1016/S0010-8545(96)90020-X

Feng, L. C., Li, X. X., Chen, R., Man, L. L., & Dong, W. K. (2023). A fluorescent "off-on-off" probe based on a new bis(salamo)-like compound for the sensitive and rapid detection of phosphates. *Journal of Molecular Structure*, *1289*, 135941. https://doi.org/10.1016/J.MOLSTRUC.2023.135941

Feng, W., Bai, L., Jia, S., & Feng, G. (2018). A novel phthalimide-rhodol-based ESIPT-FRET system for rapid colorimetric and ratiometric fluorescent detection of palladium. *Sensors and Actuators B: Chemical*, *260*, 554–562. https://doi.org/10.1016/J.SNB.2017.12.172

Following laser-induced plasma stoichiometry with atomic absorption spectroscopy. (n.d.). *ElsevierJ Merten, E Nicholas, S Ethridge, H Bariola, S Chestnut, A Anders, J Brees, M FosterSpectrochimica Acta Part B: Atomic Spectroscopy, 2023•Elsevier*. Retrieved December 22, 2024, from https://www.sciencedirect.com/science/article/pii/S0584854722002440

Fu, J., Li, B., Mei, H., Chang, Y., & Xu, K. (2019). Fluorescent schiff base probes for sequential detection of Al^{3+} and F^{-} and cell imaging applications.

Spectrochimica Acta. Part A, Molecular and Biomolecular Spectroscopy, *227*, 117678–117678. https://doi.org/10.1016/J.SAA.2019.117678

Fu, J., Yao, K., Chang, Y., Li, B., Yang, L., A, K. X.-S. A. P., & 2019, undefined. (n.d.-a). A novel colorimetric-fluorescent probe for Al3+ and the resultant complex for F− and its applications in cell imaging. *ElsevierJ Fu, K Yao, Y Chang, B Li, L Yang, K XuSpectrochimica Acta Part A: Molecular and Biomolecular Spectroscopy, 2019•Elsevier*. Retrieved December 22, 2024, from https://www.sciencedirect.com/science/article/pii/S1386142519306249

Fu, J., Yao, K., Chang, Y., Li, B., Yang, L., A, K. X.-S. A. P., & 2019, undefined. (n.d.-b). A novel colorimetric-fluorescent probe for Al3+ and the resultant complex for F− and its applications in cell imaging. *ElsevierJ Fu, K Yao, Y Chang, B Li, L Yang, K XuSpectrochimica Acta Part A: Molecular and Biomolecular Spectroscopy, 2019•Elsevier*. Retrieved December 23, 2024, from https://www.sciencedirect.com/science/article/pii/S1386142519306249

Fu, J., Yao, K., Chang, Y., Li, B., Yang, L., & Xu, K. (2019a). A novel colorimetric-fluorescent probe for Al3+ and the resultant complex for F− and its applications in cell imaging. *Spectrochimica Acta Part A: Molecular and Biomolecular Spectroscopy*, *222*, 117234. https://doi.org/10.1016/J.SAA.2019.117234

Fu, J., Yao, K., Chang, Y., Li, B., Yang, L., & Xu, K. (2019b). A novel colorimetric-fluorescent probe for Al3+ and the resultant complex for F− and its applications in cell imaging. *Spectrochimica Acta Part A: Molecular and Biomolecular Spectroscopy*, *222*, 117234. https://doi.org/10.1016/J.SAA.2019.117234

Gale, P. A., & Caltagirone, C. (2018). Fluorescent and colorimetric sensors for anionic species. *Coordination Chemistry Reviews*, *354*, 2–27. https://doi.org/https://doi.org/10.1016/j.ccr.2017.05.003

Gan, Y., Yin, G., Xu, Z., Zhou, H., Yu, T., Li, H., & Yin, P. (2023). A dual-functional fluorescent probe for simultaneous visualization and quantification of Au and Pd species in environmental and biological systems. *Chemical Engineering Journal*, *451*, 138437. https://doi.org/10.1016/J.CEJ.2022.138437

Ganguly, A., Ghosh, S., Kar, S., A, N. G.-S. A. P., & 2015, undefined. (n.d.). Selective fluorescence sensing of Cu (II) and Zn (II) using a simple Schiff base ligand: Naked eye detection and elucidation of photoinduced electron transfer (PET). *ElsevierA Ganguly, S Ghosh, S Kar, N GuchhaitSpectrochimica Acta Part A: Molecular and Biomolecular Spectroscopy, 2015•Elsevier*. Retrieved January 1, 2025, from https://www.sciencedirect.com/science/article/pii/S1386142515001651

Gao, M., & Tang, B. Z. (2017). Fluorescent Sensors Based on Aggregation-Induced Emission: Recent Advances and Perspectives. *ACS Sensors*, *2*(10), 1382–1399. https://doi.org/10.1021/ACSSENSORS.7B00551/ASSET/IMAGES/MEDIUM/SE-2017-005518_0020.GIF

Ghazali, S., Fan, J., Du, J., & Peng, X. (2019). Mito-targeted “turn-on” fluorescent probe for nickel (II) detection. *Methods*, *168*, 24–28. https://doi.org/10.1016/J.YMETH.2019.04.014

Ghorai, P., Pal, K., Karmakar, P., & Saha, A. (2020). The development of two fluorescent chemosensors for the selective detection of Zn2+ and Al3+ ions in a quinoline platform by tuning the substituents in the receptor part: Elucidation of the structures of the metal-bound chemosensors and biological studies. *Dalton Transactions*, *49*(15), 4758–4773. https://doi.org/10.1039/c9dt04902a

Ghosh, A., Mukherjee, K., Ghosh, S. K., & Saha, B. (2013). Sources and toxicity of fluoride in the environment. *Research on Chemical Intermediates*, *39*(7), 2881–2915. https://doi.org/10.1007/S11164-012-0841-1/METRICS

Goshisht, M. K., & Tripathi, N. (2021). Fluorescence-based sensors as an emerging tool for anion detection: mechanism, sensory materials and applications. *Journal of Materials Chemistry C*, *9*(31), 9820–9850. https://doi.org/10.1039/D1TC01990B

Goshisht, M., Patra, G., Advances, N. T.-M., & 2022, undefined. (2022a). Fluorescent Schiff base sensors as a versatile tool for metal ion detection: strategies, mechanistic insights, and applications. *Pubs.Rsc.OrgMK Goshisht, GK Patra, N TripathiMaterials Advances, 2022•pubs.Rsc.Org*, *3*, 2612. https://doi.org/10.1039/d1ma01175h

Goshisht, M., Patra, G., Advances, N. T.-M., & 2022, undefined. (2022b). Fluorescent Schiff base sensors as a versatile tool for metal ion detection: strategies, mechanistic insights, and applications. *Pubs.Rsc.OrgMK Goshisht, GK Patra, N TripathiMaterials Advances, 2022•pubs.Rsc.Org*, *3*, 2612. https://doi.org/10.1039/d1ma01175h

Gosi, M., Marepu, N., & Sunandamma, Y. (2021). Cyanine-based Fluorescent Probe for Cyanide Ion Detection. *Journal of Fluorescence*, *31*(5), 1409–1415. https://doi.org/10.1007/S10895-021-02771-8/METRICS

Goswami, N., Naithani, S., Goswami, T., … P. K.-S. A., & 2024, undefined. (n.d.-a). A quinoline derived Schiff base as highly selective 'turn-on'probe for fluorogenic recognition of Al3+ ion. *ElsevierN Goswami, S Naithani, T Goswami, P Kumar, S KumarSpectrochimica Acta Part A: Molecular and Biomolecular Spectroscopy, 2024•Elsevier*. Retrieved December 23, 2024, from https://www.sciencedirect.com/science/article/pii/S1386142524001379

Goswami, N., Naithani, S., Goswami, T., … P. K.-S. A., & 2024, undefined. (n.d.-b). A quinoline derived Schiff base as highly selective 'turn-on'probe for fluorogenic recognition of Al3+ ion. *ElsevierN Goswami, S Naithani, T Goswami, P Kumar, S KumarSpectrochimica Acta Part A: Molecular and Biomolecular Spectroscopy, 2024•Elsevier*. Retrieved January 2, 2025,

from https://www.sciencedirect.com/science/article/pii/S1386142524001379

Goswami, N., Naithani, S., Goswami, T., Kumar, P., Kumar, P., & Kumar, S. (2024a). Turn-on detection of Al3+ ions using quinoline-based tripodal probe: mechanistic investigation and live cell imaging applications. *Analytical Methods*, *16*(29), 5022–5031. https://doi.org/10.1039/d4ay00761a

Goswami, N., Naithani, S., Goswami, T., Kumar, P., Kumar, P., & Kumar, S. (2024b). Turn-on detection of Al3+ ions using quinoline-based tripodal probe: mechanistic investigation and live cell imaging applications. *Analytical Methods*, *16*(29), 5022–5031. https://doi.org/10.1039/d4ay00761a

Goswami, N., Naithani, S., Goswami, T., Kumar, P., & Kumar, S. (2024a). A quinoline derived Schiff base as highly selective 'turn-on' probe for fluorogenic recognition of Al3+ ion. *Spectrochimica Acta - Part A: Molecular and Biomolecular Spectroscopy*, *310*. https://doi.org/10.1016/j.saa.2024.123971

Goswami, N., Naithani, S., Goswami, T., Kumar, P., & Kumar, S. (2024b). A quinoline derived Schiff base as highly selective 'turn-on' probe for fluorogenic recognition of Al3+ ion. *Spectrochimica Acta - Part A: Molecular and Biomolecular Spectroscopy*, *310*(January), 123971. https://doi.org/10.1016/j.saa.2024.123971

Goswami, N., Naithani, S., Mangalam, J., Goswami, T., Dubey, R., Kumar, P., Kumar, P., & Kumar, S. (2023). Fluorescent and chromogenic organic probes to detect group 10 metal ions: design strategies and sensing applications. *Dalton Transactions*, *52*(41), 14704–14732. https://doi.org/10.1039/D3DT01723K

Goswami, N., Naithani, S., Mangalam, J., Transactions, T. G.-…, & 2023, undefined. (n.d.-a). Fluorescent and chromogenic organic probes to detect

group 10 metal ions: design strategies and sensing applications. *Pubs.Rsc.OrgN Goswami, S Naithani, J Mangalam, T Goswami, R Dubey, P Kumar, P Kumar, S KumarDalton Transactions, 2023•pubs.Rsc.Org*. Retrieved December 22, 2024, from https://pubs.rsc.org/en/content/articlehtml/2023/dt/d3dt01723k

Goswami, N., Naithani, S., Mangalam, J., Transactions, T. G.-…, & 2023, undefined. (n.d.-b). Fluorescent and chromogenic organic probes to detect group 10 metal ions: design strategies and sensing applications. *Pubs.Rsc.OrgN Goswami, S Naithani, J Mangalam, T Goswami, R Dubey, P Kumar, P Kumar, S KumarDalton Transactions, 2023•pubs.Rsc.Org*. Retrieved December 23, 2024, from https://pubs.rsc.org/en/content/articlehtml/2023/dt/d3dt01723k

Goyal, H., Annan, I., Ahluwalia, D., Bag, A., & Gupta, R. (2023). Discriminative 'Turn-on' Detection of Al3+ and Ga3+ Ions as Well as Aspartic Acid by Two Fluorescent Chemosensors. *Sensors*, *23*(4). https://doi.org/10.3390/s23041798

Grasso, G., Colella, F., Forciniti, S., Onesto, V., Iuele, H., Siciliano, A. C., Carnevali, F., Chandra, A., Gigli, G., & del Mercato, L. L. (2023). Fluorescent nano- and microparticles for sensing cellular microenvironment: past, present and future applications. *Nanoscale Advances*, *5*(17), 4311–4336. https://doi.org/10.1039/D3NA00218G

Gui, S., Huang, Y., Hu, F., Jin, Y., Zhang, G., Yan, L., Zhang, D., & Zhao, R. (2015a). Fluorescence turn-on chemosensor for highly selective and sensitive detection and bioimaging of al3+ in living cells based on ion-induced aggregation. *Analytical Chemistry*, *87*(3), 1470–1474. https://doi.org/10.1021/AC504153C/SUPPL_FILE/AC504153C_SI_001.PDF

Gui, S., Huang, Y., Hu, F., Jin, Y., Zhang, G., Yan, L., Zhang, D., & Zhao, R. (2015b). Fluorescence Turn-On Chemosensor for Highly Selective and Sensitive Detection and Bioimaging of Al3+ in Living Cells Based on Ion-

Induced Aggregation. *ACS PublicationsS Gui, Y Huang, F Hu, Y Jin, G Zhang, L Yan, D Zhang, R ZhaoAnalytical Chemistry, 2015•ACS Publications*, *87*(3), 46. https://doi.org/10.1021/ac504153c

Gulaboski, R. (2022). THE FUTURE OF VOLTAMMETRY. *Macedonian Journal of Chemistry and Chemical Engineering*, *41*(2), 151–162. https://doi.org/10.20450/MJCCE.2022.2555

Guo, C., Sedgwick, A. C., Hirao, T., & Sessler, J. L. (2021). Supramolecular fluorescent sensors: An historical overview and update. *Coordination Chemistry Reviews*, *427*, 213560. https://doi.org/10.1016/J.CCR.2020.213560

Guo, C., Sedgwick, A., Hirao, T., reviews, J. S.-C. chemistry, & 2021, undefined. (n.d.). Supramolecular fluorescent sensors: An historical overview and update. *ElsevierC Guo, AC Sedgwick, T Hirao, JL SesslerCoordination Chemistry Reviews, 2021•Elsevier*. Retrieved December 23, 2024, from https://www.sciencedirect.com/science/article/pii/S001085452030730X

Guo, Q., Ji, D., & Zhao, J. (2021). Theoretical insights into photochemical behavior and ESIPT mechanism for 2,6-dimethyl phenyl derivatives. *Chemical Physics Letters*, *767*, 138377. https://doi.org/10.1016/J.CPLETT.2021.138377

Gupta, A., advances, N. K.-R., & 2016, undefined. (2016). A review of mechanisms for fluorescent ’ “turn-on”’probes to detect Al 3+ ions. *Pubs.Rsc.OrgA Gupta, N KumarRSC Advances, 2016•pubs.Rsc.Org*, *6*(108), 106413–106434. https://doi.org/10.1039/c6ra23682k

Gupta, A., & Kumar, N. (2016). A review of mechanisms for fluorescent ‘“turn-on”’ probes to detect Al3+ ions. *RSC Advances*, *6*(108), 106413–106434. https://doi.org/10.1039/C6RA23682K

Gupta, A. Sen, Paul, K., & Luxami, V. (2016). Benzimidazole based ratiometric chemosensor for detection of CN− and Cu2+ ions in protic/aqueous

system: Elaboration as XOR logic operation. *Inorganica Chimica Acta*, *443*, 57–63. https://doi.org/10.1016/J.ICA.2015.11.024

Gupta, V. K., Jain, A. K., & Maheshwari, G. (2007). Aluminum(III) selective potentiometric sensor based on morin in poly(vinyl chloride) matrix. *Talanta*, *72*(4), 1469–1473. https://doi.org/10.1016/J.TALANTA.2007.01.064

Han, S., Wang, J., & Jia, S. (2015). Turn-off–on chemiluminescence determination of cyanide. *Luminescence*, *30*(1), 38–43. https://doi.org/https://doi.org/10.1002/bio.2687

Han, T., Feng, X., Tong, B., Shi, J., Chen, L., Zhi, J., & Dong, Y. (2011). A novel "turn-on" fluorescent chemosensor for the selective detection of Al3+ based on aggregation-induced emission. *Chemical Communications*, *48*(3), 416–418. https://doi.org/10.1039/C1CC15681K

He, H., Li, Y., Botany, L. H.-S. A. J. of, & 2019, undefined. (n.d.). Aluminum toxicity and tolerance in Solanaceae plants. *ElsevierH He, Y Li, LF HeSouth African Journal of Botany, 2019•Elsevier*. Retrieved December 23, 2024, from https://www.sciencedirect.com/science/article/pii/S0254629918301844

Heena, N., Naithani, S., Sangeeta, N., Guchhait, B., Goswami, T., & Kumar, S. (2024). Designing a multifunctional AIE-active fluorescent Schiff base probe: sensitive heavy metal ion recognition and water-induced aggregation. *New Journal of Chemistry*, *48*(40), 17423–17435. https://doi.org/10.1039/D4NJ02417F

Hendry-Hofer, T. B., Ng, P. C., Witeof, A. E., Mahon, S. B., Brenner, M., Boss, G. R., & Bebarta, V. S. (2019). A Review on Ingested Cyanide: Risks, Clinical Presentation, Diagnostics, and Treatment Challenges. *Journal of Medical Toxicology*, *15*(2), 128–133. https://doi.org/10.1007/S13181-018-0688-Y/METRICS

High Performance Liquid Chromatography - Heinz Engelhardt - Google Books. (n.d.). Retrieved December 17, 2024, from https://books.google.co.in/books?hl=en&lr=&id=slHxCAAAQBAJ&oi=fnd&pg=PA1&dq=high+performance+liquid+chromatography&ots=ZQNLT4MYFF&sig=RZjIzBJcNw_eAX7gUqKu4I_FrMw&redir_esc=y#v=onepage&q=high%20performance%20liquid%20chromatography&f=false

Highly selective CHEF-type chemosensor for lutetium (III) recognition in semi-aqueous media. (n.d.). *ElsevierRS Kumar, SKA Kumar, K Vijayakrishna, A Sivaramakrishna, CVSB Rao, N SivaramanSpectrochimica Acta Part A: Molecular and Biomolecular Spectroscopy, 2019•Elsevier*. Retrieved December 22, 2024, from https://www.sciencedirect.com/science/article/pii/S1386142519301131

Hou, L., Liu, T., Gong, Y., Li, J., Deng, C., Chemistry, C. Z.-… J. of, & 2020, undefined. (n.d.). A turn-on Schiff base fluorescent probe for the exogenous and endogenous Fe 3+ ion sensing and bioimaging of living cells. *Pubs.Rsc.OrgL Hou, T Liu, Y Gong, J Li, C Deng, C Zhang, Y Wang, S Shuang, W LiangNew Journal of Chemistry, 2020•pubs.Rsc.Org*. Retrieved December 22, 2024, from https://pubs.rsc.org/en/content/articlehtml/2020/nj/d0nj04315j

Hu, W., Zeng, L., Wang, Y., Liu, Z., Ye, X., & Li, C. (2016). A ratiometric two-photon fluorescent probe for fluoride ion imaging in living cells and zebrafish. *Analyst*, *141*(18), 5450–5455. https://doi.org/10.1039/c6an00905k

Huang, X., Song, J., Yung, B. C., Huang, X., Xiong, Y., & Chen, X. (2018). Ratiometric optical nanoprobes enable accurate molecular detection and imaging. *Chemical Society Reviews*, *47*(8), 2873–2920. https://doi.org/10.1039/C7CS00612H

Huang, Y., Chen, W., Dong, M., Li, N., Chen, L., Ling, L., Xu, Q., Lin, M., & Xing, Z. (2023). A novel fluorescence probe for the recognition of Cd2+ and its application. *Spectrochimica Acta Part A: Molecular and*

Biomolecular Spectroscopy, *301*, 122979. https://doi.org/10.1016/J.SAA.2023.122979

Huang, Y., Wang, F., Mu, S., Sun, X., … Q. L.-… A. P. A. M., & 2020, undefined. (n.d.). Highly selective and sensitive chemosensor for Al (III) based on isoquinoline Schiff base. *ElsevierYY Huang, FX Wang, SY Mu, X Sun, QZ Li, CZ Xie, HB LiuSpectrochimica Acta Part A: Molecular and Biomolecular Spectroscopy, 2020•Elsevier*. Retrieved December 22, 2024, from https://www.sciencedirect.com/science/article/pii/S1386142520307332

Huang, Y. Y., Wang, F. X., Mu, S. Y., Sun, X., Li, Q. Z., Xie, C. Z., & Liu, H. B. (2020a). Highly selective and sensitive chemosensor for Al(III) based on isoquinoline Schiff base. *Spectrochimica Acta Part A: Molecular and Biomolecular Spectroscopy*, *243*, 118754. https://doi.org/10.1016/J.SAA.2020.118754

Huang, Y. Y., Wang, F. X., Mu, S. Y., Sun, X., Li, Q. Z., Xie, C. Z., & Liu, H. B. (2020b). Highly selective and sensitive chemosensor for Al(III) based on isoquinoline Schiff base. *Spectrochimica Acta Part A: Molecular and Biomolecular Spectroscopy*, *243*, 118754. https://doi.org/10.1016/J.SAA.2020.118754

Huo, F., Zhang, Y., Yue, Y., Chao, J., Zhang, Y., & Yin, C. (2017). Isophorone-based aldehyde for “ratiometric” detection of cyanide by hampering ESIPT. *Dyes and Pigments*, *143*, 270–275. https://doi.org/10.1016/j.dyepig.2017.04.050

Iftikhar, R., Parveen, I., Ayesha, Mazhar, A., Iqbal, M. S., Kamal, G. M., Hafeez, F., Pang, A. L., & Ahmadipour, M. (2023a). Small organic molecules as fluorescent sensors for the detection of highly toxic heavy metal cations in portable water. *Journal of Environmental Chemical Engineering*, *11*(1), 109030. https://doi.org/10.1016/J.JECE.2022.109030

Iftikhar, R., Parveen, I., Ayesha, Mazhar, A., Iqbal, M. S., Kamal, G. M., Hafeez, F., Pang, A. L., & Ahmadipour, M. (2023b). Small organic molecules as fluorescent sensors for the detection of highly toxic heavy metal cations in portable water. *Journal of Environmental Chemical Engineering*, *11*(1), 109030. https://doi.org/10.1016/J.JECE.2022.109030

Immanuel David, C., & Lee, H. (2024). Cutting-edge advances in colorimetric and fluorescent chemosensors for detecting lethal cyanide ion: A comprehensive review. *Microchemical Journal*, *200*, 110359. https://doi.org/https://doi.org/10.1016/j.microc.2024.110359

Islam, M., Hoque, A., Baig, K., … M. S.-S. A., & 2024, undefined. (n.d.). A zwitterionic probe for ratiometric fluorescent detection of aluminium (III) ion in aqueous medium and its application in bioimaging. *ElsevierMS Islam, A Hoque, KMY Baig, M Sarmin, GK Kole, M Hoda, MA AlamSpectrochimica Acta Part A: Molecular and Biomolecular Spectroscopy, 2024•Elsevier*. Retrieved December 23, 2024, from https://www.sciencedirect.com/science/article/pii/S1386142524001719

Iyer, D. K., Shaji, A., Singh, S. P., Tripathi, A., Hazra, A., Mandal, S., & Ghosh, P. (2023). A review on rhodamine probes for metal ion recognition with a future on artificial intelligence and machine learning. *Coordination Chemistry Reviews*, *495*, 215371. https://doi.org/10.1016/J.CCR.2023.215371

Jackson, R., & Logue, B. A. (2017). A review of rapid and field-portable analytical techniques for the diagnosis of cyanide exposure. *Analytica Chimica Acta*, *960*, 18–39. https://doi.org/https://doi.org/10.1016/j.aca.2016.12.039

Jaffé, H. H., & Miller, A. L. (1966). The fates of electronic excitation energy. *Journal of Chemical Education*, *43*(9), 469–473. https://doi.org/10.1021/ED043P469

Jamuna, K., Gayathri, S., Sivakumar, S., & Ashokkumar, B. (2023). Design and development of a fluorometric and colorimetric sensor for toxic cyanide detection by pyridinium scaffolds: live cell imaging and real sample analysis. *Sensors & Diagnostics*, *2*(2), 337–346. https://doi.org/10.1039/D2SD00163B

Janata, J. (1992). Chemical Sensors. *Analytical Chemistry*, *64*(12), 196–219. https://doi.org/10.1021/AC00036A012/ASSET/AC00036A012.FP.PNG_V03

Jaszczak, E., Polkowska, Ż., Narkowicz, S., & Namieśnik, J. (2017). Cyanides in the environment—analysis—problems and challenges. *Environmental Science and Pollution Research*, *24*(19), 15929–15948. https://doi.org/10.1007/s11356-017-9081-7

Javaid, M., Haleem, A., Rab, S., Pratap Singh, R., & Suman, R. (2021). Sensors for daily life: A review. *Sensors International*, *2*, 100121. https://doi.org/10.1016/J.SINTL.2021.100121

Jayasudha, P., Manivannan, R., Kim, W., Lim, H., Patra, S. K., & Son, Y. A. (2024). Tailored fluorophore design: Enhancing selectivity for cyanide ion sensing in water and food samples, and innovative device development. *Spectrochimica Acta Part A: Molecular and Biomolecular Spectroscopy*, *314*, 124196. https://doi.org/10.1016/J.SAA.2024.124196

Jeong, Y., & Yoon, J. (2012). Recent progress on fluorescent chemosensors for metal ions. *Inorganica Chimica Acta*, *381*(1), 2–14. https://doi.org/10.1016/J.ICA.2011.09.011

Ji, P., Li, J., Wang, W., Song, Z., Zhang, Z., Wang, B., & Feng, G. (2023). A novel fluorescent molecule based on 1,2,3-triazole for determination of palladium (II) and hydrazine hydrate in aqueous system. *Spectrochimica Acta Part A: Molecular and Biomolecular Spectroscopy*, *293*, 122492. https://doi.org/10.1016/J.SAA.2023.122492

Jo, J., Olasz, A., Chen, C.-H., & Lee, D. (2013). Interdigitated Hydrogen Bonds: Electrophile Activation for Covalent Capture and Fluorescence Turn-On Detection of Cyanide. *Journal of the American Chemical Society*, *135*(9), 3620–3632. https://doi.org/10.1021/ja312313f

Jreije, I., Hadioui, M., Talanta, K. W.-, & 2022, undefined. (n.d.). Sample preparation for the analysis of nanoparticles in natural waters by single particle ICP-MS. *ElsevierI Jreije, M Hadioui, KJ WilkinsonTalanta, 2022•Elsevier*. https://doi.org/10.1016/j.talanta.2021.123060

Jun, J. V., Petersson, E. J., & Chenoweth, D. M. (2018). Rational Design and Facile Synthesis of a Highly Tunable Quinoline-Based Fluorescent Small-Molecule Scaffold for Live Cell Imaging. *Journal of the American Chemical Society*, *140*(30), 9486–9493. https://doi.org/10.1021/JACS.8B03738

Jung, H. S., Chen, X., Kim, J. S., & Yoon, J. (2013). Recent progress in luminescent and colorimetric chemosensors for detection of thiols. *Chemical Society Reviews*, *42*(14), 6019–6031. https://doi.org/10.1039/C3CS60024F

Jung, H. S., Ko, K. C., Lee, J. H., Kim, S. H., Bhuniya, S., Lee, J. Y., Kim, Y., Kim, S. J., & Kim, J. S. (2010). Rationally designed fluorescence turn-on sensors: A new design strategy based on orbital control. *Inorganic Chemistry*, *49*(18), 8552–8557. https://doi.org/10.1021/IC101165K

Juvekar, V., Park, S. J., Yoon, J., & Kim, H. M. (2021). Recent progress in the two-photon fluorescent probes for metal ions. *Coordination Chemistry Reviews*, *427*, 213574. https://doi.org/10.1016/J.CCR.2020.213574

Kalavathi, A., Saravanakumar, P., Satheeshkumar, K., Vennila, K. N., & Elango, K. P. (2023). Spectral and DFT/TD-DFT studies on turn-on fluorescent detection of Al(III) by a quinolin-8-ol-based Schiff base and its bioimaging. *Journal of Molecular Structure*, *1289*, 135895. https://doi.org/10.1016/J.MOLSTRUC.2023.135895

Kang, J., Huo, F., Zhang, Y., Chao, J., Glass, T. E., & Yin, C. (2019). A novel near-infrared ratiometric fluorescent probe for cyanide and its bioimaging applications. *Spectrochimica Acta - Part A: Molecular and Biomolecular Spectroscopy*, *209*, 95–99. https://doi.org/10.1016/j.saa.2018.10.037

Karasiński, J., Tupys, A., Yang, L., Mester, Z., Halicz, L., & Bulska, E. (2020). Novel Approach for the Accurate Determination of Se Isotope Ratio by Multicollector ICP-MS. *Analytical Chemistry*, *92*(24), 16097–16104. https://doi.org/10.1021/ACS.ANALCHEM.0C03768/ASSET/IMAGES/LARGE/AC0C03768_0003.JPEG

Karch, K. R., Snyder, D. T., Harvey, S. R., & Wysocki, V. H. (2022). Native Mass Spectrometry: Recent Progress and Remaining Challenges. *Annual Review of Biophysics*, *51*(Volume 51, 2022), 157–179. https://doi.org/10.1146/ANNUREV-BIOPHYS-092721-085421/CITE/REFWORKS

Karimi-Maleh, H., Darabi, R., Karimi, F., … C. K.-E., & 2023, undefined. (n.d.). State-of-art advances on removal, degradation and electrochemical monitoring of 4-aminophenol pollutants in real samples: a review. *ElsevierH Karimi-Maleh, R Darabi, F Karimi, C Karaman, SA Shahidi, N Zare, M Baghayeri, L FuEnvironmental Research, 2023•Elsevier*. Retrieved December 22, 2024, from https://www.sciencedirect.com/science/article/pii/S0013935123001305

Kataev, E. A. (2023). Converting pH probes into “turn-on” fluorescent receptors for anions. *Chemical Communications*, *59*(13), 1717–1727. https://doi.org/10.1039/D2CC06194E

Kateshiya, M. R., Desai, M. L., Malek, N. I., & Kailasa, S. K. (2023). Advances in Ultra-small Fluorescence Nanoprobes for Detection of Metal Ions, Drugs, Pesticides and Biomarkers. *Journal of Fluorescence*, *33*(3), 775–798. https://doi.org/10.1007/S10895-022-03115-W

Kaur, B., Kaur, N., & Kumar, S. (2018). Colorimetric metal ion sensors – A comprehensive review of the years 2011–2016. *Coordination Chemistry Reviews*, *358*, 13–69. https://doi.org/10.1016/J.CCR.2017.12.002

Kaur, B., Kaur, N., reviews, S. K.-C. chemistry, & 2018, undefined. (n.d.). Colorimetric metal ion sensors–A comprehensive review of the years 2011–2016. *ElsevierB Kaur, N Kaur, S KumarCoordination Chemistry Reviews, 2018•Elsevier*. Retrieved December 22, 2024, from https://www.sciencedirect.com/science/article/pii/S0010854517305283

Kaushal, J., Singh, S., Oswal, P., Arora, A., Structure, D. N.-… of M., & 2022, undefined. (n.d.). Suzuki− Miyaura coupling and O− arylation reactions catalysed by palladium (II) complexes of bulky ligands bearing naphthalene core, Schiff base functionality and. *Elsevier*. Retrieved December 22, 2024, from https://www.sciencedirect.com/science/article/pii/S0022286021022195

Kaushik, R., Ghosh, A., Singh, A., Gupta, P., Mittal, A., & Jose, D. A. (2016). Selective Detection of Cyanide in Water and Biological Samples by an Off-the-Shelf Compound. *ACS Sensors*, *1*(10), 1265–1271. https://doi.org/10.1021/acssensors.6b00519

Kawamichi, T., Haneda, T., Kawano, M., Nature, M. F.-, & 2009, undefined. (n.d.). X-ray observation of a transient hemiaminal trapped in a porous network. *Nature.ComT Kawamichi, T Haneda, M Kawano, M FujitaNature, 2009•nature.Com*. Retrieved January 23, 2025, from https://www.nature.com/articles/nature08326

Khalid, R., Shahzad, S. A., Assiri, M. A., Javid, T., Irshad, H., & Ullah, M. Z. (2024). AIE active fluorescent probe for the detection of cyanide ion through fluorescence enhancement in real samples: An integrated extensive fluorescence and DFT studies. *Microchemical Journal*, *200*, 110264. https://doi.org/10.1016/J.MICROC.2024.110264

Khan, J. (2023). Synthesis and Applications of Fluorescent Chemosensors: A Review. *Journal of Fluorescence*, *34*(6), 2485–2494. https://doi.org/10.1007/S10895-023-03455-1/METRICS

Kim, A., Kang, J., Jang, H., engineering, C. K.-J. of industrial and, & 2018, undefined. (n.d.). Fluorescent detection of Zn (II) and In (III) and colorimetric detection of Cu (II) and Co (II) by a versatile chemosensor. *ElsevierA Kim, JH Kang, HJ Jang, C KimJournal of Industrial and Engineering Chemistry, 2018•Elsevier*. Retrieved December 22, 2024, from https://www.sciencedirect.com/science/article/pii/S1226086X18302156

Kim, H., Lee, S., Lee, J., & Tae, J. (2010). Rhodamine triazole-based fluorescent probe for the detection of Pt 2+. *Organic Letters*, *12*(22), 5342–5345. https://doi.org/10.1021/OL102397N/SUPPL_FILE/OL102397N_SI_001.PDF

Kim, S. H., Choi, H. S., Kim, J., Lee, S. J., Quango, D. T., & Kim, J. S. (2010). Novel optical/electrochemical selective 1,2,3-triazole ring-appended chemosensor for the Al3+ ion. *Organic Letters*, *12*(3), 560–563. https://doi.org/10.1021/OL902743S/SUPPL_FILE/OL902743S_SI_001.PDF

Krämer, J., Kang, R., Grimm, L. M., De Cola, L., Picchetti, P., & Biedermann, F. (2022). Molecular Probes, Chemosensors, and Nanosensors for Optical Detection of Biorelevant Molecules and Ions in Aqueous Media and Biofluids. *Chemical Reviews*, *122*(3), 3459–3636. https://doi.org/10.1021/ACS.CHEMREV.1C00746/ASSET/IMAGES/MEDIUM/CR1C00746_0045.GIF

Krämer, J., Kang, R., Grimm, L. M., De Cola, L., Picchetti, P., & Biedermann, F. (2022). Molecular probes, chemosensors, and nanosensors for optical detection of biorelevant molecules and ions in aqueous media and biofluids. *Chemical Reviews*, *122*(3), 3459–3636.

Krewski, D., Yokel, R. A., Nieboer, E., Borchelt, D., Cohen, J., Harry, J., Kacew, S., Lindsay, J., Mahfouz, A. M., & Rondeau, V. (2007a). Human Health Risk Assessment for Aluminium, Aluminium Oxide, and Aluminium Hydroxide. *Journal of Toxicology and Environmental Health, Part B*, *10*(SUPPL. 1), 1–269. https://doi.org/10.1080/10937400701597766

Krewski, D., Yokel, R. A., Nieboer, E., Borchelt, D., Cohen, J., Harry, J., Kacew, S., Lindsay, J., Mahfouz, A. M., & Rondeau, V. (2007b). Human health risk assessment for aluminium, aluminium oxide, and aluminium hydroxide. *Taylor & Francis, E Nieboer, D Borchelt, J Cohen, J Harry, S Kacew, J Lindsay, AM Mahfouz, V RondeauJournal of Toxicology and Environmental Health, Part B, 2007•Taylor & Francis*, *10*(SUPPL. 1), 1–1. https://doi.org/10.1080/10937400701597766

Kshirsagar, N., Sonawane, R., Patil, P., … J. N.-I. C., & 2020, undefined. (n.d.). Fluorescent chemosensor for Al (III) based on chelation-induced fluorescence enhancement and its application in live cells imaging. *ElsevierN Kshirsagar, R Sonawane, P Patil, J Nandre, P Sultan, S Sehlangia, CP Pradeep, Y WangInorganica Chimica Acta, 2020•Elsevier*. Retrieved December 30, 2024, from https://www.sciencedirect.com/science/article/pii/S0020169320310045?casa_token=3CN_t90aHscAAAAA:J6h3u8X2gxaim75RxJZOFzOSxJjLYlvDaMenH-XCriBmjb2bhlqAiHJtNPhWJPGOWPIbUr6TauA

Kuhana A, T., Feng, W., & Feng, G. (2018). A simple but effective colorimetric and far-red to near-infrared fluorescent probe for palladium and its application in living cells. *Dyes and Pigments*, *152*, 112–117. https://doi.org/10.1016/J.DYEPIG.2018.01.044

Kumar, P., & Kumar, S. (2020). Copper ion luminescence on/off sensing by a quinoline-appended ruthenium(II)-polypyridyl complex in aqueous media. *Journal of Molecular Structure*, *1202*, 127242. https://doi.org/10.1016/J.MOLSTRUC.2019.127242

Kumar, P., Kumar, V., advances, R. G.-R., & 2015, undefined. (2013). Arene-based fluorescent probes for the selective detection of iron. *Pubs.Rsc.OrgP Kumar, V Kumar, R GuptaRSC Advances, 2015•pubs.Rsc.Org*, *00*, 1–3. https://doi.org/10.1039/x0xx00000x

Kumar, R. S., Ashok Kumar, S. K., Vijayakrishna, K., Sivaramakrishna, A., Brahmnanda Rao, C. V. S., Sivaraman, N., & Sahoo, S. K. (2019). Highly selective CHEF-type chemosensor for lutetium (III) recognition in semi-aqueous media. *ElsevierRS Kumar, SKA Kumar, K Vijayakrishna, A Sivaramakrishna, CVSB Rao, N SivaramanSpectrochimica Acta Part A: Molecular and Biomolecular Spectroscopy, 2019•Elsevier*, *214*, 32–39. https://doi.org/10.1016/j.saa.2019.02.003

Kumar, S., Gadiyaram, S., Tittal, R. K., Vikas D, G., & Sharma, R. (2023a). Fluorescent molecular probe to detect and differentiate Fe3+from other metal ions. *Journal of Molecular Structure*, *1290*, 135940. https://doi.org/10.1016/J.MOLSTRUC.2023.135940

Kumar, S., Gadiyaram, S., Tittal, R. K., Vikas D, G., & Sharma, R. (2023b). Fluorescent molecular probe to detect and differentiate Fe3+from other metal ions. *Journal of Molecular Structure*, *1290*, 135940. https://doi.org/10.1016/J.MOLSTRUC.2023.135940

Kumar, S., Singh, S., Kumar, A., & Kumar, P. (2021a). Recognition, mechanistic investigation and applications for the detection of biorelevant Cu2+/Fe2+/Fe3+ ions by ruthenium(II)-polypyridyl based fluorescent sensors. *Dalton Transactions*, *50*(8), 2705–2721. https://doi.org/10.1039/D0DT03488F

Kumar, S., Singh, S., Kumar, A., & Kumar, P. (2021b). Recognition, mechanistic investigation and applications for the detection of biorelevant Cu2+/Fe2+/Fe3+ions by ruthenium(ii)-polypyridyl based fluorescent sensors. *Dalton Transactions*, *50*(8), 2705–2721. https://doi.org/10.1039/d0dt03488f

Kumar, S., Singh, S., Kumar, A., Murthy, K. S. R., & Singh, A. K. (2022). pH-Responsive luminescence sensing, photoredox catalysis and photodynamic applications of ruthenium (II) photosensitizers bearing imidazo [4, 5-f][1, 10] phenanthroline scaffolds. *Coordination Chemistry Reviews*, *452*, 214272.

Kumar, S., Singh, S., Kumar, A., Transactions, P. K.-D., & 2021, undefined. (n.d.). Recognition, mechanistic investigation and applications for the detection of biorelevant Cu 2+/Fe 2+/Fe 3+ ions by ruthenium (II)-polypyridyl based fluorescent sensors. *Pubs.Rsc.OrgS Kumar, S Singh, A Kumar, P KumarDalton Transactions, 2021•pubs.Rsc.Org*. Retrieved December 22, 2024, from https://pubs.rsc.org/en/content/articlehtml/2021/dt/d0dt03488f

Kumar, V., Kim, H., Pandey, B., James, T. D., Yoon, J., & Anslyn, E. V. (2023). Recent advances in fluorescent and colorimetric chemosensors for the detection of chemical warfare agents: a legacy of the 21st century. *Chemical Society Reviews*, *52*(2), 663–704. https://doi.org/10.1039/D2CS00651K

Kumar, V., Singh, D., Kumar, P., Chaudhary, G., Singh, A. P., & Gupta, R. (2022). Turn-on fluorescent detection of nickel and zinc ions by two related chemosensors containing naphthalimide ring(s). *Journal of Molecular Structure*, *1261*, 132901. https://doi.org/10.1016/J.MOLSTRUC.2022.132901

Kursunlu, A., Bastug, E., Oguz, A., Acta, M. O.-A. C., & 2022, undefined. (n.d.). A highly branched macrocycle-based dual-channel sensor: Bodipy and pillar arene combination for detection of Sn (II) &Hg (II) and bioimaging in living cells. *ElsevierAN Kursunlu, E Bastug, A Oguz, M Oguz, M YilmazAnalytica Chimica Acta, 2022•Elsevier*. Retrieved December 22, 2024, from https://www.sciencedirect.com/science/article/pii/S0003267022001131

Lacson, C. F. Z., Lu, M.-C., & Huang, Y.-H. (2020). Fluoride network and circular economy as potential model for sustainable development-A review. *Chemosphere*, *239*, 124662. https://doi.org/https://doi.org/10.1016/j.chemosphere.2019.124662

Lakowicz, J. R. (2006). Principles of fluorescence spectroscopy. *Principles of Fluorescence Spectroscopy*, 1–954. https://doi.org/10.1007/978-0-387-46312-4/COVER

Lalitha, R., & Velmathi, S. (2023). A Study of Small Molecule-Based Rhodamine-Derived Chemosensors and their Implications in Environmental and Biological Systems from 2012 to 2021: Latest Advancement and Future Prospects. *Journal of Fluorescence 2023 34:1*, *34*(1), 15–118. https://doi.org/10.1007/S10895-023-03231-1

Lee, Y. J., Lim, C., Suh, H., Song, E. J., & Kim, C. (2014). A multifunctional sensor: Chromogenic sensing for Mn2+ and fluorescent sensing for Zn2+ and Al3+. *Sensors and Actuators B: Chemical*, *201*, 535–544. https://doi.org/10.1016/J.SNB.2014.05.035

Li, C., Hu, W., Wang, J., Song, X., Xiong, X., Analyst, Z. L.-, & 2020, undefined. (n.d.). A highly specific probe for the imaging of inflammation-induced endogenous nitric oxide produced during the stroke process. *Pubs.Rsc.OrgC Li, W Hu, J Wang, X Song, X Xiong, Z LiuAnalyst, 2020•pubs.Rsc.Org*. Retrieved December 30, 2024, from https://pubs.rsc.org/en/content/articlehtml/2020/an/d0an00824a

Li, D., Tu, S., Le, Y., Zhou, Y., Yang, L., Ding, Y., Huang, L., & Liu, L. (2023a). Development of a carbazole-based fluorescent probe for quantitative detection of fluoride ions in aqueous systems. *Chemical Papers*, *77*(3), 1741–1749. https://doi.org/10.1007/S11696-022-02557-7/METRICS

Li, D., Tu, S., Le, Y., Zhou, Y., Yang, L., Ding, Y., Huang, L., & Liu, L. (2023b). Development of carbazole-based fluorescent probe for highly sensitive application in fluoride ion detection. *Spectrochimica Acta Part A:*

Molecular and Biomolecular Spectroscopy, *285*, 121816. https://doi.org/10.1016/J.SAA.2022.121816

Li, D., Tu, S., Le, Y., Zhou, Y., Yang, L., Ding, Y., Huang, L., & Liu, L. (2023c). Development of carbazole-based fluorescent probe for highly sensitive application in fluoride ion detection. *Spectrochimica Acta Part A: Molecular and Biomolecular Spectroscopy*, *285*, 121816. https://doi.org/10.1016/J.SAA.2022.121816

Li, H., Fan, J., & Peng, X. (2013). Colourimetric and fluorescent probes for the optical detection of palladium ions. *Chemical Society Reviews*, *42*(19), 7943–7962. https://doi.org/10.1039/C3CS60123D

Li, H., Zhao, P., Zou, N., Wang, H., & Sun, K. (2017). The colorimetric and ratiometric fluorescent detection of cyanide and sulfide in live cells, application for logic gate and bioimging. *Tetrahedron Letters*, *58*(1), 30–34. https://doi.org/10.1016/j.tetlet.2016.11.088

Li, L., Wang, J., Xu, S., Li, C., & Dong, B. (2022). Recent Progress in Fluorescent Probes For Metal Ion Detection. *Frontiers in Chemistry*, *10*, 875241. https://doi.org/10.3389/FCHEM.2022.875241/BIBTEX

Li, Q., & Zhou, Y. (2023a). Recent advances in fluorescent materials for mercury(ii) ion detection. *RSC Advances*, *13*(28), 19429–19446. https://doi.org/10.1039/D3RA02410E

Li, Q., & Zhou, Y. (2023b). Recent advances in fluorescent materials for mercury(ii) ion detection. *RSC Advances*, *13*(28), 19429–19446. https://doi.org/10.1039/D3RA02410E

Li, X. X., Ma, C. Y., Du, M. X., Dong, W. K., & Ding, Y. J. (2024). A rare salamo-salophen type “on-off-on” fluorescent probe for relay recognition of Hg2+ and phosphate ions and its applications. *Journal of Molecular Structure*, *1299*, 137188. https://doi.org/10.1016/J.MOLSTRUC.2023.137188

Li, Z., Hou, J., Wang, S., Zhu, L., He, X., Chemistry, J. S.-C., & 2022, undefined. (n.d.). Recent advances of luminescent sensors for iron and copper: Platforms, mechanisms, and bio-applications. *ElsevierZ Li, JT Hou, S Wang, L Zhu, X He, J ShenCoordination Chemistry Reviews, 2022•Elsevier*. Retrieved December 23, 2024, from https://www.sciencedirect.com/science/article/pii/S0010854522002909

Li, Z., Wang, J., Chen, Y., Xiao, L., & Liu, Z. (2023). A benzothiazole-based fluorescent probe for sensing Zn2+ and its application. *Inorganica Chimica Acta*, *545*, 121275. https://doi.org/10.1016/J.ICA.2022.121275

Li, Z., Wang, J., Xiao, L., Wang, J., Acta, H. Y.-I. C., & 2021, undefined. (n.d.). A dual-response fluorescent probe for Al3+ and Zn2+ in aqueous medium based on benzothiazole and its application in living cells. *ElsevierZ Li, J Wang, L Xiao, J Wang, H YanInorganica Chimica Acta, 2021•Elsevier*. Retrieved December 23, 2024, from https://www.sciencedirect.com/science/article/pii/S0020169320313475?casa_token=4VFeGI4LN1QAAAAA:8UwTZEGDoxfyKS2IAx71HuSoykg7dXsHTzxkBKe6sifrzh-i2LEc8l3W_2Da68kr1FgZ9zmQ-fhV

Li, Z., Yu, M., Zhang, L., Yu, M., Liu, J., … L. W.-C., & 2010, undefined. (n.d.). A “switching on” fluorescent chemodosimeter of selectivity to Zn2+ and its application to MCF-7 cells. *Pubs.Rsc.OrgZ Li, M Yu, L Zhang, M Yu, J Liu, L Wei, H ZhangChemical Communications, 2010•pubs.Rsc.Org*. Retrieved December 30, 2024, from https://pubs.rsc.org/en/content/articlehtml/2010/cc/c0cc01687j

Lindsay, Sandie. (1997). *High performance liquid chromatography*. 337. https://books.google.com/books/about/High_Performance_Liquid_Chromatography.html?id=08VQA3iChOUC

Liu, B., Zhuang, J., & Wei, G. (2020a). Recent advances in the design of colorimetric sensors for environmental monitoring. *Environmental Science: Nano*, *7*(8), 2195–2213. https://doi.org/10.1039/D0EN00449A

Liu, B., Zhuang, J., & Wei, G. (2020b). Recent advances in the design of colorimetric sensors for environmental monitoring. *Environmental Science: Nano*, *7*(8), 2195–2213. https://doi.org/10.1039/D0EN00449A

Liu, H., Liu, T., Li, J., Zhang, Y., Li, J., Song, J., … J. Q.-J. of M., & 2018, undefined. (n.d.). A simple Schiff base as dual-responsive fluorescent sensor for bioimaging recognition of Zn 2+ and Al 3+ in living cells. *Pubs.Rsc.OrgH Liu, T Liu, J Li, Y Zhang, J Li, J Song, J Qu, WY WongJournal of Materials Chemistry B, 2018•pubs.Rsc.Org*. Retrieved December 22, 2024, from https://pubs.rsc.org/en/content/articlehtml/2018/tb/c8tb01743c

Liu, M., Yin, Z., Tan, Y., Li, J., Peng, H., Duan, A., Pigments, C. L.-D. and, & 2020, undefined. (n.d.). A new acylhydrazine N'-(1, 3 dimethylbutylene)-3-hydroxy-naphthohydrazide based fluorescent sensor for the detection of Ni2+. *ElsevierM Liu, Z Yin, Y Tan, J Li, H Peng, A Duan, C LuoDyes and Pigments, 2020•Elsevier*. Retrieved December 19, 2024, from https://www.sciencedirect.com/science/article/pii/S0143720820308469?casa_token=9m7fzL4V8K8AAAAA:lEV8M9cDUSuUlFZp8mHMeZmXYvrCW5ddbK8TpZfSJ5K1h6bMYk_Ynu2l1q0NvQwfV3hqoLF4xZgp

Liu, M., Zhu, H., Fang, Y., Liu, C., Li, X., Zhang, X., Ma, L., Wang, K., Yu, M., Sheng, W., & Zhu, B. (2024). An ultra-sensitive fluorescent probe for recognition of aluminum ions and its application in environment, food, and living organisms. *Spectrochimica Acta Part A: Molecular and Biomolecular Spectroscopy*, *307*, 123578. https://doi.org/10.1016/J.SAA.2023.123578

Liu, S., Zhang, L., Kim, H., Sun, J., & Yoon, J. (2024). Recent advances and challenges in monitoring chromium ions using fluorescent probes. *Coordination Chemistry Reviews*, *501*, 215575. https://doi.org/10.1016/J.CCR.2023.215575

Liu, Y., Wu, M., Zhao, J., Wang, Y., & Zhang, Y. (2022a). A simple salicylaldehyde-bearing pyrazine as a turn-on fluorescent chemosensor for

Al3+and Zn2+recognition and its applications. *Reviews in Analytical Chemistry*, *41*(1), 217–227. https://doi.org/10.1515/REVAC-2022-0043/DOWNLOADASSET/SUPPL/REVAC-2022-0043_SM.PDF

Liu, Y., Wu, M., Zhao, J., Wang, Y., & Zhang, Y. (2022b). A simple salicylaldehyde-bearing pyrazine as a turn-on fluorescent chemosensor for Al3+and Zn2+recognition and its applications. *Reviews in Analytical Chemistry*, *41*(1), 217–227. https://doi.org/10.1515/REVAC-2022-0043/HTML

Liu, Y., Zhang, Y., Sheng, M., Kang, Y., Jia, B., Li, W., & Fu, Y. (2023). A novel pyrene-based fluorescent probe for Al3+ detection. *Spectrochimica Acta Part A: Molecular and Biomolecular Spectroscopy*, *287*, 122085. https://doi.org/10.1016/J.SAA.2022.122085

Liu, Z., He, W., Reviews, Z. G.-C. S., & 2013, undefined. (2013). Metal coordination in photoluminescent sensing. *Pubs.Rsc.OrgZ Liu, W He, Z GuoChemical Society Reviews, 2013•pubs.Rsc.Org*, *42*, 1568. https://doi.org/10.1039/c2cs35363f

Lohar, S., Dhara, K., Roy, P., Sinha Babu, S. P., & Chattopadhyay, P. (2018). Highly Sensitive Ratiometric Chemosensor and Biomarker for Cyanide Ions in the Aqueous Medium. *ACS Omega*, *3*(8), 10145–10153. https://doi.org/10.1021/ACSOMEGA.8B01035

Long, D., & Yu, H. (2016). A synergistic coordination strategy for colorimetric sensing of chromium(III) ions using gold nanoparticles. *Analytical and Bioanalytical Chemistry*, *408*(29), 8551–8557. https://doi.org/10.1007/S00216-016-9990-1

Lough, W. J. ., & Wainer, I. W. . (1997). *High performance liquid chromatography : fundamental principles and practice*. 276. https://books.google.com/books/about/High_Performance_Liquid_Chromatography.html?id=9SzJGAmWIvMC

Loya, M., Ghosh, S., & Atta, A. K. (2023a). A review on dual detection of Cu2+ and Ni2+ ions by using single fluorometric and colorimetric organic molecular probes. *Journal of Molecular Structure*, *1278*, 134949. https://doi.org/10.1016/J.MOLSTRUC.2023.134949

Loya, M., Ghosh, S., & Atta, A. K. (2023b). A review on dual detection of Cu2+ and Ni2+ ions by using single fluorometric and colorimetric organic molecular probes. *Journal of Molecular Structure*, *1278*, 134949. https://doi.org/10.1016/J.MOLSTRUC.2023.134949

Lu, C., Xu, J., Song, Z., Pigments, Z. D.-D. and, & 2024, undefined. (n.d.). Advancements in ESIPT probe research over the past three years based on different fluorophores. *ElsevierC Lu, J Xu, Z Song, Z DaiDyes and Pigments, 2024•Elsevier*. Retrieved December 23, 2024, from https://www.sciencedirect.com/science/article/pii/S0143720824000597?casa_token=pTlNIFQpc_0AAAAA:5dA44YcJTeDLPqVP_xgRHIPC08XkvTRvrJaZVidlXF4DeiHskrYDKHfCW8f1vC-YJLpMwEjEDbiP

Lu, M., Qiu, S., Cui, S., Letters, S. P.-T., & 2020, undefined. (n.d.). A double target fluorescent sensor based on diarylethene for detection of Al3+ and Zn2+. *Elsevier*. Retrieved December 22, 2024, from https://www.sciencedirect.com/science/article/pii/S0040403920308509

Lu, W., Chen, J., Shi, J., Xu, L., Yang, S., & Gao, B. (2021). A novel quinoline-based turn-on fluorescent probe for the highly selective detection of Al (III) and its bioimaging in living cells, plants tissues and zebrafish. *Journal of Biological Inorganic Chemistry*, *26*(1), 57–66. https://doi.org/10.1007/S00775-020-01836-6

Ma, D. L., Lin, S., Wang, W., Yang, C., & Leung, C. H. (2017). Luminescent chemosensors by using cyclometalated iridium(iii) complexes and their applications. *Chemical Science*, *8*(2), 878–889. https://doi.org/10.1039/C6SC04175B

Ma, X., Hao, Y., Dong, X., & Xia, N. (2023). Biosensors with Metal Ion–Phosphate Chelation Interaction for Molecular Recognition. *Molecules 2023, Vol. 28, Page 4394*, *28*(11), 4394. https://doi.org/10.3390/MOLECULES28114394

Maharani, E. P., Briliana, H., Putri, E. H., Faraditta, F. S., & Az-zhaffirah, A. R. (2024). A Comprehensive Review on Atomic Absorption Spectroscopy: Principles, Techniques, and Applications. *Jurnal Ilmiah Wahana Pendidikan*, *10*(15), 20–29. https://doi.org/10.5281/ZENODO.13764070

Majhi, A., Venkateswarlu, K., & Sasikumar, P. (2024). Coumarin Based Fluorescent Probe for Detecting Heavy Metal Ions. *Journal of Fluorescence*, *34*(4), 1453–1483. https://doi.org/10.1007/S10895-023-03372-3/METRICS

Malahom, N., Ma-In, T., Naksen, P., Anutrasakda, W., Amatatongchai, M., Citterio, D., & Jarujamrus, P. (2023). Nitrogen-Doped Graphene Quantum Dots as "Off–On" Fluorescent Probes in Paper-Based Test Kits for Selective Monitoring of Cyanide in Food. *ACS Applied Nano Materials*, *6*(13), 11144–11153. https://doi.org/10.1021/acsanm.3c01109

Malkondu, S., Erdemir, S., & Karakurt, S. (2020). Red and blue emitting fluorescent probe for cyanide and hypochlorite ions: Biological sensing and environmental analysis. *Dyes and Pigments*, *174*, 108019. https://doi.org/10.1016/J.DYEPIG.2019.108019

Man, L., Wang, T., Liu, K., Hou, X., … Z. W.-J. of M., & 2024, undefined. (n.d.). A novel dual-functional half salamo-based fluorescent turn-on sensor for selectively recognition and differentiation of Zn2+ and Al3+ ions. *Elsevier*. Retrieved January 2, 2025, from https://www.sciencedirect.com/science/article/pii/S0022286024001091

Manickam, S., & Iyer, S. K. (2020). Highly sensitive turn-off fluorescent detection of cyanide in aqueous medium using dicyanovinyl-substituted

phenanthridine fluorophore. *RSC Advances*, *10*(20), 11791–11799. https://doi.org/10.1039/D0RA00623H

Manna, A., Chowdhury, S., Transactions, G. P.-D., & 2019, undefined. (2019). A novel hydrazide-based selective and sensitive optical chemosensor for the detection of Ni 2+ ions: Applications in live cell imaging, molecular logic gates and smart. *Pubs.Rsc.OrgAK Manna, S Chowdhury, GK PatraDalton Transactions, 2019•pubs.Rsc.Org*, *48*, 12336. https://doi.org/10.1039/c9dt02448d

Manna, U., Das, G., & Hossain, Md. A. (2022). Insights into the binding aspects of fluoride with neutral synthetic receptors. *Coordination Chemistry Reviews*, *455*, 214357. https://doi.org/https://doi.org/10.1016/j.ccr.2021.214357

Manoj, K. M., Ramasamy, S., Parashar, A., Gideon, D. A., Soman, V., Jacob, V. D., & Pakshirajan, K. (2020). *Acute toxicity of cyanide in aerobic respiration: Theoretical and experimental support for murburn explanation*. *11*(1), 32–56. https://doi.org/doi:10.1515/bmc-2020-0004

Martínez-Máñez, R., & Sancenón, F. (2003a). Fluorogenic and chromogenic chemosensors and reagents for anions. *Chemical Reviews*, *103*(11), 4419–4476. https://doi.org/10.1021/CR010421E/ASSET/CR010421E.FP.PNG_V03

Martínez-Máñez, R., & Sancenón, F. (2003b). Fluorogenic and Chromogenic Chemosensors and Reagents for Anions. *Chemical Reviews*, *103*(11), 4419–4476. https://doi.org/10.1021/cr010421e

Melhuish, W. H. (1961). Quantum efficiencies of fluorescence of organic substan ces: Effect of solvent and concentration of the fluorescent solute. *Journal of Physical Chemistry*, *65*(2), 229–235. https://doi.org/10.1021/J100820A009

Meng, W.-Q., Sedgwick, A. C., Kwon, N., Sun, M., Xiao, K., He, X.-P., Anslyn, E. V, James, T. D., & Yoon, J. (2023). Fluorescent probes for the detection

of chemical warfare agents. *Pubs.Rsc.OrgWQ Meng, AC Sedgwick, N Kwon, M Sun, K Xiao, XP He, EV Anslyn, TD James, J YoonChemical Society Reviews, 2023•pubs.Rsc.Org*, *52*, 601. https://doi.org/10.1039/d2cs00650b

Mohanasundaram, D., Vinoth Kumar, G. G., Kumar, S. K., Maddiboyina, B., Raja, R. P., Rajesh, J., & Sivaraman, G. (2020). Turn-on fluorescence sensor for selective detection of fluoride ion and its molecular logic gates behavior. *Journal of Molecular Liquids*, *317*, 113913. https://doi.org/10.1016/J.MOLLIQ.2020.113913

Moore, J., Fanelli, R. M., & Sekellick, A. J. (2020). High-Frequency Data Reveal Deicing Salts Drive Elevated Specific Conductance and Chloride along with Pervasive and Frequent Exceedances of the U.S. Environmental Protection Agency Aquatic Life Criteria for Chloride in Urban Streams. *Environmental Science and Technology*, *54*(2), 778–789. https://doi.org/10.1021/ACS.EST.9B04316/ASSET/IMAGES/LARGE/ES9B04316_0005.JPEG

Muhammad Shahbaz, Birra Dar, Shahzad Sharif, Aqib Khurshid, M., Sajjad Hussain, Bilal Riaz, Maryam Musaffa, Hania Khalid, Rashid Ch, A., & Abia Mahboob. (2024). Recent advances in the fluorimetric and colorimetric detection of cobalt ions. *RSC Advances*, *14*(14), 9819–9847. https://doi.org/10.1039/D4RA00445K

Murale, D. P., Haque, M. M., Hong, K. T., & Lee, J. S. (2021). A Pyridinyl-Pyrazole BODIPY as Lipid Droplets Probe. *Bulletin of the Korean Chemical Society*, *42*(1), 111–114. https://doi.org/10.1002/BKCS.12166

Naithani, S., Dubey, R., Goswami, T., Thetiot, F., & Kumar, S. (2024a). Optical detection strategies for Ni(II) ion using metal–organic chemosensors: from molecular design to environmental applications. *Dalton Transactions*, *53*(43), 17409–17428. https://doi.org/10.1039/D4DT02376E

Naithani, S., Dubey, R., Goswami, T., Thetiot, F., & Kumar, S. (2024b). Optical detection strategies for Ni(II) ion using metal–organic chemosensors: from molecular design to environmental applications. *Dalton Transactions*, *53*(43), 17409–17428. https://doi.org/10.1039/D4DT02376E

Naithani, S., Dubey, R., Goswami, T., Thetiot, F., & Kumar, S. (2024c). Optical detection strategies for Ni(ii) ion using metal–organic chemosensors: from molecular design to environmental applications. *Dalton Transactions*, *53*(43), 17409–17428. https://doi.org/10.1039/D4DT02376E

Naithani, S., Goswami, N., Singh, S., Yadav, V., Kumar, S., Kumar, P., Kumar, A., Goswami, T., & Kumar, S. (2023a). Turn-on detection of Al3+ and Zn2+ ions by a NSN donor probe: reversibility, logic gates and DFT calculations. *Analytical Methods*, *15*(44), 6021–6030. https://doi.org/10.1039/D3AY01534C

Naithani, S., Goswami, N., Singh, S., Yadav, V., Kumar, S., Kumar, P., Kumar, A., Goswami, T., & Kumar, S. (2023b). Turn-on detection of Al3+ and Zn2+ ions by a NSN donor probe: reversibility, logic gates and DFT calculations. *Analytical Methods*, *15*(44), 6021–6030. https://doi.org/10.1039/D3AY01534C

Naithani, S., Goswami, N., Singh, S., Yadav, V., Kumar, S., Kumar, P., Kumar, A., Goswami, T., & Kumar, S. (2023c). Turn-on detection of Al3+ and Zn2+ ions by a NSN donor probe: reversibility, logic gates and DFT calculations. *Analytical Methods*, *15*(44), 6021–6030. https://doi.org/10.1039/d3ay01534c

Naithani, S., Goswami, N., Yadav, V., Mangalam, J., Goswami, T., & Kumar, S. (2025). Selective Turn-On Luminescent Recognition of Perchlorate Ion Using Pyridyl-Benzimidazole–Based Probe. *Luminescence*, *40*(1), e70087. https://doi.org/10.1002/BIO.70087

Naithani, S., Goswami, T., Thetiot, F., & Kumar, S. (2023). Imidazo[4,5-f][1,10]phenanthroline based luminescent probes for anion recognition:

Recent achievements and challenges. *Coordination Chemistry Reviews*, *475*, 214894. https://doi.org/https://doi.org/10.1016/j.ccr.2022.214894

Naithani, S., Heena, Sharma, P., Layek, S., Thetiot, F., Goswami, T., & Kumar, S. (2025). Nanoparticles and quantum dots as emerging optical sensing platforms for Ni(II) detection: Recent approaches and perspectives. *Coordination Chemistry Reviews*, *524*, 216331. https://doi.org/https://doi.org/10.1016/j.ccr.2024.216331

Naithani, S., Thetiot, F., Yadav, V., Saini, S., Roy, P., Layek, S., Goswami, T., & Kumar, S. (2024a). A pyridyl-benzimidazole based ruthenium(II) complex as optical sensor: Targeted cyanide detection and live cell imaging applications. *Journal of Photochemistry and Photobiology A: Chemistry*, *453*, 115610. https://doi.org/10.1016/J.JPHOTOCHEM.2024.115610

Naithani, S., Thetiot, F., Yadav, V., Saini, S., Roy, P., Layek, S., Goswami, T., & Kumar, S. (2024b). A pyridyl-benzimidazole based ruthenium(II) complex as optical sensor: Targeted cyanide detection and live cell imaging applications. *Journal of Photochemistry and Photobiology A: Chemistry*, 115610. https://doi.org/https://doi.org/10.1016/j.jphotochem.2024.115610

Nan, X., Huyan, Y., Li, H., Sun, S., & Xu, Y. (2021). Reaction-based fluorescent probes for Hg2+, Cu2+ and Fe3+/Fe2+. *Coordination Chemistry Reviews*, *426*, 213580. https://doi.org/10.1016/J.CCR.2020.213580

Nandhini, C., Kumar, P. S., Poongodi, K., Shanmugapriya, R., & Elango, K. P. (2021). Development of simple imine based probe for selective fluorescent cyanide sensing with red-emission in solid and solution phases. *Journal of Molecular Liquids*, *327*, 114833. https://doi.org/10.1016/J.MOLLIQ.2020.114833

Nanomaterial-based electrochemical sensing platform for the determination of Olaparib. (n.d.). *ElsevierM Majidian, G Ozcelikay, A Cetinkaya, MA Unal, H Nazır, EB Atici, SA OzkanElectrochimica Acta, 2023•Elsevier*. Retrieved

December 22, 2024, from https://www.sciencedirect.com/science/article/pii/S0013468623003791

Naphthalene derived Schiff base as a reversible fluorogenic chemosensor for aluminium ions detection. (n.d.). *Elsevier, SPM Paul, A Sanmugam, A Abiram, S Murugan, RS Kumar, AI Almansour, N Arumugam…Spectrochimica Acta Part A: Molecular and Biomolecular Spectroscopy, 2024•Elsevier*. Retrieved December 23, 2024, from https://www.sciencedirect.com/science/article/pii/S1386142523014178

Nayak, P. (2002). Aluminum: Impacts and Disease. *Environmental Research*, *89*(2), 101–115. https://doi.org/10.1006/ENRS.2002.4352

Novel fluorescent microcapsules based on sporopollenin for removal and detection of Cu (II) ions in aqueous solutions: Eco-friendly design, fully. (n.d.). *ElsevierA Bilgic, A Cimen, AN Kursunlu, HS KarapınarMicroporous and Mesoporous Materials, 2022•Elsevier*. Retrieved December 22, 2024, from https://www.sciencedirect.com/science/article/pii/S1387181121007265?casa_token=uX0SjoI7q3UAAAAA:05t3pITaVqRG51KrlRqOqCoZ6MFojlIJ5YVEJsOGwji7MbnQzUMr9CTNr1M6PPbIW94vXZBurzd9

Organization, W. H. (2022). *Guidelines for drinking-water quality: incorporating the first and second addenda*. World Health Organization.

Organoselenium ligand-stabilized copper nanoparticles: development of a magnetically separable catalytic system for efficient, room temperature and. (n.d.). *ElsevierA Arora, P Oswal, S Singh, D Nautiyal, GK Rao, S Kumar, AK Singh, A KumarInorganica Chimica Acta, 2021•Elsevier*. Retrieved December 22, 2024, from https://www.sciencedirect.com/science/article/pii/S0020169321000232?casa_token=DxNrYQMssbwAAAAA:RM-PlcgCirSVsAH_FL8qtW07TJJ9wuLqNxpQ_ttEgDhCclWfnHmNBGLPZhKtMVqGZcyzb05IizG7

Osteryoung, J. (1993). Voltammetry for the Future. *Accounts of Chemical Research*, *26*(3), 77–83. https://doi.org/10.1021/AR00027A001/ASSET/AR00027A001.FP.PNG_V03

Padghan, S. D., Hu, J.-W., Hsu, Y.-H., Liu, K.-M., & Chen, K.-Y. (2024). Swift and quantitative naked-eye detection of cyanide: A dual-mode approach using an ICT-based colorimetric and ratiometric fluorescent chemodosimeter. *Dyes and Pigments*, *228*, 112229. https://doi.org/https://doi.org/10.1016/j.dyepig.2024.112229

Pak, Y., Wang, Y., Reviews, Q. X.-C. C., & 2021, undefined. (n.d.). Conjugated polymer based fluorescent probes for metal ions. *ElsevierYL Pak, Y Wang, Q XuCoordination Chemistry Reviews, 2021•Elsevier*. Retrieved December 23, 2024, from https://www.sciencedirect.com/science/article/pii/S0010854520311966

Pal, A., Karmakar, M., Bhatta, S. R., & Thakur, A. (2021). A detailed insight into anion sensing based on intramolecular charge transfer (ICT) mechanism: A comprehensive review of the years 2016 to 2021. *Coordination Chemistry Reviews*, *448*, 214167. https://doi.org/https://doi.org/10.1016/j.ccr.2021.214167

Pal, A., Sarkar, O., Pramanik, N. R., & Dey, N. (2024). Design of ESIPT-Based Fluorescent Probes for Dual-Mode Sensing of Cyanide: Application to Rapid On-Location Detection and Screening of Natural Water Samples. *Industrial and Engineering Chemistry Research*, *63*(19), 8489–8496. https://doi.org/10.1021/ACS.IECR.3C04209/SUPPL_FILE/IE3C04209_SI_001.PDF

Park, G., Lee, M., You, G., Choi, Y., Letters, C. K.-T., & 2014, undefined. (n.d.). A turn-on and reversible fluorescence sensor with high affinity to Zn2+ in aqueous solution. *Elsevier*. Retrieved December 30, 2024, from https://www.sciencedirect.com/science/article/pii/S004040391400416X

Park, S. H., Kwon, N., Lee, J. H., Yoon, J., & Shin, I. (2020a). Synthetic ratiometric fluorescent probes for detection of ions. *Chemical Society Reviews*, *49*(1), 143–179. https://doi.org/10.1039/C9CS00243J

Park, S. H., Kwon, N., Lee, J. H., Yoon, J., & Shin, I. (2020b). Synthetic ratiometric fluorescent probes for detection of ions. *Chemical Society Reviews*, *49*(1), 143–179. https://doi.org/10.1039/c9cs00243j

Patil, D., Patil, A., Khadke, N., Acta, A. B.-I. C., & 2019, undefined. (n.d.-a). Highly selective and sensitive colorimetric probe for Al3+ and Fe3+ metal ions based on 2-aminoquinolin-3-yl phenyl hydrazone Schiff base. *ElsevierDY Patil, AA Patil, NB Khadke, AV BorhadeInorganica Chimica Acta, 2019•Elsevier*. Retrieved December 22, 2024, from https://www.sciencedirect.com/science/article/pii/S002016931831747X?casa_token=4vH1GMy2BHYAAAAA:wlsUKnYK3apyNWM0r8W6ARWLgfEE5l6MvCRQpz59hyB1kY9e3D-U2KlcFXtSl4MRC29-0hrfQv57

Patil, D., Patil, A., Khadke, N., Acta, A. B.-I. C., & 2019, undefined. (n.d.-b). Highly selective and sensitive colorimetric probe for Al3+ and Fe3+ metal ions based on 2-aminoquinolin-3-yl phenyl hydrazone Schiff base. *ElsevierDY Patil, AA Patil, NB Khadke, AV BorhadeInorganica Chimica Acta, 2019•Elsevier*. Retrieved December 23, 2024, from https://www.sciencedirect.com/science/article/pii/S002016931831747X?casa_token=oCuBOzRp6X0AAAAA:fvPV8Ki_WaAF8_POGLqiw8X7pguIl9wnfii3vnwAaPjf49tAkH0wVKMgKHiIgOewGe9O5eZy12f1

Paudel, N., Dhakal, A., & Pradhanang, S. S. (2024). Analysis and Detection of Heavy Metals Content in Some Selected Packaged Fruit Juices of Kathmandu City by Flame Atomic Absorption Spectroscopy. *International Journal of Applied Sciences and Biotechnology*, *12*(3), 158–165. https://doi.org/10.3126/IJASBT.V12I3.70167

Paul, S., Karar, M., & Dey, N. (2024). Sequence specific optical recognition of dual Anions, fluoride and bisulfate ions: An update. *Journal of Molecular Liquids*, *394*, 123524. https://doi.org/10.1016/J.MOLLIQ.2023.123524

(PDF) Computer Simulation of Speciation of Trivalent Aluminum, Gadolinium and Yttrium Ions in Human Blood Plasma. (n.d.). Retrieved December 22, 2024, from https://www.researchgate.net/publication/259449565_Computer_Simulation_of_Speciation_of_Trivalent_Aluminum_Gadolinium_and_Yttrium_Ions_in_Human_Blood_Plasma

(PDF) Thermal analysis and determination of the heavy metal content of the plant Urtica Dioica L. by atomic absorption spectroscopy. (n.d.). Retrieved December 22, 2024, from https://www.researchgate.net/publication/366578266_Thermal_analysis_and_determination_of_the_heavy_metal_content_of_the_plant_Urtica_Dioica_L_by_atomic_absorption_spectroscopy

Peng, H., Peng, X., Huang, J., Huang, A., Xu, S., Zhou, J., Huang, S., & Cai, X. (2020). Synthesis and crystal structure of a novel pyridine acylhydrazone derivative as a “turn on” fluorescent probe for Al3+. *Journal of Molecular Structure*, *1212*. https://doi.org/10.1016/j.molstruc.2020.128138

Pervaiz, A., Shahzad, S. A., Assiri, M. A., Javid, T., Irshad, H., & Qvortrup, K. (2024). Cyanide and chloroform detection through J-aggregates based aggregation induced emission probe with real sample applications. *Journal of Hazardous Materials Letters*, *5*, 100132. https://doi.org/https://doi.org/10.1016/j.hazl.2024.100132

Petříček, V., Dušek, M., & Plášil, J. (2016). Crystallographic computing system Jana2006: Solution and refinement of twinned structures. *Zeitschrift Fur Kristallographie - Crystalline Materials*, *231*(10), 583–599. https://doi.org/10.1515/ZKRI-2016-1956/MACHINEREADABLECITATION/RIS

pH-Responsive luminescence sensing, photoredox catalysis and photodynamic applications of ruthenium (II) photosensitizers bearing imidazo. (n.d.). *ElsevierS Kumar, S Singh, A Kumar, KSR Murthy, AK SinghCoordination*

Chemistry Reviews, 2022•Elsevier. Retrieved December 17, 2024, from https://www.sciencedirect.com/science/article/pii/S0010854521005464

Prabha, D., Singh, D., Kumar, P., & Gupta, R. (2021). Selective Detection of Picric Acid and Pyrosulfate Ion by Nickel Complexes Offering a Hydrogen-Bonding-Based Cavity. *Inorganic Chemistry*, *60*(23), 17889–17899. https://doi.org/10.1021/ACS.INORGCHEM.1C02479

Pradhan, A. B., Mandal, S. K., Banerjee, S., Mukherjee, A., Das, S., Khuda Bukhsh, A. R., & Saha, A. (2015). A highly selective fluorescent sensor for zinc ion based on quinoline platform with potential applications for cell imaging studies. *Polyhedron*, *94*, 75–82. https://doi.org/10.1016/J.POLY.2015.04.005

Principles of Chemical Sensors. (2019). https://books.google.com/books/about/Principles_of_Chemical_Sensors.html?id=fVnK0UoGaoQC

Qi, S., Liu, W., Zhang, P., Wu, J., Zhang, H., Ren, H., Ge, J., & Wang, P. (2018). A colorimetric and ratiometric fluorescent probe for highly selective detection of glutathione in the mitochondria of living cells. *Sensors and Actuators, B: Chemical*, *270*, 459–465. https://doi.org/10.1016/j.snb.2018.05.017

Qi, Y., Tang, Z., Zhan, H., Wang, Y., Zhao, Y., Fei, X., Tian, J., Yu, L., & Liu, J. (2020). A new interpretation of the ESIPT mechanism of 2-(benzimidazol-2-yl)-3-hydroxychromone derivatives. *Spectrochimica Acta Part A: Molecular and Biomolecular Spectroscopy*, *224*, 117359. https://doi.org/10.1016/J.SAA.2019.117359

Qiao, M., Ding, L., Reviews, F. L.-C. C., & 2021, undefined. (n.d.). Surfactant assemblies encapsulating fluorescent probes as selective and discriminative sensors for metal ions. *ElsevierM Qiao, L Ding, F LvCoordination Chemistry Reviews, 2021•Elsevier*. Retrieved December

23, 2024, from https://www.sciencedirect.com/science/article/pii/S0010854520308870

Quinoline-based metal complexes: Synthesis and applications. (n.d.). *ElsevierR Kumar, A Thakur, D Chandra, AK Dhiman, PK Verma, U SharmaCoordination Chemistry Reviews, 2024•Elsevier*. Retrieved December 23, 2024, from https://www.sciencedirect.com/science/article/pii/S0010854523004423

Ragavi, S. P., Thirumalai, D., & Asharani, I. V. (2024). A Review on Small Organic Colorimetric and Fluorescent Hosts for the Detection of Cobalt and Nickel Ion. *Journal of Fluorescence*, 1–23. https://doi.org/10.1007/S10895-024-03807-5/METRICS

Randviir, E. P., & Banks, C. E. (2015). The latest developments in quantifying cyanide and hydrogen cyanide. *TrAC Trends in Analytical Chemistry*, *64*, 75–85. https://doi.org/https://doi.org/10.1016/j.trac.2014.08.009

Ray, D., & Bharadwaj, P. K. (2008). A coumarin-derived fluorescence probe selective for magnesium. *Inorganic Chemistry*, *47*(7), 2252–2254. https://doi.org/10.1021/IC702388Z

research, P. N.-E., & 2002, undefined. (n.d.). Aluminum: impacts and disease. *ElsevierP NayakEnvironmental Research, 2002•Elsevier*. Retrieved December 23, 2024, from https://www.sciencedirect.com/science/article/pii/S0013935102943525

reviews, G. F.-C. chemistry, & 1996, undefined. (n.d.). Aluminum and Alzheimer's disease: model studies. *ElsevierGD FasmanCoordination Chemistry Reviews, 1996•Elsevier*. Retrieved December 23, 2024, from https://www.sciencedirect.com/science/article/pii/S001085459690020X

Roy, S. (2025). Detection of fluoride ion by carbon dots-based fluorescent probes. *Journal of Molecular Structure*, *1319*, 139465. https://doi.org/10.1016/J.MOLSTRUC.2024.139465

Sadia, M., Khan, J., Khan, R., Shah, S. W. A., Zada, A., Zahoor, M., Ullah, R., & Ali, E. A. (2023). Synthesis and Computational Study of an Optical Fluorescent Sensor for Selective Detection of Ni2+ Ions. *ACS Omega*, *8*(30), 27500–27509. https://doi.org/10.1021/ACSOMEGA.3C03131/ASSET/IMAGES/LARGE/AO3C03131_0010.JPEG

Sahu, M., Manna, A., Chowdhury, S., advances, G. P.-R., & 2020, undefined. (2020). A novel dihydro phenylquinazolinone-based two-in-one colourimetric chemosensor for nickel (II), copper (II) and its copper complex for the fluorescent colourimetric. *Pubs.Rsc.OrgM Sahu, AK Manna, S Chowdhury, GK PatraRSC Advances, 2020•pubs.Rsc.Org*. https://doi.org/10.1039/d0ra09023a

Saleem, M., Rafiq, M., & Hanif, M. (2017). Organic Material Based Fluorescent Sensor for Hg2+: a Brief Review on Recent Development. *Journal of Fluorescence*, *27*(1), 31–58. https://doi.org/10.1007/S10895-016-1933-X

Samanta, S., Giri, P., Giri, S., Structure, A. G.-… of M., & 2023, undefined. (n.d.). Flexible HSA-interactive phenolphthalein based probe proficient at selective turn-on sensing for Zn2+ & Al3+. *Elsevier*. Retrieved December 23, 2024, from https://www.sciencedirect.com/science/article/pii/S0022286023000285

Samanta, S., Mandal, U., Das, B., … S. M.-… of P. and, & 2023, undefined. (n.d.-a). Rhodamine B-Quinoline based schiff base as fluorescent 'turn on'sensor of Al3+, Cr3+, HSO4− and its cytotoxicity and cell imaging application on TPC-1 and HtH-7. *Elsevier*. Retrieved December 22, 2024, from https://www.sciencedirect.com/science/article/pii/S101060302300271X

Samanta, S., Mandal, U., Das, B., … S. M.-… of P. and, & 2023, undefined. (n.d.-b). Rhodamine B-Quinoline based schiff base as fluorescent 'turn on'sensor of Al3+, Cr3+, HSO4− and its cytotoxicity and cell imaging application on TPC-1 and HtH-7. *Elsevier*. Retrieved December 23, 2024,

from https://www.sciencedirect.com/science/article/pii/S101060302300271X

Samanta, S. S., Giri, P. K., Giri, S., Ghosh, A., & Misra, A. (2023). Flexible HSA-interactive phenolphthalein based probe proficient at selective turn-on sensing for Zn2+ & Al3+. *Journal of Molecular Structure*, *1278*, 134927. https://doi.org/10.1016/J.MOLSTRUC.2023.134927

Sanaul Islam, M., Hoque, A., Mohamed Yusuf Baig, K., Sarmin, M., Kole, G. K., Hoda, M., & Akhtarul Alam, M. (2024). A zwitterionic probe for ratiometric fluorescent detection of aluminium(III) ion in aqueous medium and its application in bioimaging. *Spectrochimica Acta Part A: Molecular and Biomolecular Spectroscopy*, *311*, 124005. https://doi.org/10.1016/J.SAA.2024.124005

Saravana Kumar, S., Selva Kumar, R., & Ashok Kumar, S. K. (2020). An "Off-On-Off" type fluorescent chemosensor for the relay detection of Zn2+ and H2PO4− in aqueous environment. *Inorganica Chimica Acta*, *502*, 119348. https://doi.org/10.1016/J.ICA.2019.119348

Sen Gupta, A., Paul, K., & Luxami, V. (2017). A fluorescent probe with "AIE + ESIPT" characteristics for Cu2+ and F− ions estimation. *Sensors and Actuators B: Chemical*, *246*, 653–661. https://doi.org/10.1016/J.SNB.2017.02.080

Sharma, P., Naithani, S., Layek, S., Kumar, A., Rawat, R., Heena, Kaja, S., Nag, A., Kumar, S., & Goswami, T. (2023). Development of low-cost copper nanoclusters for highly selective "turn-on" sensing of Hg2+ ions. *Spectrochimica Acta Part A: Molecular and Biomolecular Spectroscopy*, *297*, 122697. https://doi.org/10.1016/J.SAA.2023.122697

Sharma, P., Naithani, S., Yadav, V., Environment, B. G.-… T. T., & 2024, undefined. (n.d.). Indium nanocubes based recyclable fluorescent chemosensor for sustainable environmental monitoring: pH-induced fluorescence transition and selective detection of. *ElsevierP Sharma, S*

Naithani, V Yadav, B Guchhait, S Kumar, T GoswamiScience of The Total Environment, 2024•Elsevier. Retrieved December 23, 2024, from https://www.sciencedirect.com/science/article/pii/S0048969724011823

Sharma, P., Naithani, S., Yadav, V., Sangeeta, Guchhait, B., Kumar, S., & Goswami, T. (2024). Indium nanocubes based recyclable fluorescent chemosensor for sustainable environmental monitoring: pH-induced fluorescence transition and selective detection of Pd(II) ions. *Science of The Total Environment*, *920*, 171043. https://doi.org/10.1016/J.SCITOTENV.2024.171043

Sharma, R., N. Chavan, S., & Lee, H. il. (2023). Fluorescent imidazolium hydrogels for tracing and recovering platinum with highest purity from spent auto catalyst. *Sensors and Actuators B: Chemical*, *396*, 134625. https://doi.org/10.1016/J.SNB.2023.134625

Sheet, S., Sen, B., Thounaojam, R., … K. A.-… of P. and, & 2017, undefined. (n.d.). Highly selective light-up Al3+ sensing by a coumarin based Schiff base probe: Subsequent phosphate sensing DNA binding and live cell imaging. *Elsevier*. Retrieved December 22, 2024, from https://www.sciencedirect.com/science/article/pii/S1010603016304956

Shekhar Samanta, S., Mandal, U., Das, B., Mandal, S., Upadhyay, P., Debraj Singh, T., & Misra, A. (2023). Rhodamine B-Quinoline based schiff base as fluorescent 'turn on' sensor of Al3+, Cr3+, HSO4− and its cytotoxicity and cell imaging application on TPC-1 and HtH-7 cell lines. *Journal of Photochemistry and Photobiology A: Chemistry*, *442*, 114806. https://doi.org/10.1016/J.JPHOTOCHEM.2023.114806

Sheldrick, G. M. (1990a). Phase annealing in SHELX-90: direct methods for larger structures. *Acta Crystallographica Section A*, *46*(6), 467–473. https://doi.org/10.1107/S0108767390000277

Sheldrick, G. M. (1990b). *SHELXL97, A Program for Crystal Structure Refinement*. https://www.scienceopen.com/book?vid=527f1309-ef7d-4d71-9985-641965ab49ab

Shellaiah, M., Thirumalaivasan, N., Aazaad, B., Awasthi, K., Sun, K. W., Wu, S. P., Lin, M. C., & Ohta, N. (2022). An AIEE Active Anthracene-Based Nanoprobe for Zn2+ and Tyrosine Detection Validated by Bioimaging Studies. *Chemosensors*, *10*(10), 381. https://doi.org/10.3390/CHEMOSENSORS10100381/S1

Shellaiah, M., Wu, Y., Analyst, H. L.-, & 2013, undefined. (n.d.). Simple pyridyl-salicylimine-based fluorescence “turn-on” sensors for distinct detections of Zn 2+, Al 3+ and OH− ions in mixed aqueous media. *Pubs.Rsc.OrgM Shellaiah, YH Wu, HC LinAnalyst, 2013•pubs.Rsc.Org*. https://doi.org/10.1039/c3an36840h

Shen, J., Wen, X., Chemical, Z. F.-S. and A. B., & 2023, undefined. (n.d.). Tandem detection of aluminum ion and norfloxacin by Au-doped copper nanoclusters based on AIE and coordination reaction. *ElsevierJ Shen, X Wen, Z FanSensors and Actuators B: Chemical, 2023•Elsevier*. Retrieved December 23, 2024, from https://www.sciencedirect.com/science/article/pii/S092540052300151X?casa_token=N9P2Iwssc60AAAAA:LE4NtBF_aK9eVEvmB4ozYqRYu0VXY0FLIGnzhhovh3_m1-aG2deaTbGprOZaCRo6O1EjMTNAzDBu

Shen, J., Wen, X., & Fan, Z. (2023). Tandem detection of aluminum ion and norfloxacin by Au-doped copper nanoclusters based on AIE and coordination reaction. *Sensors and Actuators B: Chemical*, *381*, 133436. https://doi.org/10.1016/J.SNB.2023.133436

Shen, Y., Mao, S., Chen, F., Zhao, S., Su, W., Fu, L., Zare, N., & Karimi, F. (2022). Electrochemical detection of Sudan red series azo dyes: Bibliometrics based analysis. *Food and Chemical Toxicology*, *163*, 112960. https://doi.org/10.1016/J.FCT.2022.112960

Shen, Y., Zhang, X., Zhang, Y., Li, H., & Chen, Y. (2018). An ICT-Modulated strategy to construct colorimetric and ratiometric fluorescent sensor for mitochondria-targeted fluoride ion in cell living. *Sensors and Actuators, B: Chemical*, *258*, 544–549. https://doi.org/10.1016/j.snb.2017.11.124

Shi, Y. S., Xiao, T., Yang, D. D., Xia, Z. G., & Zheng, X. J. (2024). Dynamic Fluorescence Sensing of Bromide Ions by Photochromic Bi(III)-Coordination Polymers Based on a Ligand Integrated by Naphthalene Diimides and Pyridinium in Solution and Films. *Small*, *20*(16), 2309076. https://doi.org/10.1002/SMLL.202309076

Shi, Y., Zhang, W., Xue, Y., & Zhang, J. (2023). Fluorescent Sensors for Detecting and Imaging Metal Ions in Biological Systems: Recent Advances and Future Perspectives. *Chemosensors*, *11*(4). https://doi.org/10.3390/chemosensors11040226

Singh, D., Tomar, S., Singh, S., Chaudhary, G., Singh, A. P., & Gupta, R. (2023). A fluorescent pH switch probe for the 'turn-on' dual-channel discriminative detection of magnesium and zinc ions. *Journal of Photochemistry and Photobiology A: Chemistry*, *435*, 114334. https://doi.org/10.1016/J.JPHOTOCHEM.2022.114334

Singh, G., Malik, P., Heena, Stanzin, J., Devi, S., Sharma, D., Singh, K. N., Singh, J., Singh, G., & Selvaraj, M. (2025). Coumarin modified Silatrane: A potent probe for Hg(II) ion Detection, biological evaluation and Acetylcholinesterase inhibition. *Inorganic Chemistry Communications*, *171*, 113494. https://doi.org/10.1016/J.INOCHE.2024.113494

Singh, V., Tiwari, K., Mishra, M., … N. S.-S. and A. B., & 2013, undefined. (n.d.). pyrmidine-2, 4 (1H, 3H)-dione as Al3+ selective colorimetric and fluorescent chemosensor. *ElsevierVP Singh, K Tiwari, M Mishra, N Srivastava, S SahaSensors and Actuators B: Chemical, 2013•Elsevier*. Retrieved December 23, 2024, from https://www.sciencedirect.com/science/article/pii/S092540051300364X?c

asa_token=xhIK5Df6TFMAAAAA:reXza1wErh3uL3HkIScyVzu0bznYcEPH_JiejZNw64jl4uLxEecPnEFoojOQw7TQtfu1hzLV-fhi

Singha, S., Jun, Y. W., Sarkar, S., & Ahn, K. H. (2019a). An Endeavor in the Reaction-Based Approach to Fluorescent Probes for Biorelevant Analytes: Challenges and Achievements. *Accounts of Chemical Research*, *52*(9), 2571–2581. https://doi.org/10.1021/ACS.ACCOUNTS.9B00314

Singha, S., Jun, Y. W., Sarkar, S., & Ahn, K. H. (2019b). An Endeavor in the Reaction-Based Approach to Fluorescent Probes for Biorelevant Analytes: Challenges and Achievements. *Accounts of Chemical Research*, *52*(9), 2571–2581. https://doi.org/10.1021/ACS.ACCOUNTS.9B00314

Soares-Paulino, A. A., Giroldo, L., Pradie, N. A., Reis, J. S., Back, D. F., Braga, A. A. C., Stefani, H. A., Lodeiro, C., & Dos Santos, A. A. (2020). Nanomolar Detection of Palladium (II) through a Novel Seleno-Rhodamine-based fluorescent and colorimetric chemosensor. *Dyes and Pigments*, *179*, 108355. https://doi.org/10.1016/J.DYEPIG.2020.108355

Solanki, Y. S., Agarwal, M., Gupta, A. B., Gupta, S., & Shukla, P. (2022). Fluoride occurrences, health problems, detection, and remediation methods for drinking water: A comprehensive review. *Science of The Total Environment*, *807*, 150601. https://doi.org/https://doi.org/10.1016/j.scitotenv.2021.150601

Song, X., Li, W., Xu, J., Ji, P., Li, Y., Feng, G., & Wang, B. (2023). Novel Aggregation-Induced Emission Fluorescent Molecule for Platinum(IV) Ion-Selective Recognition and Imaging of Controlled Release in Cells. *Analytical Chemistry*, *95*(7), 3883–3891. https://doi.org/10.1021/ACS.ANALCHEM.2C05650/SUPPL_FILE/AC2C05650_SI_001.PDF

Sorenson, J. R. J., Campbell, I. R., Tepper, L. B., & Lingg, R. D. (1974). Aluminum in the Environment and Human Health. *Environmental Health Perspectives*, *Vol 8*, 3–95. https://doi.org/10.1289/EHP.7483

Spectral and DFT/TD-DFT studies on turn-on fluorescent detection of Al (III) by a quinolin-8-ol-based Schiff base and its bioimaging. (n.d.-a). *Elsevier*. Retrieved December 22, 2024, from https://www.sciencedirect.com/science/article/pii/S0022286023009900

Spectral and DFT/TD-DFT studies on turn-on fluorescent detection of Al (III) by a quinolin-8-ol-based Schiff base and its bioimaging. (n.d.-b). *Elsevier*. Retrieved December 23, 2024, from https://www.sciencedirect.com/science/article/pii/S0022286023009900

Strianese, M., Robinson, J. P., Goyal, H., Annan, I., Ahluwalia, D., Bag, A., & Gupta, R. (2023). Discriminative "Turn-on" Detection of Al3+ and Ga3+ Ions as Well as Aspartic Acid by Two Fluorescent Chemosensors. *Mdpi.ComH Goyal, I Annan, D Ahluwalia, A Bag, R GuptaSensors, 2023•mdpi.Com*. https://doi.org/10.3390/s23041798

Su, H., Chen, X., & Fang, W. (2014). ON-OFF mechanism of a fluorescent sensor for the detection of Zn(II), Cd(II), and Cu(II)transition metal ions. *Analytical Chemistry*, *86*(1), 891–899. https://doi.org/10.1021/AC4034592/SUPPL_FILE/AC4034592_SI_001.PDF

Suguna, S., puthoor, A., Parimala devi, D., Abiram, A., Nandhakumar, R., & Prabhu, J. (2023). Experimental and theoretical studies on naphthalene based fluorophores: Applications in detection of Al3+ ions in water, soil, food and live cells. *Journal of Photochemistry and Photobiology A: Chemistry*, *435*, 114268. https://doi.org/10.1016/J.JPHOTOCHEM.2022.114268

Sukato, R., Sangpetch, N., Palaga, T., Jantra, S., Vchirawongkwin, V., Jongwohan, C., Sukwattanasinitt, M., & Wacharasindhu, S. (2016). New turn-on fluorescent and colorimetric probe for cyanide detection based on BODIPY-salicylaldehyde and its application in cell imaging. *Journal of Hazardous Materials*, *314*, 277–285. https://doi.org/https://doi.org/10.1016/j.jhazmat.2016.04.001

Sun, C., Miao, X., Zhang, L., Li, W., Acta, Z. C.-I. C., & 2018, undefined. (n.d.). Design and synthesis of a 2-hydroxy-1-naphthaldehyde-based fluorescent chemosensor for selective detection of aluminium ion. *ElsevierC Sun, X Miao, L Zhang, W Li, Z ChangInorganica Chimica Acta, 2018•Elsevier*. Retrieved December 22, 2024, from https://www.sciencedirect.com/science/article/pii/S0020169318301117?casa_token=C0zGSq48E-kAAAAA:5megGKDYR89inDc3e1npDkg4zMHdX6m7eoKgTZr1eem8Oa_9p5hdAp4z7lgxSFO5B9V-yQbJhNUc

Sun, H., Xu, Q., Xu, C., Zhang, Y., Ai, J., Ren, M., Liu, K., & Kong, F. (2023a). Construction of a water-soluble fluorescent probe for copper (II) ion detection in live cells and food products. *Food Chemistry*, *418*, 135994. https://doi.org/10.1016/J.FOODCHEM.2023.135994

Sun, H., Xu, Q., Xu, C., Zhang, Y., Ai, J., Ren, M., Liu, K., & Kong, F. (2023b). Construction of a water-soluble fluorescent probe for copper (II) ion detection in live cells and food products. *Food Chemistry*, *418*, 135994. https://doi.org/10.1016/J.FOODCHEM.2023.135994

Sun, Y., Hu, J. H., Qi, J., & Li, J. Bin. (2016). A highly selective colorimetric and “turn-on” fluorimetric chemosensor for detecting CN− based on unsymmetrical azine derivatives in aqueous media. *Spectrochimica Acta Part A: Molecular and Biomolecular Spectroscopy*, *167*, 101–105. https://doi.org/10.1016/J.SAA.2016.05.017

Sun, Y. X., Sun, Y. G., Deng, Z. P., Jia, Y. H., Han, W. Y., Wang, J. J., & Sun, Y. (2023). A turn-off fluorescent probe for the detection of copper(II) ion based on a salicylaldehyde derivatives Schiff-base. *Journal of Molecular Structure*, *1291*, 136069. https://doi.org/10.1016/J.MOLSTRUC.2023.136069

Suna, G., Gunduz, S., Topal, S., Ozturk, T., & Karakuş, E. (2023). A unique triple–channel fluorescent probe for discriminative detection of cyanide,

hydrazine, and hypochlorite. *Talanta*, *257*, 124365. https://doi.org/10.1016/J.TALANTA.2023.124365

Suryawanshi, S. B., Deshmukh, G. R., Bodake, A. J., & Patil, S. R. (2020). AIE Emission of SDS Capped Diphenylanthracene Nanoparticles for Selective Recognition and Estimation of Al3+ Ion in Aqueous Medium Based on Enhancement Effect and Analytical Application. *Macromolecular Symposia*, *392*(1), 2000082. https://doi.org/10.1002/MASY.202000082

Sushma, Sharma, S., & Ghosh, K. S. (2024). Fluorescence chemosensing and bioimaging of metal ions using schiff base probes working through photo-induced electron transfer (PET). *Critical Reviews in Analytical Chemistry*. https://doi.org/10.1080/10408347.2024.2418327

Tang, F. K., Zhu, J., Kong, F. K. W., Ng, M., Bian, Q., Yam, V. W. W., Tse, A. K. W., Tse, Y. C., & Leung, K. C. F. (2020). A BODIPY-based fluorescent sensor for the detection of Pt2+ and Pt drugs. *Chemical Communications*, *56*(18), 2695–2698. https://doi.org/10.1039/D0CC00027B

Thanayupong, E., Suttisintong, K., Sukwattanasinitt, M., & Niamnont, N. (2017). Turn-on fluorescent sensor for the detection of cyanide based on a novel dicyanovinyl phenylacetylene. *New Journal of Chemistry*, *41*(10), 4058–4064. https://doi.org/10.1039/C6NJ03794A

Tian, H., Qiao, X., Zhang, Z. L., Xie, C. Z., Li, Q. Z., & Xu, J. Y. (2019). A high performance 2-hydroxynaphthalene Schiff base fluorescent chemosensor for Al3+ and its applications in imaging of living cells and zebrafish in vivo. *Spectrochimica Acta Part A: Molecular and Biomolecular Spectroscopy*, *207*, 31–38. https://doi.org/10.1016/J.SAA.2018.08.063

Tian, X., Jiang, H., Wang, M., Cui, W., Guo, Y., … L. Z.-A. C., & 2023, undefined. (n.d.). Exploring the performance of quadrupole, time-of-flight, and multi-collector ICP-MS for dual-isotope detection on single nanoparticles and cells. *ElsevierX Tian, H Jiang, M Wang, W Cui, Y Guo, L Zheng, L Hu, G Qu, Y Yin, Y Cai, G JiangAnalytica Chimica Acta,*

2023•Elsevier. Retrieved December 22, 2024, from https://www.sciencedirect.com/science/article/pii/S0003267022013277

Tian, X., Tong, X., Li, Z., Li, D., Kong, Q., & Yang, X. (2018). In Vivo Fluoride Ion Detection and Imaging in Mice Using a Designed Near-Infrared Ratiometric Fluorescent Probe Based on IR-780. *Journal of Agricultural and Food Chemistry*, *66*(43), 11486–11491. https://doi.org/10.1021/ACS.JAFC.8B03736

Tomasulo, M., & Raymo, F. M. (2005). Colorimetric Detection of Cyanide with a Chromogenic Oxazine. *Organic Letters*, *7*(21), 4633–4636. https://doi.org/10.1021/ol051750m

Tsai, J. J., Zhan, Y. C., Wu, Y. Y., & Chen, Y. C. (2023). A facile switch-on fluorescence sensing method for detecting phosphates from complex aqueous samples. *Sensors and Actuators B: Chemical*, *380*, 133298. https://doi.org/10.1016/J.SNB.2023.133298

Turhan, O., Yaman, M., Dikmen, G., Nural, Y., Sarıboyacı, A. E., Tasa, B. A., Soykan, M. N., & Seferoğlu, Z. (2023). Novel fluorescent sensors based on coumarin-hydrazide-hydrazone hybrid for the detection of CN−, Co2+ and Ni2+ ions: DFT and bioimaging in living cells. *Journal of Molecular Liquids*, *392*, 123440. https://doi.org/10.1016/J.MOLLIQ.2023.123440

Turn-on detection of Al 3+ and Zn 2+ ions by a NSN donor probe: reversibility, logic gates and DFT calculations. (n.d.). *Pubs.Rsc.OrgS Naithani, N Goswami, S Singh, V Yadav, S Kumar, P Kumar, A Kumar, T GoswamiAnalytical Methods, 2023•pubs.Rsc.Org*. Retrieved December 23, 2024, from https://pubs.rsc.org/en/content/articlehtml/2023/ay/d3ay01534c

Udhayakumari, D., Naha, S., & Velmathi, S. (2017). Colorimetric and fluorescent chemosensors for Cu2+. A comprehensive review from the years 2013–15. *Analytical Methods*, *9*(4), 552–578. https://doi.org/10.1039/C6AY02416E

Vallejo, D. D., Rojas Ramírez, C., Parson, K. F., Han, Y., Gadkari, V. V., & Ruotolo, B. T. (2022). Mass Spectrometry Methods for Measuring Protein Stability. *Chemical Reviews*, *122*(8), 7690–7719. https://doi.org/10.1021/ACS.CHEMREV.1C00857

Van Acker, T., Theiner, S., Bolea-Fernandez, E., Vanhaecke, F., & Koellensperger, G. (2023). Inductively coupled plasma mass spectrometry. *Nature Reviews Methods Primers 2023 3:1*, *3*(1), 1–18. https://doi.org/10.1038/s43586-023-00235-w

Varadaraju, C., Paulraj, M. S., Tamilselvan, G., Muthu Vijayan Enoch, I. V., Srinivasadesikan, V., & Shyi-Long, L. (2019). Evaluation of metal ion sensing behaviour of fluorescent probe along with its precursors: PET-CHEF mechanism, molecular logic gate behaviour and DFT studies. *Journal of Inclusion Phenomena and Macrocyclic Chemistry*, *95*(1–2), 79–89. https://doi.org/10.1007/S10847-019-00919-5/METRICS

Villarino, N., Lavilla, I., Pena-Pereira, F., & Bendicho, C. (2024). Silver nanocluster-based colorimetric/fluorimetric dual-mode sensor for the detection of bromide and sulfite in waters and wastewaters. *Microchemical Journal*, *196*, 109685. https://doi.org/10.1016/J.MICROC.2023.109685

Vivier, V., & Orazem, M. E. (2022). Impedance Analysis of Electrochemical Systems. *Chemical Reviews*, *122*(12), 11131–11168. https://doi.org/10.1021/ACS.CHEMREV.1C00876/ASSET/IMAGES/MEDIUM/CR1C00876_0022.GIF

Wang, F., Wang, K., Kong, Q., Wang, J., Xi, D., Gu, B., Lu, S., Wei, T., & Chen, X. (2021). Recent studies focusing on the development of fluorescence probes for zinc ion. *Coordination Chemistry Reviews*, *429*, 213636. https://doi.org/10.1016/J.CCR.2020.213636

Wang, F., Wang, L., Chen, X., & Yoon, J. (2014). Recent progress in the development of fluorometric and colorimetric chemosensors for detection

of cyanide ions. *Chemical Society Reviews*, *43*(13), 4312–4324. https://doi.org/10.1039/C4CS00008K

Wang, H., Wang, B., Shi, Z., Tang, X., Dou, W., … Q. H.-B. and, & 2015, undefined. (n.d.-a). A two-photon probe for Al3+ in aqueous solution and its application in bioimaging. *ElsevierH Wang, B Wang, Z Shi, X Tang, W Dou, Q Han, Y Zhang, W LiuBiosensors and Bioelectronics, 2015•Elsevier*. Retrieved December 30, 2024, from https://www.sciencedirect.com/science/article/pii/S0956566314008057?casa_token=CEtSXpALFxkAAAAA:JCHK_0cxhCho3ZL8v1H33fA5_PS5x2liKTi-RipuZ5QjorGc5DxNzRYwinlSk06JCgslJM9r9kY

Wang, J., Hu, K., Wang, H., Sun, W., Han, L., Li, L., & Wei, Y. (2023). A novel multi-purpose convenient Al3+ ion fluorescent probe based on phenolphthalein. *Journal of Molecular Structure*, *1271*, 134085. https://doi.org/10.1016/J.MOLSTRUC.2022.134085

Wang, J., Li, Y., Li, K., Meng, X., & Hou, H. (2017). Highly Selective Turn-On Fluorescent Chemodosimeter for AlIII Detection through AlIII-Promoted Hydrolysis of C=N Double Bonds in the 8-Hydroxyquinoline Aldehyde Schiff Base. *Chemistry – A European Journal*, *23*(21), 5081–5089. https://doi.org/10.1002/CHEM.201606024

Wang, J., Pei, Y., Yan, M., Li, Y., Yang, G., … C. Q.-M., & 2021, undefined. (n.d.-b). A fast-response turn-on quinoline-based fluorescent probe for selective and sensitive detection of zinc (II) and its application. *ElsevierJT Wang, YY Pei, MY Yan, YG Li, GG Yang, CH Qu, W Luo, J Wang, QF LiMicrochemical Journal, 2021•Elsevier*. Retrieved January 1, 2025, from https://www.sciencedirect.com/science/article/pii/S0026265X20330472

Wang, J., Pei, Y., Yan, M., Li, Y., Yang, G., … C. Q.-M., & 2021, undefined. (n.d.-c). A fast-response turn-on quinoline-based fluorescent probe for selective and sensitive detection of zinc (II) and its application. *ElsevierJT Wang, YY Pei, MY Yan, YG Li, GG Yang, CH Qu, W Luo, J Wang, QF LiMicrochemical Journal, 2021•Elsevier*. Retrieved December 23, 2024,

from https://www.sciencedirect.com/science/article/pii/S0026265X20330472

Wang, K., Wang, W., Zhang, X. Y., Jiang, A. Q., Yang, Y. S., & Zhu, H. L. (2021). Fluorescent probes for the detection of alkaline phosphatase in biological systems: Recent advances and future prospects. *TrAC Trends in Analytical Chemistry*, *136*, 116189. https://doi.org/10.1016/J.TRAC.2021.116189

Wang, L., Zhang, C., He, H., Zhu, H., Guo, W., … S. Z.-I. J. of, & 2020, undefined. (n.d.-d). Cellulose-based colorimetric sensor with N, S sites for Ag+ detection. *ElsevierL Wang, C Zhang, H He, H Zhu, W Guo, S Zhou, S Wang, JR Zhao, J ZhangInternational Journal of Biological Macromolecules, 2020•Elsevier*. Retrieved December 22, 2024, from https://www.sciencedirect.com/science/article/pii/S0141813020337648

Wang, P., Fu, J., Yao, K., Chang, Y., Xu, K., B, Y. X.-S. and A., & 2018, undefined. (n.d.-e). A novel quinoline-derived fluorescent "turn-on" probe for Cu2+ with highly selectivity and sensitivity and its application in cell imaging. *ElsevierP Wang, J Fu, K Yao, Y Chang, K Xu, Y XuSensors and Actuators B: Chemical, 2018•Elsevier*. Retrieved December 22, 2024, from https://www.sciencedirect.com/science/article/pii/S0925400518312656?casa_token=CruKLaNyQVwAAAAA:6xWwNkWYrpVTpfC73NFGBa5GX2fVWQpGSfUH-C6QRFTFa1gmcGik4lujDi2iKhcdNcp-BvEm9lqh

Wang, W. (2016). Introductory Chapter: What is Chemical Sensor? *Progresses in Chemical Sensor*. https://doi.org/10.5772/64626

Wang, X., Cheng, S., Liu, C., Zhang, Y., Su, M., Rong, X., Zhu, H., Yu, M., Sheng, W., & Zhu, B. (2022). A novel ratiometric fluorescent probe for the detection of nickel ions in the environment and living organisms. *Science of The Total Environment*, *840*, 156445. https://doi.org/10.1016/J.SCITOTENV.2022.156445

Wang, X., Liu, C., Zhu, H., Cheng, S., Zhang, Y., Su, M., Rong, X., Yu, M., Sheng, W., & Zhu, B. (2022). An ultra-sensitive and highly selective fluorescent probe for nickel ions and its environmental and biological applications. *Sensors and Actuators B: Chemical*, *369*, 132300. https://doi.org/10.1016/J.SNB.2022.132300

Wang, Y., Ma, Z., Zhang, D., Deng, J., … X. C.-S. A., & 2018, undefined. (n.d.-a). Highly selective and sensitive turn-on fluorescent sensor for detection of Al3+ based on quinoline-base Schiff base. *ElsevierY Wang, ZY Ma, DL Zhang, JL Deng, X Chen, CZ Xie, X Qiao, QZ Li, JY XuSpectrochimica Acta Part A: Molecular and Biomolecular Spectroscopy, 2018•Elsevier*. Retrieved December 22, 2024, from https://www.sciencedirect.com/science/article/pii/S1386142518300672

Wang, Y., Ma, Z., Zhang, D., Deng, J., … X. C.-S. A., & 2018, undefined. (n.d.-b). Highly selective and sensitive turn-on fluorescent sensor for detection of Al3+ based on quinoline-base Schiff base. *ElsevierY Wang, ZY Ma, DL Zhang, JL Deng, X Chen, CZ Xie, X Qiao, QZ Li, JY XuSpectrochimica Acta Part A: Molecular and Biomolecular Spectroscopy, 2018•Elsevier*. Retrieved December 23, 2024, from https://www.sciencedirect.com/science/article/pii/S1386142518300672

Wolfbeis, O. S. (2005). Materials for fluorescence-based optical chemical sensors. *Journal of Materials Chemistry*, *15*(27–28), 2657–2669. https://doi.org/10.1039/B501536G

Wood, R. (2016). Acute animal and human poisonings from cyanotoxin exposure — A review of the literature. *Environment International*, *91*, 276–282. https://doi.org/https://doi.org/10.1016/j.envint.2016.02.026

World Health Organization. (2003). Cyanide in Drinking water, Guidelines for drinking-water quality. *World Health Organization*, *2*, 7.

Wu, D., Sedgwick, A. C., Gunnlaugsson, T., Akkaya, E. U., Yoon, J., & James, T. D. (2017). Fluorescent chemosensors: the past, present and future.

Chemical Society Reviews, *46*(23), 7105–7123. https://doi.org/10.1039/C7CS00240H

Wu, G., Gao, Q., Li, M., Tang, X., Lai, K. W. C., & Tong, Q. (2018). A ratiometric probe based on coumarin-quinoline for highly selective and sensitive detection of Zn2+ ions in living cells. *Journal of Photochemistry and Photobiology A: Chemistry*, *355*, 487–495. https://doi.org/10.1016/J.JPHOTOCHEM.2017.05.006

Wu, J., Liu, W., Ge, J., Zhang, H., Reviews, P. W.-C. S., & 2011, undefined. (n.d.). New sensing mechanisms for design of fluorescent chemosensors emerging in recent years. *Pubs.Rsc.OrgJ Wu, W Liu, J Ge, H Zhang, P WangChemical Society Reviews, 2011•pubs.Rsc.Org*. Retrieved December 30, 2024, from https://pubs.rsc.org/en/content/articlehtml/2011/cs/c0cs00224k

Wu, J. S., Liu, W. M., Zhuang, X. Q., Wang, F., Wang, P. F., Tao, S. L., Zhang, X. H., Wu, S. K., & Lee, S. T. (2007). Fluorescence turn on of coumarin derivatives by metal cations: A new signaling mechanism based on C=N isomerization. *Organic Letters*, *9*(1), 33–36. https://doi.org/10.1021/OL062518Z

Wu, L., Huang, C., Emery, B. P., Sedgwick, A. C., Bull, S. D., He, X.-P., Tian, H., Yoon, J., Sessler, J. L., & James, T. D. (2020). Förster resonance energy transfer (FRET)-based small-molecule sensors and imaging agents. *Chemical Society Reviews*, *49*(15), 5110–5139. https://doi.org/10.1039/C9CS00318E

Wu, S., Wang, Y., Iqbal, M., Mehmood, K., Li, Y., Tang, Z., & Zhang, H. (2022). Challenges of fluoride pollution in environment: Mechanisms and pathological significance of toxicity – A review. *Environmental Pollution*, *304*, 119241. https://doi.org/https://doi.org/10.1016/j.envpol.2022.119241

Wu, Z., & Tang, X. (2015). Visualizing Fluoride Ion in Mitochondria and Lysosome of Living Cells and in Living Mice with Positively Charged

Ratiometric Probes. *Analytical Chemistry*, *87*(17), 8613–8617. https://doi.org/10.1021/ACS.ANALCHEM.5B02578

Xia, Y. F., Bao, G. M., Peng, X. X., Wu, X. Y., Lu, H. F., Zhong, Y. F., Li, W., He, J. X., Liu, S. Y., Fan, Q., Li, S. H., Xiao, W., & Yuan, H. Q. (2022). A highly water-stable dual-emission fluorescent probe based on Eu3+-loaded MOF for the simultaneous detection and quantification of Fe3+ and Al3+ in swine wastewater. *Analytica Chimica Acta*, *1221*, 340115. https://doi.org/10.1016/J.ACA.2022.340115

Xie, Y. Q., Han, M. M., Zhang, Y. M., Chen, H., Zhang, H. B., Ren, C. Y., Li, L., Wu, R., Yao, H., Shi, X. N., Lin, Q., & Wei, T. B. (2023). A novel fluorescent probe with high sensitivity for sequential detection of CN− and Al3+ in highly aqueous medium and its applications in living cell bioimaging. *Journal of Photochemistry and Photobiology A: Chemistry*, *437*, 114488. https://doi.org/10.1016/J.JPHOTOCHEM.2022.114488

Xu, F., Leng, W., Lu, Q., Li, K., Zhang, Y., Liu, J., Xu, L., & Sheng, G. (2023). Ratiometric fluorescent sensing of phosphate ion in environmental water samples using flavin mononucleotide-functionalized Fe3O4 particles. *Science of The Total Environment*, *857*, 159249. https://doi.org/10.1016/J.SCITOTENV.2022.159249

Xu, H., Chen, W., Ju, L., and, H. L.-S. A. P. A. M., & 2021, undefined. (n.d.). A purine based fluorescent chemosensor for the selective and sole detection of Al3+ and its practical applications in test strips and bio-imaging. *ElsevierH Xu, W Chen, L Ju, H LuSpectrochimica Acta Part A: Molecular and Biomolecular Spectroscopy, 2021•Elsevier*. Retrieved December 23, 2024, from https://www.sciencedirect.com/science/article/pii/S1386142520310532

Xu, H., Chen, W., Ju, L., & Lu, H. (2021). A purine based fluorescent chemosensor for the selective and sole detection of Al3+ and its practical applications in test strips and bio-imaging. *Spectrochimica Acta Part A:*

Molecular and Biomolecular Spectroscopy, *247*, 119074. https://doi.org/10.1016/J.SAA.2020.119074

Xu, H., Zhang, S., Gu, Y., & Lu, H. (2022). Naphthalimide appended isoquinoline fluorescent probe for specific detection of Al3+ ions and its application in living cell imaging. *Spectrochimica Acta Part A: Molecular and Biomolecular Spectroscopy*, *265*, 120364. https://doi.org/10.1016/J.SAA.2021.120364

Xu, J., Jiang, R., Feng, Y., Liu, Z., Huang, J., … C. M.-C. C., & 2022, undefined. (n.d.). Functional nucleic acid-based fluorescent probes for metal ion detection. *ElsevierJ Xu, R Jiang, Y Feng, Z Liu, J Huang, C Ma, K WangCoordination Chemistry Reviews, 2022•Elsevier*. Retrieved December 23, 2024, from https://www.sciencedirect.com/science/article/pii/S0010854522000480

Xu, Z., Chen, X., Kim, H. N., & Yoon, J. (2010). Sensors for the optical detection of cyanide ion. *Chemical Society Reviews*, *39*(1), 127–137. https://doi.org/10.1039/B907368J

Yan, J. L., Zhang, L., Wu, W. N., Wang, Y., & Xu, Z. H. (2023). A novel AIRE-based fluorescent ratiometric probe with endoplasmic reticulum-targeting ability for detection of hypochlorite and bioimaging. *Bioorganic Chemistry*, *131*, 106319. https://doi.org/10.1016/J.BIOORG.2022.106319

Yan, Z., Cai, Y., Zhang, J., & Zhao, Y. (2022). Fluorescent sensor arrays for metal ions detection: A review. *Measurement*, *187*, 110355. https://doi.org/10.1016/J.MEASUREMENT.2021.110355

Yang, C., advances, J. Z.-R., & 2024, undefined. (2024a). A simple 'turn-on' fluorescence chemosensor for Al (iii) detection in aqueous solution and solid matrix. *Pubs.Rsc.Org*. https://doi.org/10.1039/d3ra06558h

Yang, C., advances, J. Z.-R., & 2024, undefined. (2024b). A simple 'turn-on' fluorescence chemosensor for Al (iii) detection in aqueous solution and solid matrix. *Pubs.Rsc.Org*. https://doi.org/10.1039/d3ra06558h

Yang, G., Li, P., Han, Y., Tang, L., Liu, Y., Xin, H., Wang, K. N., Zhao, S., Liu, Z., & Cao, D. (2023). A coumarin hydrazide Schiff base fluorescent probe for sensitively sensing Al3+ in living cells. *Materials Chemistry and Physics*, *295*, 127145. https://doi.org/10.1016/J.MATCHEMPHYS.2022.127145

Yang, P., Tang, A. L., Tan, S., Wang, G. Y., Huang, H. Y., Niu, W., Liu, S. T., Ge, M. H., Yang, L. L., Gao, F., Zhou, X., Liu, L. W., & Yang, S. (2024). Recent progress and outlooks in rhodamine-based fluorescent probes for detection and imaging of reactive oxygen, nitrogen, and sulfur species. *Talanta*, *274*, 126004. https://doi.org/10.1016/J.TALANTA.2024.126004

Yang, X., Zhang, Q., Zhang, S., Lai, M., Ji, X., Ye, Y., Li, H., & Zhao, M. (2023). Molecule fluorescent probes for sensing and imaging analytes in plants: Developments and challenges. *Coordination Chemistry Reviews*, *487*, 215154. https://doi.org/10.1016/J.CCR.2023.215154

Yang, Y.-K., & Tae, J. (2006). Acridinium Salt Based Fluorescent and Colorimetric Chemosensor for the Detection of Cyanide in Water. *Organic Letters*, *8*(25), 5721–5723. https://doi.org/10.1021/ol062323r

Yao, B., Zhang, J., Han, M., Liang, L., Li, X., Cai, X., & Leng, Y. (2023). Two novel “turn on” fluorescent probes for the determination of Al3+ and its applications. *Inorganic Chemistry Communications*, *153*, 110798. https://doi.org/10.1016/J.INOCHE.2023.110798

Ye, F. Y., Hu, M., & Zheng, Y. S. (2023). Advances and challenges of metal ions sensors based on AIE effect. *Coordination Chemistry Reviews*, *493*, 215328. https://doi.org/10.1016/J.CCR.2023.215328

Yoon, S. J., Nam, Y. S., Lee, H. J., Lee, Y., & Lee, K. B. (2019). Colorimetric probe for Ni2+ based on shape transformation of triangular silver nanoprisms upon H2O2 etching. *Sensors and Actuators B: Chemical*, *300*, 127045. https://doi.org/10.1016/J.SNB.2019.127045

Yuan, X., Zhang, W., Liu, L., Lin, Y., Xie, L., Chai, X., Xu, K., Du, G., & Zhang, L. (2023). A Chitosan-Based Fluorescent Probe Combined with Smartphone Technology for the Detection of Hypochlorite in Pure Water. *Molecules*, *28*(17), 6316. https://doi.org/10.3390/MOLECULES28176316

Yue, Y., Dong, Q., Zhang, Y., Sun, Y., Methods, Y. G.-A., & 2015, undefined. (n.d.). A highly selective “turn-on” fluorescent chemosensor based on 8-aminoquinoline for detection of Zn 2+. *Pubs.Rsc.OrgY Yue, Q Dong, Y Zhang, Y Sun, Y GongAnalytical Methods, 2015•pubs.Rsc.Org*. Retrieved January 1, 2025, from https://pubs.rsc.org/en/content/articlehtml/2015/ay/c5ay01007a

Zeng, S., Li, S. J., Sun, X. J., Li, M. Q., Ma, Y. Q., Xing, Z. Y., & Li, J. L. (2018). A naphthalene-quinoline based chemosensor for fluorescent “turn-on” and absorbance-ratiometric detection of Al3+ and its application in cells imaging. *Spectrochimica Acta - Part A: Molecular and Biomolecular Spectroscopy*, *205*, 276–286. https://doi.org/10.1016/j.saa.2018.07.039

Zeng, S., Li, S., Sun, X., Li, M., Xing, Z., Acta, J. L.-I. C., & 2019, undefined. (n.d.-a). A benzothiazole-based chemosensor for significant fluorescent turn-on and ratiometric detection of Al3+ and its application in cell imaging. *ElsevierS Zeng, SJ Li, XJ Sun, MQ Li, ZY Xing, JL LiInorganica Chimica Acta, 2019•Elsevier*. Retrieved December 22, 2024, from https://www.sciencedirect.com/science/article/pii/S0020169318313768?casa_token=lwF5PwNQ_3UAAAAA:Nn0kJVnld_pcI63tuud5EE1Hm3sj1rNaR97bn_RW5S5QM4rcZDZTNPtZ8C-cQkNUSRGXPbzeua9v

Zeng, S., Li, S., Sun, X., Li, M., Xing, Z., Acta, J. L.-I. C., & 2019, undefined. (n.d.-b). A benzothiazole-based chemosensor for significant fluorescent turn-on and ratiometric detection of Al3+ and its application in cell imaging. *ElsevierS Zeng, SJ Li, XJ Sun, MQ Li, ZY Xing, JL LiInorganica Chimica Acta, 2019•Elsevier*. Retrieved December 23, 2024, from https://www.sciencedirect.com/science/article/pii/S0020169318313768?c

asa_token=WzKeNJeA2PsAAAAA:oQxa5CaWVOi33QTSTSsvaxNPMsAKOOMLkx0DoQosaLB8SHmyCFgjNjSAc1hdTISc0ULww5aVfVd0

Zeng, S., Li, S., Sun, X., Li, M., Xing, Z., Acta, J. L.-I. C., & 2019, undefined. (n.d.-c). A benzothiazole-based chemosensor for significant fluorescent turn-on and ratiometric detection of Al3+ and its application in cell imaging. *ElsevierS Zeng, SJ Li, XJ Sun, MQ Li, ZY Xing, JL LiInorganica Chimica Acta, 2019•Elsevier*. Retrieved December 23, 2024, from https://www.sciencedirect.com/science/article/pii/S0020169318313768?casa_token=0SbyNJRBKsMAAAAA:BAxc3rV55rT3O1ScYoyJ8nWq36Z4VLkywLYRDNt2B9Ez9EwkU4HX-5OdjWiEoRM1taXMrP9yOaJH

Zhang, C., Liu, C., Nie, S., Li, X., Wang, Y., … Y. Z.-… A. P. A. M., & 2023, undefined. (n.d.). Two novel fluorescent probes based on quinolinone for continuous recognition of Al3+ and ClO−. *ElsevierC Zhang, C Liu, S Nie, X Li, Y Wang, Y Zhang, J Guo, Y SunSpectrochimica Acta Part A: Molecular and Biomolecular Spectroscopy, 2023•Elsevier*. Retrieved January 2, 2025, from https://www.sciencedirect.com/science/article/pii/S1386142523006029

Zhang, D., Yang, X., Wang, T., Ji, X., & Wu, X. (2023a). Advances in organic fluorescent probes for bromide ions, hypobromous acid and related eosinophil peroxidase-A review. *Analytica Chimica Acta*, *1244*, 340626. https://doi.org/10.1016/J.ACA.2022.340626

Zhang, D., Yang, X., Wang, T., Ji, X., & Wu, X. (2023b). Advances in organic fluorescent probes for bromide ions, hypobromous acid and related eosinophil peroxidase-A review. *Analytica Chimica Acta*, *1244*, 340626. https://doi.org/10.1016/J.ACA.2022.340626

Zhang, P., Xiong, C., Liu, Z., Chen, H., & Li, S. (2023). CsPbBr3 nanocrystals as luminescent probe for in situ detection of chloride and iodide ions in water. *Microchemical Journal*, *190*, 108651. https://doi.org/10.1016/J.MICROC.2023.108651

Zhang, S., Wang, Y., & Xu, H. (2022). A new naphthalimide-picolinohydrazide derived fluorescent “turn-on” probe for hypersensitive detection of Al3+ ions and applications of real water analysis and bio-imaging. *Spectrochimica Acta Part A: Molecular and Biomolecular Spectroscopy*, *275*, 121193. https://doi.org/10.1016/J.SAA.2022.121193

Zhao, G., Wei, G., Yan, Z., Guo, B., Guang, S., Acta, R. W.-A. C., & 2020, undefined. (n.d.). A multiple fluorescein-based turn-on fluorophore (FHCS) identified for simultaneous determination and living imaging of toxic Al3+ and Zn2+ by improved Stokes shift. *ElsevierG Zhao, G Wei, Z Yan, B Guo, S Guang, R Wu, H XuAnalytica Chimica Acta, 2020•Elsevier*. Retrieved December 23, 2024, from https://www.sciencedirect.com/science/article/pii/S0003267019312358

Zhao, J., Li, C., Wei, S., Lü, C., & Zou, L. W. (2023). A multifunctional fluorescent probe based on Schiff base with AIE and ESIPT characteristics for effective detections of Pb2+, Ag+ and Fe3+. *Spectrochimica Acta Part A: Molecular and Biomolecular Spectroscopy*, *300*, 122904. https://doi.org/10.1016/J.SAA.2023.122904

Zhao, N., Wu, Y., Wang, R., Shi, L., Analyst, Z. C.-, & 2011, undefined. (n.d.). An iridium (iii) complex of oximated 2, 2′-bipyridine as a sensitive phosphorescent sensor for hypochlorite. *Pubs.Rsc.OrgN Zhao, YH Wu, RM Wang, LX Shi, ZN ChenAnalyst, 2011•pubs.Rsc.Org*. Retrieved December 30, 2024, from https://pubs.rsc.org/en/content/articlehtml/2011/an/c1an15030h

Zheng, Y., Zhai, S. M., Xiao, M. M., Dong, P. Z., Xu, J. R., & Zhao, B. X. (2024). A novel ratiometric fluorescence probe based on the FRET-ICT mechanism for detecting fluoride ions and viscosity. *Spectrochimica Acta Part A: Molecular and Biomolecular Spectroscopy*, *309*, 123822. https://doi.org/10.1016/J.SAA.2023.123822

Zhou, F., Wang, H., Liu, P., Hu, Q., Wang, Y., … C. L.-S. A. P., & 2018, undefined. (n.d.-a). A highly selective and sensitive turn-on probe for

aluminum (III) based on quinoline Schiff's base and its cell imaging. *ElsevierF Zhou, H Wang, P Liu, Q Hu, Y Wang, C Liu, J HuSpectrochimica Acta Part A: Molecular and Biomolecular Spectroscopy, 2018•Elsevier*. Retrieved December 22, 2024, from https://www.sciencedirect.com/science/article/pii/S1386142517307217

Zhou, F., Wang, H., Liu, P., Hu, Q., Wang, Y., … C. L.-S. A. P., & 2018, undefined. (n.d.-b). A highly selective and sensitive turn-on probe for aluminum (III) based on quinoline Schiff's base and its cell imaging. *ElsevierF Zhou, H Wang, P Liu, Q Hu, Y Wang, C Liu, J HuSpectrochimica Acta Part A: Molecular and Biomolecular Spectroscopy, 2018•Elsevier*. Retrieved December 23, 2024, from https://www.sciencedirect.com/science/article/pii/S1386142517307217

Zhou, J., Xu, S., Yu, Z., Ye, X., Dong, X., & Zhao, W. (2019). Two-channel responsive fluorescent probe of meso carboxylate of BODIPY with AIE characteristics for fast detection of palladium. *Dyes and Pigments*, *170*, 107656. https://doi.org/10.1016/J.DYEPIG.2019.107656

Zhou, L., Feng, Y., Cheng, J., Sun, N., Zhou, X., & Xiang, H. (2012). Simple, selective, and sensitive colorimetric and ratiometric fluorescence/phosphorescence probes for platinum(ii) based on Salen-type Schiff bases. *RSC Advances*, *2*(28), 10529–10536. https://doi.org/10.1039/C2RA21254D

Zhou, P., Aggregate, K. H.-, & 2022, undefined. (2022). ESIPT-based AIE luminogens: Design strategies, applications, and mechanisms. *Wiley Online LibraryP Zhou, K HanAggregate, 2022•Wiley Online Library*, *3*(5). https://doi.org/10.1002/agt2.160

Zhou, L. Sen, Zhang, X. Y., & Huang, Y. (2024). High selective, sensitive, reversible and imaging application sensor for Aluminium detection. *Journal of Molecular Structure*, *1310*, 138357. https://doi.org/10.1016/J.MOLSTRUC.2024.138357

Zhou, T., Wang, J., Xu, J., Zheng, C., Niu, Y., Wang, C., Xu, F., Yuan, L., Zhao, X., Liang, L., & Xu, P. (2020). A Smart Fluorescent Probe for NO Detection and Application in Myocardial Fibrosis Imaging. *Analytical Chemistry*, *92*(7), 5064–5072. https://doi.org/10.1021/ACS.ANALCHEM.9B05435

Zhou, W., Saran, R., reviews, J. L.-C., & 2017, undefined. (2017). Metal sensing by DNA. *ACS PublicationsW Zhou, R Saran, J LiuChemical Reviews, 2017•ACS Publications*, *117*(12), 8272–8325. https://doi.org/10.1021/acs.chemrev.7b00063

Zhou, Y., Yang, X., Jang, W. J., Yan, M., & Yoon, J. (2025). Binding- and activity-based small molecule fluorescent probes for the detection of Cu+, Cu2+, Fe2+ and Fe3+ in biological systems. *Coordination Chemistry Reviews*, *522*, 216201. https://doi.org/10.1016/J.CCR.2024.216201

Zhou, Z., Niu, W., Lin, Z., Cui, Y., Tang, X., Chemistry, Y. L.-I., & 2020, undefined. (n.d.). A novel "turn-off" fluorescent sensor for Al3+ detection based on quinolinecarboxamide-coumarin. *Elsevier*. Retrieved December 22, 2024, from https://www.sciencedirect.com/science/article/pii/S1387700320307589?casa_token=P4FfjEdnyToAAAAA:tRZQyLyxiQHoIIE0KpOwoDOxAmD1WsfaOtR1roeO8_y_INKAnT838_578AiVPUcjkuxAI1sWZ6T5

Zhu, J., Hu, L., Meng, X., Li, F., Wang, W., Shi, G., Molecules, Z. W.-, & 2023, undefined. (2023). Synergism of Photo-Induced Electron Transfer and Aggregation-Induced Quenching Mechanisms for Highly Sensitive Detection of Silver Ion and Captopril. *Mdpi.ComJ Zhu, L Hu, X Meng, F Li, W Wang, G Shi, Z WangMolecules, 2023•mdpi.Com*. https://doi.org/10.3390/molecules28093650

Zhu, X., Wang, J., Zhang, J., Chen, Z., Zhang, H., & Zhang, X. (2015). Imaging of fluoride ion in living cells and tissues with a two-photon ratiometric fluorescence probe. *Sensors (Switzerland)*, *15*(1), 1611–1622. https://doi.org/10.3390/s150101611

Zhu, Z. X., Yu, D. D., Liu, Z. G., Huang, Y. W., Zhou, A. Y., Chen, Z. W., Sun, J., Wang, X., Jin, L. T., & Cong, W. T. (2017). A naphthalene derivative as ‘turn-on’ fluorescent chemosensor for the highly selective and sensitive detection of Al3+. *Luminescence*, *32*(7), 1307–1312. https://doi.org/10.1002/BIO.3326

Zou, X., Hu, J., Zhu, H., Chen, Q., & Gong, Z. (2023). Ultrasensitive turn-off fluorescence detection of iodide using carbon dots/gold nanocluster as fluorescent nanoprobe. *Microchemical Journal*, *185*, 108275. https://doi.org/10.1016/J.MICROC.2022.108275

LIST OF PUBLICATIONS

- **Nidhi Goswami,** Sudhanshu Naithani, Jimmy Mangalam, Tapas Goswami, Ritesh Dubey, Pramod Kumar, Pankaj Kumar, and Sushil Kumar, "Fluorescent and chromogenic organic probes to detect group 10 metal ions: design strategies and sensing applications" *Dalton transactions,* vol. 52, pp. 14704–14732, 2023, https://doi.org/10.1039/D3DT01723K.
- **Nidhi Goswami**, Sudhanshu Naithani, Tapas Goswami, Pankaj Kumar, and Sushil Kumar, "A quinoline derived Schiff base as highly selective 'turn-on' probe for fluorogenic recognition of Al^{3+} ion" *Spectrochimica Acta Part A: Molecular and Biomolecular Spectroscopy*, vol. 310, pp. 123971, 2024, https://doi.org/10.1016/j.saa.2024.123971.
- **Nidhi Goswami**, Sudhanshu Naithani, Tapas Goswami, Pankaj Kumar, Pramod Kumar, and Sushil Kumar, "Turn-on detection of Al^{3+} ions using quinoline-based tripodal probe: mechanistic investigation and live cell imaging applications", *Analytical methods*, vol. 16, pp. 5022-5031, 2024, https://doi.org/10.1039/D4AY00761A.
- **Nidhi Goswami,** Sudhanshu Naithani, Jimmy Mangalam, Vikas Yadav, Saakshi Saini, Partha Roy, Tapas Goswami, and Sushil Kumar, "Imidazo-phenanthroline based ratiometric optical sensing platform for cyanide and fluoride ion", *Spectrochimica Acta Part A: Molecular and Biomolecular Spectroscopy,* vol. 338, pp. 126123, 2025, https://doi.org/10.1016/j.saa.2025.126123.
- **N. Goswami *et* al.** Fluorogenic probes based on 2,2'-thiobis(ethylamine) binding motifs: Selective analyte detection and emerging opportunities (communicated)
- **N. Goswami *et* al.** Isolation and characterization of the labile tetrahedral intermediate in the Al(III)-catalyzed hydration of aromatic aldehydes (Under process)

Other publications

- Sudhanshu Naithani, **Nidhi Goswami**, Sain Singh, Vikas Yadav, Sanjay Kumar, Pramod Kumar, Amit Kumar, Tapas Goswami, and Sushil Kumar, "Turn-on detection of Al^{3+} and Zn^{2+} ions by a NSN donor probe: reversibility, logic gates and DFT calculations", *Analytical methods*, vol. 15(44), pp. 6021–6030, 2024, https://doi.org/10.1039/D3AY01534C.
- Sudhanshu Naithani, **Nidhi Goswami,** Vikas Yadav, Jimmy Mangalam, Tapas Goswami, and Sushil Kumar, "Selective turn-on luminescent recognition of perchlorate ion using pyridyl-benzimidazole-based probe", vol. 40, s2025, 10.1002/bio.70087.
- Amit Chauhan, **Nidhi Goswami** *et* al., "Optical detection of Al^{3+} and Fe^{3+} via multiple readout using a Ru(II)-terpyridyl platform: Insights from experimental and theoretical studies", Inorganica Chimica Acta, 2025, vol. 581, pp. 122650, 2025, https://doi.org/10.1016/j.ica.2025.122650.

CONFERENCES

- **N. Goswami *et* al.**, Sustainability Fair 2.0 4th International Sustainability Conference on Health, Safety, Fire and Environmental Advances (HSFEA 2023) organized by UPES, Dehradun.
- **N. Goswami *et* al.**, IYRC-2024 organized by UPES, Dehradun (28-29th Feb 2024).
- **N. Goswami *et* al.**, ICRAAST-1.0 organized by UPES, Dehradun (29-31st May 2024)
- **N. Goswami *et* al.**, IAC-2024 organized by CSIR-IIP, Dehradun (5-7th Jun 2024).

WORKSHOPS

- 1st Annual Celebration of Research Week Sustainability Cluster at UPES, Dehradun (29 Dec 2021)
- Two days workshop (Funding opportunities and project writing) (4-5 Apr 2022)
- Workshop (Essentials of Research Article writing at UPES) (19 Jan 2022)
- Sustainability in Water & Environment in the Department of Chemical Engineering and Technology, IIT BHU, Varanasi (26th & 27th Feb 2024).

Nidhi Goswami_Thesis_05 Feb 2025_plag.docx

My Files

My Files

Bennett University

Document Details

Submission ID

trn:oid:::29034:81138917

Submission Date

Feb 5, 2025, 3:00 PM GMT+5:30

Download Date

Feb 26, 2025, 8:26 PM GMT+5:30

File Name

Nidhi Goswami_Thesis_05 Feb 2025_plag.docx

File Size

84.0 MB

215 Pages

51,488 Words

308,074 Characters

1% Overall Similarity

The combined total of all matches, including overlapping sources, for each database.

Filtered from the Report

- Bibliography
- Quoted Text
- Cited Text
- Small Matches (less than 14 words)

Exclusions

- 198 Excluded Matches

Match Groups

35 Not Cited or Quoted 1%
Matches with neither in-text citation nor quotation marks

0 Missing Quotations 0%
Matches that are still very similar to source material

0 Missing Citation 0%
Matches that have quotation marks, but no in-text citation

0 Cited and Quoted 0%
Matches with in-text citation present, but no quotation marks

Top Sources

0% Internet sources
1% Publications
1% Submitted works (Student Papers)

Integrity Flags

2 Integrity Flags for Review

Replaced Characters
112 suspect characters on 65 pages
Letters are swapped with similar characters from another alphabet.

Hidden Text
9 suspect characters on 2 pages
Text is altered to blend into the white background of the document.

Our system's algorithms look deeply at a document for any inconsistencies that would set it apart from a normal submission. If we notice something strange, we flag it for you to review.

A Flag is not necessarily an indicator of a problem. However, we'd recommend you focus your attention there for further review.

Match Groups

- **35** Not Cited or Quoted 1%
  Matches with neither in-text citation nor quotation marks
- **0** Missing Quotations 0%
  Matches that are still very similar to source material
- **0** Missing Citation 0%
  Matches that have quotation marks, but no in-text citation
- **0** Cited and Quoted 0%
  Matches with in-text citation present, but no quotation marks

Top Sources

0% Internet sources
1% Publications
1% Submitted works (Student Papers)

Top Sources

The sources with the highest number of matches within the submission. Overlapping sources will not be displayed.

1	Publication	Suban K. Sahoo. "Fluorescent Chemosensing and Bioimaging", CRC Press, 2024	<1%
2	Publication	Pragyan Parimita Dash, Dhvani A. Patel, Patitapaban Mohanty, Rubi Behura, S. Be...	<1%
3	Publication	Gurdeep Kaur, Iqubal Singh, Runjhun Tandon, Nitin Tandon. "Recent advanceme...	<1%
4	Internet	dokumen.pub	<1%
5	Publication	Jen-Tsung Chen. "Biotechnology, Multiple Omics, and Precision Breeding in Medic...	<1%
6	Publication	I. Hamzi. "Colorimetric andFluorometric N-Acylhydrazone-based Chemosensors f...	<1%
7	Publication	Ankita Roy, Mahasweta Nandi, Partha Roy. "Dual chemosensors for metal ions: A ...	<1%
8	Internet	pubs.acs.org	<1%
9	Submitted works	VIT University on 2019-03-23	<1%
10	Submitted works	VIT University on 2020-07-16	<1%

11 Submitted works

Indian Institute of Technology, Madras on 2024-08-02 <1%

12 Internet

orbi.uliege.be <1%

13 Submitted works

National Institute Of Technology, Tiruchirappalli on 2024-02-23 <1%

14 Publication

Cheng, Zehua. "Fluorescent Detection of Pesticide Residues and Heavy Metal Ions... <1%

15 Publication

Rajendran Nagarajan, Chitra Varadaraju, Ki Hwan Lee. "Recent advancements in t... <1%

16 Submitted works

Southern Methodist University on 2024-06-19 <1%

17 Publication

Tung, Matthew. "The Development of Photosensitizers: Addressing Limitations in... <1%